

THESIS ON CIVIL ENGINEERING F52

**Propagation and Run-up of Nonlinear Solitary
Surface Waves in Shallow Seas and
Coastal Areas**

ARTEM RODIN

TUT
PRESS

TALLINN UNIVERSITY OF TECHNOLOGY
Institute of Cybernetics
Laboratory of Wave Engineering

**The thesis was accepted for the defence of the degree of Doctor of Philosophy
in Engineering on 26 March 2015**

Supervisors: Prof. Dr. Tarmo Soomere
Dr. Ira Didenkulova
Institute of Cybernetics, Tallinn University of Technology, Estonia

Opponents: Prof. Dr. Stanisław R. Massel
Institute of Oceanology, Polish Academy of Sciences, Sopot,
Poland

Prof. Dr. Peter A. Davies
School of Engineering, Physics and Mathematics, University of
Dundee, United Kingdom

Defence of the thesis: 04 May 2015

Declaration:

Hereby I declare that this doctoral thesis, my original investigation and achievement, submitted for the doctoral degree at Tallinn University of Technology, has not been submitted for a doctoral or an equivalent academic degree.

/Artem Rodin/



Copyright: Artem Rodin, 2015
ISSN 1406-4766
ISBN 978-9949-23-757-9 (publication)
ISBN 978-9949-23-758-6 (PDF)

EHITUS F52

**Pikkade mittelineaarsete lainete
dünaamika ja lainerünnak**

ARTEM RODIN

Contents

List of publications constituting the thesis	6
List of figures	6
Introduction	11
Run-up of long waves	13
Wave systems produced by ships sailing at large Froude numbers	15
Ship-induced solitary waves of depression as a concealed hazard	16
Freak and extreme waves and their run-up and inundation	18
The objectives and outline of the thesis	19
Approbation of the results	21
1. Nonlinear wave dynamics and run-up in the coastal zone	23
1.1. Mathematical model of nonlinear shallow-water waves	23
1.2. CLAWPACK software package	26
1.3. Run-up of waves of elevation on a beach	30
1.4. Run-up of waves of depression	34
1.5. The effect of solitary wave amplitude and polarity on the run-up	37
2. Observed run-up of vessel waves	39
2.1. The complexity of ship-induced wave systems	39
2.2. Experimental study of ship wakes in Tallinn Bay	42
2.3. Statistics of single vessel waves and their run-up	43
2.4. Run-up of individual vessel waves	49
3. Ship-induced solitary waves of depression	51
3.1. Ship-induced depressions in shallow areas	51
3.2. Ship-induced solitary waves of depression in the Venice Lagoon	54
3.3. Numerically simulated Riemann waves	57
3.4. Propagation of ship-induced depressions into the Venice Lagoon	62
4. Rogue waves and extreme run-up in the coastal zone	67
4.1. Rogue waves in the nearshore	67
4.2. Wind wave measurements and data processing	68
4.3. Statistics of rogue waves in low wind conditions	70
4.4. Run-up of severe storm waves on the Estonian coast	71
Conclusions	77
Summary of the results	77
Main conclusions proposed to defend	79
Recommendations for further work	80
Bibliography	82
Acknowledgements	95
Abstract	96
Resümee	97
Appendix A: Curriculum Vitae	98
Appendix B: Elulookirjeldus	106

List of publications constituting the thesis

The thesis is based on five academic publications, which are referred to in the text as Paper I, Paper II, Paper III, Paper IV and Paper V. Papers I–III and V are indexed by the ISI Web of Science Core Collection database and Paper IV is indexed by the SCOPUS database:

- Paper I Didenkulova I., **Rodin A.** 2013. A typical wave wake from high-speed vessels: its group structure and run-up. *Nonlinear Processes in Geophysics*, 20, 179–188.
- Paper II Parnell K.E., Soomere T., Zaggia L., **Rodin A.**, Lorenzetti G., Rapaglia J., Scarpa G.M. 2015. Ship induced solitary Riemann waves of depression in Venice Lagoon. *Physics Letters A*, 379, 555–559.
- Paper III **Rodin A.**, Soomere T., Parnell K.E., Zaggia L. 2015. Numerical simulation of the propagation of ship-induced Riemann waves of depression into the Venice Lagoon. *Proceedings of the Estonian Academy of Sciences*, 64, 22–35.
- Paper IV Didenkulova I., **Rodin A.** 2012. Statistics of shallow water rogue waves in Baltic Sea conditions: the case of Tallinn Bay. In: *IEEE/OES Baltic 2012 International Symposium*, 8–11 May 2012, Klaipėda, Lithuania; Proceedings. IEEE, 6 pp., doi: 10.1109/BALTIC.2012.6249221
- Paper V **Rodin A.**, Didenkulova I., Nikolkina I. 2014. Run-up of large storm waves on Estonian coasts of the Baltic Sea. In: *IEEE/OES Baltic 2014 International Symposium*, 26–29 May 2014, Tallinn, Estonia; Proceedings. IEEE, 5 pp., doi: 10.1109/BALTIC.2014.6887886

List of figures

- Figure 1.** The composite geometry of the run-up problem.....30
- Figure 2.** Run-up and reflection of a small-amplitude (weakly nonlinear) solitary wave of elevation ($A = 0.1$ m) from a sloping beach.....31
- Figure 4.** Run-up and reflection of a very high solitary wave of elevation ($A = 3.5$ m) from a sloping beach: $x-t$ diagram. The scale at the right indicates the distance of the water surface from the bottom.33
- Figure 5.** Vertical oscillations of the waterline for various amplitudes of the initial solitary wave of elevation.....33
- Figure 6.** Comparison of numerical simulations with predictions of the analytical theory for a 0.05 m high weakly nonlinear wave of elevation.34
- Figure 7.** Run-up and reflection of a solitary wave of depression with $A = 0.1$ m from a sloping beach.34

Figure 8. Run-up and reflection of a solitary wave of depression with an almost limiting amplitude ($A = -3.499$ m) from a sloping beach: $x-t$ diagram. The scale at the right indicates the distance of the water surface from the bottom.	35
Figure 9. Run-up and reflection of a solitary wave of depression with an almost limiting amplitude ($A = -3.499$ m) from a sloping beach.	36
Figure 10. Vertical oscillations of the shoreline for various amplitudes of solitary waves of depression.....	36
Figure 11. Comparison of numerical simulations with predictions of the analytical theory for initially 0.05 m high weakly nonlinear solitary waves of depression.....	36
Figure 12. Run-up and run-down heights versus the initial wave amplitude.	37
Figure 13. Run-up/run-down ratios versus the initial wave amplitude.....	38
Figure 14. Ratio of run-down heights to run-up heights R_{down}/R_{up} versus the initial wave amplitude.....	38
Figure 15. Scheme of the wave pattern excited by a high-speed vessel sailing at a subcritical speed (Soomere, 2009).	40
Figure 16. Sketch map of the Baltic Sea and location of the study site in Tallinn Bay (Paper I).	42
Figure 17. High-speed vessel wakes at Pikakari Beach. Run-up was tracked with the help of the measurement staff at the shore. Wave properties were recorded farther using a tripod (Paper I).	43
Figure 18. Vessel wakes from a) the <i>SuperStar</i> (18 June 2009, 16:15), b) the <i>Star</i> (20 June 2009, 12:10) (Paper I).	44
Figure 19. Averaged distribution of all recorded vessel wave heights. The red dashed line corresponds to the Rayleigh distribution ($\sigma = 0.12$ m) and the black solid line to the Weibull distribution ($\sigma = 0.16$ m, $q = 1.53$), fitted using the maximum likelihood estimate (Paper I).	45
Figure 20. Averaged distribution of all recorded run-up heights of vessel waves. The red dashed line corresponds to the Rayleigh distribution ($\sigma = 0.38$ m) and the black solid line to the Weibull distribution ($\sigma = 0.56$ m, $q = 2.77$), fitted using the maximum likelihood estimate (Paper I).	46
Figure 21. Mean run-up and wave heights in the wakes, calculated from the original data (red squares) and reconstructed from the Rayleigh (blue circles) and Weibull (black triangles) distributions. Blue solid and black dashed lines correspond to the regression curves fitted to the results calculated from the Rayleigh and Weibull distributions, respectively (Paper I).....	47

Figure 22. Wave heights (blue circles) and corresponding run-up heights (red triangles) within the wake from a) the *SuperStar* (19 June 2009, 19:15), b) the *Star* (20 June 2009, 12:10) and c) the *Viking XPRS* (21 June 2009, 13:50) (Paper I).....48

Figure 23. Wave amplification rate on Pikakari Beach for waves from a) the *SuperStar*, b) the *Star*, c) the *Viking XPRS*. Dashed lines correspond to Eq. (27), dotted lines to the calculation of breaking run-up with the characteristic periods of 6 s (blue) and 14 s (black) and the black solid line corresponds to Eq. (28). Some smaller waves with heights <20 cm may have the amplification rate matching that of theoretical estimations for non-breaking waves (black dashed line) (Paper I). ..49

Figure 24. The study area in the Malamocco–Marghera industrial channel. White triangles in the inset indicate the locations of pressure sensors in Figure 25 (Papers II and III).53

Figure 25. Cross-section of the Malamocco–Marghera channel at the measurement site (Figure 24). The location of pressure sensors (B0–B3, W0–W3) is indicated by triangles. The distance is referenced to the western channel marker and the depth is referenced to the local tidal datum (0.26 m below mean sea level) (Paper II).54

Figure 26. An example of 24-h-long record of water level, restored from the pressure signal, at the banks of the Malamocco–Marghera channel. The location of the devices at the western (coastal, B0–B3) and eastern (lagoon, W0–W3) sides of the channel are indicated in Figure 25. The record begins at 12:00 on 01 April 2014. Data for locations W2 and W3 (used to characterize the wake of the *Abu Dhabi Star* below and in Paper II) are partly missing due to equipment failure. Note that gauge B3 was moved by a strong wake about 3 h after the record began (Paper III).55

Figure 27. Disturbances induced by the *Abu Dhabi Star*, *Domenico Ievoli* and *Pessada*. Data for W0 for the passage of the *Pessada* are missing due to equipment failure. The largest depressions caused the drying of the coastal slope at location B3. The position of the surface is presented according to the actual water depths at the time of ship passage (Paper II).56

Figure 28. The appearance of a depression pulse with an initial amplitude of 1 m in the navigation channel and over its lagoonside slope at time instants 0, 150 and 300 s. Note the development of a counter-propagating reflected wave at 150 and 300 s. The bold line in the right upper part of the panel represents the model seabed (only shown for the water depths <5 m) (Paper III).60

Figure 29. Water surface time series in a wake produced by the *Vigor SW* on the western (coastal) side of the channel around 13:20 on 01 April 2014 (Paper III)...60

Figure 30. Propagation of a numerically simulated Riemann wave matching the depression created by the *Pessada* over the lagoonside bank of the channel at measurement sites W1–W3 (data from W0 are absent due to equipment failure) on 28 March 2014 at 8:30. Red: measured profiles; blue: simulated profiles (Paper III).61

Figure 31. Propagation of a numerically simulated Riemann wave matching the depression created by the *Vigor SW* over the beachside bank of the channel at measurement sites B0–B3 on 01 April 2014 at 13:20. Red: measured profiles; blue: simulated profiles (Paper III).....62

Figure 32. Simulated and measured trough amplitudes for all 12 vessels. Blue dashed line: the regression lines for measurement sites B1–B3 and W1–W3; black dotted line: the regression line for the most distant sites B3 and W3 (Paper III)....63

Figure 33. Space–time ($x-t$) diagram of the simulated wave profile produced by the depression wave with the initial amplitude $A_0 = 1$ m propagating into the lagoon with a constant water depth of 2 m (Paper III). The scale at the right indicates the distance of the water surface from the undisturbed position.65

Figure 34. Temporal evolution of the amplitude of initial Gaussian-shaped depressions matching the measured wakes at the channel margin. The parameters in Eq. (28) are as follows: *Vigor SW* (01 April 2014 at 13:20): $A_0 = 1$ m, $l = 200$ m; *Domenico Ievoli* (22 April 2014 at 06:50): $A_0 = 0.92$ m, $l = 100$ m; *Pessada* (28 March 2014 at 8:30): $A_0 = 0.65$ m, $l = 182.5$ m; *Abu Dhabi Star* (01 April 2014 at 15:38): $A_0 = 0.8$ m, $l = 195$ m (Paper III).....66

Figure 35. Numerically simulated trough profiles in the lagoon after 300 s propagation time. The different locations of the wave trough are caused by different propagation speeds in Eq. (4) (Paper III).....66

Figure 36. Frequency of occurrence of significant wave heights in different sections of the record. White and blue bars correspond to the values of H_S obtained using down-crossing and up-crossing methods, respectively (Paper IV). 69

Figure 37. Examples of low-resolution short rogue waves measured on 30 June (a) and 17 June 2009 (b) (Paper IV).70

Figure 38. Groups of rogue waves measured on 25 June 2009 (Paper IV).70

Figure 39. Scatter diagram for rogue wave height H_r and significant wave height H_S for rogue waves identified using up-crossing (a) and down-crossing (b) approaches. Red squares correspond to low-resolution rogue waves (Paper IV)....71

Figure 40. Amplification factor of rogue waves identified using up-crossing (a) and down-crossing (b) approaches. Red squares show low-resolution rogue waves (Paper IV).71

Figure 41. Distributions of the crest heights A_+ (a) and trough depressions A_- of rogue events (b). White and red bars correspond to all rogue events found using the up-crossing method and to only high-resolution events respectively; light and dark blue bars correspond to all rogue events found by the down-crossing method and to only high-resolution events, respectively (Paper IV).72

Figure 42. Distributions of rogue wave heights identified using the up-crossing (a) and down-crossing (b) approaches. White columns correspond to the full rogue wave dataset and blue columns to high-resolution events (Paper IV).....	72
Figure 43. Locations of 18 beach profiles along Estonian coasts used in Didenkulova et al. (2013b) and Paper V.	74
Figure 44. Comparison of calculated and estimated run-up heights (Paper V).	75
Figure 45. Calculated and estimated run-up heights versus significant wave height (Paper V).	75
Figure 46. Wave amplification on the beach (ratio of the run-up height to the significant wave height) versus significant wave height (Paper V).	76

Introduction

The dynamics of nonlinear waves on the water surface is a traditional research field in fluid mechanics. Its various aspects have been addressed in a number of classic books (Lamb, 1916; Stoker, 1957; Kochin, 1964; Whitham, 1974; Sedov, 1977; Sretensky, 1977; Lighthill, 1978). While considerable progress has been achieved in the analytical research of linear and weakly nonlinear waves since the seminal book of Whitham (1974) and enormous progress has been made in the numerical analysis of various nonlinear problems of wave motion, many issues of nonlinear wave dynamics are still under intense research. The practical importance of these studies becomes *inter alia* evident through the hazardous nature of large and steep sea waves. The motion of such waves often leads to the damage of even the most contemporary ships (Nikolkina and Didenkulova, 2011, 2012; Bitner-Gregersen et al., 2013), destruction of offshore and coastal engineering structures and loss of life. The associated nonlinear effects such as wave breaking in the nearshore or wave run-up (Didenkulova, 2009a) and set-up (Dean and Bender, 2006) in the vicinity of the shoreline endanger the users of the coastal zone at a considerable distance from the waterline and elevation from the still water level.

The dynamics of so-called long waves has particular importance in the understanding of several core marine-induced dangers. This concept is associated with the ratio of the length of the wave to the water depth. Waves are called long (equivalently, water is called shallow) if the wave length at least 20 times exceeds the depth of the water. In essence, virtually all waves attacking the gently sloping shoreline can be treated as long waves starting from a certain depth. Thus, their impact on coastal communities, port and coastal structures cannot be underestimated. A striking example of such waves is a tsunami that is often a long wave even in the open ocean. The devastating 2004 tsunami in the Indian Ocean and another event in 2011 in Japan took the lives of almost 300,000 people and also demonstrated the fragility of the existing technological solutions by, e.g., severely damaging a nuclear power plant. Meteorological tsunamis are equally dangerous. They may create flooding similar to storm surges resulting from the passage of cyclones, lead to coastal flooding and loss of life, like the fatal meteorological tsunami that struck Nagasaki Bay in Japan in 1979 (Hibiya and Kajiura, 1982). Their smaller counterparts are compact groups of ship waves created at relatively large sailing speeds (Didenkulova et al., 2011c).

It is generally desirable to apply as simple concepts and techniques as possible to the description of wave motion. Waves in the coastal zone are transformed and amplified due to effects of wave shoaling, refraction, diffraction and wave breaking. This is a challenge with respect to coastal engineering and marine safety, where it is often important to take account of the impact of waves at the coast based on offshore wave conditions. The linear wave theory, although it provides a fairly good description of many offshore wave properties and gives a flavour about how the ocean waves are transformed at certain depths, is generally not applicable

to steep and high waves in the nearshore. Various weakly nonlinear approaches allow further description of the motion of relatively high and steep waves but they also fail in many occasions of practical interest.

The process of nonlinear transformation of long waves (equivalently, waves in shallow water) has for decades been extensively studied in the framework of nonlinear shallow water theory (Stoker, 1957; Shuleykin, 1968; Arseniev and Shelkovnikov, 1991). Although this problem can nowadays be analysed by means of numerically solving the nonlinear Euler or Navier–Stokes equations, it is still desirable to create a simpler (semi-)analytic description of the related fundamental phenomena.

The most interesting aspects are how nonlinear waves break, exert run-up or form a shock wave. The shock wave formation is often observed in the coastal zone, for example, when a tidal wave enters the estuary (Favre, 1935; Nakamura, 1973; Tsuji et al., 1991), straits (Pelinovsky and Troshina, 1994), a shallow channel (Wu and Tian, 2000; Caputo and Stepanyants, 2003) or a narrow bay (Zahibo et al., 2006b) as a bore-like phenomenon (Nakamura, 1973). Various problems associated with the wave dynamics and shape before breaking, incl. its spectrum and the breaking time, have been studied from a number of viewpoints (Pelinovsky, 1982; Zahibo et al., 2008).

The dynamics of breaking waves is mostly studied numerically. There are very few analytical results, except for several idealized cases. If the wave is long enough, the shock area occupies a small part of the wave front, the internal structure of the shock can be neglected and it can be approximated as a rupture (hydraulic jump) that separates areas with constant flow velocity (Courant and Friedrichs, 1948; Stoker, 1957; Voltsinger et al., 1989). Depending on the height of the bore, different types of shock waves may occur: so-called “parabolic waves”, hydraulic jumps or undular bores. The first two occasions can be adequately addressed using shallow-water equations in divergence form with appropriate boundary conditions at the discontinuity. However, dispersion effects are important during the evolution of a bore and, e.g., the Korteweg–de Vries–Burgers equation should be applied to describe the structure of the shock.

There are still numerous occasions when simplified approaches do not provide an adequate representation of the propagation and transformation of nonlinear waves in the marine environment. In particular, the analysis of several classes of rogue waves and long-living deep depressions in shallow water requires the use of more general concepts. The dynamics of long-living depression waves (Rapaglia et al., 2011) that are rare in natural conditions but produced by ships in certain occasions is particularly interesting. Nonlinearity can be arbitrarily strong for shallow-water waves of depression and the asymptotic estimates and weakly nonlinear models are not always applicable to their description. For example, the classical Korteweg–de Vries (KdV) model indicates that a sequence of elevation waves is rapidly formed from an initial depression (Arcas and Segur, 2012). The leading elevation wave, developed at the rear end of the depression, is up to twice the height of the depression according to the weakly nonlinear model (Grimshaw et

al., 2014). However this feature is not evident in field data presented in Paper II. A possible framework for addressing this problem is provided in terms of Riemann or simple waves (Papers II and III) that have an exact analytical description (Pelinovsky, 1982; Voltsinger et al., 1989; Didenkulova et al., 2006a).

Run-up of long waves

It is well known that the elevation, to which the wave motion may bring water at the shoreline may be much larger than the wave height. The problem of wave run-up is a classical research field of ocean and coastal engineering. The pioneering work of Carrier and Greenspan (1958) has provided a rigorous analytical solution for several features of run-up of idealized non-breaking waves on a plane beach. The idea of the reduction of nonlinear shallow-water equations to their linear counterparts using the Legendre (hodograph) transformation has since then been exploited in hundreds of studies.

The majority of the existing research addresses the run-up of incident waves of various shapes on a plane beach. The properties of run-up have been established for a variety of single disturbances such as solitons (Pedersen and Gjevik, 1983; Synolakis, 1987; Shermeneva and Shugan, 2006; Antuono and Brocchini, 2008, 2010), sine pulses (Mazova et al., 1991; Shermeneva and Shugan, 2006), Lorentz pulses (Pelinovsky and Mazova 1992), Gaussian pulses (Carrier et al., 2003; Kanoglu, 2004; Kanoglu and Synolakis, 2006; Antuono and Brocchini, 2007), N-waves (Tadepalli and Synolakis, 1994, Kanoglu, 2004; Antuono and Brocchini, 2007; Madsen and Shaffer, 2010), some specific localized disturbances (Tinti and Tonini, 2005; Pritchard and Dickinson, 2007; Dobrokhotov and Tirozzi, 2010) and nonlinearly deformed (asymmetric) waves (Didenkulova et al., 2006a, 2007a,b, 2008; Didenkulova and Pelinovsky, 2008; Didenkulova, 2009). Similar studies have been performed for different regular wave trains such as sine waves (Madsen and Fuhrman, 2008), cnoidal wave trains (Synolakis et al., 1988; Synolakis, 1991) and “characterized tsunami waves” (Tinti and Tonini, 2005; Madsen and Shaffer, 2010). The same approach has recently been applied to irregular wave fields (Didenkulova et al., 2010, 2011b; Denissenko et al., 2011, 2013; Didenkulova and Pelinovsky, 2011b) and irregular beach shapes (Dutykh et al., 2011).

Other studies involve research into the influence of bottom friction on the run-up height (Bernatsky and Nosov, 2012) and possible resonance effects (Stefanakis et al., 2011; Ezersky et al., 2013a,b). The listed studies have assumed that the waves are unidirectional and incidentally approach a homogeneous beach. The effects associated with the spatial structure of the approaching wave and more complicated shape of the seabed have been addressed in recent studies of wave run-up in long and narrow bays with various cross-sections (Zahibo et al., 2006a; Choi et al., 2008; Didenkulova and Pelinovsky, 2009, 2011a,b,c; Rybkin et al., 2014).

Most of the papers cited above address the run-up phenomena when undulating wave sequences or single waves of positive polarity (waves of elevation or solitary

crests) propagate to a beach. It is not unexpected that these waves may induce significant flooding of the shore. The situation may be even richer in content and dangerous if the leading wave of elevation is preceded by a solitary wave of depression (either a single trough or a trough–crest system similar to a N-wave). The presence of the precursor disturbance in the form of a depression leads to a substantial increase in the run-up height of the leading wave of elevation (Soloviev and Mazova, 1994; Tadepalli and Synolakis, 1994). The N-wave effect becomes evident for both waves of small (but finite) amplitude in the framework of linear or weakly nonlinear theory and for large-amplitude strongly nonlinear (but still non-breaking) waves.

Many properties of the run-up phenomena substantially depend on the history of the propagation of the wave in deeper regions before the wave approaches the nearshore. These properties vary depending not only on the propagation distance along an idealized basin of constant depth but also on the polarity of the approaching wave (Didenkulova et al., 2006b; Zahibo et al., 2008; Pelinovsky and Rodin, 2011, 2012). It is well known that different polarities of the incident wave result in different manifestations of linear effects during the propagation of even very small-amplitude waves. For example, the dependence of the wave propagation speed on the local water depth leads to the steepening of the wave front. As the instantaneous water depth under the wave trough is smaller than under the crest, nonlinear effects are always stronger at the wave trough than at the wave crest. This difference may markedly impact several properties of non-breaking wave run-up on a beach (Didenkulova et al., 2014).

Analysis of the run-up of large-amplitude and gradually breaking waves is generally quite complicated and extensive and meaningful results have been obtained only for the case of fully developed bores (Shen and Meyer, 1963; Sachdev and Seshadri, 1976). It is therefore important to study single waves rolling ashore in a wide range of their height when the wave breaks before landfall, and its shape can be approximated by a fully developed bore. Only the first steps have been made in this direction (Li and Raichlen, 2002; Madsen and Fuhrman, 2008).

The situation is particularly complicated in many realistic situations where the wave propagates over a wide relatively shallow area before it exerts run-up. In these occasions even relatively small-amplitude waves may be considerably affected by nonlinear effects. These effects are different for waves of different polarities (Didenkulova et al., 2014), in particular because the effect of nonlinearity impacts differently waves of opposite polarities that propagate over shallow areas. These differences have been extensively studied in tsunami research (e.g., Carrier et al., 2003; Fernando et al., 2008). However, most of the relevant studies have only addressed the classical solitary wave solutions to (weakly) nonlinear shallow-water equations, which are waves of elevation. A large part of this thesis is focused on the analysis of propagation, transformation and run-up of strongly nonlinear long-living waves of depression.

Wave systems produced by ships sailing at large Froude numbers

Similarly to moving atmospheric pressure patterns that are able to generate meteorological tsunamis, virtually all moving vessels produce certain disturbances of the water surface. The key properties of waves excited by vessels that sail steadily over a relatively deep sea area are adequately described by the classical theory of linear (Kelvin) ship waves (e.g., Wehausen, 1973; Newman, 1977; Lighthill, 1978; Kuznetsov et al., 2002). This theory reasonably depicts not only the geometry of wave crests but also several features of the spatio-temporal distribution of single wave heights.

An increase in the vessel speed in relatively shallow water leads to an increase in the depth(-based) Froude number $F_d = v/\sqrt{gH}$ (defined as the ratio of the ship's speed v to the maximum phase speed of linear water waves \sqrt{gH} for the given depth H). The implementation of larger ships means an increase in the length Froude number. Any of these changes may lead to various changes in the vessel wave pattern. The shallow-water effect becomes essential when $F_d > 0.6$ (Lee et al., 1989), when unsteady wave components can be generated (Akylas, 1984; Mei, 1986) but in some cases it is notable even at $F_d \sim 0.2$. An increase in the depth Froude number is associated not only with the widening of the area filled with waves (Kelvin wedge) that are stationary with respect to the ship (Sorensen, 1973) but also with the generation of long and long-crested, almost non-dispersive leading waves and with a variety of nonlinear phenomena (Papers II and III).

A wide range of specific types of disturbances has been described in the international literature, from high and long leading waves (Parnell and Kofoed-Hansen, 2001), packets of relatively short waves resembling Schrödinger solitons (Brown et al., 1989), solitary waves of elevation (Neuman et al., 2001; Garel et al., 2008) and cnoidal wave trains (Soomere et al., 2005) moving ahead of the vessel up to associated depression areas (Soomere, 2007) and phenomena that transport large amounts of water to adjacent shores (Soomere et al., 2011). These constituents, some of them qualitatively different from the usual wind waves or components of the linear Kelvin wake, have been observed around the world, e.g., in the Venice Lagoon, Italy (Rapaglia et al., 2011), Savannah River, Georgia (Houser, 2011), New Zealand and Denmark (Parnell and Kofoed-Hansen, 2001) and Tallinn Bay, Estonia (Parnell et al., 2008).

The waves excited by contemporary large strongly powered vessels can be a major contributor of energy and especially energy flux even to sections of coasts that are exposed to significant natural hydrodynamic loads (Soomere, 2005a; Soomere et al., 2009). The actual effect of vessel-induced disturbances depends upon the features of the coastal environment and on the difference in the properties of vessel waves and the existing hydrodynamic loads. Even though the importance of waves from high-speed vessels in the evolution of low- and medium-energy coasts has been demonstrated and quantified for different basins and environments (Parnell and Kofoed-Hansen, 2001; Soomere, 2005a), the reasons for such a strong impact still remain largely unclear. A possible explanation is the net transport of

water, excited by ships sailing at transcritical speeds and directed towards the adjacent coasts. This signal may lead to significant water level set-up exactly when groups of high vessel waves arrive. The joint effect of this set-up and intense waves may cause a rapid reaction of the coast (Soomere et al., 2011).

Ship wakes are transient wave events that often involve a combination of several linear and nonlinear wave components (Soomere, 2007). Their impact on the coast is often highly variable due to wave interaction with bottom topography (Torsvik et al., 2009a). Given the number of factors influencing ship wakes listed above, it is difficult to accurately predict the wake impact at a particular stretch of the coastline even if the parameters related to the ship route, ship dimensions and ship speed are known. Likewise, it is also difficult to identify the source of individual wake components, given a measurement record of a wake event at the coast. It is well known that wave energy is dissipated in the surf zone, due to wave breaking and reflection as waves interact with bottom topography. However, only a few studies have been made on the transformation of ship wakes in shallow water (Belibassakis, 2003; Didenkulova et al., 2009a; Torsvik et al., 2009a).

Another contribution to the impact of vessel waves on the coastal processes is the specific group structure of such sets of waves. Quite often the largest, the longest and the most asymmetric waves arrive first and somewhat shorter, lower and more symmetric waves come later. This structure produces the possibility of almost continuous sequence of high run-up events that is untypical of wind waves. This option and the underlying characteristic properties of vessel-induced wave groups are experimentally studied in Paper I and Chapter 2 of this thesis for Pikakari Beach in Tallinn Bay, the Baltic Sea.

Ship-induced solitary waves of depression as a concealed hazard

Many constituents of wakes of large contemporary ships, from the classical Kelvin waves to intricate nonlinear phenomena at transcritical speeds (Soomere, 2007) and to Mach-type systems at supercritical speeds (Rabaud and Moisy, 2013; Darmon et al., 2014), may become hazardous for people, their property and the ecosystem. It is commonly believed that the largest environmental impacts come from long and long-crested groups of high, almost non-dispersive waves (Parnell and Kofoed-Hansen, 2001; Soomere, 2005a). Solitonic precursor waves are less known but in some occasions equally hazardous components. These nonlinear disturbances have usually small amplitudes but may still drive large water velocities (Neuman et al., 2001), bring substantial amounts of water to the shore (Soomere et al., 2011) or, when crossing each other, build long-living rogue waves (Peterson et al., 2003).

The motion of a ship at finite depths at moderate or large depth Froude numbers always produces a depression region. This phenomenon is frequently called Bernoulli wake (Graff, 1962; Jiang, 2001). In some cases it may appear at as low depth Froude numbers as 0.13 (Janson, 2002). In numerical reconstructions it becomes usually evident as an elongated region of depression of nearly uniform depth (Baines, 1997; Torsvik et al., 2009a,b). Its most well-known consequence is

the drawdown effect of the vessel. This effect is commonly called squat (Constantine, 1961; Naghdi and Rubin, 1984; Millward 1996; Gourlay and Tuck 2001; Gourlay, 2003, 2006). Although it occurs also in open shallow sea areas, it is usually addressed in the context of navigation channels where it may form structures similar to undular bore (Akylas, 1984; Grimshaw and Smyth, 1986; Lee et al., 1989).

If a shallow navigation channel that hosts large and relatively rapidly sailing ships has adjacent water areas, the vessel-induced depressions are not necessarily limited to the channel area. The moving depressions may cause extensive dropdown in the water level in adjacent harbours (Forsman, 2001) or spread to a distance of many hundreds of metres from the channel over adjacent shallow areas (Ravens and Thomas 2008; Rapaglia et al., 2011). The resulting events have a characteristic dominant trough that is often followed by small crests (Gelinis et al., 2013). This appearance suggests that linear or weakly nonlinear theories may not be able to properly describe the long-term evolution of such depressions.

Particularly interesting features of ship wakes may become evident in a fairly realistic situation where a navigation channel has extensive shallow banks. This situation is typical if the channel is dredged in a shallow lagoon or a tidal estuary. In such situations the standard depth Froude number not necessarily characterizes the sailing regime properly. Numerical simulations suggest that unexpectedly high waves may occur at relatively modest Froude numbers (Torsvik et al., 2009b).

Another important aspect is the development of dangerous water level drawdowns at the banks of navigable rivers (Balzerek and Kozlowski, 2007). The generated depression waves are particularly deep if the waterway is surrounded by wide shallow-water areas, as is the case in the Venice Lagoon (Rapaglia et al., 2011). As demonstrated in Paper II, ships of fairly moderate size (blocking coefficient or width \times draught of the vessel / cross-sectional area of the channel in the range of 0.07–0.14) and sailing at depth Froude numbers of 0.37–0.5 may produce up to 2.5 m deep depressions in locations where the water depth is about 4 m. It is usually thought that the depression area is concentrated in the vicinity of the moving vessel. As substantial waves of depression have been reported at a distance of many hundreds of metres from the channel (Rapaglia et al., 2011), it is likely that in some situations the ship-induced depressions may start travelling as free waves.

The rear of the measured depressions often involves a bore-like feature (Ravens and Thomas, 2008). These events commonly have a characteristic deep leading trough, followed by a set of crests at longer distances from the generation area (Gelinis et al., 2013). These features are consistent with the common scenarios of non-dispersive propagation of waves of depression that are prone to the formation of *V*-like shapes with an extremely steep, bore-like rear slopes (Didenkulova et al., 2014). This feature, evidently driven by nonlinearity, explains well why ship-induced depression waves may play a great role in sediment resuspension in shallow lagoons and estuaries (Rapaglia et al., 2011; Gelinis et al., 2013; Göransson et al., 2014). These waves decrease in height away from the channel but

they obviously remain strongly nonlinear in the Venice Lagoon with the average depth of only 0.8 m. Although weakly nonlinear theories may replicate qualitative features of the propagation of such depressions (Grimshaw et al., 2014), their quantitative analysis evidently requires the application of fully nonlinear approaches. In this thesis these structures are addressed in the above-mentioned framework of fully nonlinear Riemann waves.

Freak and extreme waves and their run-up and inundation

Rogue waves (also called freak, monster or killer waves) on the sea surface are extremely dangerous phenomena that have been the subject of serious study within the framework of nonlinear wave theory over the last 20 years since the famous Draupner's New Year Wave (Haver, 2005). The existing mechanisms of freak wave generation are summarized in recent books and reviews (Kurkin and Pelinovsky 2004; Dysthe et al., 2008; Garrett and Gemmrich, 2009; Kharif et al., 2009). Usually two main factors of the evolution of such waves are taken into account: dispersion (associated with the difference in propagation speeds of the individual spectral components in deeper waters) and nonlinearity (leading to modulational instability of waves and change in the speed of their spread).

Many freak waves occur in shallow water and are effectively long waves. A possible source of shallow-water rogue waves is soliton interaction driven by crossing systems of long and long-crested waves produced by ships sailing at moderate and high Froude numbers (Peterson et al., 2003). Although most of the rogue wave studies have addressed deep-water conditions (Kharif et al., 2009), such waves may have an even larger impact in the coastal zone that is often densely populated by smaller ships, recreational boats and coastal engineering structures. Recent statistics (Nikolkina and Didenkulova, 2011, 2012; Liu, 2007) indicates that a large proportion of accidents which result in human loss and/or damage to ships occur in the shallow part of the ocean, near the shore or even on the beach. For example, 50% of all accidents caused by the killer waves in 2006–2010, occurred on the coast, 38.5% in shallow water and only 11.5% in the deep part of the ocean and on the high seas. Seven ship losses and 14 ship damages were reported in shallow waters (Nikolkina and Didenkulova, 2011). The resulting damage is also comparatively large in the coastal zone. From 131 lives lost owing to the freak waves for these years, 79 occurred in shallow water and 46 on the beach.

Only a few studies address processes that cause the formation of freak waves in shallow water (Peterson et al., 2003; Soomere and Engelbrecht, 2005; Pelinovsky et al., 2008; Chambarel et al., 2009; Didenkulova and Pelinovsky, 2011b; Didenkulova et al., 2011c). The disproportionately large reported loss of lives and different kinds of damages caused by rogue waves in the nearshore calls for the progress towards better understanding of shallow-water rogue waves. An important contribution to this goal is careful documentation of the related extreme events and

extraction of statistics and properties of events similar to rogue waves everywhere where single waves are reliably measured for a long enough time interval.

One such attempt towards more reliable statistics of the occurrence of smaller rogue wave events is presented in Paper IV. It is based on the perception that large waves may severely attack certain types of the coastal profiles (Didenkulova and Pelinovsky, 2011a), causing impacts that can be called rogue run-up events or situations that may serve as a great danger for people at the coast. More generally, from the point of view of coastal structure design or spatial planning of the low-lying areas, it is very important to have an estimate of the maximum expected inundation and run-up. This analysis is usually performed using different empirical approximations (Hunt, 1959; Battjes, 1974; Guza and Thornton, 1982; Holman, 1986; Powell, 1990; Nielsen and Hanslow, 1991). An overview of empiric formulas available in the literature is given in Matias et al. (2012). These formulas have been obtained by means of field observations or by special flume experiments in specific conditions and are thus directly applicable in a limited range of situations. As waves in many locations of the relatively gently sloping nearshore of Estonia can be generally treated as long waves already before breaking, it is acceptable to perform similar estimates using nonlinear shallow-water theory similarly to the evaluation of the propagation of vessel-induced waves (Paper V, Chapter 4 of this thesis).

The objectives and outline of the thesis

The studies presented in this thesis target the propagation, transformation, reflection and run-up of long strongly nonlinear waves in the coastal environment, with specific focus on long-living waves of depression that are naturally generated by ships sailing in relatively shallow waters. The particular objectives are as follows:

- to develop a technique for quantitative replication of the propagation and run-up of long almost non-dispersive strongly nonlinear shallow-water waves of elevation and depression;
- to evaluate the properties of usual and extreme run-up events of large wind waves and wave groups induced by high-speed vessels;
- to reconstruct the properties and propagation range of long vessel-induced solitary waves of depression in a shallow-water lagoon.

The propagation of long waves of appreciable amplitude in relatively shallow sea areas is intrinsically nonlinear. Chapter 1 introduces nonlinear shallow-water equations that are suitable for the description of the propagation, transformation and reflection of such long-living waves (both waves of elevation and depression) under the assumption that the effects of dispersion and breaking are insignificant (Section 1.1). The idealized particular solutions of these equations for the constant-depth water are known as Riemann or simple waves. This framework, although it ignores several features of realistic wave propagation, replicates some core

properties of their nonlinear evolution that are overlooked by simpler approaches in terms of a strictly hyperbolic system of equations.

The central numerical tool presented in Chapter 1 (Section 1.2) for solving such equations is the CLAWPACK software package (LeVeque R.J., Berger M.J. et al., CLAWPACK Software 4.6.2, www.clawpack.org). This software is applied in Sections 1.3–1.5 to study the dependence of the propagation, run-up and reflection of initially smooth disturbances (elevations and depressions) on their height in a composite basin containing a section of constant depth and a section with a sloping beach. The results have been accepted for publication as a chapter (Rodin A., Didenkulova I., Pelinovsky E. Numerical study for run-up of breaking waves of different polarities on a sloping beach) in the second edition of the collection *Extreme Ocean Waves* (ed. by Pelinovsky E., Kharif C.; to be published by Springer in summer 2015). As the collection has not yet been published, the results are described in a more detailed manner than the outcome of already published studies in other chapters.

Chapter 2 complements the theoretical estimates of run-up heights and the ratio of the run-up height to the offshore height of the incident waves with similar information from *in situ* measurements in Tallinn Bay, the Baltic Sea. As the generation of single disturbances in the marine environment is complicated, the material relies on measurements of the relevant properties of short groups of vessel-induced waves. The properties of approaching waves were measured in the relatively deep nearshore where the waves were far from breaking. A side goal was to shed some light on why ship wakes may substantially modify the natural course of beach processes (Didenkulova et al., 2011).

The chapter starts with a short insight into the major problems resulting from the frequent presence of high vessel-induced waves (Section 2.1). This material is followed by a description of the study area and the experimental set-up in Section 2.2. Section 2.3 presents an attempt to develop a proper analytical description of the frequency of occurrence of vessel-induced waves of different height and a similar description of their run-up heights and to evaluate the average amplification of waves during the run-up process. The analysis of interrelations of the height and run-up of individual waves in Section 2.4 suggests that the specific group structure of the wave wake together with general rules of the run-up of single waves may be the likely reason for the unexpectedly strong impact of vessel waves on the shore.

Chapter 3 focuses on the description and analysis of long-living strongly nonlinear depression waves produced by ships sailing in a navigation channel in the Venice Lagoon. Section 3.1 presents an overview of nonlinear components of wakes of vessels sailing at moderate depth Froude numbers in relatively shallow water. The measurements of vessel wakes described in Section 3.2 suggest that the largest depressions are strongly nonlinear entities that may almost dry the seabed in shallow areas adjacent to the navigation channel. This feature motivates to use the fully nonlinear theory of shallow-water waves and the framework of Riemann waves (Section 1.1) for their analysis. The propagation of such depressions as free waves into and through shallow water surrounding the navigation channel is

analysed using the CLAWPACK software described in Section 1.2. This software acceptably replicates the main properties of the evolution of the depressions such as the rapid formation of front/rear asymmetry and a steep rear front.

The central question addressed in Sections 3.3 and 3.4 is how far these deep waves of depression may propagate from the region of generation. To shed light on this question, first several dozen reconstructions of the wave shape and properties over a relatively short distance are compared with the results of measurement. The resulting statistics provides a flavour about the reliability of these reconstructions. The evolution of several examples of the observed depressions is then tracked over many hundred metres in the lagoon. The core result is a rough estimate of the distance, at which such depressions still have a substantial amplitude and are capable of providing high near-bottom velocities.

The appearance of the highest vessel-induced waves is frequently associated with the phenomenon of rogue waves that are often believed to be an intrinsic feature of severe seas in the offshore (Section 4.1). Rogue waves may, however, appear also in quite low wind wave conditions and in shallow waters. Chapter 4 first provides evidence of the presence and appearance of two distinct populations of small-amplitude rogue waves in the nearshore (Section 4.2). The relevant measurements were complementary to the measurements of vessel waves discussed in Chapter 2 that were performed in the nearshore of Tallinn Bay during the absence of vessel wakes in 2.7 m deep water over about two weeks. The statistics of rogue waves involves various kinds of rogue events (incl. crests and troughs), identified using both the up-crossing and down-crossing methods (Section 4.3) as well as separate statistics of rogue wave troughs and crests. The outcome demonstrates new effects, typical for shallow-water rogue waves, which are very much bathymetry-dependent (Didenkulova and Pelinovsky, 2011b; Slunyaev et al., 2011)

As demonstrated in Section 2.4, the run-up properties and statistics of (predominantly random) wind waves are not necessarily the same as similar quantities for (predominantly transient events of) ship wakes. Section 4.4 presents an attempt to estimate numerically the maximum inundation of selected sections of Estonian sea coasts based on the severest wave fields taken from 35-year wave simulations with the WAM model forced by COSMO winds in the presence of ice. The estimates of maximum run-up not necessarily match similar estimations made using different express formulas for run-up heights.

Approbation of the results

The basic results described in this thesis have been presented by the author at the following international conferences:

Rodin A. 2014. Influence of wave breaking effects on wave transformation and run-up on the beach. Poster presentation at the *EGU General Assembly 2014* (27 April–02 May 2014, Vienna, Austria).

- Rodin A.**, Didenkulova I. 2014. Shallow water freak waves: the case of Tallinn Bay the Baltic Sea. Poster presentation at the *EGU General Assembly 2014* (27 April–02 May 2014, Vienna, Austria).
- Rodin A.**, Didenkulova I., Nikolkina I. 2014. Run-up of large storm waves on Estonian coasts of the Baltic sea. Poster presentation at the *6th IEEE/OES Baltic International Symposium* (26–29 May 2014, Tallinn, Estonia).
- Rodin A.**, Didenkulova I. 2014. Transformation and run-up of large-amplitude nonlinear waves from high-speed ferries in the coastal zone of the Baltic sea. Poster presentation at the *6th IEEE/OES Baltic International Symposium* (26–29 May 2014, Tallinn, Estonia).
- Didenkulova I., **Rodin A.** 2014. Transformation and run-up of large-amplitude ship waves in the coastal areas of the Baltic Sea. Oral presentation at the *XX International scientific and technological conference “Information Systems and Technologies 2014”* (18 April 2014, Nizhny Novgorod, Russia) (in Russian).
- Didenkulova I., **Rodin A.** 2013. Peculiarities of the ship wake structure. Poster presentation at the *9th Baltic Sea Science Congress* (26–30 August 2013, Klaipeda, Lithuania).
- Didenkulova I., **Rodin A.** 2013. Properties of shallow water rogue waves in the Baltic Sea. Poster presentation at the *9th Baltic Sea Science Congress* (26–30 August 2013, Klaipeda, Lithuania).
- Didenkulova I., **Rodin A.** 2012. Statistics of wake groups produced by fast ferries. Oral presentation at the *XVIII International scientific and technological conference “Information Systems and Technologies 2012”* (18–20 April 2012, Nizhny Novgorod, Russia) (in Russian).
- Didenkulova I., **Rodin A.** 2012. Statistics of shallow water rogue waves in Baltic Sea conditions: the case of Tallinn Bay. Oral presentation at the *IEEE/OES Baltic International Symposium* (08–11 May 2012, Klaipeda, Lithuania).
- Rodin A.** 2012. Ship waves in Tallinn Bay, Baltic sea: their parameters, group structure and run-up. Oral presentation at the *IEEE/OES Baltic International Symposium* (08–11 May 2012, Klaipeda, Lithuania).
- Rodin A.**, Didenkulova I. 2012. A typical wave wake from high-speed vessels: its group structure and run-up. Oral presentation at the *EGU General Assembly 2012* (22–27 April 2012, Vienna, Austria).
- Didenkulova I., Pelinovsky E., **Rodin A.** 2012. Formation of shallow water rogue waves taking into account wave breaking effects. Poster presentation at the *EGU General Assembly 2012* (22–27 April 2012, Vienna, Austria).
- Didenkulova I., **Rodin A.** 2012. Statistics of waves within a ship wake. Poster presentation at the *EGU General Assembly 2012* (22–27 April 2012, Vienna, Austria).

1. Nonlinear wave dynamics and run-up in the coastal zone

The propagation of small-amplitude non-breaking waves, regardless their polarity, is usually reproduced well both in numerical computations and in predictions of different versions of weakly nonlinear shallow-water theory. In many occasions even the linear approach works well. The waves approaching the shore, however, intrinsically develop nonlinear qualities at some stage of their motion. Nonlinear effects become increasingly important when the wave amplitude increases or if one has to track the long-term evolution of even initially small-amplitude waves, e.g., in studies of the run-up of initially small waves that are located far from the shoreline. With a further increase in the wave amplitude, the wave starts to break or transforms into a shock wave (similar to a bore) before approaching the shore. A proper description of such waves requires the application of advanced mathematical models and numerical methods capable of replicating the core features of such strongly nonlinear behaviour.

A large part of the analysis in this thesis relies on nonlinear shallow-water equations. Their particular solutions for constant water depth are known as Riemann waves. Although several important features of wave propagation, such as dispersion or interaction with the bottom, cannot be reproduced in terms of Riemann waves, this framework and the CLAWPACK software package allow for extensive numerical study of the propagation, transformation, reflection and run-up of long partially breaking solitary waves of various polarities in both ideal conditions (in a composite basin containing a section of constant depth and a section with a sloping beach) and in a realistic situation in the Venice Lagoon.

The mathematical model appropriate for the description of strongly nonlinear non-dispersive shallow-water waves is briefly presented in Section 1.1. It mostly follows Papers II and III. Section 1.2 provides a description of the CLAWPACK software and its upgrade used in this thesis. The course and properties of the run-up for incident solitary waves of elevation and depression are described in Sections 1.3 and 1.4, respectively. A comparison of run-up characteristics for waves of different polarities is performed in Section 1.5.

1.1. Mathematical model of nonlinear shallow-water waves

As described in Introduction, in many occasions both ship-induced disturbances and natural wave motions may have so large amplitudes that the linear theory fails to describe their properties and even common weakly nonlinear approaches (such as the Korteweg–de Vries equation or its generalizations) are not applicable to their replication. Following the ideas developed by Didenkulova et al. (2006) and Zahibo et al. (2008), an attempt is made in Papers II and III to reproduce the key properties of deep ship-induced depressions using the fully nonlinear one-dimensional shallow-water equations (Whitham, 1974):

$$\frac{\partial u}{\partial t} + u \frac{\partial u}{\partial x} + g \frac{\partial \eta}{\partial x} = 0, \quad \frac{\partial \eta}{\partial t} + \frac{\partial}{\partial x} [(h + \eta)u] = 0. \quad (1)$$

Here h is the unperturbed water depth, η is the water surface displacement with respect to the calm water surface located at $z = 0$, $u(x, t)$ is the depth-averaged horizontal velocity of the water flow (called flow speed below), $g = 9.81 \text{ m/s}^2$ is acceleration due to gravity, x is the horizontal coordinate and t is time.

The use of Eqs. (1) for studies of wave motion is only justified if dispersion and dissipation can be neglected. This condition is not always applicable to ocean waves. For example, even extremely long tsunami waves experience a certain level of dispersion (Pelinovsky, 1982). The main advantage of Eqs. (1) is that they are valid for waves of arbitrary amplitude and, formally, exact up to wave breaking. Therefore, they can be applied to the motion of relatively large waves on the above-mentioned condition that dispersion and breaking do not play a major role. Another, even more important benefit from the viewpoint of this thesis is their ability to describe waves of elevation and depression in the same framework. Differently from common weakly nonlinear equations for water waves, which often only allow solitary waves of elevation as their valid solutions (Grimshaw et al., 2014), the analytical solutions to Eqs. (1) may equally well be long-living waves of depression.

It is convenient to employ Eqs. (1) in the flux form:

$$\frac{\partial H}{\partial t} + \frac{\partial}{\partial x} (Hu) = 0, \quad \frac{\partial (Hu)}{\partial t} + \frac{\partial}{\partial x} \left(Hu^2 + \frac{gH^2}{2} \right) = 0, \quad (2)$$

where $H(x, t) = h(x) + \eta(x, t)$ is the instantaneous thickness of the water column. Similarly to Eqs. (1), Eqs. (2) are exact in the framework of the shallow water theory and are valid for any amplitude of disturbances up to the wave breaking.

A classical solution to Eqs. (1, 2) in a basin of constant depth is the so-called simple or Riemann wave. The propagation of Riemann waves can be described in terms of the shape of the water surface $H(x, t)$ and the associated flow speed:

$$H(x, t) = H_0[x - V(x, t)t], \quad u(x, t) = 2 \left[\sqrt{gH(x, t)} - \sqrt{gh} \right], \quad (3)$$

where $H(x, t)$ reflects the relocation of the disturbance over the water surface, $H_0(x)$ is the initial shape of the disturbance, $V(x, t)$ is the (local) speed of wave propagation, \sqrt{gH} and \sqrt{gh} are so-called linear long wave speeds (the maximum phase and group speed for linear surface waves at a given depth) for water depths of H and h , respectively.

Solutions of this type are widely used, e.g., in nonlinear acoustics (Rudenko and Soluyan, 1977; Engelbrecht et al., 1988; Gurbatov et al., 1990). Although the shallow-water environment (that supports surface waves with partially transversal motions of the medium) and media supporting acoustic waves (that are longitudinal waves) are not fully equivalent, this concept has also been applied in the theory of

shallow-water waves (Voltsinger et al., 1989). It has been demonstrated that many properties of water waves can be replicated and forecast (at least qualitatively) using the approach of Riemann waves (Didenkulova et al., 2006b; Zahibo et al., 2008; Pelinovsky and Rodin, 2011). All analytical and numerical results of wave propagation and run-up presented in the thesis have been obtained using Eqs. (1).

The solution (3) describes the nonlinear deformation of waves with the steepening of their front slope. A detailed analysis of such a deformation of shallow-water waves and changes in their spectral composition up to the breaking was carried out in Didenkulova et al. (2006b).

It is straightforward to derive from Eqs. (3) the following expression for the (local) speed of nonlinear wave propagation:

$$V(x,t) = 3\sqrt{gH(x,t)} - 2\sqrt{gh}. \quad (4)$$

Commonly for long water waves (Pelinovsky, 1982; Dean and Dalrymple, 1991), this speed depends on the total water depth H at a particular location and thus varies along the wave profile.

The results of a number of numerical experiments with the propagation of Riemann waves over a sea area of constant depth are available in several papers (Stoker, 1957; Shuleykin, 1968; Pelinovsky, 1982).

According to Eq. (3), the propagation speed of an elevation (positive disturbance of the water surface, wave crest) is always greater than the linear long wave speed. This means that the higher parts of the disturbance tend to propagate faster than the lower ones. As a result, over time the waves of elevation tend to become steeper and a single wave crest develops a steep front.

The propagation of waves of depression to some extent deviates from the motion of waves of elevation. According to Eq. (4), the depressed parts of the disturbance propagate slower than the linear long wave speed \sqrt{gh} . Therefore, for waves of depression the presence of nonlinearity is associated with the formation of a characteristic skewed shape with a steep *rear* slope (Whitham, 1974; Didenkulova et al., 2006b; Zahibo et al., 2008).

While a Riemann wave of elevation can, formally, be of any height, the height of long-living Riemann waves of depression is indirectly limited by a specific manifestation of strong nonlinearity. Namely, there is an implicit limit for the formation of the steep rear slope. From Eq. (4) it follows that if the height of the initial disturbance η exceeds the threshold $|\eta| = (5/9)h$, the trough velocity becomes negative. This means that different parts of the wave profile start to propagate in different directions. As a consequence, the steepness of the rear front increases rapidly and the wave breaks almost instantaneously (or, equivalently, a shock wave appears) (Didenkulova et al., 2006b; Zahibo et al., 2008). Therefore, nonlinear effects are often more pronounced for waves of depression than for more common waves of elevation.

The discussed condition is equivalent to the requirement that in long-living Riemann waves of depression the thickness of the water sheet at the deepest point of the trough should always be

$$H > H_{cr} = \frac{4}{9}h. \quad (5)$$

In other words, a Riemann wave of depression can only propagate over a reasonable distance if its trough is not too deep. It is not clear what exactly will happen if the condition (5) is no more met because Eqs. (1) fail to describe the further behaviour of the disturbance. Technically, at the critical amplitude the nonlinear wave speed V becomes zero and the nonlinearity parameter (defined as the ratio of the velocity of water particles u to the wave propagation speed), equivalently, the Mach number u/V , becomes infinite. The wave may disintegrate into a smaller wave and a reflected wave from the shock front (Pelinovsky and Rodin, 2012). It is, however, more likely that a bore-like feature is formed and that intense turbulence rapidly damps the energy of the motion.

The applicability of this approach to the description of large shallow-water waves and an analysis of wave propagation, transformation and reflection in the nearshore are addressed numerically in Sections 1.3–1.5 for a particular set-up. The parameters of the set-up match the dimensions used for a recent set of experiments performed in the Large Wave Flume (Grosse Wellenkanal, GWK, Hannover, Germany) (Denissenko et al., 2013; Didenkulova et al., 2013a).

1.2. CLAWPACK software package

Following the experience gathered in previous research (Stoker, 1957; Mei, 1986; Voltsinger et al., 1989; Arseniev and Shelkovnikov, 1991; Pelinovsky, 1996; LeVeque, 2002), the propagation of various strongly nonlinear disturbances in shallow water is analysed in this thesis using the software package CLAWPACK (Conservation LAWs PACKAge). This is a free package developed by Professor Randall J. LeVeque (University of Washington, USA). It is written in FORTRAN and Python languages and is based on a Godunov-type method (a version of the finite-volume method). Its major advantage for studies of ship-induced long-living waves of depressions is its ability to properly represent solutions for dynamic problems that involve (or may develop) discontinuities within the computational domain.

Technically, CLAWPACK was developed for solving one-, two- and three-dimensional time-dependent hyperbolic systems of differential equations (or systems of such equations) that are written in the form of conservation laws. The condition for the equation to be hyperbolic implicitly means the guarantee that the problem in question, roughly speaking, is well-posed and can be locally solved for arbitrary initial data along any non-characteristic hypersurface (LeVeque, 2002). This software can be used to solve also non-conservative systems, (systems of equations with variable coefficients and/or containing forcing terms. The package includes an algorithm for adaptive mesh refinement (AMRCLAW) and an option for parallel processing of the calculations (MPI, Multi Processors Interface).

In order to solve Eqs. (1) using CLAWPACK, the equations should be first written in terms of conservation laws. In the absence of external forces the most general form of representation of these laws can be written in the matrix form:

$$q_t + [f(q)]_x = 0. \quad (6)$$

Here the variable q is a vector function that involves all the components of wave motion. This package is also capable of solving more general hyperbolic systems of equations, written in a non-conservative form (LeVeque, 2002):

$$q_t + A(q, x, t)q_x = \psi(x, t), \quad (7)$$

where ψ is another vector function describing the external forces.

The main requirement for Eqs. (2) to be eligible for the CLAWPACK package is that this system of equations must be strictly hyperbolic. This property means that the matrix A must be real and all its eigenvalues must be different. It is straightforward to demonstrate that this condition is satisfied for the nonlinear shallow-water equations (2) in a constant-depth water body $h = \text{const}$. It is convenient to rewrite Eqs. (2) in a matrix form:

$$\begin{bmatrix} H \\ Hu \end{bmatrix}_t + \begin{bmatrix} uH \\ Hu^2 + \frac{1}{2}gH^2 \end{bmatrix}_x = 0. \quad (8)$$

Let us denote $q_1 = H$, $q_2 = Hu$, $\vec{q} = (q_1, q_2)$, $\vec{f} = (f_1, f_2)$ and

$$\vec{f}^T = \begin{bmatrix} Hu \\ Hu^2 + \frac{1}{2}gH^2 \end{bmatrix} = \begin{bmatrix} q_2 \\ \frac{q_2^2}{q_1} + \frac{1}{2}gq_1^2 \end{bmatrix}. \quad (9)$$

These equations can be equivalently rewritten in the quasilinear form:

$$q_t^T + F(\vec{q})q_x^T = 0, \quad (10)$$

where

$$F(\vec{q}) = \begin{bmatrix} 0 & 1 \\ -\frac{q_2^2}{q_1^2} + gq_1 & 2\frac{q_2}{q_1} \end{bmatrix} = \begin{bmatrix} 0 & 1 \\ -u^2 + gH & 2u \end{bmatrix}. \quad (11)$$

The eigenvalues of the resulting equation have the meaning of the speed of wave propagation. The equation for the eigenvalues is

$$|F(\vec{q}) - \lambda E| = \begin{vmatrix} -\lambda & 1 \\ -u^2 + gH & 2u - \lambda \end{vmatrix} = 0. \quad (12)$$

The roots of Eq. (12) are the eigenvalues of the matrix (11):

$$\lambda_1 = u - \sqrt{gH}, \quad \lambda_2 = u + \sqrt{gH}, \quad (13)$$

equivalently:

$$\lambda_1 = \frac{q_2}{q_1} - \sqrt{gq_1}, \quad \lambda_2 = \frac{q_2}{q_1} + \sqrt{gq_1}. \quad (14)$$

The obtained eigenvalues are obviously different except in the case $H = 0$ when also so-called Riemann invariants (Whitham, 1974), defined as

$$V_1 = u + 2\sqrt{gH}, \quad V_2 = u - 2\sqrt{gH}, \quad (15)$$

coalesce. This case corresponds to the edge of the water sheet. It is the most problematic issue in the calculation of wave run-up on the shore in many numerical approaches, including this model where it was resolved only recently.

The corresponding eigenvectors of the matrix $F(\vec{q})$ are

$$\vec{r}_1^T = \begin{bmatrix} 1 \\ u - \sqrt{gH} \end{bmatrix}, \quad \vec{r}_2^T = \begin{bmatrix} 1 \\ u + \sqrt{gH} \end{bmatrix}. \quad (16)$$

The eigenvalues λ_1 , λ_2 and eigenvectors for the system in question are functions of q . The eigenvectors are associated with the above-mentioned Riemann invariants, which are widely used, for example, in nonlinear acoustics or shallow-water theory as the most convenient way to solve specific problems.

The core of CLAWPACK for solving one-dimensional problems (which is the focus in this thesis) relies on basic algorithms for solving hyperbolic systems of equations. These algorithms are gradually upgraded from version to version. The package was implemented initially in FORTRAN 77 but from version 4.6 it was adapted to the modern compiler gfortran. All plugins (independently compiled modules, which are dynamically linked to the main program) for the user interface in version 4.3 have been implemented in FORTRAN 90. Starting from version 4.6.1, the Python software is extensively used.

The user is asked to introduce the following information in one *.py file in a convenient format: the number of grid cells, the size of the computational domain, the number of equations, the initial time step and the maximum time step (the use of a fixed time step is also allowed), the desired and the critical value of the Courant number, the type of boundary conditions to be applied at the borders of the computational domain (the choice is between zero extrapolation, periodic boundary conditions, a solid wall and user-defined boundary conditions) and the type of initial conditions (initial displacement and/or initial velocity).

Simulations in the thesis are made using two versions of the CLAWPACK package: CLAWPACK 4.3 (released in April 2006) and CLAWPACK 4.6.2 (released in May 2012). The earlier version of CLAWPACK for solving hyperbolic systems of shallow-water equations offers a finite volume method, implemented using the Roe scheme (Roe, 1981). This algorithm allows describing the

emergence and propagation of shock waves with high accuracy, which is important from the viewpoint of the problem in this thesis. The CLAWPACK version 4.3 was comparatively nonflexible in terms of user-driven modification of initial and boundary conditions. Adding forcing terms to the initial equations was not straightforward and the use (by default) of the Matlab tool for visualization of the results required additional efforts.

Earlier versions of CLAWPACK such as version 4.3 did not allow for the replication of the movement of water on the dry shore, a process that is important, e.g., for modelling the propagation of waves of depression in the Venice Lagoon (Paper II). The modification of the algorithms towards the replication of this feature is given in LeVeque (2010) and was implemented in CLAWPACK, starting from version 4.6.2 in May 2012. The newer versions also allow adding extra (forcing and other) terms into Eqs. (2) and to conveniently specify many interim outputs. Visualization and editing of graphical results are carried out now by iPython native tools such as iPython sandbox. This greatly simplifies and reduces the cost of using CLAWPACK. Other parts of CLAWPACK do not have a graphical interface. As all interim results are stored in ASCII format, it is straightforward to employ any visualization environment.

As the simultaneous assignment of the initial disturbance and the initial velocity field was not foreseen in the standard package CLAWPACK 4.6.2, the relevant modifications were made to the code for the purposes of this thesis. To properly use the software and to appropriately interpret the calculation results, I participated in the Gene Golub SIAM Summer School 2012 (Monterey, USA, 29 July to 10 August 2012) “Simulation and Supercomputing in the Geosciences” where Professor Randall J. LeVeque provided training on CLAWPACK 4.6.2 and on the branch GEOCLAW.

These packages serve as advanced tools for the numerical modelling of long waves in the ocean with geo-referencing. The advantages of the new version CLAWPACK (and, in particular, GEOCLAW) include automatic protection against any violation of the Courant condition

$$\frac{u\Delta t}{\Delta x} \leq 1, \quad (17)$$

where Δt is a time step, Δx is a space step and u is a flow rate. In previous versions the user had only an option to passively track the instantaneous Courant number. If its values were not satisfactory (≥ 1), the calculations were halted. Starting from version 4.6.2, the software contains an automatic adaptation scheme of the spatial step to a given time step to meet condition (17). This improvement greatly facilitates the work with CLAWPACK in general.

The newer versions of the software allow the use of variable water depth in the entire computational domain (including the real bathymetry in the one- and two-dimensional case). This is complemented by the algorithms that are designed to solve the interaction of water with a dry bottom (LeVeque and George, 2008). Starting from version 4.6.2, a new method in the basic algorithm was implemented.

The user has now a choice between the so-called Roe solver mentioned above (first-order accuracy, representing a finite-volume method) and a finite-difference Lax–Wendroff method of second order (Lax and Wendroff, 1960).

The CLAWPACK package has been extensively tested and validated in the international literature (e.g., LeVeque and George, 2008; Berger et al., 2011; Gonzalez et al., 2011). The tests include comparisons between the analytical solution and laboratory experiments with the run-up of a single wave on a gently sloping beach and on a composite beach (LeVeque and George, 2008; Gonzalez et al., 2011) as well as comparisons with experimental and field data about the run-up of a single wave on a conical island and the run-up of a tsunami on a complex three-dimensional island.

Rodin and Pelinovsky (2014) provide a comparison of theoretical estimates of single wave’s splash on the solid wall with the results of CLAWPACK. They specifically tested the accuracy of the conservation laws during wave propagation. Both the mass (H) and momentum (Hu) conservation laws were preserved with an accuracy less than 10^{-8} for a wide range of amplitudes and spatial and temporal extensions of the waves.

1.3. Run-up of waves of elevation on a beach

The ability of the CLAWPACK package to reproduce the long-term propagation and reflection of nonlinear shallow-water waves over composite bathymetry (area of constant depth adjacent to a sloping beach) is demonstrated for the idealized case of wave run-up along a plane beach (Figure 1). The composite geometry of the bottom profile contains a 250 m long basin of constant water depth (3.5 m) and a plane rigid beach with a slope 1:6. The spatial step is 0.1 m and the time step is 0.5 s in all calculations presented in this chapter. These values satisfy Courant’s criterion. The boundary condition at the left border of the computational domain $x=0$ corresponds to free wave propagation across the border. The boundary condition $H(x,t)=0$ at the shore reflects free oscillations of the moving shoreline $x(t)$.

The initial conditions correspond to the solitary wave of elevation or depression (called pulse below) concentrated in the constant-depth area $x < 250$ m and

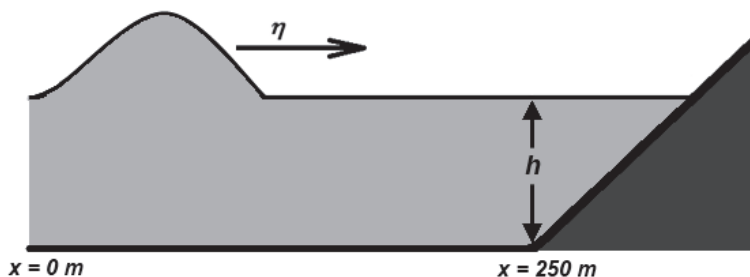


Figure 1. The composite geometry of the run-up problem.

propagating onshore:

$$\eta_{in}(x,0) = A \cosh^{-2} \frac{x-x_0}{L}, \quad u_{in}(x,0) = 2\left(\sqrt{g[h+\eta_{in}(x,0)]} - \sqrt{gh}\right), \quad (18)$$

where L is the characteristic half-wavelength. As the hyperbolic cosine increases rapidly with the increase in its argument, the “step” in the water surface at $x = 250$ m is very small and does not affect the calculations. It is easy to show analytically that the rigorous solution of the system (2) for initial conditions (18) represents a Riemann wave (Pelinovsky and Rodin, 2011, 2012)

$$H(x,t) = H_0[x - V(H)t], \quad (19)$$

where $H_0(x) = h + \eta_{in}(x,0)$ is the initial wave shape. The characteristic half-wavelength was set to $L = 11$ m that corresponds to a half-wave period of 2 s in all simulations. The maximum of the initial pulse is located at $x_0 = 50$ m. The wave amplitude A varied from 0.05 m to 3.5 m for waves of elevation and from -0.05 m to -3.49 m (to keep the water layer continuous) for waves of depression.

Small-amplitude waves of elevation climbed the beach and reflected from it without breaking (Figure 2, $A = 0.1$ m). Even though nonlinearity was weak, the nonlinear effects were still present and led to gradual wave steepening. This process is clearly seen at $t = 30$ s. The wave run-up height for this case is 0.43 m, which exceeds the initial wave amplitude by more than four times and is consistent with observations in Section 2.4. The travel time to the shore is 40 s. The reflected wave has a sign-variable shape as predicted by the analytical theory. The amplitude of the reflected wave (0.08 m at $t = 70$ s, Figure 2) is less than the amplitude of the incident wave. The decrease in the amplitude reflects both wave transformation and spreading in space of the initially compact pulse. The reflected wave is further affected by nonlinear effects and develops a very steep section on its front slope

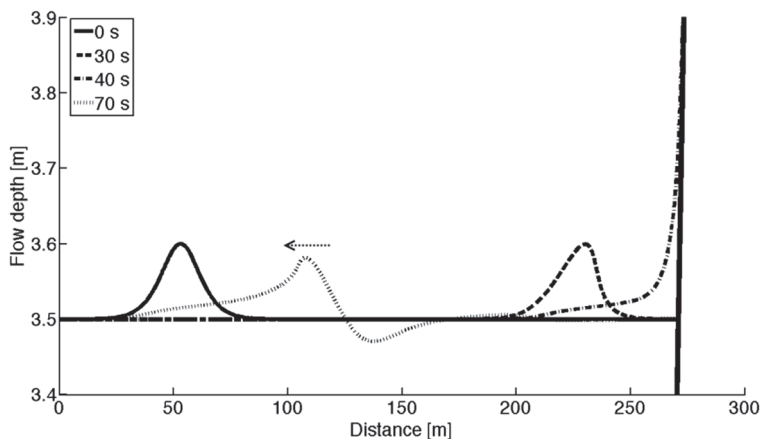


Figure 2. Run-up and reflection of a small-amplitude (weakly nonlinear) solitary wave of elevation ($A = 0.1$ m) from a sloping beach.

near the crest. Interestingly, the reflected wave contains a weak elevation after the trough. This feature apparently emerges due to the joint impact of the wave with the sloping beach and the point matching the slope with constant depth. This tail is not observed in asymptotic analytical considerations (Didenkulova et al., 2006a, 2007b), where the latter interaction is neglected.

An increase in the wave amplitude leads to a much more pronounced impact of nonlinear effects. A pulse with the initial amplitude $A = 0.5$ m rapidly obtains an almost vertical front slope. On a realistic beach it would apparently break or possibly split up into a number of KdV solitons depending on the amplitude of the initial pulse (Favre, 1935; Stoker, 1957; Nakamura, 1973; Teles da Silva, 1990; Docherty and Chanson, 2010), but in the simulations it is transformed into a shock wave that propagates faster than the weakly nonlinear wave above. The maximum run-up height $R = 1.44$ m is achieved at a slightly earlier time $t = 37.5$ s. Therefore, the run-up ratio $R/A = 2.88$ is less than in the previous non-breaking case. The decrease in the run-up ratio is related to the wave breaking and associated dissipation of wave energy. However, the reflected wave does not break. Its amplitude is equal to 0.31 m at $t = 70$ s.

Further increase in the wave amplitude leads to its faster propagation, earlier breaking and quicker dissipation. For a wave with $A = 1.5$ m the maximum run-up height $R = 2.83$ m ($R/A = 1.88$) is achieved at $t = 34.5$ s. The reflected wave decays rapidly. Its amplitude (0.67 m at $t = 70$ s) is almost 45% of the initial wave amplitude. An extremely high-amplitude wave ($A = 3.5$ m, equal to the water depth) breaks almost instantaneously. Its shape becomes triangular and its front moves quicker than the waves of smaller amplitude (Figures 3 and 4).

The wave reaches its maximum run-up height of 4.84 m in 30.5 s. The run-up ratio decreases significantly to 1.38. The reflected wave at $t = 60$ s has an amplitude of 1.24 m, which is approximately 35% of the initial wave amplitude. The length of the reflected wave increases with an increase in its amplitude. This

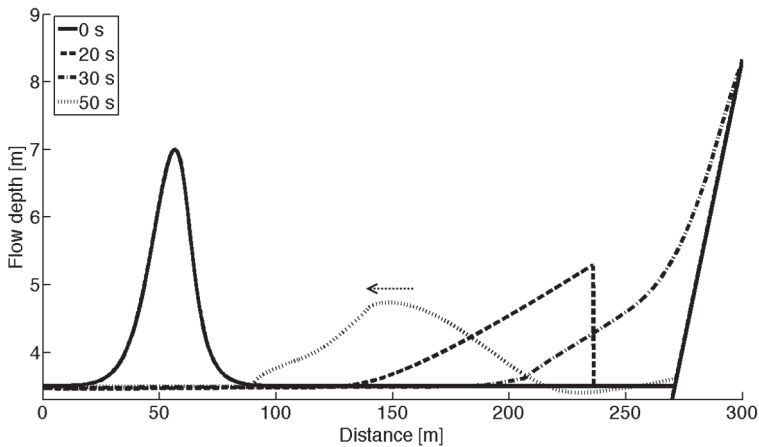


Figure 3. Run-up and reflection of a very high solitary wave of elevation ($A = 3.5$ m) from a sloping beach.

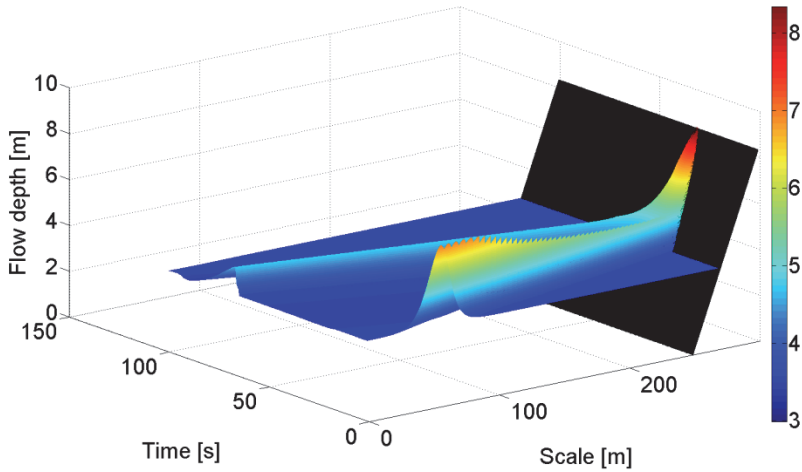


Figure 4. Run-up and reflection of a very high solitary wave of elevation ($A = 3.5$ m) from a sloping beach: $x-t$ diagram. The scale at the right indicates the distance of the water surface from the bottom.

reflects the properties of shock waves approaching the beach: they have a longer spatial extension than the incident wave. Interestingly, the reflected waves have always a smooth shape in contrast to large-amplitude breaking incident waves.

The run-up of waves of elevation induces significant flooding of the coast (Figure 5). The extension of the flooding increases with an increase in the initial wave height. The ebb (run-down) is much weaker than the run-up and the maximum water dropdown decreases with an increase in the initial wave height.

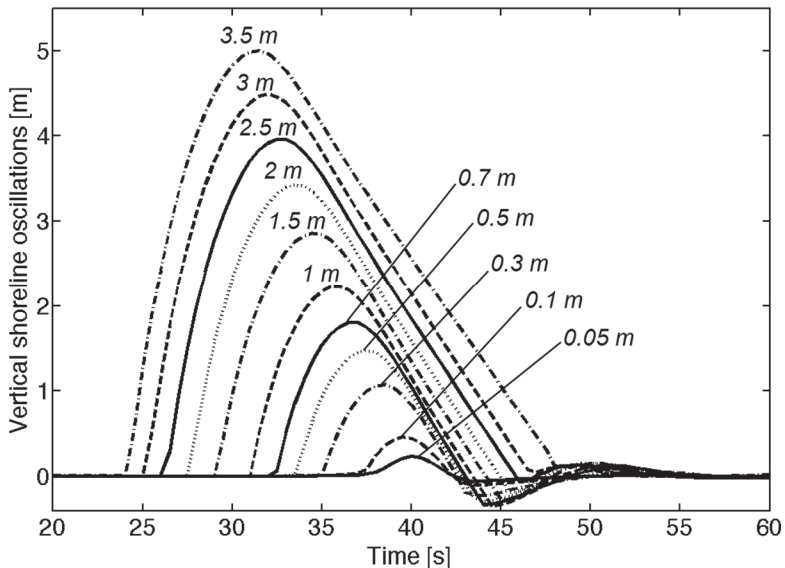


Figure 5. Vertical oscillations of the waterline for various amplitudes of the initial solitary wave of elevation.

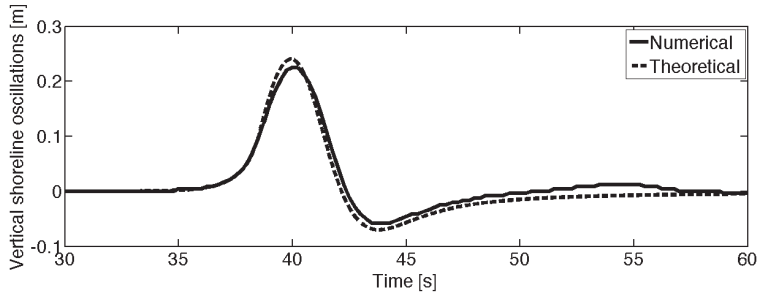


Figure 6. Comparison of numerical simulations with predictions of the analytical theory for a 0.05 m high weakly nonlinear wave of elevation.

For waves of very large amplitude (≥ 2.5 m) there is almost no ebb stage at all. The duration of the flooding is also longer than for the temporal extension of the ebb phase, and it increases with an increase in the initial wave amplitude. The simulated behaviour of the oscillations of the waterline for weakly nonlinear non-breaking wave run-up matches well the predictions of the analytical theory (Figure 6) obtained using the procedure described in Didenkulova (2009) and Didenkulova et al. (2006a, 2007b).

1.4. Run-up of waves of depression

The run-up of a solitary wave of depression (a single trough) of small amplitude (0.1 m) in the same geometry leads, in general, to a sign-inverted pattern of the run-up of waves of elevation (Figure 7). The maximum run-up height $R = 0.17$ m is approximately half of the run-down level (0.33 m), but still higher than the initial wave amplitude. The run-down ratio $\hat{R}/A = 3.3$ is less than the corresponding run-up ratio for an equivalent wave of elevation. The reflected wave starts from a trough that is followed by a wave crest. Due to the resulting large surface elevation

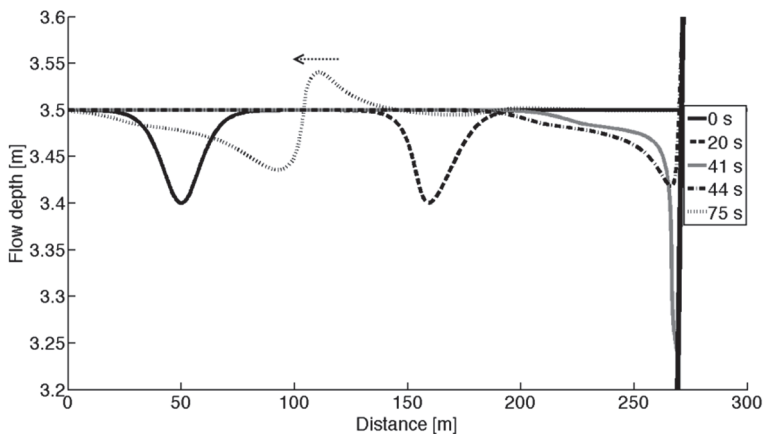


Figure 7. Run-up and reflection of a solitary wave of depression with $A = 0.1$ m from a sloping beach.

difference at the wave front, its steepness increases significantly as a result of nonlinear effects.

When the initial pulse amplitude is 0.5 m, the maximum run-up and run-down heights of the wave are $R = 0.53$ m and $\hat{R} = 0.83$ m, respectively. Importantly, the time to reach the maximum run-up/run-down height is longer than the small-amplitude case. This feature reflects the property of depression waves discussed in Section 1.1: their (nonlinear) speed of propagation is less than the linear speed of long-wave propagation. The run-down ratio $\hat{R}/A = 1.66$ is also less than in the previous case, apparently because of breaking effects that are also visible in the shape of the reflected wave. With an increase in the wave amplitude, nonlinear effects leading to wave breaking become more prominent.

A wave of depression with an almost limiting amplitude $A = -3.499$ m involves only a very thin film of water at the bottom below the wave trough. As expected, in this case nonlinear effects are the largest and result in a strong and rapid wave transformation (Figure 8). The wave breaks almost immediately. This process leads to a significant decrease in the wave amplitude (Figure 9) and the maximum run-up and run-down heights (0.83 m and 1.49 m respectively, this is about 40% less than the initial wave amplitude). The reflected wave also breaks after some time.

The run-up of a solitary wave of depression leads to a comparatively strong ebb and flood (Figure 10). As expected, the duration and magnitude of the ebb are generally longer than those of the flood. Both run-up and run-down heights increase with an increase in the initial wave amplitude. Similarly to the analysis of the run-up of waves of elevation in Section 1.3, numerical results for the non-breaking run-up of comparatively small waves of depression match well the predictions of the analytical theory (Figure 11).

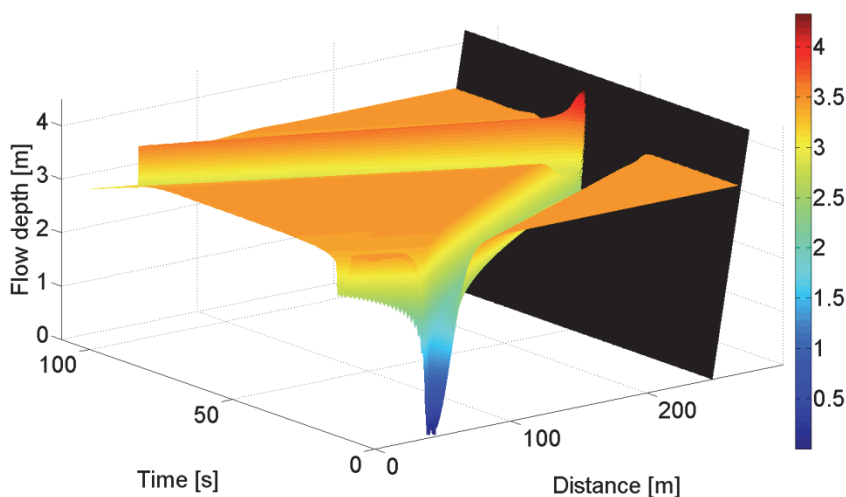


Figure 8. Run-up and reflection of a solitary wave of depression with an almost limiting amplitude ($A = -3.499$ m) from a sloping beach: $x-t$ diagram. The scale at the right indicates the distance of the water surface from the bottom.

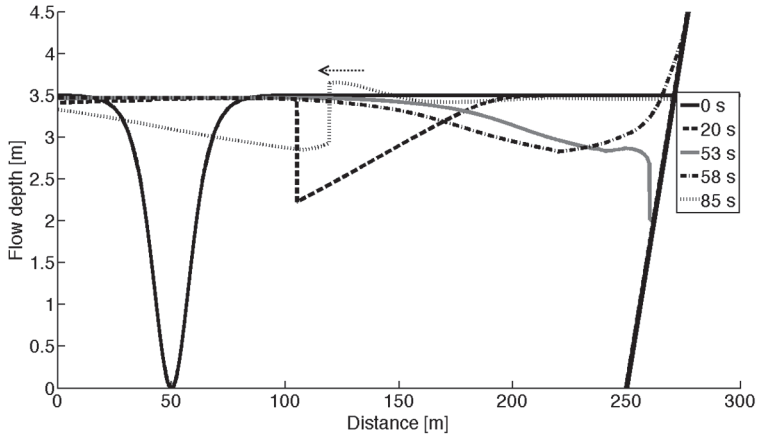


Figure 9. Run-up and reflection of a solitary wave of depression with an almost limiting amplitude ($A = -3.499$ m) from a sloping beach.

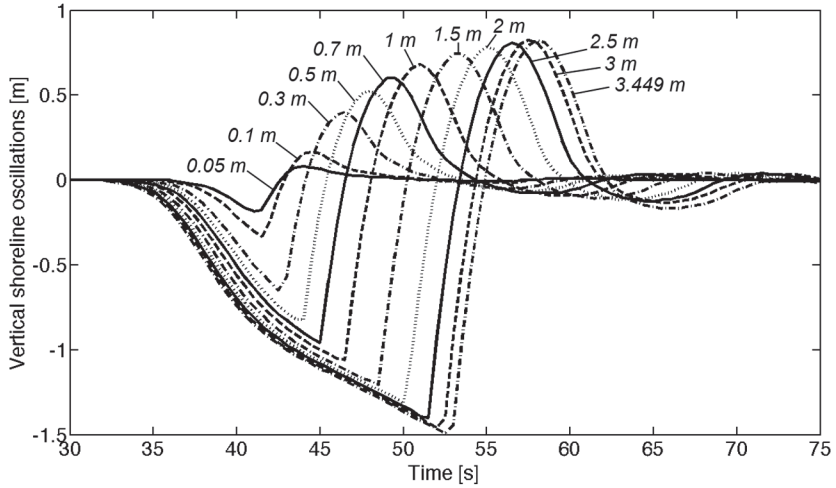


Figure 10. Vertical oscillations of the shoreline for various amplitudes of solitary waves of depression.

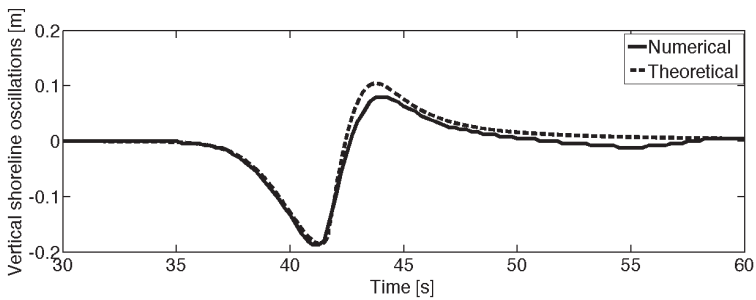


Figure 11. Comparison of numerical simulations with predictions of the analytical theory for initially 0.05 m high weakly nonlinear solitary waves of depression.

1.5. The effect of solitary wave amplitude and polarity on the run-up

Sections 1.3 and 1.4 have demonstrated that both run-up and run-down heights increase with an increase in the initial wave amplitude of both waves of elevation and depression. The analytical theory of the run-up of weakly nonlinear waves predicts a linear dependence of these heights on the initial amplitude. The simulated relationships between these parameters are far from linear (Figure 12). It is likely that this deviation for large-amplitude (strongly nonlinear) waves is related to the energy dissipation due to wave breaking.

The run-up height of waves of elevation increases with an increase in the wave amplitude, while the run-down height behaves non-monotonically and tends to zero for large-amplitude waves. The run-down height of waves of depression exceeds the associated run-up height, but these values approach a constant and remain comparable even for very large initial amplitudes similarly to non-breaking waves (Didenkulova et al., 2014). The ratios of run-up or run-down heights to the initial wave amplitude decrease monotonically with an increase in the amplitude of waves of elevation (Figure 13). It is likely that this feature again reflects wave breaking effects. The ratio of run-down heights to run-up heights (Figure 14) is a non-monotonic function of the initial wave amplitude for waves of depression. Its minimum value (1.55) is achieved for initial wave amplitudes of 0.5–1 m (about 15–35% of the undisturbed water depth). For waves of elevation, the difference in run-down and run-up heights is significantly larger than for waves of depression.

The behaviour of wave travel time (to the instant of the maximum run-up height) is also different for waves of different polarity. For waves of elevation it decreases with an increase in the wave amplitude. This property is explained by the formation of a high-amplitude wave or a shock wave that propagates faster than a linear wave (Figure 5). Contrariwise, the travel time of waves of depression

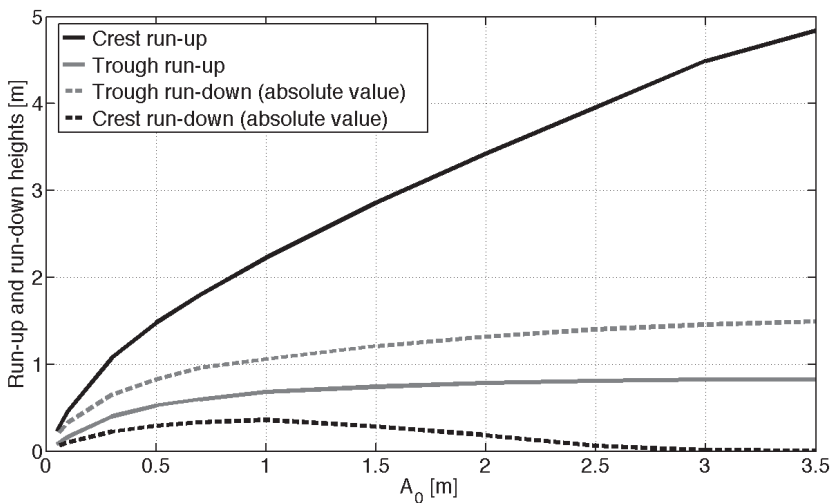


Figure 12. Run-up and run-down heights versus the initial wave amplitude.

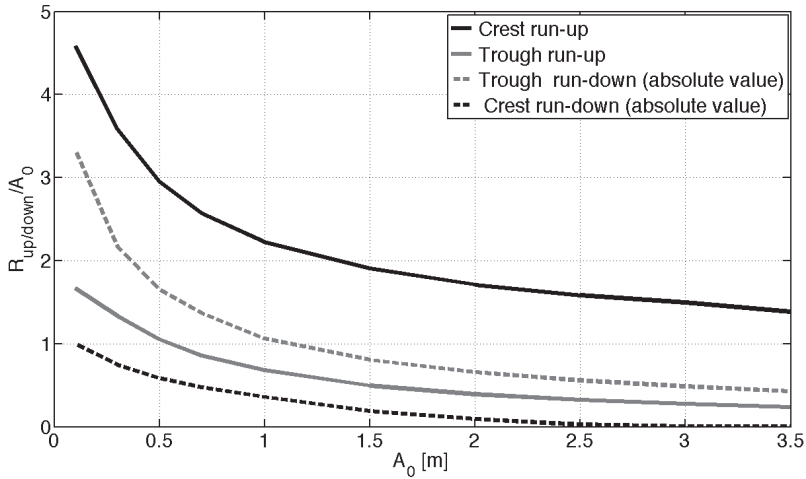


Figure 13. Run-up/run-down ratios versus the initial wave amplitude.

increases with the increase in the wave amplitude as a deep trough or a shock wave of negative polarity propagates slower than a linear wave (Figure 9).

For practical applications it is important to know how soon the maximum inundation occurs after the wave front arrives. For waves of elevation, the flood front duration initially decreases with an increase in the wave amplitude. This can be explained by an increase in the steepness of the wave climbing the beach. For very large initial waves strong dissipation damps the wave front and the flood is governed by the tail of the shock wave, and the duration of the flood front increases again. For waves of depression, the ebb front duration monotonically grows with an increase in the initial amplitude. This reflects the asymmetry of the depression waves: the flood duration is governed by a shock wave at the rear of the entire disturbance.

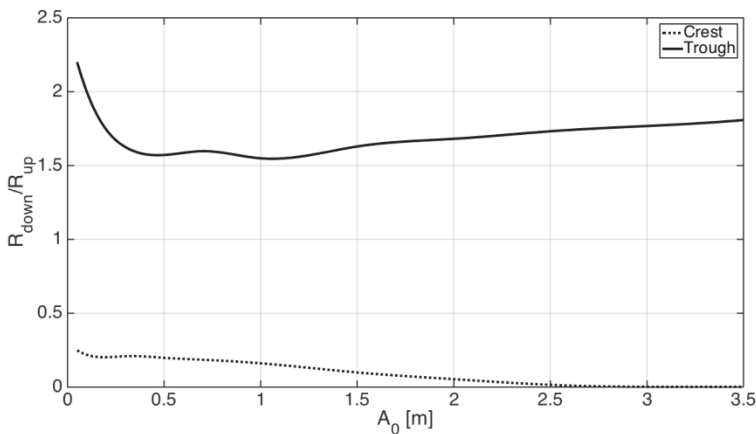


Figure 14. Ratio of run-down heights to run-up heights R_{down}/R_{up} versus the initial wave amplitude.

2. Observed run-up of vessel waves

The frequent presence of large and long water waves induced by high-speed vessels in Tallinn Bay is a major new factor of hydrodynamic pressure (Soomere, 2005a) that may even override the natural hydrodynamic activity in this part of the Baltic Sea during relatively calm seasons (Kelpšaitė et al., 2009). The leading ship-induced waves have considerably longer periods and often approach the shore from directions, from which storm waves are infrequent. These features enhance the potential of ship wakes to modify the natural course of beach processes (Didenkulova et al., 2011c; Pindsoo et al., 2014) and to disturb marine habitats in the coastal zone (Erm and Soomere, 2006; Erm et al., 2011).

This chapter and Paper I address another potential reason for the unexpectedly strong impact of vessel waves on the shores of Tallinn Bay. Namely, the specific group structure of the wave wake in combination with general properties of the run-up of single waves may substantially modify the run-up process of single vessel waves. The analysis is based on a detailed experimental study of the impact of the group structure of these wakes on run-up heights of single vessel waves at Pikakari Beach in Tallinn Bay. The specific structure of frequency modulated wave packets induced by high-speed vessels leads to a long sequence of very high wave run-up events at the coast, even when the offshore wave heights are moderate. The analysis is complemented with the evaluation of the ratio of the run-up height to the offshore wave height.

Section 2.1 provides a short insight into the major problems associated with high vessel-induced waves in the coastal zone largely following Paper III. The study area in the Baltic Sea and the experimental set-up for the measurements of vessel waves and their run-up are described in Section 2.2. Statistical properties of vessel waves and their amplification during the run-up process are discussed in Section 2.3. Section 2.4 is devoted to the analysis of interrelations of the height and run-up of individual waves. The presentation in Sections 2.2–2.4 follows Paper I.

2.1. The complexity of ship-induced wave systems

As discussed in Introduction and in Papers I–III, the system of ship-induced waves changes considerably when ships sail at depth Froude numbers larger than about 0.5. The related effects became common after the new generation of large and powerful ships operating at cruise speeds up to 30 knots and regularly sailing at $F_d > 0.6$ was introduced in the 1990s (Parnell and Kofoed-Hansen, 2001; Parnell et al., 2007; 2008; Soomere, 2007). A large part of the energy of the resulting wave systems is concentrated into two or three packets of long waves that are only weakly dispersive (Figure 15).

Paper III provides a short overview of specific effects that may become evident when ships are sailing at large Froude numbers. The wave groups produced by ships sailing at depth Froude numbers in a so-called high-speed subcritical range

0.5–0.85 usually consist of a few crests. As such groups often remain compact over substantial distances, they may serve as a source of great danger to the people (Hamer, 1999) and the environment. While the wakes of ships sailing at lower depth Froude numbers are usually problematic only in the immediate vicinity of the sailing line, the wakes generated at larger Froude numbers remain dangerous at a distance of many kilometres from the sailing line (Soomere, 2005; Parnell et al., 2007).

The system of vessel-induced undulations is often preceded by solitary waves of elevation called precursor solitons (Ertekin et al., 1984). Such solitary disturbances may be generated already starting from depth Froude numbers as low as about 0.2 (Ertekin et al., 1986). Although their amplitude is normally very small, their propagation is often associated with high water velocities (Neuman et al., 2001), elevated shoreline water levels (Soomere et al., 2011) or the ability of building long-living rogue waves in shallow water (Peterson et al., 2003).

Recently, it has been demonstrated that an increase in the length-based Froude number may cause specific types of ship wave systems that resemble the Mach cone (Rabaud and Moisy, 2013; Darmon et al., 2014). While in the classic Kelvin wave theory the highest waves are located at the border of the Kelvin wedge, for Mach-type wakes the highest waves may occur inside this wedge (Noblesse et al., 2014).

These high waves are often much longer than natural waves in sheltered or semi-sheltered environments. They may seriously threaten ecosystems (Ali et al., 1999) and serve as a source of acute danger for the users of the nearshore (Hamer, 1999) and the coast (Krylov, 2003). These impacts are a natural consequence of intense traffic of large and powerful ships in regions where the levels of natural wave energy are normally small. In many regions of the world that are exposed to heavy ship traffic, even in coastal areas with relatively high natural wave energy

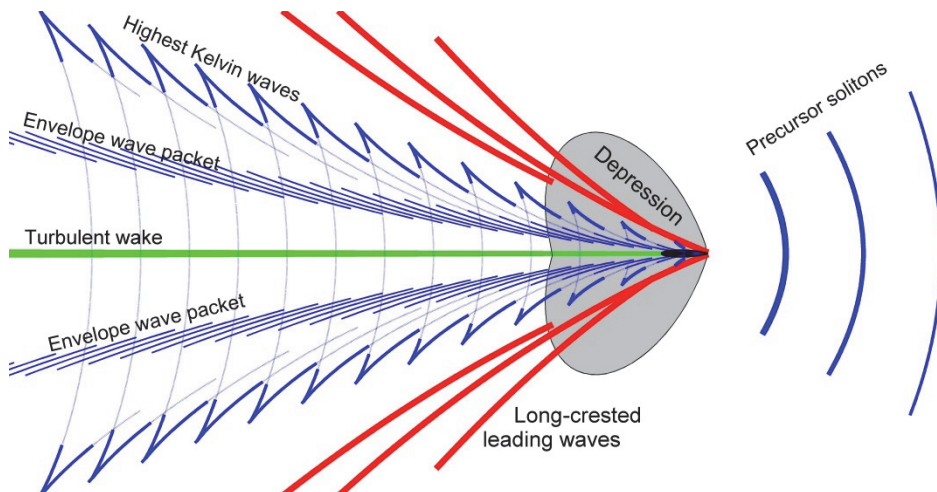


Figure 15. Scheme of the wave pattern excited by a high-speed vessel sailing at a subcritical speed (Soomere, 2009).

levels, vessel wakes have become a major factor in the dynamics of the coastal zone (Parnell and Kofoed-Hansen, 2001; Soomere, 2007).

The ever widening impact of ship-induced waves and the growing awareness about the related adverse effects has led to various attempts towards the regulation of ship traffic. The first attempts in this direction focused on the limitation of maximum wave heights (Stumbo et al., 1999; Parnell and Kofoed-Hansen, 2001; Varyani, 2006). More generally, the existing regulations aim at setting limits for a single property of the wave field (usually the highest waves) or, alternatively, for a characteristic single wave component of the entire vessel-driven system of disturbances (Macfarlane et al., 2014).

These attempts, although appreciable, only provide a partial solution because a craft that operates at comparatively large speeds in relatively shallow water normally produces a variety of disturbances. This system may contain, additionally to more or less regular undulations, also solitary waves of elevation or depression, or drive an elevation of the water level in the nearshore (Soomere et al., 2011). The resulting extremely complex wave pattern may substantially vary both in physical and spectral space (Torsvik and Soomere, 2008; Sheremet et al., 2013; Torsvik et al., 2015). As a limiting case, a ship in a channel may even produce a conditionally stable supercritical bore (Gourlay, 2001; Gourlay and Cook, 2004) that causes an abrupt elevation of water level and may result in a surge wave at the coast.

Many of the listed components are capable of providing serious damage to the coastal environment. Their impact may substantially depend on the local conditions. For example, in the Marlborough Sounds, New Zealand, the wakes of high-speed ferries caused rapid and significant accretion of sediment (Parnell and Kofoed-Hansen, 2001). In contrast, in Tallinn Bay, Estonia, basically similar groups of vessel waves resulted in rapid erosion of the normally accreting beach at the island of Aegna (Parnell et al., 2008; Soomere et al., 2009).

The highest and longest ship waves recorded at the coasts of Tallinn Bay often reached over 1 m above still water level. Several examples extended even higher than 1.5 m above calm water level (Didenkulova et al., 2009a; Torsvik et al., 2009a). On a few days there was evidence of overwash deposits at heights about 2 m above still water level (Soomere et al., 2009). The presence of vessel wakes led to rapid loss of sediments, with a rate up to 1 m³ per metre of the coastline by a wake of one vessel (Soomere et al., 2009). The combined effect of vessel wakes and wind waves produced a stable convex nearshore beach profile at Pikakari Beach of Tallinn Bay (Didenkulova and Soomere, 2011). It has a specific shape that allows anomalous “non-reflecting” wave behaviour (Didenkulova et al., 2009b).

The ability of the groups of long and long-crested waves to modify the shores (incl. the capability to easily smooth out the emerging berm) may be connected with their ability to exert very large run-up events (Didenkulova et al., 2009a; Soomere et al., 2009). These events and records motivated a detailed study of run-up properties of vessel waves in Paper I.

2.2. Experimental study of ship wakes in Tallinn Bay

Tallinn Bay (Figure 16) is one of the most famous venues of studies into waves produced by ships sailing at relatively high speeds in comparatively shallow water (Parnell et al., 2008). It is one of the few locations open to relatively high waves where high and long vessel waves substantially contribute to the overall hydrodynamic activity (Kelpšaitė et al., 2009) and sediment transport processes (Pindsoo et al., 2014) during certain seasons. The background for this uncommonly large proportion of vessel wakes is that this bay, located in the almost tideless Baltic Sea, is sheltered from predominant storm directions. The bay is characterized by a relatively mild (the significant wave height exceeds 0.5 m with a probability of 10%) but extremely intermittent (100-yr maximum wave heights exceed 4 m) wind wave climate. As the fetch length is relatively short, the peak periods of wind waves are usually well below 3 s, reach 4–6 s in strong storms and only infrequently exceed 7–8 s (Soomere, 2005b).

This water body with a size of about 10 km × 20 km hosts intense traffic of large high-power ferries that sail at cruise speeds up to 30 knots (depth Froude numbers 0.6–0.8; Parnell et al., 2008) at a distance of about 2.5 km from the coast (Torsvik et al., 2009a; Soomere et al., 2011). The main reason for extensive environmental impact of vessel waves in Tallinn Bay is that vessel wave periods (8–15 s, since 2007 usually below 10 s) considerably exceed typical periods of wind waves in this bay (Soomere, 2005a; Parnell et al., 2008). The heights of the largest waves were up to 2 m before 2007 (Soomere, 2005a) but have remained below 1.4 m since 2008 (Parnell et al., 2008; Kurennoy et al., 2009, 2011).

As the waves produced by powerful large ships normally approach in well-defined groups of ~10 single crests, the associated wave set-up is usually minor. It is possible to recognize the run-up of almost all wave crests and to associate the



Figure 16. Sketch map of the Baltic Sea and location of the study site in Tallinn Bay (Paper I).

run-up values with the properties of single waves seaward from the surf zone. Paper I provides an insight into measurements of the properties of vessel wakes and their impact on coasts. The experiment was performed at Pikakari Beach (Figure 16) in 2009 under reasonable environmental conditions (wind wave heights mostly about 10 cm and reaching 40 cm during three days). The focus was on the waves produced by three conventional ships with lengths of about 200 m and operational speeds of 25–27.5 knots, sailing from Helsinki to Tallinn. The parameters of vessels, generated waves and the variability and internal structure of the wakes are described in Kurennoy et al. (2009) and Torsvik et al. (2015).

The wave profiles were recorded from 17 June till 1 July 2009 at 5 Hz using a downward-looking ultrasonic echosounder. The device was mounted on a stable tripod in about 2.7 m deep water approximately 100 m from the shoreline and 2.4 km from the sailing line. The record contains 66 clearly identifiable wakes: 29 from the *Star*, 23 from the *SuperStar* and 14 from the *Viking XPRS*. The maximum wave heights (up to 1 m) corresponded to the longest waves with periods of 8–10 s. As typical wind wave periods were 2–3 s, these vessel waves were clearly distinguishable from the natural wave background.

The maximum run-up heights were evaluated visually following the inundation of each wave crest (Figure 17). The video recordings started on 12 June, that is, earlier than the echosounder was mounted (Paper I) and this data set contains more recordings of vessel waves: 86 wakes in total, 36 from the *Star*, 31 from the *SuperStar* and 19 from the *Viking XPRS*. As the distance between the echosounder and the shore was about 2–3 wavelengths (Figure 17), large waves kept their identity and it was possible to follow the propagation of each crest up to the shore and to link the properties of each wave measured by the echosounder and its run-up at the shore.

2.3. Statistics of single vessel waves and their run-up

The data set described in the previous section allows for a detailed study of the

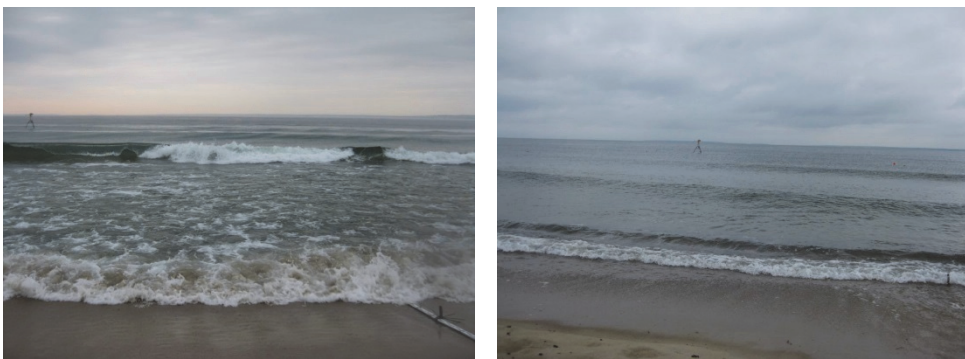


Figure 17. High-speed vessel wakes at Pikakari Beach. Run-up was tracked with the help of the measurement staff at the shore. Wave properties were recorded farther using a tripod (Paper I).

statistics of vessel-induced waves and corresponding run-ups. All measured wave systems had a structure characteristic of ships sailing at high but still subcritical depth Froude numbers about 0.6–0.8 (Soomere, 2007; Parnell et al., 2008). The chirp-like signal (Torsvik et al., 2015) recorded by the echosounder consisted of frequency modulated packets. The largest and longest waves arrived first and both the amplitude and period of subsequent waves gradually decreased (Figure 18). The cases where the groups of waves with different heights and periods are clearly separable (Figure 18a) evidently reflect ships sailing at larger depth Froude numbers. The highest waves (with a height of up to 1 m and exerting a run-up up to 1.4 m) usually belonged to the first group.

Single waves were extracted from the signal using the classical zero-upcrossing method (IAHR, 1989). The empirical distributions of the wave heights generated by the three ships were very similar to each other, peaked at 8–10 cm and moderately skewed towards larger wave heights. Most of the waves were <30 cm high. The number of very high waves was rather small. The distributions rapidly decayed starting from 0.14 m (Paper I). Waves higher than 40 cm constituted, on average, about 2% of all waves (1% for the *Viking XPRS*, 2% for the *Star* and 3% for the *SuperStar*).

The similarity of these distributions for all ships (Paper I) evidently reflects the similarity of lengths, widths, draughts and operational speeds of the three ships (Parnell et al., 2008; Kurennoy et al., 2009). The average distribution of wave heights that incorporates 66 events (Figure 19) reasonably replicates the shape and properties of similar distributions for different ships. All the distributions in question had a general appearance resembling either a Rayleigh or a Weibull distribution. Based on this appearance, the distributions of single vessel wave heights H were approximated by these commonly used probability density functions (PDF) in wave statistics. A Rayleigh distribution

$$f_R(H, \sigma) = \frac{H}{\sigma^2} \exp\left[-\frac{H^2}{2\sigma^2}\right] \quad (20)$$

is fully described by only one (scale) parameter σ and describes, e.g., amplitudes of narrow-band wave fields (Longuet-Higgins, 1952). The scale parameter of a

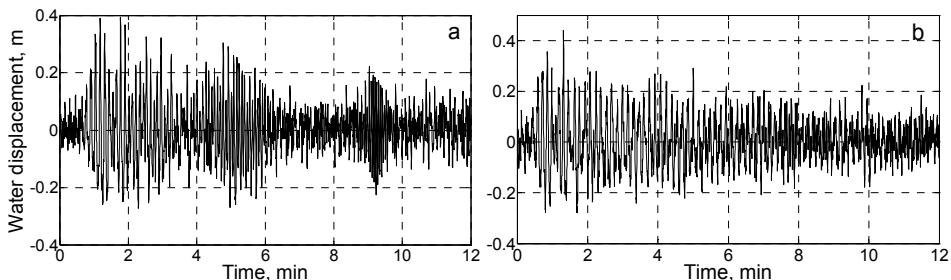


Figure 18. Vessel wakes from a) the *SuperStar* (18 June 2009, 16:15), b) the *Star* (20 June 2009, 12:10) (Paper I).

Rayleigh distribution equals to the mode of the pool of values.

As the PDFs of realistic ocean wave heights often deviate from a Rayleigh distribution, a more general Weibull distribution is often used for the description of both single wave heights and wave fields with various average properties (Battjes, 1971). This distribution has a PDF described by two parameters – a scale parameter σ and a shape parameter q :

$$f_w(H, \sigma, q) = \frac{q}{\sigma} \left(\frac{H}{\sigma} \right)^{q-1} \exp \left[- \left(\frac{H}{\sigma} \right)^q \right]. \quad (21)$$

The parameters of these theoretical PDFs are evaluated for all discussed empirical distributions of vessel wave heights using a nonlinear least-squares method. A Rayleigh distribution unsatisfactorily matches the joint empirical PDF (Figure 19) and similar distributions for single ships (Paper I). The best fit is observed for the *Viking XPRS* that sails at lower speeds than the other ships (Parnell et al., 2008; Kurennoy et al. 2009). This observation suggests that the mismatch of the empirical distribution and a Rayleigh distribution may be a specific feature of sailing at large depth Froude numbers.

A Weibull distribution seems to be a fairly good model for the heights of waves of each ship (Paper I) as well as for their joint distribution (Figure 19). Although it slightly underestimates the proportion of small (~ 10 cm) waves, it describes well the distribution of larger wave heights (> 15 cm). The underestimation of small waves may reflect the presence of the wind wave background that contained an appreciable amount of small waves < 10 cm on several days of the experiment.

The scale parameter σ was almost the same (0.12 m) for the distribution in Figure 19 and for similar distributions for particular vessels (0.12 m for the *Star*, 0.13 m for the *SuperStar* and 0.11 m for the *Viking XPRS*). It was slightly larger for Weibull distributions: 0.16 m for the joint distribution and for the *SuperStar*, and 0.15 m for the *Star* and the *Viking XPRS*.

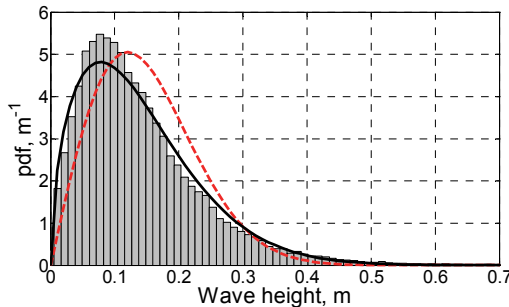


Figure 19. Averaged distribution of all recorded vessel wave heights. The red dashed line corresponds to the Rayleigh distribution ($\sigma = 0.12$ m) and the black solid line to the Weibull distribution ($\sigma = 0.16$ m, $q = 1.53$), fitted using the maximum likelihood estimate (Paper I).

The shape parameter q in the Weibull distribution varies more significantly. It was 1.53 for the overall distribution, 1.45 for the *Star*, 1.52 for the *SuperStar* and 1.71 for the *Viking XPRS*. Paper I provides an interpretation of this variation based on the physical meaning of this parameter from the viewpoint of the Glukhovsky distribution. This distribution was developed semi-empirically for the description of wind wave statistics at intermediate depths in the coastal zone of the Caspian Sea by including the water depth as an additional parameter (Glukhovsky, 1966). Both the Weibull and Glukhovsky distributions represent a generalization of the Rayleigh distribution. For their comparison it is convenient to consider cumulative distribution functions (CDF). For Weibull distributions it has the following form:

$$F_w(H, \sigma, q) = 1 - \exp\left[-\left(\frac{H}{\sigma}\right)^q\right]. \quad (22)$$

The CDF of the Glukhovsky distribution is (Glukhovsky, 1966)

$$F_G(H, \bar{H}, h) = 1 - \exp\left[-\frac{\pi}{4\left(1 + \frac{\bar{H}}{\sqrt{2\pi h}}\right)}\left(\frac{H}{\bar{H}}\right)^{\frac{2}{1-\bar{H}/h}}\right], \quad (23)$$

where \bar{H} is the mean wave height and h is the water depth. A comparison of Eqs. (22) and (23) reveals that the two CDFs are identical if

$$q = \frac{2}{1 - \bar{H}/h}, \quad \sigma = \bar{H} \left(\frac{4}{\pi} + \left(\frac{2}{\pi}\right)^{3/2} \frac{\bar{H}}{h} \right)^{\frac{1-\bar{H}/h}{2}}. \quad (24)$$

The water depth at the location of the tripod was $h = 2.7$ m and the mean height of all waves reflected in Figure 19 was $\bar{H} = 0.14$ m. These values correspond to

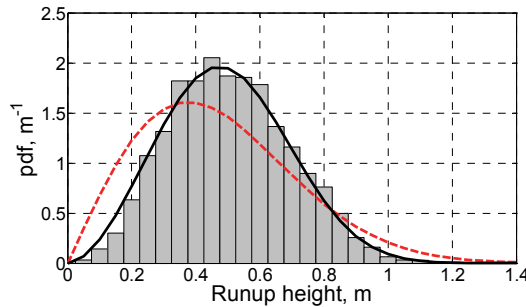


Figure 20. Averaged distribution of all recorded run-up heights of vessel waves. The red dashed line corresponds to the Rayleigh distribution ($\sigma = 0.38$ m) and the black solid line to the Weibull distribution ($\sigma = 0.56$ m, $q = 2.77$), fitted using the maximum likelihood estimate (Paper I).

$\sigma \approx 0.16$ m and $q \approx 2.1$, which are close to the values evaluated from the original data.

The distributions of run-up heights of waves of single ships and the joint distribution (Figure 20) are almost symmetric. They are all peaked at 0.3–0.6 m and have almost coinciding modes at 0.4–0.5 m (Paper I). Paper I makes an attempt to approximate these distributions by Rayleigh and Weibull distributions PDFs (Figure 20). While the Rayleigh distribution fails to match the shape of the empirical distributions of run-up heights, the Weibull distribution works quite well for this data set. However, its shape parameters are more diverse for run-up heights. The mode of the Rayleigh distribution is $\sigma = 0.38$ m for the joint distribution and for waves produced by the *Star*, 0.40 m for the *SuperStar* and 0.33 m for the *Viking XPRS*. Similarly to vessel wave heights, the scale parameter in Weibull distributions for run-up heights is larger than for the Rayleigh distribution. It is $\sigma = 0.56$ m for the joint distribution and for the *Star*, 0.59 m for the *SuperStar* and 0.49 m for the *Viking XPRS*. The shape parameter is $q = 2.77$ for the overall distribution, 2.75 for the *Star*, 2.93 for the *SuperStar* and 2.70 for the *Viking XPRS* (Paper I).

The established parameters of theoretical distributions allow calculating the corresponding mean wave and run-up heights from the analytical expressions of the relevant distributions:

$$\bar{H} = \int_0^{\infty} Hf(H)dH, \quad (25)$$

where $f(H)$ stands for any of the above-discussed distributions. As expected, the values of mean wave and run-up heights, calculated from the original data and reconstructed from the obtained Rayleigh and Weibull distributions, have a reasonable match for the overall statistics and for each vessel (Figure 21). Theoretical values calculated from Eq. (23) for the Rayleigh distribution tend to underestimate the observed average run-up height by 10–20%.

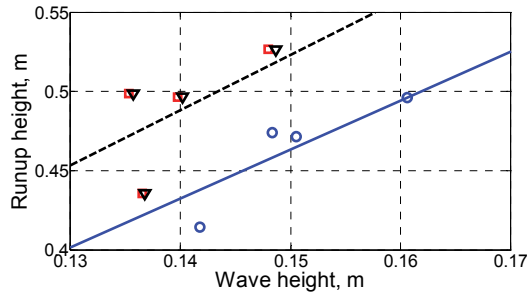


Figure 21. Mean run-up and wave heights in the wakes, calculated from the original data (red squares) and reconstructed from the Rayleigh (blue circles) and Weibull (black triangles) distributions. Blue solid and black dashed lines correspond to the regression curves fitted to the results calculated from the Rayleigh and Weibull distributions, respectively (Paper I).

The performed analysis makes it possible to relate the heights of vessel waves in the 2.7 m deep nearshore and the run-up heights (Paper I) and thus to some extent quantify the wave amplification at the shore (Figure 21). Although the corresponding regression lines are based on only four points, they still indicate an interesting trend. The average run-up heights can be expressed as follows:

$$\bar{R} = Q\bar{H}, \quad (26)$$

where $Q \approx 3.1$ for the best-match Rayleigh distribution and $Q \approx 3.5$ for a similar Weibull distribution. Consistently with the underestimation of run-up heights, fitting to the Rayleigh distribution gives a smaller amplification rate at the coast.

The validity of this estimate can be roughly evaluated by comparison of the theoretical amplification rates of non-breaking sinusoidal waves with a period of $T = 10$ s (which is the period of the largest vessel waves). The amplification rate R/H of such a wave on a plane beach in the framework of shallow-water theory is (Didenkulova et al., 2007a)

$$\frac{R}{H} = \pi \sqrt{\frac{2L}{T\sqrt{gh}}} \approx 6. \quad (27)$$

Here $L = 100$ m is the distance to the shore and $h = 2.7$ m is the water depth. Thus, the average amplification rate of vessel waves' height in the realistic run-up process is about half the one predicted by Eq. (27). The difference can be explained by the impact of the breaking of vessel waves (see Figure 17).

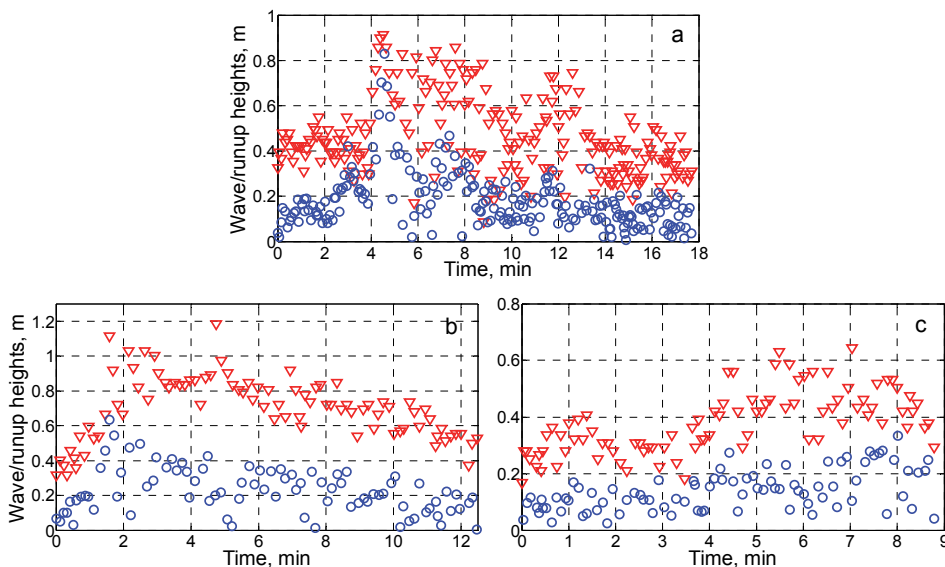


Figure 22. Wave heights (blue circles) and corresponding run-up heights (red triangles) within the wake from a) the *SuperStar* (19 June 2009, 19:15), b) the *Star* (20 June 2009, 12:10) and c) the *Viking XPRS* (21 June 2009, 13:50) (Paper I).

2.4. Run-up of individual vessel waves

Paper I also presents an attempt to better understand the link between the nearshore wave heights and run-up properties of individual waves on the example of three sets of vessel waves in question. Careful synchronization of the clocks of the echosounder and the video system made it possible to identify the run-up of most of the waves higher than 10 cm in the wake. The analysis was performed for a wake from the *SuperStar* on 19 June 2009 at 19:15, from the *Star* on 20 June 2009 at 12:10 and from the *Viking XPRS* on 21 June 2009 at 13:50.

A comparison of the relevant data (Figure 22) indicates a fairly good correlation between wave and run-up heights. Although larger waves generally produce larger run-up heights, the maximum run-up events do not always correspond to the maximum wave height. Moreover, numerous unremarkable waves result in an almost the same run-up height as the outstanding highest wave (Figure 22). This can be partially explained by different periods of single waves.

The subsequent approach of three wave groups with different periods is clearly

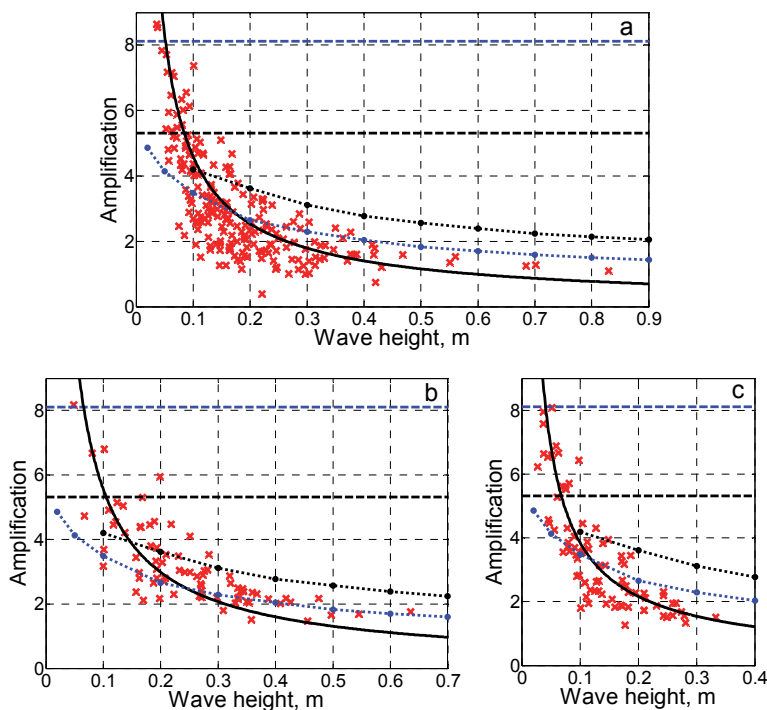


Figure 23. Wave amplification rate on Pikakari Beach for waves from a) the *SuperStar*, b) the *Star*, c) the *Viking XPRS*. Dashed lines correspond to Eq. (27), dotted lines to the calculation of breaking run-up with the characteristic periods of 6 s (blue) and 14 s (black) and the black solid line corresponds to Eq. (28). Some smaller waves with heights <20 cm may have the amplification rate matching that of theoretical estimations for non-breaking waves (black dashed line) (Paper I).

seen in the time-frequency spectrum (Paper I). The first group with a peak period at 8 s arrives first. The second group with a peak period of 5 s arrives three minutes later and a group of waves with periods about 4 s approaches after three more minutes. This structure of the entire wake is characteristic of ships sailing at depth Froude numbers 0.6–0.8 (Soomere, 2007; Torsvik et al., 2015).

The presence of relatively large run-up events in the later phase of the arrival of vessel waves is consistent with Eq. (27), which signals that the run-up height increases with a decrease in the wave period (Paper I). This effect may partially explain why vessel waves often cause rapid beach erosion (Soomere, 2005; Parnell et al., 2007). The group structure of the wake dictates that, unlike narrow-banded groups of wind waves, vessel waves with very large run-up heights arrive over a long time interval, and this may result in an anomalous impact on the coast.

As discussed above, wave breaking may substantially affect the beaching of large waves and reduce their run-up. Very often the largest vessel waves break far before they reach the shoreline (Figure 17). Smaller waves have generally stronger amplification rates than the larger ones (Figure 23). The observed properties qualitatively match the results of the numerical simulation of the amplification of waves approaching Pikakari Beach, performed with the CLAWPACK package using the original profile of Pikakari Beach measured during the experimental campaign (Section 1.2). Consistently with observations, the calculated amplification rate decreases with an increase in the wave height. The evolution of larger waves that are more prone to breaking, matches well the simulated results for breaking waves, while smaller waves behave similarly to the results of simulations of non-breaking waves.

The amplification rates for waves produced by all three vessels (Figure 23) match well the empirical power regression curve derived in Paper I

$$\frac{R}{H} = aH^{-b}, \quad (28)$$

where the coefficient b varies within $0.75 \leq b \leq 0.95$ depending on the vessel and the dimensional coefficient a changes within the range $0.4 \leq a \leq 1.0$. The approximation (28) can be used for estimates of run-up heights from vessel-generated waves.

3. Ship-induced solitary waves of depression

The properties of waves generated by large and powerful vessels have received considerable attention in the international scientific literature (Soomere, 2005, 2009). The high hydrodynamic loads associated with the leading large and long waves are often considered to be of the largest environmental significance (Parnell and Kofoed-Hansen, 2001). With the exception of studies of sediment resuspension and turbidity (e.g., Rapaglia et al., 2011; Göransson et al., 2014), only few studies treat the impacts of depression waves produced by ships (Forsman, 2001). While the generation of a depression wave (Bernoulli wake) by ships sailing in shallow water has been known for a long time and the associated phenomenon of squat is well understood, it was recognized only recently that ship-induced depressions may occur at a substantial distance from the fairway (Rapaglia et al., 2011) where they eventually propagate as free waves.

This chapter focuses on deep depression waves excited by ships of fairly modest size and sailing at moderate depth Froude numbers in the Malamocco–Marghera channel in the Venice Lagoon. Section 3.1 presents a short insight into the relevant literature (mostly following Paper III) and then depicts the study area of large waves of depression and experimental set-up in the Venice Lagoon in spring 2014. Section 3.2 presents an overview of the properties of the largest measured depressions on banks of the navigation channel (Paper II). As their amplitude is comparable with the water depth, it is reasonable to use the technique of Riemann waves and the relevant software described in Chapter 1 for their analysis.

Section 3.3 is targeted to the development of a simple approach for the replication of these depression waves by means of the specification of a smooth disturbance at a certain distance from the shallow area and by letting it to propagate along the slope of the navigation channel. This includes a comparison of real wakes and their numerical counterparts on the banks. Finally, Section 3.4 aims at understanding how far such structures can propagate into the lagoon as compact entities of potentially dangerous height. The field data measured in spring 2014 are used to initialize simulations of the propagation of their idealized counterparts – solitary Riemann waves of depression.

3.1. Ship-induced depressions in shallow areas

It is often assumed that among vessel-generated disturbances long and high leading waves of the entire wake provide the most significant environmental impacts (Soomere, 2005a, 2009). These groups are almost non-dispersive in relatively shallow sea areas and, similarly to tsunamis (Didenkulova et al., 2011c), may propagate over considerable distances as compact entities. They may cause environmental damage and hazard to people and property even at remote locations. Their height and steepness (and consequently water velocities) are often amplified by shoaling and/or in the process of run-up (Section 2.3).

This viewpoint implicitly reflects the properties of solutions of common equations for weakly nonlinear water waves such as KdV or Kadomtsev–Pethviashvili equations. As discussed in Introduction, these equations may only have waves of elevation as their valid solitary-wave solutions. Indeed, ships sailing at moderate depth Froude numbers usually produce also solitary waves (precursors) of elevation (Ertekin et al., 1986; Neuman et al., 2001; Soomere, 2007).

The system of disturbances excited by a moving ship is richer than just a set of waves of elevation or undulations. Several effects become evident when sailing at moderate and high depth Froude numbers (equivalently, in relatively shallow water). In such a regime the formation of a depression region (often called Bernoulli wake) is as common as the production of waves of elevation (Akylas, 1984; Grimshaw and Smyth, 1986; Lee et al., 1989).

The presence of a depression can be to a certain extent analysed by another common class of weakly nonlinear disturbances – solutions of the KdV equation called undular bore. The related phenomena have been known theoretically for more than 60 years (Benjamin and Lighthill, 1954; Peregrine, 1966) and are common in numerical experiments of one-dimensional ship motion. The vessel moving at a constant speed produces a gradually lengthening region of depression of nearly uniform depth (Baines, 1997; Torsvik et al., 2007, 2009a). This is a reflection of a well-known drawdown effect called squat in navigational channels (Constantine, 1961; Graff, 1962; Naghdi and Rubin, 1984). This major source of danger for navigation in very shallow channels and especially at large blocking coefficients (Millward, 1996; Gourlay, 2003) has been well documented (e.g. Gourlay and Tuck, 2001; Gourlay, 2006) and its forecast is made routinely for major navigation channels (El-Kader et al., 2003).

Possible problems of ship-driven depressions are commonly related to their penetration to harbours adjacent to the navigation channel (Forsman, 2001) or to their potential impact on river banks (Balzerek and Kozłowski, 2007). Another issue has been raised for ships sailing in channels dredged into the very shallow Venice Lagoon where they produce very large waves of depression (Rapaglia et al., 2011; Gelinas et al., 2013), whereas waves of elevation are insignificant. As the channels are surrounded by extensive lagoon areas, these depressions can propagate to a considerable distance (up to 500 m, Rapaglia et al., 2011) away from the navigation channel. These disturbances drive possibly significant but likely not exceptional water velocities (cf. Rapaglia et al., 2011) in the channel itself but serve as an important agent of resuspension in large parts of the lagoon.

The Venice Lagoon is known as the biggest lagoon not only in Italy but in the entire Mediterranean region (Brambati et al., 2003; Madricardo and Donnici, 2014). While its surface area is as large as about 550 km², its average depth is only 0.8 m. Water circulation and dynamics in this extremely shallow water body is mainly controlled by tides that have excursion between 0.3 and 1.1 m. The lagoon has only three tidal inlets with depths ranging from about 10 to >17 m for the Malamocco inlet. Water exchange between the open sea and the interior of the lagoon is conducted by numerous tidal channels (Paper III).

The lagoon has been subject to extensive anthropogenic interventions through the centuries. The natural sediment deposition around the city of Venice was prevented by diversions of the Brenta and Piave Rivers directly into the sea. These works were completed already in the 16th century. Simultaneously, the barrier islands separating the lagoon from the Adriatic Sea were stabilized with seawalls in the 18th century. The three inlets were protected by the construction of jetties by the early 20th century (Brambati et al., 2003). These works were complemented by dredging several artificial waterways that today have depths of 10 m or more.

One of the largest interventions was the construction of a navigation channel that connects the Porto Marghera Industrial Zone (Figure 24) to the Malamocco inlet. The Malamocco–Marghera channel (locally known as Canale dei Petroli) first leads to the south of Porto Marghera along the mainland coast for 14 km and then turns towards the Malamocco inlet (Rapaglia et al., 2011). It has a total length of 20 km, a total width of about 200 m in the east–west section and 100 m in the north–south section and a width of the navigable bottom of 60 m. With a design depth of 12 m, this channel is able to accommodate relatively large vessels.

Although the channel definitely has a great role in the development of the economy of the entire region, its environmental impacts have been of significant concern (Rapaglia et al., 2011; Gelinis et al., 2013). Bathymetric surveys (Sarretta et al., 2010) have indicated intense erosion of the central lagoon from 1970 to 2000. This process has been partially related to the ship traffic in this channel.

The measurements, data from which are used in Papers II and III, were performed in the north–south oriented section of the Malamocco–Marghera channel (Figure 24). The cross-section of the channel is slightly asymmetric. The bottom of the channel (the navigable area) is 11–12 m deep (Figure 25) and is

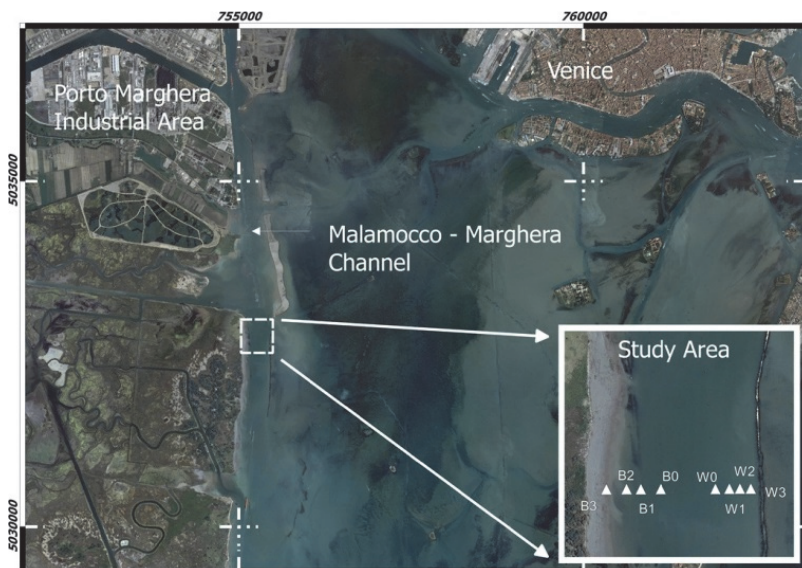


Figure 24. The study area in the Malamocco–Marghera industrial channel. White triangles in the inset indicate the locations of pressure sensors in Figure 25 (Papers II and III).

surrounded by relatively steep slopes ($\sim 10\%$) that have a width of 30–40 m.

A specific feature of the channel is the presence of wide gently sloping shallow banks at both sides. The western (mainland) bank is about 150 m wide, has an almost constant slope of $\sim 3\%$ from the channel margin and ends with an about 1 m high erosion scarp at the shoreline. The eastern (lagoon) bank gently (with a slope of $\sim 2\%$) rises from the channel margin over about 90 m wide area to a depth of about 2 m. At this location a semi-permeable rock wall prevents the propagation of ship-generated wakes into the lagoon (but still ensures water exchange between the channel and the rest of the lagoon).

The measurements of the properties of ship-induced disturbances presented in Paper II and used in Paper III to initialize the simulations of wave propagation into the lagoon were performed at eight locations at the banks (Figure 25). Wave properties were reconstructed from pressure fluctuations that were recorded at either 2 or 5 Hz. Four sensors were mounted on the seabed (locations B1–B3 and W1–W3 in Figure 25) or connected to the channel markers (B0 and W0). The instruments had a maximum synchronization error of ± 10 s (Paper II). The possible de-synchronization is immaterial from the viewpoint of studies in Papers II and III that rely on the magnitude and shape of the ship-generated disturbances.

3.2. Ship-induced solitary waves of depression in the Venice Lagoon

The records of vessel wakes contain four sampling periods of 2 to 6 days in March and April 2014. The original record involves semi-diurnal tidal signal (Figure 26). The entire data set contains about 90 examples of ship wakes (Paper II). The data for three ships in Figure 27 illustrate the range of appearances of the wakes for ships with similar parameters. Consistently with Rapaglia et al. (2011) and Gelinas et al. (2013), the ships did not produce any large-amplitude wave groups or precursors of elevation. This feature is not fully unexpected as the speeds of ships (retrieved from data transmitted by the Automatic Identification System) were in the range of 7–11.4 knots, which corresponds to $F_d = 0.34$ – 0.53 (Paper II).

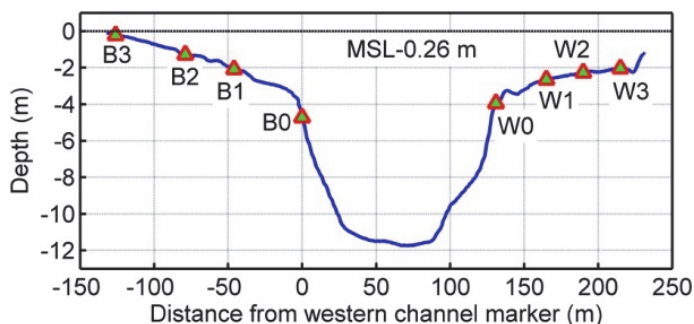


Figure 25. Cross-section of the Malamocco–Marghera channel at the measurement site (Figure 24). The location of pressure sensors (B0–B3, W0–W3) is indicated by triangles. The distance is referenced to the western channel marker and the depth is referenced to the local tidal datum (0.26 m below mean sea level) (Paper II).

The predominant feature of all large ship-induced water level disturbances was a deep depression. The depressions had an almost perfectly symmetric shape (understood as the shape of the course of the water level in time coordinates) at the margins of the channel (locations B0 and W0 in Figure 27). The simulations based on weakly nonlinear approaches suggest that ship-induced depressions should develop an elongated almost horizontal trough with time (Torsvik et al., 2009b; Torsvik et al., 2009a). The recorded depressions, however, had a characteristic *V*-shaped trough, although the ships have already sailed along the channel for a relatively long time. This feature suggests that the depressions apparently had strongly nonlinear nature.

The clearly distinguishable depression lasted typically ~ 80 s. The deep trough was often preceded by a small wave of elevation and followed by another wave or sequence of waves. The typical duration of the entire disturbance to the calm water level was ~ 400 s. Similarly to the extensive variability in the properties of waves of elevation excited by ships sailing at relatively large depth Froude numbers in water of basically constant depth (Kurennoy et al., 2009), the properties of the depression waves recorded at the study site varied significantly. The largest water level dropdown at the western edge of the channel (location B0) was 2.52 m (measured from still water level; 2.58 m when measured from the crest of a small but quite long wave of elevation that preceded the depression) at the coastal side of the channel in the wake of the *Abu Dhabi Star*. This was a relatively large but not exceptional ship sailing at a moderate speed (Paper II). The largest depressions reported in Paper II were >1.5 m and thus considerably exceeded the similar parameters of waves of depressions reported in the scientific literature (Balzerek and Kozłowski, 2007; Rapaglia et al., 2011; Göransson et al., 2014).

The properties of the largest depressions and accompanying smaller waves were often markedly different on opposite sides of the channel. For example, the water

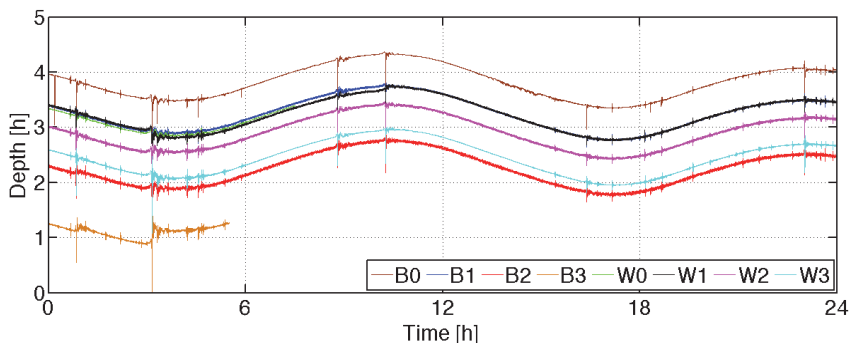


Figure 26. An example of 24-h-long record of water level, restored from the pressure signal, at the banks of the Malamocco–Marghera channel. The location of the devices at the western (coastal, B0–B3) and eastern (lagoon, W0–W3) sides of the channel are indicated in Figure 25. The record begins at 12:00 on 01 April 2014. Data for locations W2 and W3 (used to characterize the wake of the *Abu Dhabi Star* below and in Paper II) are partly missing due to equipment failure. Note that gauge B3 was moved by a strong wake about 3 h after the record began (Paper III).

level dropdown excited by the above-discussed passage of the *Abu Dhabi Star* was much less, about 1.6 m at the lagoonside channel marker. It is hypothesized in Paper II that this feature may be associated either with a shifted position of the ship with respect to the channel axis or with the different morphology of the channel slopes and banks.

The shape of the depression and of the entire wake system changed when the wave propagated over the banks. The depth of the largest troughs usually decreased to some extent but did not change significantly when the wake was propagating over the banks starting from devices B1 and W1. Only at site B3 (in very shallow

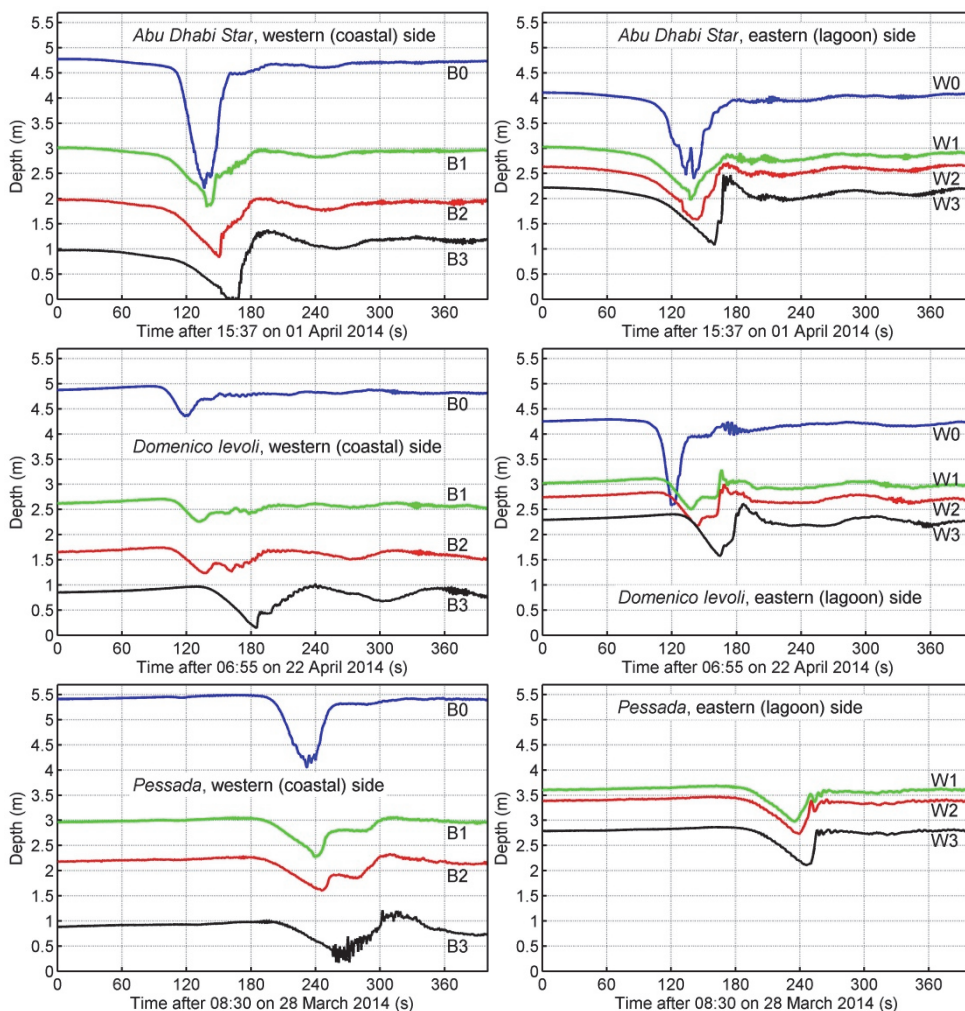


Figure 27. Disturbances induced by the *Abu Dhabi Star*, *Domenico Ievoli* and *Pessada*. Data for W0 for the passage of the *Pessada* are missing due to equipment failure. The largest depressions caused the drying of the coastal slope at location B3. The position of the surface is presented according to the actual water depths at the time of ship passage (Paper II).

water) a certain increase in the wave height was observed.

The most significant process during the wave propagation from the channel margin was an increase in the asymmetry of the wave profile. The wave front became gradually less steep. The rear slope rapidly steepened and became bore-like already at locations B1 and W1. In some occasions a relatively short wave of elevation was developed immediately after the steep rear slope had passed. This asymmetry is characterized in Paper III in terms of the ratio of typical values of the rear slopes to front slopes. This ratio is usually <1.5 at sites W0 and B0 but increases to the level of 2–3 at sites B1 and B2, and becomes as large as ~ 10 at sites W3 and B3.

The typical shape of the depression wave on the banks is strongly skewed *V*-like disturbance. A step or a sequence of steps is often present on the rear slope of the depression wave. It is debatable which mechanism causes this feature. For example, incipient undular bore formation probably modifies the wake of the *Pessada* at W1–W3 (Figure 27). Alternatively, reflection from the bottom may impact the wake of the *Domenico Ievoli* at sites B3 and W1–W3. This property matches a similar feature in numerical simulations of Riemann waves (Rodin and Pelinovsky, 2014).

Paper II discusses several environmental consequences of the propagation of such waves of depression into the shallow lagoon. It is natural to assume that the greatest water velocities and thus intense sediment resuspension would occur during the passage of the rear slope of the waves. The associated highly energetic events may resuspend large amounts of fine sediment from the lagoon bed. This suspended material can be transported by tidal currents to various locations, including the navigation channel that may need frequent dredging, or the material may be carried out of the lagoon (Rapaglia et al., 2011; Gelinis et al., 2013).

3.3. Numerically simulated Riemann waves

The material presented in Section 3.2 and in Paper II shows that linear and weakly nonlinear approaches fail to replicate the properties and propagation of the largest depressions already at the margin of the Malamocco–Marghera channel. None of the recorded depressions had an elongated trough with an almost horizontal bottom that is suggested by weakly nonlinear simulations of ship motion in shallow channels (Torsvik et al., 2007, 2009a). Even though the depressions had an almost symmetric shape in time coordinates at the margins of the channel, they rapidly became asymmetric when propagating over the banks (Figure 27).

Consistently with the weakly nonlinear propagation of solitary depression waves (Grimshaw et al., 2014), the ship-induced troughs developed a sequence of waves of elevation at the end of the rear slope. The maximum surface elevation often exceeded the undisturbed level for some time after the rear slope had passed. This feature, together with the development of steps at the rear slope, is also consistent with the strongly nonlinear propagation of such disturbances as described below.

The level of nonlinearity is often evaluated as the ratio of the height of the disturbance to the water depth. This ratio is usually ~ 0.1 for larger ships and about 0.25 in extreme occasions (like for the wake of the *Abu Dhabi Star*). This ratio is mostly reasonable (~ 0.3) even for the largest depression waves at the border of the navigation channel. Even though the heights of some depression waves decrease to some extent away from the channel margin, a depression of about 0.5 m often penetrates to the 2–4 m deep banks where it is evidently strongly nonlinear.

Papers II and III make an attempt to employ the framework of simple or Riemann waves (Section 1.1) to describe and model the evolution and propagation of ship-induced solitary depression waves. As discussed in Chapter 1, Eqs. (2) do not take dispersion and breaking into account and thus Riemann waves only conditionally describe shallow-water waves. In spite of its obvious limitations, this technique has been successfully applied to the analysis of long waves (Didenkulova et al., 2006b; Zahibo et al., 2008; Pelinovsky and Rodin, 2012).

As the crests of ship-induced waves are generally parabolic and have relatively low curvature at longer distances from the hull (Lee and Grimshaw, 1990; Didenkulova et al., 2011c), it is apparently acceptable to assume that the depression waves have (at least locally) straight crests. The motion of very long waves over very shallow water in ideal conditions can then be approximately described by Eqs. (1) (Whitham, 1974). The typical duration of ship-induced depressions (60–80 s) indicates that they are extremely long when propagating over the banks of the channel with a depth of 2–4 m, and even longer (in comparison with the water depth) in 1–2 m deep water in the rest of the lagoon.

The most interesting question is how far such disturbances may travel into the lagoon. To answer this question to some extent, the wave measurements described in Section 3.2 and in Paper II are used to initialize the calculations of the propagation of Riemann waves of depression over shallow areas in conditions similar to the banks of the Malamocco–Marghera channel in Paper III.

A comparison of the wave speed with the arrival of the deepest part of the disturbances at subsequent sites (Figure 27) indicates that the wave front moved obliquely (at an angle of about 45° according to Rapaglia et al. (2011)) with respect to the channel margin. This means that the surface elevation recordings at sites B1–B3 and W1–W3 reflect different parts of the wave crest. As the existing data set did not allow for a reliable specification of the wave direction, the analysis in Papers II and III proceeds from the assumption that the channel and its banks are homogeneous along the sailing line and the ships are moving at a constant speed. In such a situation the mismatch of the wave propagation direction with the orientation of the line of measurement devices (Figure 24) only leads to a certain shift in the timing of the measured and simulated disturbances and thus is immaterial for the results of the study.

The tracking of ship-induced wave propagation and transformation is performed in Papers II and III using the CLAWPACK software described in Section 1.2. During the simulations, the mass conservation law was satisfied with an accuracy of $10^{-6}\%$, which is at the same level as in earlier numerical experiments with

Riemann waves (Didenkulova et al., 2011a). To avoid wave energy reflection from the border of the computational domain, Sommerfeld-type artificial radiation conditions (Sommerfeld, 1949) were applied at each side of the domain.

The bottom profile within the channel and its banks in Figure 25 was linearly interpolated to a grid with a step of 20 cm based on measurements that had a resolution of approximately 1 m (Paper II). A refinement of the grid step by 2–3 times led to maximum differences in wave amplitudes of less than 0.5%. The water depth was assumed to be constant in the interior of the lagoon. The time step (0.5 s) was restricted by the Courant–Friedrichs–Levy condition.

The measured data sets describe the temporal evolution of the water surface at a certain location, while the simulation of waves of depression using Eqs. (2) requires information about the spatial structure of the wave. It is not straightforward to use for this purpose the measured depressions because it is not clear whether they were forced disturbances or were already propagating as free waves. To resolve this problem, an indirect way of the initialization of the simulations was used in Papers II and III. The approach is based on the assumption that the leading wave of depression of ships moving in a strongly nonlinear regime is a generally symmetric trough with a shape that resembles an inverted (negative polarity) PDF of a Gaussian distribution (Torsvik and Soomere, 2008; Torsvik et al., 2009b). The simulations were initialized with such a function. This procedure makes use of the tendency of the formation of a specific skewed V -like shape of the depression at the channel margins. This shape is a natural consequence of the evolution of initially symmetric depressions (Pelinovsky and Rodin, 2012).

Therefore, it was implicitly assumed that the trough was already a free wave at the margin of the channel and that after some time (or at a certain distance from the sailing line) the basic features (shape, asymmetry, etc.) of the troughs are no longer directly connected with the properties of the ship hull and are defined by generic rules that govern the propagation of depressions of a certain amplitude. This assertion was tested by a series of simulations, in which the initial shape matched an inverted KdV soliton. The exact shape of the initial pulse only insignificantly affected the results of numerical simulations at the channel margins.

Based on the listed arguments, simulations in Papers II and III used a Gaussian bell shape of negative polarity

$$H_0(x) = A_0 \exp\left(-\frac{x^2}{l^2}\right) \quad (29)$$

to initialize the shape of the water surface matching ship-driven disturbances. Here A_0 is the initial amplitude of the trough and l is its characteristic half-width. The flow speed was defined using Eqs. (3) and the sign of the velocities was chosen to match the wave propagation away from the channel.

The amplitude, location (in space) and width of the initial shape were adjusted iteratively, using the philosophy of inverse modelling to match the maximum depth and width of the measured depression at sites W0 or B0. The evolution of the

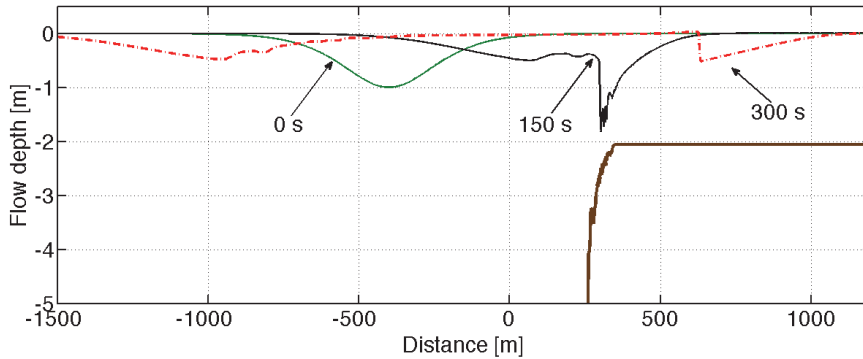


Figure 28. The appearance of a depression pulse with an initial amplitude of 1 m in the navigation channel and over its lagoonside slope at time instants 0, 150 and 300 s. Note the development of a counter-propagating reflected wave at 150 and 300 s. The bold line in the right upper part of the panel represents the model seabed (only shown for the water depths <5 m) (Paper III).

initial disturbance (29) was first simulated over some distance along the channel bottom, and then it was let to propagate along the slope of the channel (Figure 28).

The resulting trough shape was visually compared with the measured wave profiles for a medium-sized ship *Vigor SW* at the channel margin (Figure 29). This vessel was chosen for the comparisons because its wake had a depth of almost exactly 1 m. The best match of the two shapes was found for the initial propagation time of 150 s along the channel bottom (Figure 28). This time was used to initialize all simulations. The parameters of the initial disturbance were found separately for each wake from the match of the simulated depression with the measured signal at the channel margins (W0 or B0). The initial amplitude A_0 was adjusted to match the maximum simulated depression with the measured water level dropdown.

The parameter l in Eq. (28) was adjusted so that the widths of the simulated and measured depressions coincided at the level of 1/3 of the maximum depth (cf.

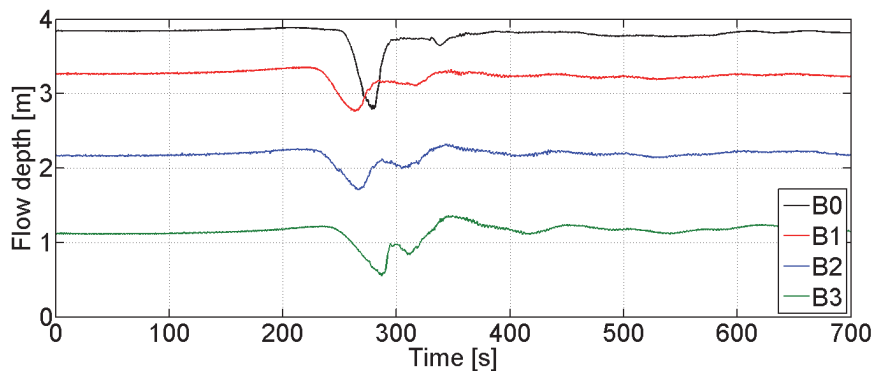


Figure 29. Water surface time series in a wake produced by the *Vigor SW* on the western (coastal) side of the channel around 13:20 on 01 April 2014 (Paper III).

Didenkulova et al., 2008). As expected from earlier numerical experiments with solitary Riemann waves of depression (Pelinovsky and Rodin, 2011, 2012; Section 1.4), the height of the initial smooth Gaussian-shaped depressions slightly increased during this part of numerical propagation and rapidly upsurged at the slopes of the channel.

In spite of this indirect manner of specification of the initial wave profile and long propagation along the channel for 600–700 m (Figure 28), the appearance of the simulated signal replicates the well-known features of the propagation of solitary depressions such as a gradual decrease in the front slope and simultaneous increase in the rear slope (Figure 30). A certain time shift between the measured and simulated waves evidently reflects the mismatch of the propagation direction of the simulated and measured depressions.

The further development of rear–front asymmetry (defined above) and the course of the wave height are appreciably replicated at the lagoonside sites W1 and W2 (Figure 30) but less satisfactorily at the coastal side sites B1 and B2 (Figure 31). The asymmetry of the simulated trough at times exceeds the asymmetry of the measured depression wave by an order of magnitude. This mismatch is usually associated with the development of a step in the rear slope of one of the profiles. The emergence of such steps (or a sequence of steps) is characteristic of the propagation of large-amplitude Riemann waves of depression from smooth initial disturbances (Didenkulova et al., 2011a). The replication of these steps (that are apparently fingerprints of reflected waves that occur if $|\eta_{max}| \rightarrow (5/9)h$, Section 1.1) is not perfect although qualitative match is evident at

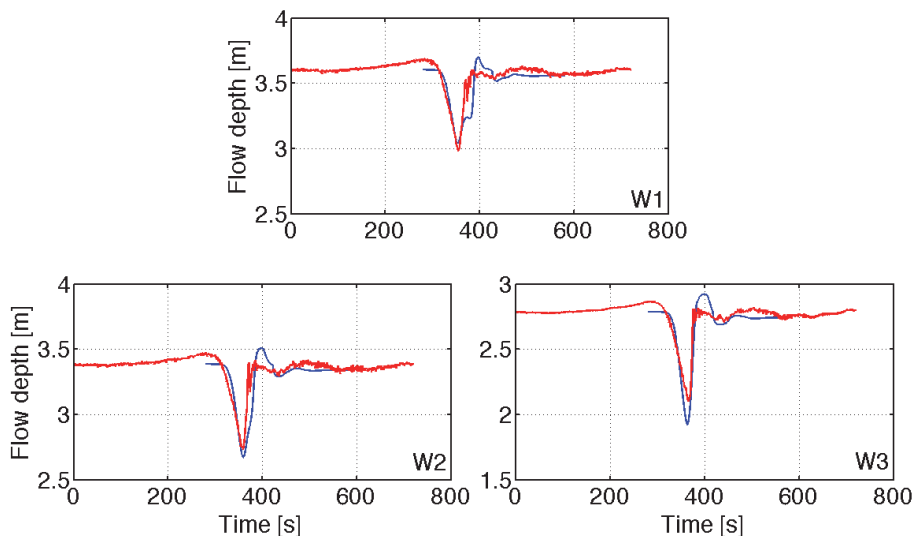


Figure 30. Propagation of a numerically simulated Riemann wave matching the depression created by the *Pessada* over the lagoonside bank of the channel at measurement sites W1–W3 (data from W0 are absent due to equipment failure) on 28 March 2014 at 8:30. Red: measured profiles; blue: simulated profiles (Paper III).

all sites.

The propagation of the largest depressions, both measured (Figure 30) and simulated along the western (coastal) bank of the channel, led to almost drying out of the seabed (Paper II) and the condition $|\eta_{max}| > (5/9)h$ was often met starting from a certain location. It is likely that the wave propagated into the even shallower area as a bore. These cases can still be reasonably well described by the numerical solution in use (Pelinovsky and Rodin, 2012).

3.4. Propagation of ship-induced depressions into the Venice Lagoon

Paper III provides results of simulations of all large depression waves recorded during one of the observation campaigns represented in Figure 26. The data set involves three continuous records, about 30–36 h each, and contains 20 identifiable wakes. The larger wakes were associated with 12 different ships (Table 1 in Paper III). Five smaller wakes remained unidentified. To make the results comparable with the ones presented above and in Paper II, the simulations of the wake of the *Domenico Ievoli* recorded on 22 April 2014 were added into the pool. As separate runs were made for waves measured at each of the channel margins, 40 simulations were used in the analysis. The numerical results were compared with a total of 269 records of the depressions from single measurement devices. The undisturbed water level in each simulation was chosen to match the actual water level at the time of the relevant ship passage.

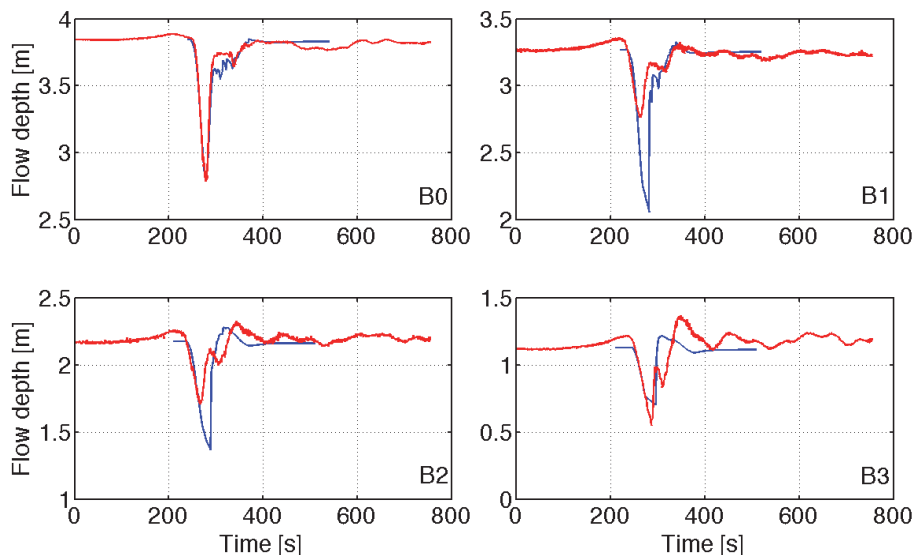


Figure 31. Propagation of a numerically simulated Riemann wave matching the depression created by the *Vigor SW* over the beachside bank of the channel at measurement sites B0–B3 on 01 April 2014 at 13:20. Red: measured profiles; blue: simulated profiles (Paper III).

The wake of the *Vigor SW* with a height of 1 m at the lagoonside channel margin is chosen in Paper III to represent typical examples of relatively large depressions (Figures 30 and 31). The further propagation of this wake is analysed over both the beachside and lagoonside banks of the channel. The height of the depression is underestimated at intermediate locations W1, W2, B1 and B2 (Figure 31). On some other occasions it is replicated adequately at all measurement sites (Figure 30). Interestingly, the match of the simulated and measured wave heights is particularly good at locations W3 and B3. The mismatch is larger for the largest wakes (Figure 27).

The numerical model tends to overestimate the wave height in most of the locations (Figure 32). If locations B0 and W0 used for the calibration are excluded, the formal linear regression line is

$$H_{\max(\text{measured})} = 0.27 H_{\max(\text{simulated})} + 0.32. \quad (30)$$

The simulations overestimate, on average, the wave amplitude by more than 40%. It is natural that the match of measured and simulated heights is almost perfect for the locations, based on which the parameters A_0 and l in Eq. (29) were evaluated. The maximum water level dropdown is often overestimated by a factor of two or even more in locations B1, B2, W1 and W2.

Consistently with above, Figure 32 demonstrates that, on average, the match of the measured and simulated wave heights is much better at the most remote measurement sites B3 and W3. This feature suggests that the numerical approach in use may fail to exactly reproduce some properties of the short-term propagation

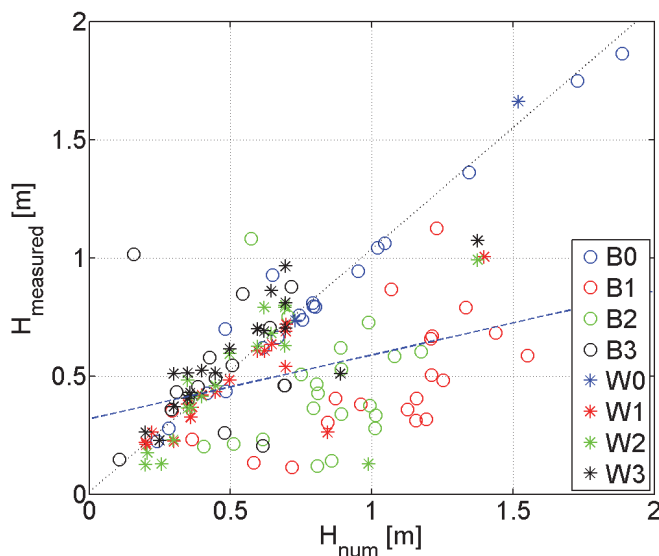


Figure 32. Simulated and measured trough amplitudes for all 12 vessels. Blue dashed line: the regression lines for measurement sites B1–B3 and W1–W3; black dotted line: the regression line for the most distant sites B3 and W3 (Paper III).

of depression waves over the banks of the channel. However, it seems to adequately replicate the long-term evolution of these waves and eventually gives a good insight into their fate in the lagoon interior. In general, it demonstrates a fair agreement between calculated and real data, notwithstanding the crudeness of the introduced approximations.

The average deviation of the simulated wave heights R^{num} from the measured ones R^{real} at different measurement sites is evaluated in Paper III using the classical root-mean-square (rms) difference

$$\delta = \sqrt{\frac{1}{N} \sum_{n=1}^N (R_n^{num} / R_n^{real} - 1)^2} . \quad (31)$$

Here N is the total number of comparable pairs of the wave heights. The rms difference δ reaches 0.36 m for the entire pool of data at W1–W3 and B1–B3. The average deviation is much less, 0.26 m, for the lagoonside most remote site W3.

Paper III makes an attempt to estimate the practical significance of the permeable rock wall at the lagoonside bank of the Malamocco–Marghera channel in terms of the risk of penetration of high-amplitude depressions followed by bore-like phenomena into the Venice Lagoon if the wall were absent. This numerical experiment is relevant for many other sections of the channel that are not protected by such a wall. The idea was to ignore the wall and to look at the further propagation of the above-discussed waves of depression in water of a constant depth of 2 m. As the above simulations were in good agreement with the measured data at the most distant site W3, it is likely that the simulations give a fair insight into the fate of such solitary troughs in the lagoon interior. The use of a constant water depth in the lagoon is motivated simply by the absence of high-resolution data from the lagoon. This simplification overlooks the situation during low tide when the water depth is generally much less than 2 m. As the focus of Paper III was the far-field behaviour of the vessel wakes, also the possible fate of those depressions was investigated that actually propagated towards the coast.

A usual requirement for the “safe” vessel-induced wave height H_{max} (in metres) is (Parnell and Kofoed-Hansen, 2001)

$$H_{max} \leq 0.5 \sqrt{\frac{4.5}{T}} . \quad (32)$$

This height should be measured at a still water depth of 3 m. The usual period T of high vessel waves is 9–12 s (Parnell and Kofoed-Hansen, 2001; Soomere, 2007). For waves with a period of 12.5 s the “safe” height is $H_{max} = 0.3$ m and expression (32) becomes irrelevant for even longer waves. It is likely that waves of depression < 0.3 m are already weakly nonlinear in the Venice Lagoon and evidently rapidly lose their bore-like appearance (Grimshaw et al., 2014). Based on these arguments, it was assumed that a “safe” trough amplitude in the Venice Lagoon is 0.3 m.

An initial depression (29) with $A_0 = 1$ m and $l = 200$ m matches well the appearance of the wake of the *Vigor SW* (Figure 31) and is generally representative

of the relatively large wakes that occur frequently in the Malamocco–Marghera channel. The height of such waves would remain well over 0.3 m after a long incursion into the lagoon (Figure 33). Its height decreases to 0.3 m only after the wave has travelled about 1500 m over the lagoon. Even if the possible overestimation of the height of the depression is taken into account (cf. Eq. (30)), the wave will cover at least 700–900 m before it decreases to 0.3 m. The results match the data from Rapaglia et al. (2011): a 0.8 m high wave remained >0.3 m high at a distance of about 300 m from the channel margin.

The properties of different simulated wakes evolve in a similar manner (Figure 34). The wave amplitude increases rapidly when the wave propagates along the side slope of the channel and reaches a maximum value near the channel margin. The amplitudes of different initial disturbances level off rapidly (after ~ 50 s or ~ 200 m in the lagoon). Further changes in the depressions are almost independent of the initial properties.

As the ship that produced the largest depression waves (*Abu Dhabi Star*, Section 3.2) was not the largest one and was sailing at a reasonable speed, even higher wakes may be possible in the Malamocco–Marghera channel. To understand how even larger-amplitude troughs may behave over the banks of the channel and in the lagoon, a hypothetical case with a characteristic half-size $l = 182.5$ m and an extremely high initial amplitude of 2.5 m was considered in Paper III. This hypothetical initial disturbance evolves into an unrealistically deep depression (almost 6 m) at a certain location along the channel slope. As expected, its height is rapidly reduced to the level comparable to measured wakes.

The heights of all simulated wakes level off rapidly after reaching the bank of the channel (Figure 34). Therefore, wakes of several ships may produce

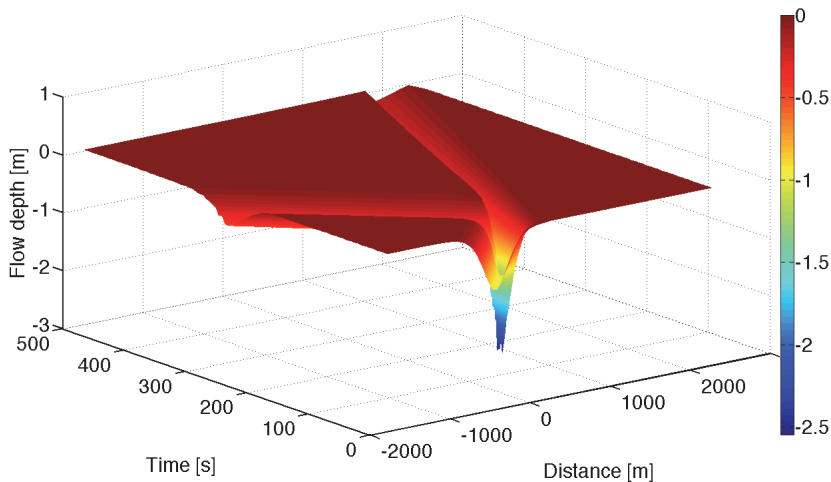


Figure 33. Space–time (x – t) diagram of the simulated wave profile produced by the depression wave with the initial amplitude $A_0 = 1$ m propagating into the lagoon with a constant water depth of 2 m (Paper III). The scale at the right indicates the distance of the water surface from the undisturbed position.

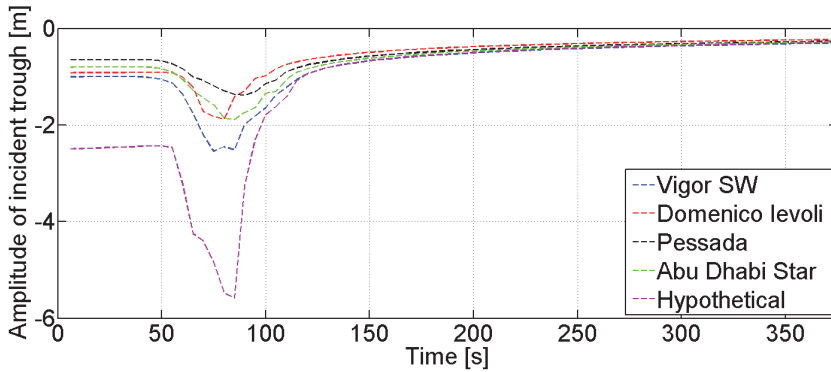


Figure 34. Temporal evolution of the amplitude of initial Gaussian-shaped depressions matching the measured wakes at the channel margin. The parameters in Eq. (28) are as follows: *Vigor SW* (01 April 2014 at 13:20): $A_0 = 1$ m, $l = 200$ m; *Domenico Ievoli* (22 April 2014 at 06:50): $A_0 = 0.92$ m, $l = 100$ m; *Pessada* (28 March 2014 at 8:30): $A_0 = 0.65$ m, $l = 182.5$ m; *Abu Dhabi Star* (01 April 2014 at 15:38): $A_0 = 0.8$ m, $l = 195$ m (Paper III).

depressions of the maximum possible amplitude in the Venice Lagoon. Their further propagation is almost independent of their initial amplitude. Consequently, even relatively modest depressions may persist over long distances.

Although detailed shapes of the depressions in question may be substantially different at the channel margins (Figures 30 and 31) these shapes also become similar after some time (Figure 35). They keep a characteristic gently sloping front and a very steep rear even at a distance of >1 km from the channel. Therefore, it is likely that the bore-like shape of the rear depression waves is preserved over substantial distances.

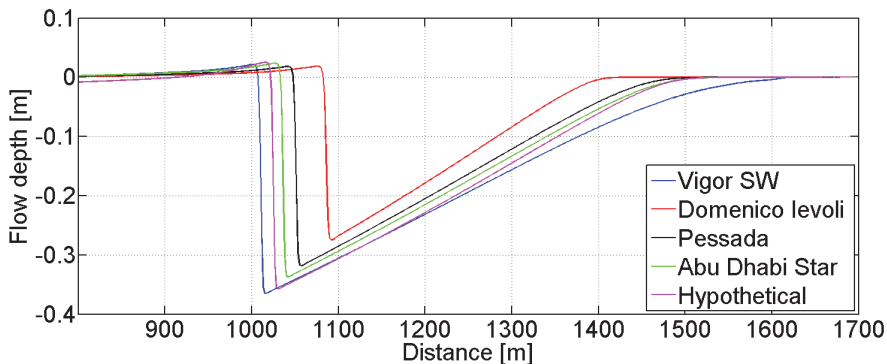


Figure 35. Numerically simulated trough profiles in the lagoon after 300 s propagation time. The different locations of the wave trough are caused by different propagation speeds in Eq. (4) (Paper III).

4. Rogue waves and extreme run-up in the coastal zone

Storm waves are one of the major sources of risk not only to offshore seafarers but also to the users of the nearshore and the coast. Among those, rogue waves that literally emerge from nowhere and similar events of extreme wave run-up during strong storms apparently have the largest damaging potential. The generation of rogue waves by various mechanisms may occur in both deep ocean and in the nearshore (Didekulova et al., 2013c). However, the effects originating from the presence of cross-seas or from the redirection of waves by other processes obviously are more frequent in shallow water because of the impact of bathymetry (Soomere, 2010). Moreover, several types of geometric focusing often occur in coastal areas. Therefore, it is likely that rogue wave phenomena might happen even more frequently in the nearshore regions.

This chapter starts with a short introduction in Section 4.1 into the basic concept of rogue waves and an insight into the existing studies of the damaging potential of rogue waves in the nearshore. The appearance of small-amplitude rogue waves that develop on the wind wave background in relatively shallow water is described based on records of sea surface elevation in Tallinn Bay, the Baltic Sea (Section 4.2). The statistics of different kinds of rogue events, rogue wave crests and troughs and the overall frequency of occurrence of rogue waves identified using zero-upcrossing and zero-downcrossing methods is presented in Section 4.3 following Paper IV.

The analysis of the potential wave run-up and associated maximum inundation on a selection of Estonian coasts of the Baltic Sea, conducted based on 35-year wind wave simulations with the wave model WAM, is presented in Section 4.4. The numerically calculated run-up of severe storm waves using the CLAWPACK software (see Section 1.2) for 18 beach profiles is based on the 35-year maximum significant wave heights and corresponding periods. The estimates of maximum run-up are compared with the estimations made using different run-up formulas, available in the literature. This analysis mostly follows Paper V.

4.1. Rogue waves in the nearshore

Studies of unexpectedly high (so-called rogue) waves were boosted after the so-called “New Year Wave” was unambiguously measured on 1 January 1995 at the Statoil-operated Draupner platform in the North Sea. This event made clear that such waves not only exist but also constitute a serious threat for navigation and oil and gas platforms.

The phenomenon of freak or rogue waves is an intrinsic quality of ocean wave fields. The frequency of occurrence of single waves of different height in a narrow-banded wave field (that is common in seas and oceans) can be adequately approximated with a Weibull distribution discussed in Section 2.3. A fundamental feature of this type of wave fields is that there is no formal limitation for the wave

height. The most probable maximum height of a single wave in a storm that contains N waves is $\hat{h}_{\max} = H_S \sqrt{0.5 \ln N}$ (Longuet-Higgins, 1952). Therefore, the longer the storm with a given significant wave height H_S is, the higher single waves may be.

Extremely large waves are unlikely because wave storms are usually not very long. Values exceeding $2H_S$ are expected to occur once out of $e^8 \approx 2891$ waves, that is, once in ~ 10 h in the open ocean conditions or once in 6–7 h in the Baltic Sea. They, however, occur with a certain frequency and even cases with the wave height of $4H_S$ have been recorded. Waves with the height exceeding $2H_S$ (in some definitions $2.2H_S$) are called freak or rogue waves (Kharif et al., 2011). As they have basically the same periods as their neighbours, they are much steeper and thus much more dangerous to ships and offshore and coastal engineering structures.

The research into the properties and driving mechanisms of rogue waves has historically been focused on rogue events in deep water. A large number of ship accidents are associated to collisions with rogue waves (Toffoli et al., 2005). However, the discussed specification of rogue waves does not include any limitation for the water depth. As discussed in the Introduction, rogue waves also occur at the coast and in the nearshore. These areas are often populated by smaller (fishing or recreational) boats and yachts and by people swimming or staying on the beach. Due to the more intense use of such regions the number of accidents with smaller vessels and associated loss of lives are substantially larger in the coastal zone than in deep waters (Nikolkina and Didenkulova, 2011, 2012). This feature underlines the importance of studies into rogue waves in shallow water and in the coastal zone and in particular the necessity of their direct measurements.

The existing pool of studies of rogue events and relevant records in the coastal zone is rather limited (Chien et al., 2002; Cherneva et al., 2005; Baschek and Imai, 2011). Relatively recent studies on the statistics of rogue waves in the coastal zone of the Baltic Sea based on measurements conducted near the coast of Aegna in the northern part of Tallinn Bay have highlighted the presence of different populations of small-scale rogue waves. This area seems to host two different types of rogue waves with respect to their typical amplification factor (the ratio of the height of a single rogue wave to the significant wave height of the background wave field) (Didenkulova and Anderson, 2010; Didenkulova, 2011).

4.2. Wind wave measurements and data processing

The data set analysed in Paper IV has been collected in the southern part of Tallinn Bay in the nearshore of Pikakari Beach (Figure 16). The equipment and setup of measurements are described in Section 2.1 and in more detail in Paper I. The data used here represent a two-week (from 17 June to 1 July 2009) high-resolution and high-frequency record of water surface elevation at 5 Hz in relatively calm weather conditions. As the daytime sections of the record contain an almost incessant field of vessel-generated waves, only night data (from 0:00 to 7:00 when ship traffic was low or missing) are employed. The events associated with occasional ship passages

during the night were removed manually. Such removal was possible because ship-induced waves had a different period and a specific wake structure (Didenkulova et al., 2013b; Torsvik et al., 2015).

The records that contained only wind waves were divided into 274 sections with a duration of 20 min. Single waves were selected using both up-crossing and down-crossing methods (IAHR, 1989), after which the significant wave height H_s was calculated for each section. Although these methods led to almost coinciding statistical properties of wave fields within the sections (Figure 36), they allowed identifying different rogue wave events. The significant wave height was rather low (below 40 cm) during the entire experiment and most of the time even below 10 cm.

Following the classical rogue wave definition, single rogue waves and sequences of rogue waves (rogue events) were identified as the waves whose wave height H_f at least twice exceeds the significant wave height within the given 20-min interval, that is, the waves for which $H_f / H_s \geq 2$ (Kharif et al., 2009).

The up-crossing method revealed 51 rogue waves or events and the down-crossing method 55 rogue waves out of almost 180 000 single waves. According to a Rayleigh distribution, a rogue wave would occur once in about 3000 waves (Section 4.1); that is, about 60 times for our data set. Thus, the Rayleigh distribution tends to slightly overestimate the frequency of occurrence of rogue waves in our record. This feature matches similar results for the northern part of Tallinn Bay, near the coast of Aegna (Figure 16) (Didenkulova and Anderson, 2010).

The characteristic wave periods varied from 2 to 4 s and were sometimes even shorter. In these cases the sampling rate (5 Hz) was insufficient to properly resolve steep slopes of rogue waves (Figure 37). These records (10 identified using the up-crossing and 12 using the down-crossing method) are marked as low-resolution records in Paper IV

In addition to single rogue waves, three rogue wave groups were identified by the down-crossing method (Figure 38) on 25 June 2009 under mild wave

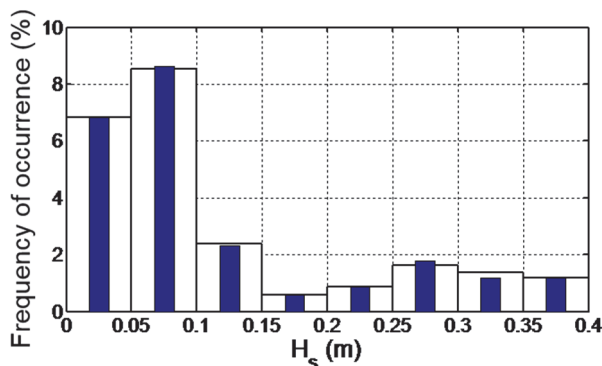


Figure 36. Frequency of occurrence of significant wave heights in different sections of the record. White and blue bars correspond to the values of H_s obtained using down-crossing and up-crossing methods, respectively (Paper IV).

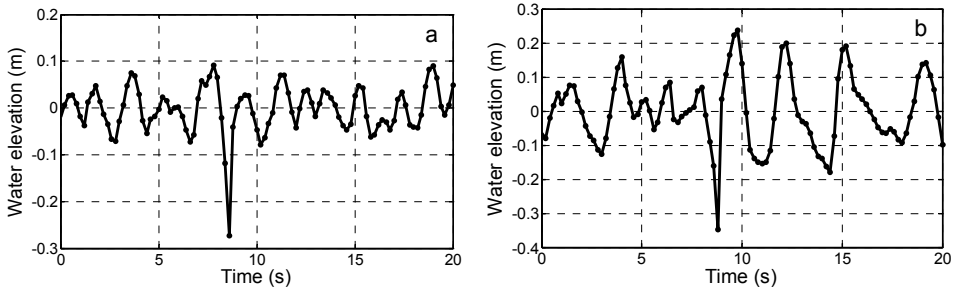


Figure 37. Examples of low-resolution short rogue waves measured on 30 June (a) and 17 June 2009 (b) (Paper IV).

conditions (wave heights no more than 15 cm). One of these events represents a typical envelope-like shape for the deep-water wave group that contains two high waves (Figure 38a).

This group was measured just before the weather changed and the wave amplitude started to grow. In other two cases two groups contained two rogue waves that were separated by slightly lower waves (Figure 38b). The periods of all three rogue waves were in the range of 1.5–1.8 s. This corresponds to values of kh in the range of 3.3–4.8 that are larger than $kh > 1.36$. Therefore the observed rogue wave groups represented deep-water rogue waves. No similar groups were identified in 2008 during an experiment near the coast of Aegna (Didenkulova and Anderson, 2010; Didenkulova, 2011).

4.3. Statistics of rogue waves in low wind conditions

A comparison of the rogue wave height H_f with the significant wave height H_s in the corresponding section of the record for different wave shapes among the total of 51+55 rogue waves (Figure 39) indicates that the identified cases are mostly close to the $H_f = 2H_s$ line. Only a few rogue waves (mostly low-resolution ones) are markedly higher than $2H_s$. This feature is consistent with the typical statistics of rogue waves (Kharif et al., 2009) as very large rogue waves are unlikely to occur in relatively short wave records.

The amplification factor (Figure 40) also indicates that this ratio is close to 2 for

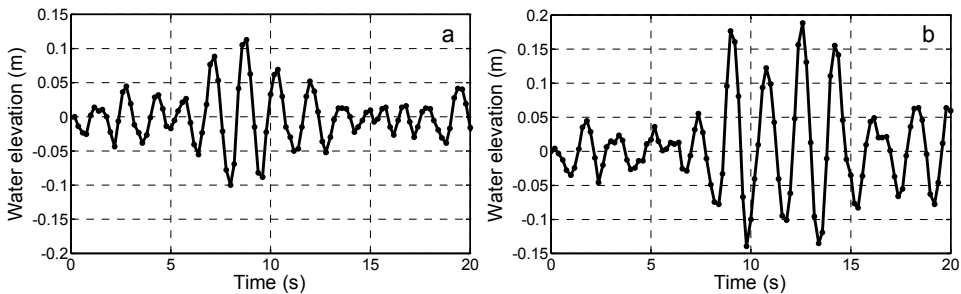


Figure 38. Groups of rogue waves measured on 25 June 2009 (Paper IV).

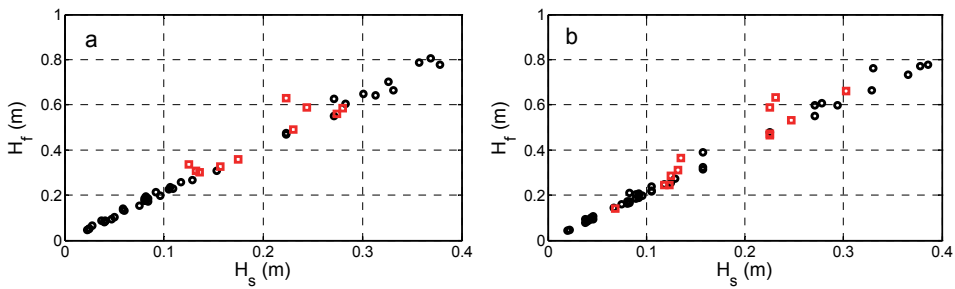


Figure 39. Scatter diagram for rogue wave height H_f and significant wave height H_s for rogue waves identified using up-crossing (a) and down-crossing (b) approaches. Red squares correspond to low-resolution rogue waves (Paper IV).

larger rogue waves but is occasionally much larger for some low resolution rogue waves. This feature was also observed in 2008 near the coast of Aegna (Didenkulova and Anderson, 2010). Similarly to the analysis in Didenkulova and Anderson (2010), no clear relationship between the amplification factor and H_f or H_s can be identified.

The distributions of the frequency of occurrence of the heights of the two rogue wave sets identified from the up-crossing and down-crossing analysis (Figure 41) are fairly similar. This feature suggests that the associated distributions of the steepness of front and rear slopes are also similar. Smaller rogue waves (<20 cm) tend to have a steep front. The majority of low-resolution waves had intermediate values of H_f (30–70 cm).

The distribution of the heights of rogue wave crests and troughs (measured from the undisturbed water surface, Figure 42) reveals a certain asymmetry. At a very low wave background (wave amplitudes below 10 cm) rogue waves have more likely a deep wave trough, while for wave fields with amplitudes over 40 cm the presence of a high rogue crest is more probable.

4.4. Run-up of severe storm waves on the Estonian coast

Paper V focuses on the problem of the evaluation of maximum inundation on

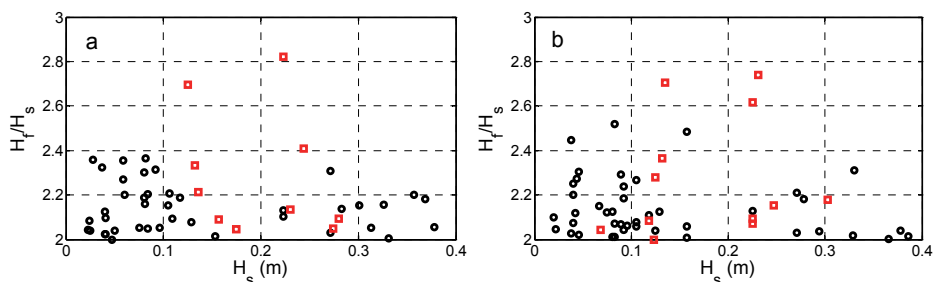


Figure 40. Amplification factor of rogue waves identified using up-crossing (a) and down-crossing (b) approaches. Red squares show low-resolution rogue waves (Paper IV).

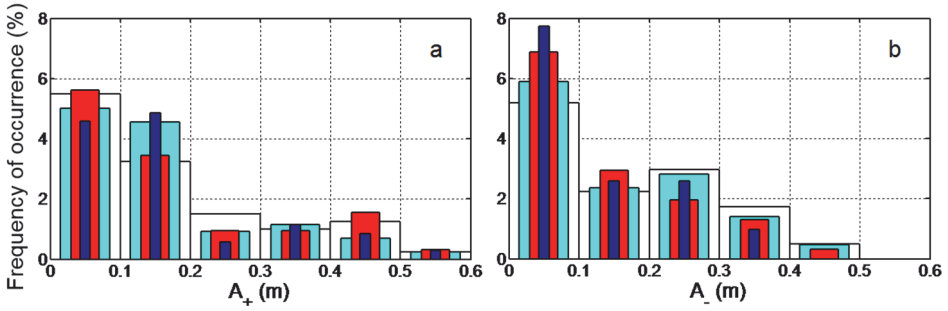


Figure 41. Distributions of the crest heights A_+ (a) and trough depressions A_- of rogue events (b). White and red bars correspond to all rogue events found using the up-crossing method and to only high-resolution events respectively; light and dark blue bars correspond to all rogue events found by the down-crossing method and to only high-resolution events, respectively (Paper IV).

selected segments of the Estonian coasts of the Baltic Sea through wave run-up during the severest storms. The idea was to compare the results of calculations based on Eqs. (1) and predictions of the common relationships for the dependence of the run-up height on the beach slope α and the incident wave height H that are often used in coastal engineering.

More than half century ago Hunt (1959) proposed the following empirical formula for the run-up height R based on numerous flume tests:

$$R = H\xi, \text{ where } \xi = \alpha \sqrt{\frac{\lambda}{H_0}}. \quad (33)$$

Here H_0 is the mean wave height and λ is the length of incident waves in deep water. The quantity ξ is the so-called Iribarren number, also called the surf-similarity parameter.

Battjes (1974) included significant wave height H_S into Eq. (33) instead of mean wave height. The maximum run-up height on a dissipative sandy beach can be described as a linear function of H_S (Guza and Thornton, 1982):

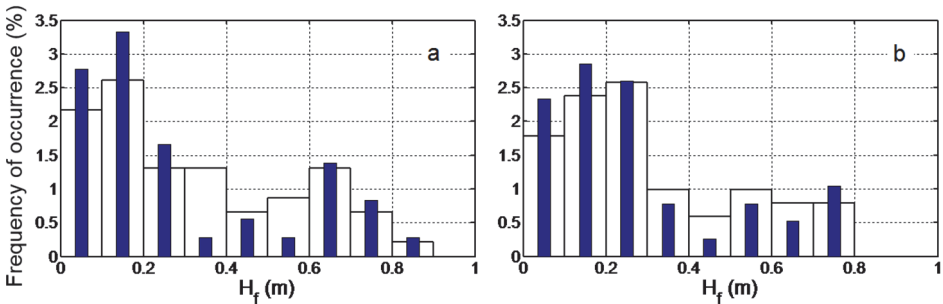


Figure 42. Distributions of rogue wave heights identified using the up-crossing (a) and down-crossing (b) approaches. White columns correspond to the full rogue wave dataset and blue columns to high-resolution events (Paper IV).

$$R = 0.035 + 0.71H_s . \quad (34)$$

Powell (1990) introduced the following expression for the highest run-up on a gravel beach based on experiments with random waves in a flume:

$$R = H_s \left(2.86 - 62.69 \left(\frac{H_s}{\lambda} \right) + 443.29 \left(\frac{H_s}{\lambda} \right)^2 \right). \quad (35)$$

Sandy beaches may be fairly different, from reflective to dissipative ones. Based on extensive measurements, Holman (1986) and Nielsen and Hanslow (1991) proposed the following formula for beaches with slopes <0.1 :

$$R = 0.05 \sqrt{H_{rms} \lambda}, \quad (36)$$

where $H_{rms} = H_s / \sqrt{2}$ is the deep-water rms wave height. As most of Estonian sedimentary coasts have gentle slopes, almost all the profiles used in Paper V are flatter than this value. For beaches with slopes ≥ 0.1 the run-up height is

$$R = 0.6\xi. \quad (37)$$

Wave conditions along the entire Estonian coast have been extracted from 35-year wind wave simulations with the wave model WAM forced by COSMO winds in the presence of ice (Nikolkina et al., 2014). The analysis is applied to a pool of representative beach profiles along the Estonian Baltic Sea coast, where repeated topographic profilings have been performed by the Geological Survey of Estonia in the framework of the state monitoring programme of beaches (Figure 43). Small-scale and temporary features of these profiles were eliminated and the most typical bottom profile for each beach was specified by using an average of the entire set of the profiles measured in 2006–2011 (Suuroja et al., 2007, 2008, 2009, 2010, 2011) in 18 different locations of the Estonian coast. If the profile was too short for numerical calculations (incl. the cases when its highest point remained below the maximum run-up height of the severest numerically modelled waves), it was extended using GEBCO maps (<http://www.gebco.net>). The range of beach slopes turned out very diverse: from 0.009 for Harilaid to 0.121 for Naissaar coasts. Most of the slopes were, however, between 0.02 and 0.05.

The maximum significant wave heights and corresponding peak periods in these locations were detected in the grid cells of the WAM model nearest to the shoreline. Such cells had water depths from 9 to 28 m and were located at distances from 1 to 8 km from the shore (Paper V). The peak periods during the roughest seas varied from 8 to 11 s and the significant wave heights ranged between 3.3 and 7.5 m.

The run-up of waves on the selected beaches was evaluated in Paper V in the framework of the shallow-water approximation using the CLAWPACK software package (Section 1.2) and the above-described measured profiles. The time and space steps were 1 m and 1 s, respectively, in all calculations. The beaching waves

were assumed to be regular and monochromatic (with the height matching the numerically simulated largest significant wave height and the associated peak period matching the simulated period) and to approach the shore incidentally. While the first two assumptions are realistic and widely used, in many occasions the highest waves approach the Estonian coastline under relatively large angles (Soomere et al., 2013; Viška and Soomere, 2013).

Wave parameters, numerically calculated run-up heights and inundation distances (Paper V) suggest that the maximum run-up heights of about 3 m are likely at Aegna, Naissaar and Osmussaar. Such events may lead to the flooding of several houses located near the waterline on Aegna where the inundation distance can be up to 35 m. Large inundation distances (23–27 m) are likely at Osmussaar, Nõva (where the run-up height was modest, about 1.2 m) and Harilaid (run-up height 1.6 m). The wave run-up of about 2 m is expected at the Kakumäe location but owing to the large coastal slope the inundation distance is only 14 m. This densely populated area is, however, highly vulnerable to wave-induced hazards. The inundation distance was comparatively large, 19 m, for Pirita. In other considered locations the maximum run-up heights were below 1.6 m and the associated inundation distances less than 14 m.

Express formulas (34) and (35) generally provide larger estimates of run-up heights than numerical results (Figure 44). The mismatch apparently stems from the specific type of the studied beaches (Soomere and Healy, 2011), to which these formulas are not directly applicable. For instance, Eq. (35) was elaborated based on experiments (Powell, 1990) with random waves in a 42 m long flume with a water

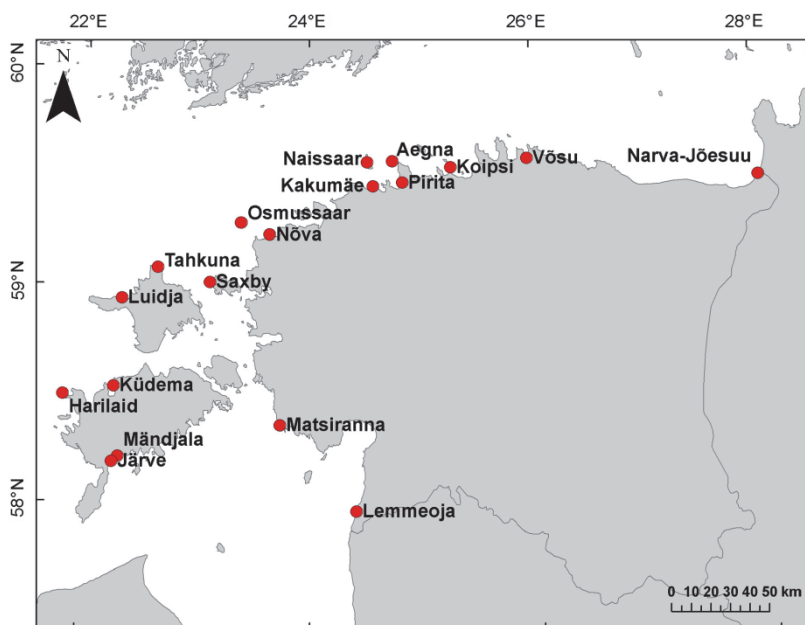


Figure 43. Locations of 18 beach profiles along Estonian coasts used in Didenkulova et al. (2013b) and Paper V.

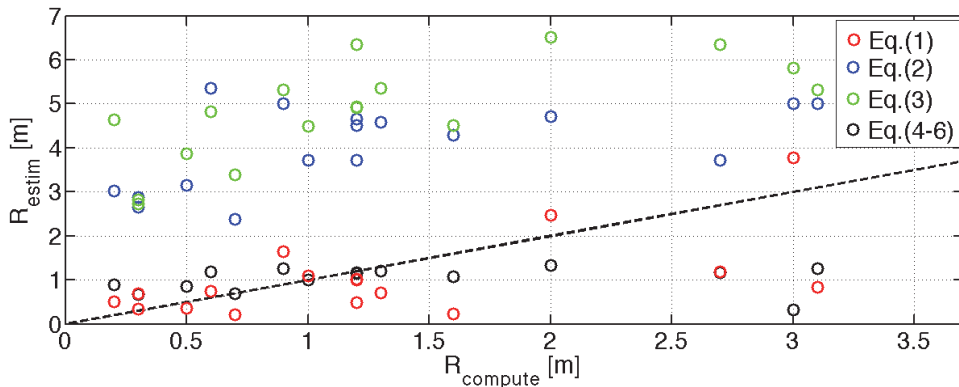


Figure 44. Comparison of calculated and estimated run-up heights (Paper V).

depth of 0.7–0.9 m. The composition of the beach matched the granular composition of typical United Kingdom beaches. Consistently with this feature, Eq. (35) gives a reasonable estimate for gravel beaches at the shores of Aegna and Osmussaar (Paper V).

The linear dependence of the run-up height on the wave height expressed in Eq. (34) obviously has a limited scope of applicability. It was elaborated for dissipative sandy beaches based on field data from the Pacific coast of the United States of America (California, Torrey Pines Beach). The underlying data set included only certain wave regimes from those that occur in this area. The beach slope varied between 0.02 and 0.05 and incident wave heights from 0.5 to 1.5 m (that is, much less than the above-considered values for Estonian coasts). The mismatch between the estimates using Eq. (34) and simulated results is thus not surprising.

The match of the results in Paper V with the outcome of approximations (33) and (36)–(37) is better apparently because some of the wave regimes used in their derivation overlapped with those applied at the Estonian coasts. Formula (33) was

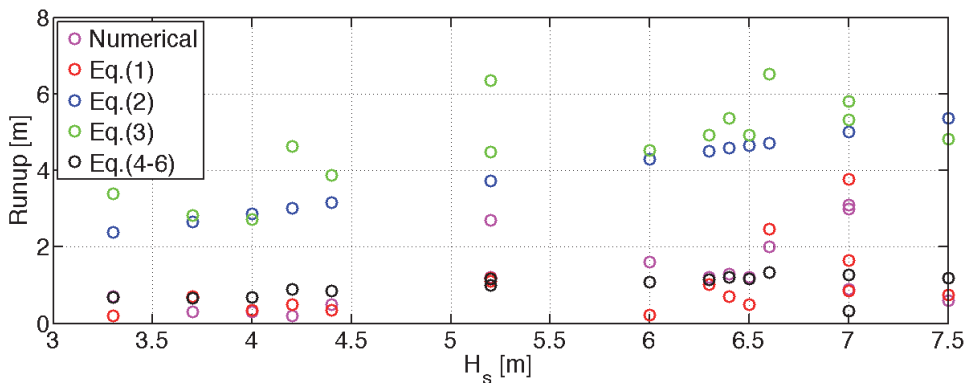


Figure 45. Calculated and estimated run-up heights versus significant wave height (Paper V).

based on flume experiments, where run-up heights were measured on a porous, rough beach with a constant slope from 0.1 to 0.33 (Hunt, 1959). The data set covers a wide range of wave regimes. Approximations (36)–(37) were derived using field data from natural beaches of the US Atlantic coast in North Carolina. The incident wave heights varied from 0.4 to 4 m (Holman, 1986), wave periods from 6 to 16 s and beach slopes from 0.07 to 0.20.

Although all listed express formulas and simulations show that the run-up height increases with an increase in the significant wave height (Figure 45), the growth rates estimated from different approximations are fairly different. The smallest growth is observed for approximations (33) and (36)–(37) (Figure 46).

In conclusion, the run-up heights of extreme wind waves estimated by some widely used engineering formulas match well the numerical calculations performed in the framework of nonlinear shallow-water theory. However, some express formulas deviate from these calculations.

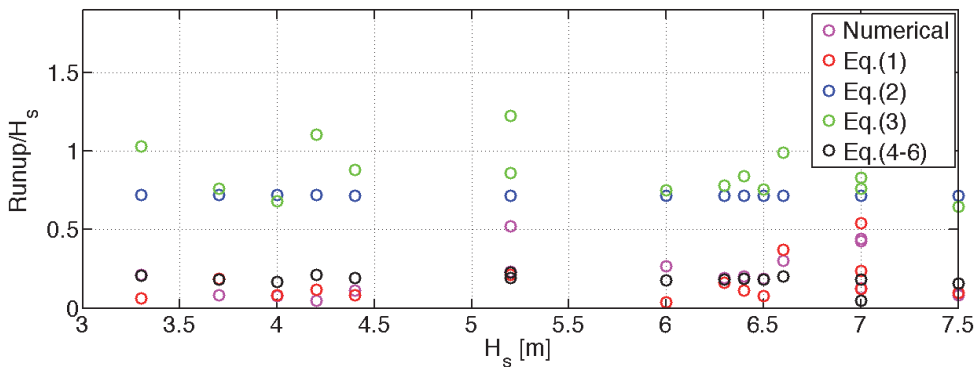


Figure 46. Wave amplification on the beach (ratio of the run-up height to the significant wave height) versus significant wave height (Paper V).

Conclusions

Summary of the results

The presented studies address various aspects of the propagation, transformation, reflection and run-up of long strongly nonlinear waves in idealized conditions and in the marine environment. The focus is on the long-term evolution of solitary waves of both polarities and on the properties of the run-up of extreme storm waves and short wave groups excited by ships sailing in relatively shallow water.

The run-up of long partially breaking solitary waves of elevation and depression was studied numerically in the framework of the nonlinear shallow-water theory for a composite beach geometry where a section of constant depth ends with a sloping beach. An increase in the initial amplitude of waves of elevation leads to an increase in the run-up height of wave crests. The run-down height first increases but decreases for even larger waves and almost vanishes for very large waves. The properties of the run-up of waves of depression (single troughs) vary in a qualitatively similar manner. The asymmetry of the process becomes clearly evident for large waves: a shock wave is formed at the rear slope of depressions. Both run-up and run-down heights of waves of depression increase with an increase in the initial wave amplitude, resulting in comparable magnitudes of flood and ebb distances. Thus, an initially negative pulse is able to exert substantial run-up on a beach. Nonlinear effects impact the waves of depression more strongly than the waves of elevation and lead to wave breaking and energy dissipation.

The experiments conducted at Pikakari Beach in Tallinn Bay, the Baltic Sea, show that a Weibull distribution appropriately describes the distribution of both offshore wave heights and the corresponding run-up heights of waves generated by large ships sailing at reasonable Froude numbers. The run-up of vessel waves is, on average, about 3.5 times as large as their height at a distance of 100 m from the shoreline. Owing to the characteristic group structure of the wake of such vessels (the largest and longest waves are followed by lower and shorter waves), large run-up heights occur during almost the entire duration of the wake. This feature may result in uncommonly large impact of vessel wakes on the shore, the rapid beach erosion included. This property is further enhanced by the impact of breaking on the run-up of the largest waves. Smaller waves (<20 cm) exert relatively large run-up and can be described in terms of long non-breaking waves on a plane beach.

Based on measurements in the Venice Lagoon it was shown that unexpectedly high (up to 2.5 m) solitary depression waves were generated by moderately-sized ships sailing at moderate depth Froude numbers (<0.5) and blocking coefficients (<0.14) in the Malamocco–Marghera channel with shallow banks. These extremely long (typical periods of 40–50 s and lengths of 250–300 m) waves were described in terms of nonlinear simple or Riemann waves in very shallow water (2–3 m). Nonlinear effects rapidly (within less than 10 s and over a distance of a few tens of metres) build up a steep, bore-like rear slope of such waves. A temporary step-like profile of the rear slope is also occasionally observed.

The possibility for these depression waves to propagate virtually freely away from the navigation channel and to penetrate onto wide and shallow shoals (estuary, river bank, shallow lagoon, etc.) was analysed numerically. These extremely long waves experience transformations characteristic of strongly nonlinear Riemann waves on the water surface. Their front keeps a modest slope but their rear develops an extremely steep, near-breaking slope, or even a bore-like feature at a distance of much less than 100 m from the channel margin. The resulting water velocities and the overall possible environmental impact are likely much larger than those derived from common expressions for linear or weakly nonlinear waves.

The simulations demonstrate that disturbances of considerable amplitude continue to move as a strongly nonlinear wave to a substantial distance. Their amplitudes rapidly (within 20–30 s) level off and the multi-step structure of the rear slope disappears. The disturbance obtains a shape characteristic of Riemann waves of depression: a relatively gentle slope followed by a steep rear.

The amplitude of these solitary waves of depression for the disturbances that are representative of the wakes frequently occurring in the Venice Lagoon remains at dangerous levels (>0.3 m) for distances of more than 1 km in the idealized 2 m deep lagoon. As the lagoon depth is commonly even smaller, the nonlinear effects are eventually greater than in the performed simulations and the steep bore-like feature may persist for an even longer time. The heights of all such depressions become almost independent of their initial properties. This suggests that even ships of inconsiderable size, sailing speed and blocking coefficient may generate wakes that travel as compact entities over extensive areas of the lagoon and provide increased levels of environmental impact.

The frequency of occurrence of rogue waves (waves whose height is at least twice the significant wave height) in low wave conditions in the nearshore was studied based on the two-week high-resolution record of the water surface in the coastal zone of the Baltic Sea. Rogue waves were identified using both zero-upcrossing and zero-downcrossing methods. A Rayleigh distribution slightly overestimates the frequency of occurrence of rogue waves. Almost all rogue waves, except the three identified by the down-crossing method, are single waves. In very low wave conditions (wave amplitudes <10 cm) it is more probable to meet a single rogue trough than a high wave crest, while for wave amplitudes >40 cm a high crest is more probable. For smaller waves (wave heights below 20 cm) a steep front can be observed, rather than a steep rear slope.

The specific coastal hazard associated with unexpected run-up of severe storm waves was assessed for a selection of Estonian coasts on 35-year wind wave simulations with the WAM model forced by COSMO winds. The wave run-up height and inundation distance were evaluated numerically using nonlinear shallow-water theory. The results were used to analyse the applicability of common empirical express formulas to wind wave run-up. It was shown that the most vulnerable zones among the selected segments were located at the coasts of Aegna and in the Kakumäe area.

Main conclusions proposed to defend

1. The properties of the run-up of long strongly nonlinear solitary waves of different polarities were compared on the basis of numerical simulations using the CLAWPACK software. Nonlinear effects and energy dissipation caused by wave breaking are more prominent for waves of depression rather than for waves of elevation.
2. Interrelations between the heights of single waves and their run-up heights were analysed for transient groups of waves generated by large ships sailing at a relatively large speed in water of limited depth. The experimental data from Tallinn Bay, the Baltic Sea, show that both wave heights and the associated run-up heights are well described by a Weibull distribution. On average, the run-up heights of vessel waves are ~ 3.5 times as large as their heights at a distance 100 m from the shoreline.
3. The main reason for a long sequence of very large run-up heights during almost the entire duration of the wave wake from vessels sailing at relatively large depth Froude numbers is the chirp structure (the largest and longest waves are followed by lower and shorter waves) of such wakes. This feature may be a major reason for the rapid reaction of beaches to fast vessel wakes.
4. Based on the measurements in the Venice Lagoon it is shown that up to 2.5 m high solitary depression waves are generated by ships of moderate size sailing in a navigation channel with shallow banks. These waves, interpreted as strongly nonlinear simple or Riemann waves, rapidly build up a bore-like rear slope and occasionally a step-like profile. Their main properties are replicated using the CLAWPACK software.
5. The penetration of vessel-generated solitary depression waves into the Venice Lagoon was analysed numerically using the nonlinear shallow-water theory and the CLAWPACK software. The measured depressions were replicated using initially smooth free waves. It is demonstrated that vessel-driven depressions of substantial height (>30 cm) often propagate for more than 1 km into the lagoon. Their front slopes become gradually less steep but the rear slopes preserve extremely steep bore-like appearance.
6. The properties of small-scale rogue waves in the coastal zone were studied based on the experimental data measured in Tallinn Bay, the Baltic Sea. The rogue wave troughs are more likely to occur at low wind wave conditions (amplitudes below 10 cm), while rogue wave crests are more probable for wave amplitudes over 40 cm.
7. The potential of unexpected run-up of severe storm waves on Estonian coasts was assessed based on a 35-year wave reconstruction. It is demonstrated that several express methods for run-up properties are not applicable to storm waves on the Estonian coasts. The most vulnerable coastal segments in terms of inundation were found on the island of Aegna and in the Kakumäe area.

Recommendations for further work

Several results of this thesis have been obtained in highly idealized situations and are thus only conditionally applicable to the practical use in the marine environment or in other water bodies. A relatively simple first step would be to understand whether or how long various disturbances maintain a certain information about their initial shape, equivalently, for which distances it is acceptable to replace the initial (e.g., vessel-induced) wave by a smooth counterpart that only matches the core feature of the disturbance. Combined with the feature established in the thesis (that after a certain propagation time the height of the waves of depression mostly depends on the propagation distance), this knowledge may eventually be converted into simple express formulas and methods for the evaluation of far-field properties and associated environmental impact of, e.g., ship-induced waves of depression.

A major limitation is that the analysis, although it takes various nonlinear effects into account, is restricted to the one-dimensional setting in the framework considering the waves approaching perpendicular to the coast. Even though this viewpoint is often acceptable in the open ocean conditions where remote swells frequently approach the shore almost incidentally, in the majority of realistic cases, from ship wakes to tsunamis, the waves either approach the coast obliquely or the nearshore cannot be adequately approximated by a plane seabed. Therefore, in order to obtain more reliable results for applications it is necessary to establish how the disturbances addressed in the thesis would behave in common versions of the two-dimensional geometry of the basin. This research should be complemented with a detailed analysis of the processes that occur if such disturbances obliquely approach a shore with a simple geometry. A further research in this direction would involve running simulations of the propagation of long nonlinear waves on a real bathymetry to take all local bathymetric and topographic effects into account.

A justification of the simple classical model of nonlinear shallow-water dynamics used in this thesis is its simplicity that allows for straightforward interpretation of a large part of the results and to a certain extent guarantees the applicability and stability of the numerical scheme. Its major drawback is that it neglects several core processes that intrinsically affect the dynamics of waves in the marine environment such as dispersion and dissipation. Also, wave breaking is considered in a rather primitive and generalized way, so that many related processes, from whitecapping to various kinds of wave transformation due to wave plunging or spilling, are not taken into account. In order to evaluate the adequacy of this simplified approach, I definitely plan to address these effects with more advanced models, such as fully nonlinear Euler or Navier–Stokes equations, potential flow theory, or SPH-models.

Although, formally, the framework of Riemann waves seems to have very good performance for the replication of properties of long-living ship-induced depressions in very shallow water, the results should still be understood as indicative. The technique of Riemann waves has been developed and works

properly for acoustic waves but water waves are intrinsically different. In particular, the results and scenarios that incorporate self-reflection of the deepest part of the trough may be problematic and cannot be relied upon without a further proof. The obtained results are definitely correct within the limits of shallow-water approximation used in the thesis but real water waves are a part of a much more complicated system. It is likely that the formation of a steep rear of such waves is accompanied by intense generation of turbulence. This process may suppress or even prevent the self-reflection. To shed further light on this problem, I would like to re-model the propagation of deep solitary depression waves using fully nonlinear (and fully dispersive) Navier–Stokes equations, for example, using the popular MITgcm model.

Finally, the thesis does not address the most intriguing question why ships of moderate size and sailing at fairly low Froude numbers produced exceptionally large waves of depression in the Malamocco–Marghera channel but at the same time virtually failed to produce any considerable waves of elevation or undulations. It is likely that the reason is somehow connected to the specific geometry of the situation: the navigation channel has wide shallow banks. Further numerical experiments with fully nonlinear three-dimensional equations of hydrodynamics may shed light to this question as well, and I would like to initiate such experiments in the future.

Bibliography

- Akylas T. 1984. On the excitation of long nonlinear water waves by a moving pressure distribution. *Journal of Fluid Mechanics*, 141, 455–466.
- Ali M.M., Murphy K.J., Langendorff J. 1999. Interrelations of river ship traffic with aquatic plants in the River Nile, Upper Egypt. *Hydrobiologia*, 415, 93–100.
- Antuono M., Brocchini M. 2007. The boundary value problem for the nonlinear shallow water equation. *Studies in Applied Mathematics*, 119, 71–91.
- Antuono M., Brocchini M. 2008. Maximum run-up, breaking conditions and dynamical forces in the swash zone: a boundary value approach. *Coastal Engineering*, 55, 732–740.
- Antuono M., Brocchini M. 2010. Solving the nonlinear shallow-water equations in physical space. *Journal of Fluid Mechanics*, 643, 207–232.
- Arcas D., Segur H. 2012. Seismically generated tsunamis. *Philosophical Transactions of the Royal Society*, 370, 1505–1542.
- Arseniev A.S., Shelkovnikov N.K. 1991. *Dynamics of Long Sea Waves*. Moscow: Moscow State University, 88 pp. (in Russian)
- Baines P.G. 1997. *Topographic Effects in Stratified Flows*. Cambridge University Press, XVI, 482 pp.
- Balzerek H., Kozłowski J. 2007. Ship-induced riverbank and harbour damage. Evidence for claims processing. *Hydro International*, 11(8), 2–7.
- Baschek B., Imai J. 2011. Rogue wave observations off the US west coast. *Oceanography*, 24(2), 158–165.
- Battjes J.A. 1971. Long-term wave height distributions at seven stations around the British Isles. *Deutsche Hydrographische Zeitschrift*, 25, 179–189.
- Battjes J.A. 1974. Runup distributions of waves breaking on slopes. *Journal of the Waterways, Harbors, and Coastal Engineering*, 97(WW1), 91–114.
- Belibassakis K.A. 2003. A coupled-mode technique for the transformation of ship-generated waves over variable bathymetry regions. *Applied Ocean Research*, 25, 321–336.
- Benjamin T.B., Lighthill M. J. 1954. On cnoidal waves and bores. *Proceedings of the Royal Society of London A*, 224, 448–460.
- Berger M., George D., LeVeque R.J., Mandli K. 2011. The GeoClaw software for depth-averaged flows with adaptive refinement. *Advances in Water Resources*, 34(9), 1195–1206.
- Bernatskiy A., Nosov M. 2012. The role of bottom friction in models of nonbreaking tsunami wave runup on the shore. *Izvestiya, Atmospheric and Oceanic Physics*, 48, 427–431.
- Bitner-Gregersen E.M., Eide L.I., Hørte T., Skjong R. 2013. *Ship and Offshore Structure Design in Climate Change Perspective*. Springer Briefs in Climate Studies, 69 pp.

- Brambati A., Carbognin L., Quaia T., Teatini P., Tosi, L. 2003. The Lagoon of Venice: geological setting, evolution and land subsidence. *Episodes*, 26(3), 264–265.
- Brown E.D., Buchsbaum S.B., Hall R.E., Penhune J.P., Schmitt K.F., Watson K.M., Wyatt D.C. 1989. Observations of a nonlinear solitary wave packet in the Kelvin wake of a ship. *Journal of Fluid Mechanics*, 204, 263–293.
- Caputo J.-G., Stepanyants Y.A. 2003. Bore formation, evolution and disintegration into solitons in shallow inhomogeneous channels. *Nonlinear Processes in Geophysics*, 10, 407–424.
- Carrier G.F., Greenspan H.P. 1958. Water waves of finite amplitude on a sloping beach. *Journal of Fluid Mechanics*, 4, 97–109.
- Carrier G.F., Wu T.T., Yeh H. 2003. Tsunami run-up and draw-down on a plane beach. *Journal of Fluid Mechanics*, 475, 79–99.
- Chambarel J., Kharif C., Touboul J. 2009. Head-on collision of two solitary waves and residual falling jet formation. *Nonlinear Processes in Geophysics*, 16, 111–122.
- Cherneva Z., Petrova P., Andreeva N., Guades Soares C. 2005. Probability distributions of peaks, troughs and heights of wind waves measured in the black sea coastal zone. *Coastal Engineering*, 52, 599–615.
- Chien H., Kao C.-C., Chuang L.Z.H. 2002. On the characteristics of observed coastal freak waves. *Coastal Engineering Journal*, 44(4), 301–319.
- Choi B.H., Pelinovsky E., Kim D.C., Didenkulova I. 2008. Two and three-dimensional computation of solitary wave runup on non-plane beach. *Nonlinear Processes in Geophysics*, 15, 489–502.
- Constantine T. 1961. On the movement of ships in restricted waterways. *Journal of Fluid Mechanics*, 9, 247–256.
- Courant R., Friedrichs K.O. 1948. *Supersonic flow and shock waves*. Interscience Publishers, New York, XVI, 464 pp.
- Darmon A., Benzaquen M., Raphael E. 2014. Kelvin wake pattern at large Froude numbers. *Journal of Fluid Mechanics*, 738, R3.
- Dean R.G., Bender C.J. 2006. Static wave set-up with emphasis on damping effects by vegetation and bottom friction. *Coastal Engineering*, 53, 149–165.
- Dean R.G., Dalrymple R.A. 1991. *Water Wave Mechanics for Engineers and Scientists*. World Scientific, 353 pp.
- Denissenko P., Didenkulova I., Pelinovsky E., Pearson J. 2011. Influence of the nonlinearity on statistical characteristics of long wave runup. *Nonlinear Processes in Geophysics*, 18, 967–975.
- Denissenko P., Didenkulova I., Rodin A., Listak M., Pelinovsky E. 2013. Experimental statistics of long wave runup on a plane beach. *Journal of Coastal Research*, Special Issue 65, 195–200.

- Didenkulova I. 2009. New trends in the analytical theory of long sea wave runup. In: Quak E., Soomere T. (eds.), *Applied Wave Mathematics: Selected Topics in Solids, Fluids, and Mathematical Methods*. Springer, 265–296.
- Didenkulova I. 2011. Shapes of freak waves in the coastal zone of the Baltic Sea (Tallinn Bay). *Boreal Environment Research*, 16(Suppl. A), 138–148.
- Didenkulova I., Anderson C. 2010. Freak waves of different types in the coastal zone of the Baltic Sea. *Natural Hazards and Earth System Sciences*, 10(9), 2021–2029.
- Didenkulova I., Pelinovsky E. 2008. Run-up of long waves on a beach: The influence of the incident wave form. *Oceanology*, 48, 1–6.
- Didenkulova I., Pelinovsky E. 2009. Non-dispersive traveling waves in inclined shallow water channels. *Physics Letters A*, 373(42), 3883–3887.
- Didenkulova I., Pelinovsky E. 2011a. Nonlinear wave evolution and runup in an inclined channel of a parabolic cross-section. *Physics of Fluids*, 23 (8), 086602.
- Didenkulova I., Pelinovsky E. 2011b. Rogue waves in nonlinear hyperbolic systems (shallow-water framework). *Nonlinearity*, 24, R1–R18.
- Didenkulova I., Pelinovsky E. 2011c. Runup of tsunami waves in U-shaped bays. *Pure and Applied Geophysics*, 168, 1239–1249.
- Didenkulova I., Soomere T. 2011. Formation of two-section cross-shore profile under joint influence of random short waves and groups of long waves. *Marine Geology*, 289, 29–33.
- Didenkulova I., Zahibo N., Kurkin A.A., Levin B.V., Pelinovsky E.N., Soomere T. 2006a. Runup of nonlinearly deformed waves on a coast. *Doklady Earth Sciences*, 411, 1241–1243.
- Didenkulova I., Zahibo N., Kurkin A., Pelinovsky E.N. 2006b. Steepness and spectrum of a nonlinearly deformed wave on shallow waters. *Izvestiya, Atmospheric and Oceanic Physics*, 42, 773–776.
- Didenkulova I., Kurkin A., Pelinovsky E. 2007a. Run-up of solitary waves on slopes with different profiles, *Izvestiya, Atmospheric and Oceanic Physics*, 43, 384–390.
- Didenkulova I., Pelinovsky E., Soomere T., Zahibo N. 2007b. Runup of nonlinear asymmetric waves on a plane beach. In: Kundu A. (ed.), *Tsunami and nonlinear waves*, Springer Berlin Heidelberg, 175–190.
- Didenkulova I., Pelinovsky E., Soomere T. 2008. Run-up characteristics of tsunami waves of “unknown” shapes. *Pure and Applied Geophysics*, 165, 2249–2264.
- Didenkulova I., Parnell K.E., Soomere T., Pelinovsky E., Kurennoy D. 2009a. Shoaling and runup of long waves induced by high-speed ferries in Tallinn Bay. *Journal of Coastal Research*, Special Issue 56, 491–495.
- Didenkulova I., Pelinovsky E., Soomere T. 2009b. Long surface wave dynamics along a convex bottom. *Journal of Geophysical Research–Oceans*, 114, C07006.

- Didenkulova I.I., Sergeeva A.V., Pelinovsky E.N., Gurbatov S.N. 2010. Statistical estimates of characteristics of long-wave run-up on a beach. *Izvestiya, Atmospheric and Oceanic Physics*, 46, 530–532.
- Didenkulova I., Pelinovsky E., Rodin A. 2011a. Nonlinear interaction of large-amplitude unidirectional waves in shallow water. *Estonian Journal of Engineering*, 17(4), 289–300.
- Didenkulova I., Pelinovsky E., Sergeeva A. 2011b. Statistical characteristics of long waves nearshore. *Coastal Engineering*, 58, 94–102.
- Didenkulova I., Pelinovsky E., Soomere T. 2011c. Can the waves generated by fast ferries be a physical model of tsunami? *Pure and Applied Geophysics*, 168, 2071–2082.
- Didenkulova, I.I., Nikolkina, I.F., Pelinovsky, E.N. 2013. Rogue waves in the basin of intermediate depth and the possibility of their formation due to the modulational instability. *JETP Letters*, 97(4), 194–198.
- Didenkulova I., Denissenko P., Rodin A., Pelinovsky E. 2013a. Effects of wave asymmetry on its runup on a beach. *Journal of Coastal Research*, Special Issue 65, 207–212.
- Didenkulova I., Sheremet A., Torsvik T., Soomere T. 2013b. Characteristic properties of different vessel wake signals. *Journal of Coastal Research*, Special Issue 65, 213–218.
- Didenkulova I., Soomere T., Pindsoo K., Suuroja S. 2013c. On the occurrence of non-reflecting cross-shore profiles along Estonian coasts of the Baltic Sea, *Estonian Journal of Engineering*, 19(2), 110–123.
- Didenkulova I.I., Pelinovsky E.N., Didenkulov O.I. 2014. Run-up of long solitary waves of different polarities on a plane beach. *Izvestiya, Atmospheric and Oceanic Physics*, 50(5), 532–538.
- Dobrokhotov S.Y., Tirozzi B. 2010. Localized solutions of one-dimensional non-linear shallow-water equations with velocity $c = x^{1/2}$. *Russian Mathematical Survey*, 65, 177–179.
- Docherty N.J., Chanson H. 2010. Characterization of unsteady turbulence in breaking tidal bores including the effects of bed roughness. In: *Hydraulic Model Report No. CH76/10*, School of Civil Engineering, University of Queensland, Australia, 112 pp.
- Dutykh D., Labart C., Mitsotakis D. 2011. Long wave runup on random beaches. *Physical Review Letters*, 107, Art. No. 184504.
- Dysthe K., Krogstad H.E., Muller P. 2008. Oceanic rogue waves. *Annual Review of Fluid Mechanics*, 40, 287–310.
- El-Kader F.A., El-Soud M.S.A., El-Serafy K., Hassan E.A. 2003. An integrated navigation system for Suez Canal (SCINS). *Journal of Navigation*, 56, 241–255.

- Engelbrecht J.K., Fridman V.E., Pelinovski E.N. 1988. *Nonlinear Evolution Equations, Pitman Research Notes in Mathematics Series*. Longman Scientific and Technical, London, 180, 121 pp.
- Erm A., Soomere T. 2006. The impact of fast ferry traffic on underwater optics and sediment resuspension. *Oceanologia*, 48(S), 283–301.
- Erm A., Alari V., Lips I., Kask J. 2011. Resuspension of sediment in a semi-sheltered bay due to wind waves and fast ferry wakes. *Boreal Environment Research*, 16, 149–163.
- Ertekin R.C., Webster W.C., Wehausen J.V. 1984. Ship-generated solitons. In: *Proceedings of 15th Symposium on Naval Hydrodynamics*, Hamburg, Federal Republic of Germany, September 2–7, National Academy Press, Washington, D.C., 347–364.
- Ertekin R.C., Webster W.C., Wehausen J.V. 1986. Waves caused by a moving disturbance in a shallow channel of finite width. *Journal of Fluid Mechanics*, 169, 275–292.
- Ezersky A., Abcha N., Pelinovsky E. 2013a. Physical simulation of resonant wave run-up on a beach. *Nonlinear Processes in Geophysics*, 20, 35–40.
- Ezersky A., Tiguercha D., Pelinovsky E. 2013b. Resonance phenomena at the long wave run-up on the coast. *Natural Hazards and Earth System Sciences*, 13, 2745–2752.
- Favre H. 1935. *Etude Théorique et Expérimentale des Ondes de Translation dans les Canaux Découverts (Theoretical and Experimental Study of Travelling Surges in Open Channels)*, Dunod Edition, Paris, France, 215 pp. (in French).
- Fernando H.J.S., Braun A., Galappatti R., Ruwanpura J., Wirisinghe S.C. 2008. Tsunamis: manifestation and aftermath. In: *Large Scale Disasters*, Cambridge University Press, Cambridge, 258–292.
- Forsman B. 2001. From bow to beach. *SSPA Highlights*, 3, 4–5.
- Garel E., Fernández L.L., Collins M. 2008. Sediment resuspension events induced by the wake wash of deep-draft vessels. *Geo-Marine Letters*, 28, 205–211.
- Garrett C., Gemmrich J. 2009. Rogue Waves. *Physics Today*, 62(6), 62–63.
- Gelinas M., Bokuniewicz H., Rapaglia J., Lwiza K.M.M. 2013. Sediment resuspension by ship wakes in the Venice Lagoon. *Journal of Coastal Research*, 29, 8–17.
- Glukhovskiy B.H. 1966. *Issledovanie morskogo vetrovogo volnenia (Study of sea wind waves)*. Leningrad, Gidrometeoizdat, 283 pp. (in Russian).
- Göransson G., Larson M., Althage J. 2014. Ship-generated waves and induced turbidity in the Göta alv River in Sweden. *Journal of Waterway, Port, Coastal, and Ocean Engineering*, 140, Art. No. 04014004, [http://dx.doi.org/10.1061/\(ASCE\)WW.1943-5460.0000224](http://dx.doi.org/10.1061/(ASCE)WW.1943-5460.0000224).
- Gonzalez F.I., LeVeque R.J., Chamberlain P., Hirai B., Varkovitzky J., George D.L. 2014. *Validation of the GeoClaw Model*. Technical Report prepared for the National Tsunami Hazard Mitigation Program,

- <http://www.depts.washington.edu/clawpack/links/nthmp-benchmarks/>
 Accessed 26.02.2014.
- Gourlay T.P. 2001. The supercritical bore produced by a high-speed ship in a channel. *Journal of Fluid Mechanics*, 434, 399–409.
- Gourlay T.P. 2003. Ship squat in water of varying depth. *International Journal of Maritime Engineering*, 145, 1–8.
- Gourlay T.P. 2006. A simple method for predicting the maximum squat of a high-speed displacement ship. *Marine Technology*, 43, 146–151.
- Gourlay T.P., Cook S. 2004. Flow past a ship radiating a bore in a channel. *Journal of Engineering for the Maritime Environment*, 218, 31–40.
- Gourlay T.P., Tuck E.O. 2001. The maximum sinkage of a ship. *Journal of Ship Research*, 45, 50–58.
- Graff W. 1962. Untersuchungen über die Ausbildung des Wellenwiderstandes im Bereich der Stauwellengeschwindigkeit in flachem, seitlich beschränktem Fahrwasser. *Schiffstechnik*, 9, 110–122 (in German).
- Grimshaw R.H.J., Smyth N. 1986. Resonant flow of a stratified flow over topography. *Journal of Fluid Mechanics*, 169, 429–464.
- Grimshaw R.H.J., Hunt J.C.R., Chow K.W. 2015. Changing forms and sudden smooth transitions of tsunami waves. *Journal of Ocean Engineering and Marine Energy*, doi: 10.1007/s40722-014-0011-1
- Gurbatov S.N., Malakhov A.N., Saichev A.I. 1990. *Nonlinear Random Waves and Turbulence in Nondispersive Media*. Moskva, Nauka, 214 pp. (in Russian).
- Guza R.T., Thornton E.B. 1982. Swash oscillations on a natural beach. *Journal of Geophysical Research*, 87(C1), 483–491.
- Hamer M. 1999. Solitary killers. *New Scientist*, 163(2201), 18–19.
- Haver S. 2005. A possible freak wave event measured at the Draupner Jacket January 1 1995. In: Olagnon M., Prevosto M. (eds.) *Rogue Waves 2004*, IFREMER, Brest, 20–22.
- Hibiya T., Kajiura K. 1982. Origin of the Abiki phenomenon (a kind of seiche) in Nagasaki Bay. *Journal of the Oceanographical Society of Japan*, 38, 172–182.
- Holman R.A. 1986. Extreme value statistics for wave runup on a natural beach. *Coastal Engineering*, 9, 527–544.
- Houser C. 2011. Sediment resuspension by vessel-generated waves along the Savannah River, Georgia. *Journal of Waterway, Port, Coastal, and Ocean Engineering*, 137(5), 246–257.
- Hunt J.A. 1959. Design of seawalls and breakwaters, *Journal of the Waterways and Harbors Division, ASCE*, 85(WW3), 123–152.
- [IAHR 1989]. IAHR working group on wave generation and analysis. 1989. List of sea-state parameters. *Journal of the Waterways, Port, Coastal, and Ocean Engineering, ASCE*, 115, 793–808.

- Janson C.E. 2002. Bernoulli waves in deep and shallow water at low speed. *Ship Technology Research*, 49, 142–147.
- Jiang T. 2001. *Ship Waves in Shallow Water*. Fortschritt-Berichte VDI, VDI Verlag, Düsseldorf, Germany, Reihe 12, Nr. 466, 152 pp.
- Kânoğlu U. 2004. Nonlinear evolution and runup-drawdown of long waves over a sloping beach. *Journal of Fluid Mechanics*, 513, 363–372.
- Kânoğlu U., Synolakis C. 2006. Initial value problem solution of nonlinear shallow water-wave equations. *Physical Review Letters*, 97, Art. No. 148501.
- Kelpšaitė L., Parnell K.E., Soomere T. 2009. Energy pollution: the relative influence of wind-wave and vessel-wake energy in Tallinn Bay, the Baltic Sea, *Journal of Coastal Research*, Special Issue 56, 812–816.
- Kharif Ch., Pelinovsky E., Slunyaev A. 2009. *Rogue Waves in the Ocean*. Springer, 216 pp.
- Kochin N.E. 1964. *Theoretical Hydrodynamics*. Interscience, 577 pp.
- Krylov A.N. 2003. On the wave resistance and large ship waves. In: *My Memoirs*, Politechnika, Sankt-Petersburg, 364–368 (in Russian).
- Kurennoy D., Soomere T., Parnell K.E. 2009. Variability in the properties of wakes generated by high-speed ferries. *Journal of Coastal Research*, Special Issue 56, 519–523.
- Kurennoy D., Parnell K.E., Soomere T. 2011. Fast-ferry generated waves in south-west Tallinn Bay. *Journal of Coastal Research*, Special Issue 64, 165–169.
- Kurkin A.A., Pelinovsky E.N. 2004. *Freak waves: Facts, Theory and Modelling*. Nizhny Novgorod State University, 157 pp. (in Russian).
- Kuznetsov N., Maz'ya V., Vainberg B. 2002. *Linear Water Waves: A Mathematical Approach*. Cambridge University Press, 532 pp.
- Lamb H. 1916. *Hydrodynamics*. Cambridge: The University Press, 708 pp.
- Lax P.D., Wendroff B. 1960. Systems of conservation laws. *Communications on Pure and Applied Mathematics*, 13(2), 217–237.
- Lee S.J., Grimshaw R.H.J. 1990. Upstream-advancing waves generated by three-dimensional moving disturbances. *Physics of Fluids A*, 2, 194–201.
- Lee S.J., Yates G.T., Wu T.Y. 1989. Experiments and analyses of upstream-advancing solitary waves generated by moving disturbances. *Journal of Fluid Mechanics*, 199, 569–593.
- LeVeque R.J. 2002. *Finite Volume Methods for Hyperbolic Problems*. Cambridge University Press, Cambridge, 580 pp.
- LeVeque R.J. 2010. A well-balanced path-integral f-wave method for hyperbolic problems with source terms. *Journal of Scientific Computing*, 48, 209–226.
- LeVeque R.J., George D.L. 2008. High-resolution finite volume methods for the shallow water equations with bathymetry and dry states. In: Liu P.L., Synolakis C., Yeh H. (eds.), *Advanced Numerical Models for Simulating*

- Tsunami Waves and Runup*, Advances in Coastal and Ocean Engineering, World Scientific, 10, 43–73.
- Li Y., Raichlen F. 2002. Non-breaking and breaking solitary wave run-up. *Journal of Fluid Mechanics*, 456, 295–318.
- Lighthill J. 1978. *Waves in Fluids*. Cambridge University Press, 504 pp.
- Liu P.C. 2007. A chronology of freak wave encounters. *Geofizika*, 24, 57–70.
- Longuet-Higgins M.S. 1952. On the statistical distributions of sea waves. *Journal of Marine Research*, 11(3), 245–265.
- Macfarlane G.J., Duffy J.T., Bose N. 2014. Rapid assessment of boat-generated waves within sheltered waterways. *Australian Journal of Civil Engineering*, 12(1), 31–40.
- Madricardo F., Donnici S. 2014. Mapping past and recent landscape modifications in the Lagoon of Venice through geophysical surveys and historical maps. *Anthropocene*, 6, 86–96.
- Madsen P.A., Fuhrman D.R. 2008. Run-up of tsunamis and periodic long waves in terms of surf-similarity. *Coastal Engineering*, 55, 209–223.
- Madsen P.A., Schaffer H.A. 2010. Analytical solutions for tsunami run-up on a plane beach: single waves, N -waves and transient waves. *Journal of Fluid Mechanics*, 645, 27–57.
- Matias A., Williams J.J., Masselink G., Ferreira Ó. 2012. Overwash threshold for gravel barriers. *Coastal Engineering*, 63, 48–61.
- Mazova R.K., Osipenko N.N., Pelinovsky E.N. 1991. Solitary wave climbing a beach without breaking. *Rozprawy Hydrotechniczne*, 54, 71–80.
- Mei C.C. 1986. Radiation of solitons by slender bodies advancing in a shallow channel. *Journal of Fluid Mechanics*, 162, 53–67.
- Millward A. 1996. A review of the prediction of squat in shallow water. *Journal of Navigation*, 49, 77–88.
- Naghdi P.M., Rubin M.B. 1984. On the squat of a ship. *Journal of Ship Research*, 28, 107–117.
- Nakamura S. 1973. On the hydraulic bore and application of the results of its studies to the problems of generation and propagation of tsunamis. *Volny tsunami. Trudy Sakh-KNII, Yuzhno-Sakhalinsk*, 32, 129–151 (in Russian).
- Neuman D.G., Tapio E., Haggard D., Laws K.E., Bland R.W. 2001. Observation of long waves generated by ferries. *Canadian Journal of Remote Sensing*, 27, 361–370.
- Newman J.N. 1977. *Marine Hydrodynamics*, MIT Press, 418 pp.
- Nielsen P., Hanslow D.J. 1991. Wave runup distributions on natural beaches. *Journal of Coastal Research*, 7(4), 1139–1152.
- Nikolkina I., Didenkulova I. 2011. Rogue waves in 2006–2010. *Natural Hazards and Earth System Sciences*, 11, 2913–2924.

- Nikolkina I., Didenkulova I. 2012. Catalogue of rogue waves reported in media in 2006–2010. *Natural Hazards*, 61(3), 989–1006.
- Nikolkina I., Soomere T., Räämet A. 2014. Multidecadal ensemble hindcast of wave fields in the Baltic Sea. In: *The 6th IEEE/OES Baltic Symposium Measuring and Modeling of Multi-Scale Interactions in the Marine Environment, May 26–29, Tallinn Estonia*. IEEE Conference Publications, Piscataway, N.J., 9 pp.
- Noblesse F., He J., Zhu Y., Hong L., Zhang C., Zhu R., Yang C. 2014. Why can ship wakes appear narrower than Kelvin's angle? *European Journal of Mechanics B/Fluids*, 46, 164–171.
- Parnell K.E., Kofoed-Hansen H. 2001. Wakes from large high-speed ferries in confined coastal waters: Management approaches with examples from New Zealand and Denmark. *Coastal Management*, 29(3), 217–237.
- Parnell K.E., McDonald S.C., Burke A.E. 2007. Shoreline effects of vessel wakes, Marlborough Sounds, New Zealand. *Journal of Coastal Research*, Special Issue 50, 502–506.
- Parnell K.E., Delpêche N., Didenkulova I., Dolphin T., Erm A., Kask A., Kelpšaitė L., Kurennoy D., Quak E., Räämet A., Soomere T., Terentjeva A., Torsvik T., Zaitseva-Pärnaste I. 2008. Far-field vessel wakes in Tallinn Bay. *Estonian Journal of Engineering*, 14(4), 273–302.
- Parnell K.E., Soomere T., Zaggia L., Rodin A., Lorenzetti G., Rapaglia J., Scarpa G. M. 2015. Ship-induced solitary Riemann waves of depression in Venice Lagoon. *Physics Letters A*, 379(6), 555–559.
- Pedersen G., Gjevik B. 1983. Runup of solitary waves. *Journal of Fluid Mechanics*, 142, 283–299.
- Pelinovsky E.N. 1982. *Nonlinear Dynamics of Tsunami Waves*. Gorky, Institute of Applied Physics, 226 pp. (in Russian).
- Pelinovsky E.N. 1996. *Tsunami Wave Hydrodynamics*. Institute Applied Physics Press, Nizhny Novgorod. 276 pp. (in Russian).
- Pelinovsky E., Mazova R. 1992. Exact analytical solutions of nonlinear problems of tsunami wave run-up on slopes with different profiles. *Natural Hazards*, 6, 227–249.
- Pelinovsky E.N., Rodin A.A. 2011. Nonlinear deformation of a large-amplitude wave on shallow water. *Doklady Physics*, 56(5), 305–308.
- Pelinovsky E.N., Rodin A.A. 2012. Transformation of a strongly nonlinear wave in a shallow-water basin. *Izvestiya, Atmospheric and Oceanic Physics*, 48, 343–349.
- Pelinovsky E.N., Troshina E.N. 1994. Propagation of long waves in straits. *Journal of Physical Oceanography*, 5(1), 43–48.
- Pelinovsky E., Kharif Ch., Talipova T. 2008. Large-amplitude long wave interaction with a vertical wall. *European Journal of Mechanics B/Fluids*, 27, 409–418.

- Peregrine D.H. 1966. Calculations of the development of an undular bore. *Journal of Fluid Mechanics*, 25, 321–330.
- Peterson P., Soomere T., Engelbrecht J., van Groesen E. 2003. Soliton interaction as a possible model for extreme waves in shallow water. *Nonlinear Processes in Geophysics*, 10, 503–510.
- Pindsoo K., Eelsalu M., Soomere T., Tõnisson H. 2014. An estimate of the impact of vessel wakes on coastal processes: a case study for Aegna, Estonia. In *The 6th IEEE/OES Baltic Symposium Measuring and Modeling of Multi-Scale Interactions in the Marine Environment, May 26–29, Tallinn Estonia*. IEEE Conference Publications, Piscataway, N.J.
- Powell K.A. 1990. Predicting short term profile response for shingle beaches, *HRWallingford SR Rept*, 1990, 219.
- Pritchard D., Dickinson L. 2007. The near-shore behaviour of shallow-water waves with localized initial conditions. *Journal of Fluid Mechanics*, 591, 413–436.
- Rabaud M., Moisy F. 2013. Ship wakes: Kelvin or Mach angle? *Physical Review Letters*, 110, Art. No. 214503.
- Rapaglia J., Zaggia L., Ricklefs K., Gelinas M., Bokuniewicz H. 2011. Characteristics of ships' depression waves and associated sediment resuspension in Venice Lagoon, Italy. *Journal of Marine Systems*, 85(1–2), 45–56.
- Ravens T.M., Thomas R.C. 2008. Ship wave-induced sedimentation of a tidal creek in Galveston bay. *Journal of Waterway, Port, Coastal, and Ocean Engineering*, 134, 21–29.
- Roe P.L. 1981. Approximate Riemann solvers, parameter vectors and difference schemes. *Journal of Computational Physics*, 43, 357–372.
- Rodin A.A., Pelinovsky E.N. 2014. *The Dynamics of Long Waves in the Coastal Zone, Taking into Account Breaking Effects*. Nizhny Novgorod, NSTU, 93 pp. (in Russian)
- Rudenko O., Soluyan S. 1977. *Theoretical Foundations of Nonlinear Acoustics*. Plenum, New York, 274 pp.
- Rybkin A., Pelinovsky E., Didenkulova I. 2014. Nonlinear wave run-up in bays of arbitrary cross-section: generalization of the Carrier-Greenspan approach. *Journal of Fluid Mechanics*, 748, 416–432.
- Sachdev P.L., Seshadri V.S. 1976. Motion of a bore over a sloping beach: an approximate analytical approach. *Journal of Fluid Mechanics*, 78(3), 481–487.
- Sarretta A., Pillon S., Molinaroli E., Guerzoni S., Fontolan G. 2010. Sediment budget in the Lagoon of Venice, Italy. *Continental Shelf Research*, 30, 934–949.
- Sedov L.I. 1977. *Mechanics of Continuous Media*. Moscow, Nauka, 1060 pp. (in Russian).
- Shen M.C., Meyer R.E. 1963. Climb of a bore on a beach. Part 3. Run-up. *Journal of Fluid Mechanics*, 16(1), 113–125.

- Sheremet A., Gravois U., Tian M. 2013. Boat-wake statistics at Jensen Beach, Florida. *Journal of Waterway, Port, Coastal, and Ocean Engineering*, 139, 286–294.
- Shermeneva M., Shugan I. 2006. The computations of the wave runup on gentle beach. *Letters to Journal of Technical Physics*, 32, 33–38.
- Shuleykin V.V. 1968. *Physics of the Sea*. Moscow, Nauka, 1083 pp. (in Russian).
- Slunyaev A., Didenkulova I., Pelinovsky E. 2011. Rogue waters. *Contemporary Physics*, 52(6), 571–590.
- Soloviev S.L., Mazova R.K. 1994. On the influence of sign of leading tsunami wave on run-up height on the coast. *Science of Tsunami Hazards*, 12, 25–31.
- Sommerfeld A. 1949. *Partial Differential Equations in Physics*. Elsevier, 334 pp.
- Soomere T. 2005a. Fast ferry traffic as a qualitatively new forcing factor of environmental processes in non-tidal sea areas: a case study in Tallinn Bay, Baltic Sea. *Environmental Fluid Mechanics*, 5(4), 293–323.
- Soomere T. 2005b. Wind wave statistics in Tallinn Bay. *Boreal Environment Research*, 10(2), 103–118
- Soomere T. 2007. Nonlinear components of ship wake waves. *Applied Mechanics Reviews*, 60(3), 120–138.
- Soomere T. 2009. Long ship waves in shallow water bodies. In: Quak E., Soomere T. (eds.), *Applied Wave Mathematics: Selected Topics in Solids, Fluids, and Mathematical Methods*. Springer, 193–228.
- Soomere T. 2010. Rogue waves in shallow water. *European Physical Journal Special Topics*, 185, 81–96.
- Soomere T., Healy T.R. 2011. On the dynamics of “almost equilibrium” beaches in semi-sheltered bays along the southern coast of the Gulf of Finland. In: Harff J., Björck S., Hoth P. (eds.), *The Baltic Sea Basin*. Central and Eastern European Development Studies, Part 5, Springer, Heidelberg Dordrecht London New York, 255–279.
- Soomere T., Põder R., Rannat K., Kask A. 2005. Profiles of waves from high-speed ferries in the coastal area. *Proceedings of the Estonian Academy of Sciences, Engineering*, 11(3), 245–260.
- Soomere T., Parnell K.E., Didenkulova I. 2009. Implications of fast ferry wakes for semi-sheltered beaches: a case study at Aegna Island, Baltic Sea. *Journal of Coastal Research*, Special Issue 56, 128–132.
- Soomere T., Parnell K.E., Didenkulova I. 2011. Water transport in wake waves from high-speed vessels. *Journal of Marine Systems*, 88, 74–81.
- Soomere T., Pindsoo K., Bishop S.R., Käär A., Valdmann A. 2013. Mapping wave set-up near a complex geometric urban coastline. *Natural Hazards and Earth System Sciences*, 13(11), 3049–3061.
- Sorensen R.M. 1973. Ship-generated waves. *Advances in Hydrosience*, 9, 49–83.
- Spielvogel L.Q. 1975. Runup of single waves on a sloping beach. *Journal of Fluid Mechanics*, 74, 685–694.

- Sretensky L.N. 1977. *The Theory of Wave Motions of a Fluid*. Moscow, Nauka, 816 pp.
- Stefanakis T.S., Dias F., Dutykh D. 2011. Local run-up amplification by resonant wave interactions. *Physical Review Letters*, 107, Art. No. 124502.
- Stoker J.J. 1957. *Water waves: Mathematical Theory with Applications*. New York: Interscience Publishers, 567 pp.
- Stumbo S., Fox K., Dvorak F., Elliot L. 1999. The prediction, measurement, and analysis of wake wash from marine vessels. *Marine Technology and SNAME News*, 36, 248–260.
- Suuroja S., Karimov M., Talpas A., Suuroja K. 2007. Mererannikute seire. Aruanne riikliku keskkonnaseire alamprogrammi Mererannikute seire täitmisest 2006, aastal, Tallinn (in Estonian).
- Suuroja S., Talpas A., Suuroja K. 2008. Eesti Riikliku Keskkonnaseire mererannikute seire allprogrammi 2007. a. aastaaruanne, Tallinn (in Estonian).
- Suuroja S., Talpas A., Suuroja K. 2009. Eesti Riikliku Keskkonnaseire mererannikute seire allprogrammi 2008. a. aastaaruanne, Tallinn (in Estonian).
- Suuroja S., Talpas A., Suuroja K. 2010. Eesti Riikliku Keskkonnaseire mererannikute seire allprogrammi 2009. a. aastaaruanne, Tallinn (in Estonian).
- Suuroja S., Talpas A., Suuroja K. 2011. Eesti Riikliku Keskkonnaseire mererannikute seire allprogrammi 2010. a. aastaaruanne, Tallinn (in Estonian).
- Synolakis C.E. 1987. The runup of solitary waves. *Journal of Fluid Mechanics*, 185, 523–545.
- Synolakis C.E. 1991. Tsunami runup on steep slopes: How good linear theory really is? *Natural Hazards*, 4, 221–234.
- Synolakis C.E., Deb M.K., Skjelbreia J.E. 1988. The anomalous behavior of the run-up of cnoidal waves. *Physics of Fluids*, 31, 3–5.
- Tadepalli S., Synolakis C.E. 1996. Model for the leading waves of tsunamis. *Physical Review Letters*, 77, 2141–2144.
- Tadepalli S., Synolakis C.E. 1994. The runup of *N*-waves. *Proceedings of the Royal Society of London*, 445, 99–112.
- Teles da Silva A.F., Peregrine D.H. 1990. Non steady computations of undular and breaking bores. In: *Proceedings of the 22nd International Congress on Coastal Engineering, Delft*. ASCE, New York, 1, 1019–1032.
- Tinti S., Tonini R. 2005. Analytical evolution of tsunamis induced by near-shore earthquakes on a constant-slope ocean. *Journal of Fluid Mechanics*, 535, 33–64.
- Toffoli A., Lefèvre J.M., Bitner-Gregersen E., Monbaliu J. 2005. Towards the identification of warning criteria: Analysis of a ship accident database. *Applied Ocean Research*, 27(6), 281–291.
- Torsvik T., Soomere T. 2008. Simulation of patterns of wakes from high-speed ferries in Tallinn Bay. *Estonian Journal of Engineering*, 14(3), 232–254.

- Torsvik T., Didenkulova I., Soomere T., Parnell K.E. 2009a. Variability in spatial patterns of long nonlinear waves from fast ferries in Tallinn Bay. *Nonlinear Processes in Geophysics*, 16, 351–363.
- Torsvik T., Pedersen G., Dysthe K. 2009b. Waves generated by a pressure disturbance moving in a channel with a variable cross-sectional topography. *Journal of Waterway, Port, Coastal, and Ocean Engineering*, 135(3), 120–123.
- Torsvik T., Soomere T., Didenkulova I., Sheremet A. 2015. Identification of ship wake structures by a time-frequency method. *Journal of Fluid Mechanics*, 765, 229–251.
- Tsuji Y., Yanuma T., Murata I., Fujiwara C. 1991. Tsunami ascending in rivers as an undular bore. *Natural Hazards*, 4, 257–266.
- Varyani K. 2006. Full scale study of the wash of high speed craft. *Ocean Engineering*, 33, 705–722.
- Viška M., Soomere T. 2013. Simulated and observed reversals of wave-driven alongshore sediment transport at the eastern Baltic Sea coast. *Baltica*, 26(2), 145–156.
- Voltsinger N.E., Klevanniy K.A., Pelinovskiy E.N. 1989. *Long-Wave Dynamics of Coastal Zone*. Gidrometeoizdat, 272 pp. (in Russian).
- Wehausen J.V. 1973. The wave resistance of ships. *Advances in Applied Mechanics*, 13, 93–244.
- Whitham G.B. 1974. *Linear and Nonlinear Waves*. Wiley, New York, 635 pp.
- Wu Y.H., Tian J.-W. 2000. Mathematical analysis of long-wave breaking on open channels with bottom friction. *Ocean Engineering*, 26, 187–201.
- Zahibo N., Pelinovsky E., Golinko V., Osipenko N. 2006a. Tsunami wave runup on coasts of narrow bays. *International Journal of Fluid Mechanics Research*, 33, 106–118.
- Zahibo N., Pelinovsky E., Talipova T., Kozelkov A., Kurkin A. 2006b. Analytical and numerical study of nonlinear effects at tsunami modeling. *Applied Mathematics and Computation*, 174(2), 795–809.
- Zahibo N., Didenkulova I., Kurkin A., Pelinovsky E. 2008. Steepness and spectrum of nonlinear deformed shallow water wave. *Ocean Engineering*, 35, 47–52.

Acknowledgements

I am using this opportunity to express my gratitude to everyone who supported me throughout the course of my PhD study.

I am thankful to my supervisors, President of Estonian Academy of Sciences, Professor Tarmo Soomere and Doctor Ira Didenkulova for their aspiring and patient guidance, invaluable constructive criticism and friendly advice during these years. I am sincerely grateful to them for sharing their truthful and illuminating views on an infinite number of issues related to my study. This thesis has not been possible without them.

I express my warm thanks to Professor Efim Pelinovsky for the help, support and guidance during my study. Without him I would not be inspired to start my academic career.

I would also like to thank all the colleagues from the Laboratory of Wave Engineering, who are my good friends always willing to help and give their best suggestions, particularly Dr. Maija Viška, Dr. Andrea Giudici, Dr. Tomas Torsvik, Dr. Bert Viikmäe, Katri Pindsoo and Maris Eelsalu.

I am grateful to my parents Lyudmila Rodina and Alexander Rodin for their unconditional love and endless patience. I wouldn't be who I am today if it weren't for them.

Especially I would like to thank Natalya Chaykovskaya for waiting me and fighting alone with almost all of the circumstances during these four years, for her endless love and support. I dedicate this thesis to her.

* * *

The studies were supported by DoRa scholarship funded from the European Social Fund.

Abstract

The thesis addresses the dynamics of long waves and the properties of their run-up in the framework of nonlinear shallow water theory as well as related topics of rogue waves and run-up of extreme storm waves and transient wave groups. The focus is on the evolution of long-living solitary waves of depression in the marine environment.

The transformation and run-up of long partially breaking solitary waves of both polarities is studied numerically using the CLAWPACK software for a composite basin containing a section of constant depth and a section with a sloping beach. It is demonstrated that nonlinear effects and energy dissipation by wave breaking are more pronounced for waves of depression than for waves of elevation. These processes lead to a marked asymmetry of the run-up for waves of different polarities, to the formation of a shock wave at the rear slopes of depressions and to substantial run-up heights of the depression waves on a beach.

Interrelations between the offshore wave height and the run-up height of single waves are studied numerically in the above framework and experimentally for transient groups of vessel-induced waves with chirp-like group structure in the marine environment recorded at Pikakari Beach (Tallinn Bay, the Baltic Sea). The wave heights within a wake and their run-up heights are reasonably described by a Weibull distribution. It is shown that the specific group structure of vessel wakes (frequency modulated packets with gradually decreasing periods and heights) leads to a sequence of high wave run-up events, even when the original wave heights are rather moderate, and potentially to uncommonly large impact on the coast.

Based on wave recordings in the Venice Lagoon it is established that unexpectedly high (~2.5 m) solitary depression waves may be generated by ships of moderate size and sailing at relatively low speeds in a channel having shallow banks. The properties of these waves (interpreted as long-living strongly nonlinear solitary Riemann waves of depression) are reproduced numerically. Such waves rapidly develop up a steep bore-like rear slope that occasionally contains a temporary multi-step profile. It is demonstrated that such vessel-driven depressions of substantial height (>0.3 m) may propagate for more than 1 km from channel into the nearby lagoon while keeping the steep bore-like rear slope.

The statistics and appearance of small-amplitude rogue waves in shallow water are analysed based on records of sea surface elevation in Tallinn Bay in relatively calm weather conditions. Almost all identified rogue waves are single waves. A Rayleigh distribution slightly overestimates the frequency of occurrence of rogue waves. In very low wave conditions (<10 cm) single rogue troughs are more probable than a crest, while for amplitudes >20 cm high crests are more probable.

The extension of maximum inundation of Estonian coasts is evaluated based on the outcome of 35-year wind wave simulations and numerical simulations using the CLAWPACK software. The results were used to analyse the applicability of common empirical express formulas to wind wave run-up.

Resüme

Doktoritöös käsitletakse pikkade tugevalt mittelineaarsete üksiklainete dünaamikat madalatel merealadel madala vee võrrandite raames, lainerünnaku (*run-up*) probleemikat laevalainete ja ekstreemsete tormilainete kontekstis ning ebatavaliselt kõrgete üksiklainete esinemise statistikat väikese lainekõrguse tingimustes. Keskne teema on erinevat liiki laevalainete (pikaealiste üksikute lainevagude ja kindlapiiriliste lainerühmade) kaugmõju väga madalatel merealadel ja nendega külgnevatel rannikutel.

Mittelineaarsete üksiklainete levimist ja lainerünnakut analüüsitakse numbriliselt (CLAWPACK tarkvaraga) idealiseeritud situatsioonis, kus lai konstantse sügavusega mereala külgneb tasapinnalise rannaga. Näidatakse, et mittelineaarsed efektid ja murdumisest tulenev sumbumine ilmnevad üksikute lainevagude puhul märksa tugevamalt kui üksikute laineharjade puhul. Need tingivad erineva polaarusega lainete levimise ja lainerünnaku omaduste tugeva asümmeetria. Lainevao taganõlval moodustub hüpe või lööklaine ning lainevao jõudmisel rannale võib vesi jõuda peaaegu sama kaugele sisemaale kui laineharja puhul.

Avamerel esinenud lainekõrguse ja üksikute lainete lainerünnaku kõrguse vahelisi seoseid analüüsitakse nii numbriliselt kui ka Tallinna lahes Pikakari rannas mõõdetud laevalainete rühmade omaduste alusel. Nii laevalainete kõrgused kui ka nende lainerünnaku kõrgused kirjelduvad hästi Weibulli jaotusega. Näidatakse, et laevalainete kindlapiiriliste rühmade spetsiifilise nn. siristuse (*chirp*) struktuuri (pikkadele lainetele järgnevad lühemad) tõttu jätkuvad kõrged lainerünnakud pikka aega ka siis, kui laevalainete kõrgus aegamisi väheneb. Seetõttu mõjutab laevade järellainetus randu märksa tugevamini kui sama kõrgusega tuulelained.

Veneetsia laguunis läbi viidud mõõdistuste alusel demonstreeritakse, et seelstes kanalites suhteliselt tagasihoidlike mõõtmetega ja mõistliku kiirusega liikuvad laevad tekitavad väga sügavaid (~2,5 m) lainevagusid juhul, kui kanalit ümbritseb lai madalaveeline ala. Selliseid lainevagusid interpreteeritakse tugevalt mittelineaarsete Riemanni üksiklainetena. Nende omadusi analüüsitakse numbriliste meetoditega. Näidatakse, et nende lainete taganõlv areneb kiiresti järsuks booritaoliseks struktuuriks. Taolised *V*-kujulised üksiklained levivad enam kui 0,3 m sügavuste ohtlikult järsu tagaseinaga häiritustena rohkem kui 1 km kaugusel laevateest.

Tagasihoidliku kõrgusega loodusliku lainetuse foonil arenevate mini-hiidlainete esinemissagedust ja kuju analüüsitakse Pikakari ranna lähistel tehtud veepinna kuju täppismõõdistuste alusel. Mini-hiidlainete seas domineerivad üksikud laineharjad või -vaod. Rayleigh jaotus hindab nende esinemissagedust veidi üle. Väga väikeste lainekõrguste puhul (<10 cm) on ülekaalus sügavad lainevaod, kuid >20 cm lainekõrguse puhul on ülekaalus üksikud kõrged laineharjad. Maksimaalse lainerünnaku parameetreid 18 Eesti ranniku lõigus analüüsitakse neis kohtades 35 aasta jooksul esinenud kõrgeimate lainete omaduste alusel CLAWPACK tarkvaraga. Demonstreeritakse, et vaid osa avaookeani randade jaoks tuletatud lainerünnaku hindamise ekspresmeetoditest sobivad Eesti tingimuste jaoks.

Appendix A: Curriculum Vitae

1. Personal data

Name	Artem Rodin
Date and place of birth	21.02.1987, Nizhny Novgorod, Russia
Address	Akadeemia tee 21, 12618 Tallinn
Phone	(+372) 620 4178
e-mail	artem@ioc.ee

2. Education

Educational institution	Graduation year	Education (field of study / degree)
Nizhny Novgorod State Technical University	2010	Applied Mathematics / MSc
Nizhny Novgorod State Technical University	2008	Applied Mathematics / BSc

3. Language competence/skills

Language	Level
Russian	native language
English	fluent
Estonian	basic skills

4. Special courses and further training

Period	Educational or other organisation
Jul.-Aug. 2012	Gene Golub SIAM Summer School <i>Simulation and Supercomputing in the Geosciences</i> , USA
Sep. 2011	BalticWay Summer School <i>Preventive methods for coastal protection</i> , Lithuania

5. Professional employment

Period	Organisation	Position
Feb. 2011 – to date	Institute of Cybernetics, Tallinn University of Technology	Technician
Sep. 2007 – Jan. 2011	MERA Networks	Software designer

6. Research activity: Publications

Research papers in journals indexed by the Web of Science Core Collection database (1.1):

Parnell K.E., Soomere T., Zaggia L., **Rodin A.**, Lorenzetti G., Rapaglia J., Scarpa G.M. 2015. Ship induced solitary Riemann waves of depression in Venice Lagoon. *Physics Letters A*, 379, 555–559.

- Rodin A.**, Soomere T., Parnell K.E., Zaggia L. 2015. Numerical simulation of propagation of ship-induced Riemann waves of depression into Venice Lagoon. *Proceedings of the Estonian Academy of Sciences*, 64, 22–35.
- Denissenko P., Didenkulova I., **Rodin A.**, Listak M., Pelinovsky E. 2013. Experimental statistics of long wave runup on a plane beach. *Journal of Coastal Research*, 65(1), 195–200.
- Didenkulova I., **Rodin A.** 2013. A typical wave wake from high-speed vessels: its group structure and run-up. *Nonlinear Processes in Geophysics*, 20(1), 179–188.
- Didenkulova I., Denissenko P., **Rodin A.**, Pelinovsky E. 2013. Effect of asymmetry of incident wave on the maximum runup height. *Journal of Coastal Research*, 65(1), 207–212.
- Pelinovsky E.N., **Rodin A.A.** 2013. Nonlinear effects at the initial stage of tsunami-wave development. *Izvestiya, Atmospheric and Oceanic Physics*, 49(5), 548–553.
- Pelinovsky E.N., **Rodin A.A.** 2012. Transformation of a strongly nonlinear wave in a shallow-water basin. *Izvestiya, Atmospheric and Oceanic Physics*, 48(3), 343–349.
- Pelinovsky E.N., **Rodin A.A.** 2011. Nonlinear deformation of a large-amplitude wave on shallow water. *Doklady Physics*, 56(5), 305–308.
- Peer-reviewed articles in other international journals (1.2) and collections (3.1) indexed by the Web of Science Core Collection or SCOPUS database:*
- Rodin A.**, Didenkulova I., Nikolkina I. 2014. Run-up of large storm waves on Estonian coasts of the Baltic Sea. In: *IEEE/OES Baltic 2014 International Symposium*, 26–29 May 2014, Tallinn, Estonia; Proceedings. IEEE, 5 pp.
- Родин А.А.** 2013. Численные расчеты наката обрушенных одиночных волн на плоский откос. *Труды Нижегородского государственного технического университета им. П.Е. Алексеева*, 1(98), 36–43.
- Пелиновский Д.Е., Гиниятуллин А.Р., Панфилова Ю.А., Шургалина Е.Г., **Родин А.А.** 2013. Аналитические приближения уединенных волн в зернистых кристаллах. *Труды Нижегородского государственного технического университета им. П.Е. Алексеева*, 3(100), 55–69.
- Didenkulova I., **Rodin A.** 2012. Statistics of shallow water rogue waves in Baltic Sea conditions: the case of Tallinn Bay. In: *IEEE/OES Baltic 2012 International Symposium*, 8–11 May 2012, Klaipėda, Lithuania; Proceedings. IEEE, 6 pp.
- Rodin A.A.**, Didenkulova I.I., Pelinovsky E.N. 2012. Взаимодействие уединенных волн большой амплитуды в мелководном бассейне. *Фундаментальные исследования*, 11(3), 710–714.
- Didenkulova I., Pelinovsky E., **Rodin A.** 2011. Nonlinear interaction of large-amplitude unidirectional waves in shallow water. *Estonian Journal of Engineering*, 17(4), 289–300.

Scholarly monographs (2.1):

Родин А.А., Пелиновский Е.Н. 2014. *Динамика длинных волн в прибрежной зоне моря с учетом эффектов обрушения*. Нижегородский гос. техн. ун-т им. Р.Е. Алексеева, монография, 83 с.

Articles/chapters in books (3.1) and (3.2):

Denissenko P., Pearson J., **Rodin A.**, Didenkulova I. 2014. Long waves climbing the slopes of different roughness: run-up height and the load on individual roughness elements. In: *Proceedings of HYDRALAB IV Joint User Meeting*, Lisbon, July 2014, TA-FZK-03, 1–6.

Диденкулова И.И., Пелиновский Е.Н., **Родин А.А.** 2012. Формирование экстремальных волн на мелкой воде с учетом обрушения. *Фундаментальная и прикладная гидрофизика*, Санкт-Петербург, Наука, 5(1), 89–98.

Талипова Т.Г., Пелиновский Е.Н., Куркина О.Е., Диденкулова И.И., **Родин А.А.**, Панкратов А.С., Наумов А.А., Гиниятуллин А.Р., Николкина И.Ф. 2012. Распространение волны конечной амплитуды в стратифицированной жидкости переменной глубины. In: *Современная наука: исследования, идеи, результаты, технологии. 10th International Scientific Conference „Actual problems of thermal physics and fluid dynamics“*, Киев: НПВК Триакон, 144–150.

Николкина И.Ф., **Родин А.А.**, Пелиновский Е.Н. 2009. Нелинейные волны в медленных гравитационных потоках на склоне. In: *Труды II международной заочной научно-практической конференции „Человек: Наука, Техника и Время“*, Ульяновск, 197–200.

Abstracts of conference presentations (5.2):

Didenkulova I., Pelinovsky E., Didenkulov O., **Rodin A.** 2015. Run-up of long solitary waves of different polarities on a plane beach. *Geophysical Research Abstracts*, 17, EGU2015-1241.

Parnell K.E., Soomere T., Zaggia L., **Rodin A.** 2015 Dynamics of ship-induced solitary wave troughs in Venice Lagoon. *Geophysical Research Abstracts*, 17, EGU2015-7118.

Pelinovsky E., Chaykovskaya N., **Rodin A.** 2015 Research of large-amplitude waves evolution in the framework of shallow-water equations and their implication for people’s safety in extreme situations. *Geophysical Research Abstracts*, 17, EGU2015-5224.

Didenkulova I., Denissenko P., **Rodin A.**, Pearson J. 2014. Experimental study of the runup of long nonlinear regular and irregular waves. *Geophysical Research Abstracts*, 16, EGU2014-16403.

Rodin A. 2014. Influence of wave breaking effects on wave transformation and run-up on the beach. *Geophysical Research Abstracts*, 16, EGU2014-14319.

Rodin A. 2014. Peculiarities of long wave transformation waves in nonlinear hyperbolic systems (shallow-water framework). In: *Mathematics and*

- Engineering in Marine and Earth Problems*, 22–25 July 2014, Aveiro, Portugal, Book of Abstracts, 109–111.
- Rodin A.**, Didenkulova I. 2014. Shallow water freak waves: the case of Tallinn Bay the Baltic Sea. *Geophysical Research Abstracts*, 16, EGU2014-7042.
- Rodin A.**, Didenkulova I. 2014. Transformation and run-up of large-amplitude nonlinear waves from high-speed ferries in the coastal zone of the Baltic Sea. In: *Measuring and Modeling of Multi-Scale Interactions in the Marine Environment: IEEE/OES Baltic Symposium 2014*, 26–29 May 2014, Tallinn, Estonia. Book of Abstracts. Tallinn, Tallinn University of Technology, 106.
- Rodin A.**, Didenkulova I., Nikolkina I. 2014. Run-up of large storm waves on estonian coasts of the Baltic Sea. In: *Measuring and Modeling of Multi-Scale Interactions in the Marine Environment: IEEE/OES Baltic Symposium 2014*, 26–29 May 2014, Tallinn, Estonia. Book of Abstracts. Tallinn, Tallinn University of Technology, 107.
- Rodin A.**, Pelinovsky E. 2014. Deformation of long large-amplitude waves in finite-depth fluid. In: Salupere A., Maugin, G.A. (eds.) *IUTAM Symposium on Complexity of Nonlinear Waves*, 8–12 September, 2014, Tallinn. Book of Abstracts. Tallinn, Institute of Cybernetics at Tallinn University of Technology, 99–100.
- Torsvik T., Herrmann H., Didenkulova I., **Rodin A.**, Quak E. 2014. Analysis of ship wake structures by use of time-frequency methods. In: Salupere A., Maugin G.A. (eds.), *IUTAM Symposium on Complexity of Nonlinear Waves*, 8–12 September, 2014, Tallinn: Book of Abstracts. Tallinn, Institute of Cybernetics at Tallinn University of Technology, 125–126.
- Диденкулова И.И., **Родин А.А.** 2014. Трансформация и накат корабельных волн большой амплитуды в прибрежных зонах Балтийского моря. In: *XX Международная научно-техническая конференция „Информационные системы и технологии“ ИСТ–2014*, 18 апреля 2014. Материалы конференции. Нижний Новгород, Нижегородский государственный технический университет, (IT Forum 2020), 374.
- Родин А.А.** 2014. Расчет высоты заплеска сильно нелинейных волн на вертикальную стенку. In: *XX Международная научно-техническая конференция „Информационные системы и технологии“ ИСТ–2014*, 18 апреля 2014. Материалы конференции. Нижний Новгород, Нижегородский государственный технический университет, (IT Forum 2020), 375.
- Шургалина Е.Г., **Родин А.А.** 2014. Боры разных типов на мелкой воде и адекватные математические модели. In: *XX Международная научно-техническая конференция „Информационные системы и технологии“ ИСТ–2014*, 18 апреля 2014. Материалы конференции. Нижний Новгород, Нижегородский государственный технический университет, (IT Forum 2020), 403.
- Didenkulova I., Denissenko P., Listak M., **Rodin A.**, Pelinovsky E. 2013. Effects of wave asymmetry on its runup on a beach. In: Russell P.E., Masselink G.

- (eds.) *ICS2013 International Coastal Symposium 2013*, 8–12 April 2013, Book of Abstracts, Plymouth University, CERF, 370.
- Didenkulova I., Denissenko P., **Rodin A.**, Listak M., Pelinovsky E. 2013. Effects of wave asymmetry on its runup on a beach: theory and experiment. In: *International Conference Caribbean Waves 2*, 22–25 January 2013, Gosier, Guadeloupe, F.W.I., Conference Program and Abstract Book, 103.
- Didenkulova I., Denissenko P., **Rodin A.**, Pelinovsky E. 2013. Statistics of long wave runup on a plane beach, based on the data from the Large Wave Flume (GWK), Hannover, Germany. *Geophysical Research Abstracts*, 15, EGU2013-3641.
- Didenkulova I., **Rodin A.** 2013. “Parabolic cap” model for gravity flows and shallow water waves. In: *BSSC 9th Baltic Sea Science Congress 2013: New Horizons for Baltic Sea Science*, 26–30 August 2013, Klaipėda, Lithuania. Abstract Book. Klaipėda, Coastal Research and Planning Institute of Klaipėda University (KU CORPI), 158.
- Didenkulova I., **Rodin A.** 2013. Peculiarities of the ship wake structure. In: *BSSC 9th Baltic Sea Science Congress 2013: New Horizons for Baltic Sea Science*, 26–30 August 2013, Klaipėda, Lithuania. Abstract Book. Klaipėda, Coastal Research and Planning Institute of Klaipėda University (KU CORPI), 32.
- Didenkulova I., **Rodin A.** 2013. Properties of shallow water rogue waves in the Baltic Sea. In: *BSSC 9th Baltic Sea Science Congress 2013: New Horizons for Baltic Sea Science*, 26–30 August 2013, Klaipėda, Lithuania. Abstract Book. Klaipėda, Coastal Research and Planning Institute of Klaipėda University (KU CORPI), 33.
- Диденкулова И.И., Денисенко П.В., **Родин А.А.** 2013. Исследование влияния асимметрии падающей волны на максимальную высоту наката. In: *XIX Международная научно-техническая конференция „Информационные системы и технологии“ ИСТ–2013*, 19 апреля 2013. Материалы конференции. Нижний Новгород, Нижегородский государственный технический университет, (IT Forum 2020), 397.
- Родин А.А.** 2013. Динамика волн цунами в очаге. In: *XIX Международная научно-техническая конференция „Информационные системы и технологии“ ИСТ–2013*, 19 апреля 2013. Материалы конференции. Нижний Новгород, Нижегородский государственный технический университет, (IT Forum 2020), 406.
- Родин А.А.**, Пелиновский Е.Н., Талипова Т.Г., Куркин А.А. 2013. Оценки параметров волны прорыва возникающей вследствие разрушения плотины Горьковской ГЭС. In: *XIX Международная научно-техническая конференция „Информационные системы и технологии“ ИСТ–2013*, 19 апреля 2013. Материалы конференции. Нижний Новгород, Нижегородский государственный технический университет, (IT Forum 2020), 407.

- Didenkulova I., Pelinovsky E., **Rodin A.** 2012. Formation of shallow water rogue waves taking into account wave breaking effects. *Geophysical Research Abstracts*, 14, EGU2012-113
- Didenkulova I., **Rodin A.** 2012. Statistics of waves within a ship wake. *Geophysical Research Abstracts*, 14, EGU2012-110.
- Pelinovsky E., Slunyaev A., Didenkulova I., Sergeeva A., Talipova T., Nikolkina I., **Rodin A.**, Shurgalina E. 2012. Shallow rogue waves: observations, laboratory experiments, theories and modeling. In: *6th International Conference "Solitons, Collapses and Turbulence: Achievements, Developments and Perspectives"*, The Conference Program & Proceedings, Russia, Novosibirsk, Akademgorodok, 4–8 June 2012. Novosibirsk, Russian Academy of Sciences, 112–113.
- Rodin A.**, Didenkulova I. 2012. A typical wave wake from high-speed vessels: its group structure and run-up. *Geophysical Research Abstracts*, 14, EGU2012-752.
- Rodin A.**, Didenkulova I., Pelinovsky E. 2012. Nonlinear interaction of large-amplitude unidirectional waves in shallow water. *Geophysical Research Abstracts*, 14, EGU2012-112.
- Rodin A.**, Didenkulova I. 2012. Ship waves in Tallinn Bay, Baltic Sea: Their parameters, group structure and runup. In: *2012 IEEE/OES Baltic International Symposium "Ocean: Past, Present and Future. Climate Change Research, Ocean Observation & Advances Technologies for Regional Sustainability"*, May 8–11, 2012, Klaipėda, Lithuania, Presentation Abstracts. Klaipėda, Baltic Valley, 39.
- Rodin A.**, Didenkulova I. 2012. Statistics of shallow water rogue waves in Baltic Sea conditions: the case of Tallinn Bay. In: *2012 IEEE/OES Baltic International Symposium "Ocean: Past, Present and Future. Climate Change Research, Ocean Observation & Advances Technologies for Regional Sustainability"*, May 8–11, 2012, Klaipėda, Lithuania, Presentation Abstracts. Klaipėda, Baltic Valley, 42.
- Диденкулова И.И., **Родин А.А.** 2012. Статистика волновых групп от быстроходных судов. In: *XVIII Международная научно-техническая конференция „Информационные системы и технологии“ ИСТ–2012*, 18–20 апреля, 2012. Материалы конференции. Нижний Новгород, Нижегородский государственный технический университет, (IT Forum 2020), 359.
- Родин А.А.** 2012. Взаимодействие однонаправленных мелководных волн. In: *XVIII Международная научно-техническая конференция „Информационные системы и технологии“ ИСТ–2012*, 18–20 апреля, 2012. Материалы конференции. Нижний Новгород, Нижегородский государственный технический университет, (IT Forum 2020), 360.
- Родин А.А.**, Диденкулова И.И., Пелиновский Е.Н. 2012. Экстремальные волны на мелкой воде. In: *XIV Международная молодежная научно-*

- техническая конференция „Будущее Технической Науки“, Нижний Новгород, 18 мая, 2012. Тезисы докладов. Нижний Новгород, НГТУ им. П.Е. Алексеева, 425–426.
- Chaykovskaya N., **Rodin A.** 2012. The role of PR in the formation of psychological readiness for rogue wave events. *Geophysical Research Abstracts*, 14, EGU2012-1516.
- Pelinovsky E., Slunyaev A., Didenkulova I., Kharif Ch., Talipova T., Sergeeva A., Shurgalina E., **Rodin A.** 2011. Rogue waves in the ocean as a part of marine natural hazards. In: *19th Caribbean Geological Conference*, Le Gosier – Guadeloupe – French West Indies, 21–24 March 2011. Programme and Abstract Book. Le Gosier, Universite des Antilles et de la Guyane, 74.
- Chaykovskaya N., **Rodin A.** 2011 Psychological characteristics of human behavior at a rogue-wave event. *Geophysical Research Abstracts*, 13, EGU 2011-3981.
- Чайковская Н.А., **Родин А.А.** 2011 Психологическое сопровождение действий человека в стрессовых ситуациях. In: *Труды межрегиональной научно-практической конференции преподавателей, практических психологов и студентов „Современная психология в экономике, политике и социальной сфере“*, Нижний Новгород, НГТУ им. П.Е. Алексеева, 2011.
- Pelinovsky E., **Rodin A.** 2011. Large-amplitude simple and shock waves in shallow water. *Geophysical Research Abstracts*, EGU2011-62.
- Rodin A.**, Pelinovsky E. 2011. Transformation of large-amplitude nonlinear wave in shallow water. In: *8th Baltic Sea Science Congress*, 22–26 August, 2011, St.Petersburg, Russia. Book of Abstracts. St. Petersburg, RSHU, 270.
- Родин А.А.**, Чайковская Н.А. 2011. Исследования эволюции волн большой амплитуды в рамках уравнений мелкой воды и их значение для обеспечения безопасности людей в экстремальных ситуациях. In: *XVII Международная научно-техническая конференция „Информационные системы и технологии“ ИСТ–2011*, 26–28 апреля, 2011. Материалы конференции. Нижний Новгород, Нижегородский государственный технический университет, (IT Forum 2020), 420–421.
- Чайковская Н.А., **Родин А.А.** 2011 Психологические особенности поведения человека в экстремальных условиях. In: *Труды III международной заочной научно-практической конференции „Человек: Информация, технология, знак“*, Ульяновск, Изд-во УлГТУ, 1, 108–111.
- Чайковская Н.А., **Родин А.А.** 2010. Исследование особенностей массового поведения в экстремальных условиях в курсе „Психология массовых коммуникаций“. In: *Труды I международной научно-практической конференции „Актуальные проблемы социальной коммуникации“*, Нижний Новгород, НГТУ, 431–433.
- Rodin A.** 2010. Interactive decision: expert method in natural hazards. *Geophysical Research Abstracts*, EGU2010-15217.
- Шапошников Д.Е., **Родин А.А.** 2010. Метод интерактивной оценки параметров модели принятия решения . In: *XVI Международная научно-*

техническая конференция „Информационные системы и технологии“ ИСТ–2010, 23 апреля 2010. Материалы конференции. Нижний Новгород, Нижегородский государственный технический университет, (IT Forum 2020), 270.

Шапошников Д.Е., **Родин А.А.** 2010. Теоретическая модель принятия решения в условиях неопределенности. In: *Тезисы докладов 20-й Международной НТК по графическим информационным технологиям и системам „КОГРАФ-2010“*, 9 апреля 2010. Нижний Новгород, НГТУ, ISBN 978-5-9902087-1-1.

Куркин А.А., Козелков А.С., **Родин А.А.** 2004. Количественная оценка цунамиопасности и схема цунамирайонирования для побережья бассейна карибского моря. In: *Будущее технической науки: сборник материалов III Международной молодежной научно-технической конференции*, 26–27 мая 2004. Тезисы докладов. Нижний Новгород, НГТУ им. Р.Е. Алексеева, 432–433.

Appendix B: Elulookirjeldus

1. Isikuandmed

Ees- ja perekonnanimi Artem Rodin
Sünniaeg ja -koht 21.02.1987, Nižni Novgorod, Venemaa
Aadress Akadeemia tee 21, 12618 Tallinn
Telefon (+372) 620 4178
e-mail artem@ioc.ee

2. Hariduskäik

Õppeasutus	Lõpetamise aeg	Haridus (eriala / kraad)
Nizhny Novgorodi Riiklik Tehnikaülikool	2010	Matemaatika magister
Nizhny Novgorodi Riiklik Tehnikaülikool	2008	Matemaatika bakalaureus

3. Keelteoskus

Keel	Tase
inglise	kõrgtase
vene	emakeel
eesti	algtase

4. Täiendõpe

Õppimise aeg	Täiendõppe läbiviija nimetus
Juuni–August 2012	Gene Golub SIAM suvekool <i>Simulation and Supercomputing in the Geosciences</i> , USA
September 2011	BalticWay suvekool <i>Preventiivsed meetodid keskkonna kaitseks</i> , Klaipėda, Leedu

5. Teenistuskäik

Töötamise aeg	Tööandja nimetus	Ametikoht
Veebr. 2011 – tänaseni	Tallinna Tehnikaülikool, Küberneetika Instituut	tehnik
Sept. 2007 – Jaan. 2008	MERA Networks	tarkvara insener

6. Teadustegevus

Avaldatud teadusartiklite ja konverentsiteeside ning peetud konverentsiettekannete loetelu on toodud ingliskeelse CV juures.

Paper I

Didenkulova I., **Rodin A.** 2013. A typical wave wake from high-speed vessels: its group structure and run-up. *Nonlinear Processes in Geophysics*, 20, 179–188.



A typical wave wake from high-speed vessels: its group structure and run-up

I. Didenkulova^{1,2} and A. Rodin^{1,2}

¹Laboratory of Wave Engineering, Institute of Cybernetics at Tallinn University of Technology, Akadeemia tee 21, 12618 Tallinn, Estonia

²Nizhny Novgorod State Technical University, Nizhny Novgorod, Russia

Correspondence to: I. Didenkulova (ira@cs.ioc.ee)

Received: 2 September 2012 – Revised: 4 February 2013 – Accepted: 4 February 2013 – Published: 26 February 2013

Abstract. High-amplitude water waves induced by high-speed vessels are regularly observed in Tallinn Bay, the Baltic Sea, causing intense beach erosion and disturbing marine habitants in the coastal zone. Such a strong impact on the coast may be a result of a certain group structure of the wave wake. In order to understand it, here we present an experimental study of the group structure of these wakes at Pikakari beach, Tallinn Bay. The most energetic vessel waves at this location (100 m from the coast at the water depth 2.7 m) have amplitudes of about 1 m and periods of 8–10 s and cause maximum run-up heights on a beach up to 1.4 m. These waves represent frequency modulated packets where the largest and longest waves propagate ahead of other smaller amplitude and period waves. Sometimes the groups of different heights and periods can be separated even within one wave wake event. The wave heights within a wake are well described by the Weibull distribution, which has different parameters for wakes from different vessels. Wave run-up heights can also be described by Weibull distribution and its parameters can be connected to the parameters of the distribution of wave heights 100 m from the coast. Finally, the run-up of individual waves within a packet is studied. It is shown that the specific structure of frequency modulated wave packets, induced by high-speed vessels, leads to a sequence of high wave run-ups at the coast, even when the original wave heights are rather moderate. This feature can be a key to understanding the significant impact on coasts caused by fast vessels.

1 Introduction

Waves induced by high-speed vessels, the depth Froude number (the ratio of the ship's speed and the maximum phase speed of linear water waves for the given depth) of which during the regular sailing regime exceeds 0.6, have become a subject of intensive study in the last ten years after the new generation of large and powerful ships operating at cruise speeds up to 30 knots has been introduced (Parnell and Kofoed-Hansen, 2001; Parnell et al., 2007, 2008; Soomere, 2007; Kurennoy et al., 2009, 2011; Torsvik et al., 2009; Rapaglia et al., 2011). It has been demonstrated that these waves can be a major contributor of energy to sections of coasts that are exposed to significant natural hydrodynamic loads (Soomere, 2005a). The actual effect depends upon the features of the coastal environment and the existing hydrodynamic loads. In this context, specific types of disturbances, such as high leading waves, monochromatic packets of relatively short waves, solitary and cnoidal wave trains ahead of the vessel and associated depression areas, all qualitatively different from the usual wind waves or constituents of the linear Kelvin wake, are extremely important (Brown et al., 1989; Neuman et al., 2001; Garel et al., 2008). These specific wave disturbances have been observed, for example, in the Venice Lagoon, Italy (Rapaglia et al., 2011), Savannah River, Georgia (Houser, 2011), New Zealand and Denmark (Parnell and Kofoed-Hansen, 2001) and Tallinn Bay, Estonia (Parnell et al., 2008).

All of these cases are characterized by the serious damage of coastal environment. In the Marlborough Sounds, New Zealand, the introduction of high-speed ferries was accompanied by rapid and significant accretion

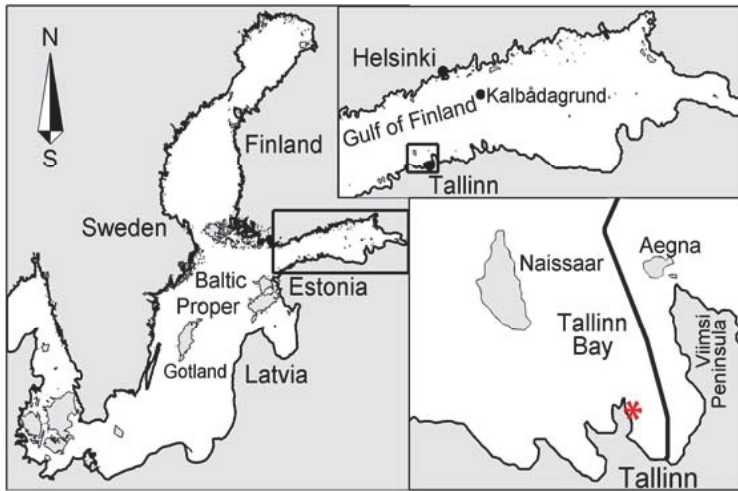


Fig. 1. Location scheme of the Baltic Sea and the study site.



Fig. 2. High-speed vessel wakes at the Pikakari beach, Tallinn Bay, Baltic Sea.

(Parnell and Kofoed-Hansen, 2001). In contrast, in Tallinn Bay, Estonia, long and energetic groups of vessel waves resulted in dramatic erosion of initially accreting beach at Aegna Island (Parnell et al., 2008; Soomere et al., 2009). These groups could easily smooth out the emerging berm and sometimes exert very large run-up events (Didenkulova et al., 2009a; Soomere et al., 2009). The highest and longest ship waves from the first group reached over 1 m above still water level with several examples going over 1.5 m above still water level (Didenkulova et al., 2009a; Torsvik et al., 2009). However, on a few days there was evidence of overwash deposits at heights about 2 m above water level (Soomere et al., 2009). The loss of sediments caused by one vessel wake was up to 1 m^3 per meter of the coastline (Soomere et al., 2009). At Pikakari beach in Tallinn Bay, wake-induced sediment transport produced a stable convex nearshore beach profile (Didenkulova and Soomere, 2011) similar to a spe-

cific shape of the coast, which allows anomalous “nonreflecting” wave behavior (Didenkulova et al., 2009b).

Even though the significant effect of waves from high-speed vessels on low-energy coasts has been demonstrated for different basins and environments, the reason of its such strong impact still remains unclear. It can be partially connected to the net transport of water, excited by ships sailing at transcritical speeds, which may produce water level set-up under groups of high vessel waves and result in a rapid reaction of the coast (Soomere et al., 2011). This effect may also be reinforced by the specific group structure of vessel-induced waves, when the largest, the longest and the most asymmetric waves come first and more symmetric waves of smaller amplitude and period come after. The characteristic properties of these groups are experimentally studied in this paper for Pikakari beach in Tallinn Bay, the Baltic Sea.

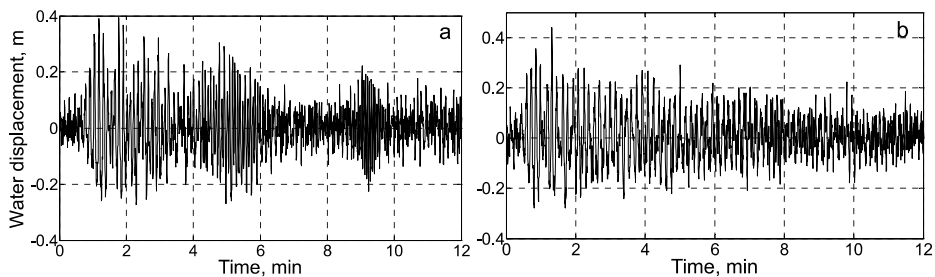


Fig. 3. Vessel wakes from (a) *SuperStar* (18 June 2009), (b) *Star* (20 June 2009).

2 Experimental set-up

Tallinn Bay is a semi-sheltered bay in the almost tideless Baltic Sea, which is characterized by the relatively mild wind wave climate. The peak periods of wind waves are usually well below 3 s, reaching 4–6 s in strong storms and only in exceptional cases exceeding 7–8 s (Soomere, 2005b). The significant wave height in the bay exceeds 0.5 m with a probability of 10% (Soomere, 2005b).

In contrast to this low wind wave activity, Tallinn Bay regularly hosts fast vessel traffic, with fairways located close to the shoreline and vessels operating at cruise speeds up to 30 knots (Parnell et al., 2008; Torsvik et al., 2009; Soomere et al., 2011). Fast vessel generated waves considerably exceed typical periods and heights of wind waves (Soomere, 2005a; Parnell et al., 2008). The periods of the highest waves are of 8–15 s and their heights are up to 2 m depending on location (Parnell et al., 2008; Kurennoy et al., 2009, 2011).

An experiment focusing on the properties of vessel wakes and their impact on coasts was performed at the Pikakari beach, Tallinn Bay (Fig. 1) during the high traffic period from 12 June till 1 July 2009. The environmental conditions in the period of the experiment were rather low, with the wind wave background mostly of about 10 cm and reaching 40 cm during three days. The vessels of our interest were the high-speed ferries *Star*, *SuperStar* and *Viking XPRS*, following routes Helsinki–Tallinn. All three vessels are large conventional ships with lengths of about 200 m and operational speeds of 30 knots, which are capable to generate large-amplitude, long and long-crested waves in Tallinn bay. However, due to the variability in ship track and its speed along the track, the parameters of ship generated waves may vary, their averaged values are described in Kurennoy et al. (2009). Vessel generated waves were recorded using a downward-looking ultrasonic echo sounder (LOG aLevel®) with a sampling frequency of 5 Hz, mounted on a stable tripod approximately 100 m from the shoreline, 2.4 km from the sailing line at a water depth of about 2.7 m from 17 June till 1 July 2009, and were studied overall and with respect to the type of the vessel. The record contains 66 clearly identifiable wakes:

29 from *Star*, 23 from *SuperStar* and 14 from *Viking XPRS*. Maximum wave heights (up to 1 m) occurred exclusively for the longest waves with periods ~ 10 s whereas typical wind wave periods were 2–3 s.

In addition, maximum run-ups of all wake waves were measured at the coast manually, by following the inundation of each wake wave and using video recording from 12 June till 1 July 2009. Since the distance between the echo sounder and coastal measurements was rather short (slightly more than 2 wavelengths), it was easy to follow the propagation of each particular wave up to the coast. A wake shoaling on the beach at the experiment site is shown in Fig. 2. On the coast, one can see a pole for the run-up measurements and farther offshore a tripod, where sea level oscillations were recorded.

The time of video-recording was synchronized with the time of the echo sounder, so it was possible to link the wave height measured at the echo sounder and run-up at the coast for each wave in the wake. In total, run-ups from 86 wakes were measured: 36 of them from *Star*, 31 from *SuperStar* and 19 from *Viking XPRS*.

3 Statistics of waves and corresponding run-ups in the wake

The data set at Pikakari beach, Tallinn Bay, allows for a detailed study of the statistics of vessel-induced waves and corresponding run-ups. The most energetic vessel waves at this location have amplitudes of about 1 m and periods of 8–10 s with maximum run-up heights up to 1.4 m.

All measured wave wakes have a specific structure of frequency modulated packets, where the largest and longest waves come first and waves of smaller amplitude and period after (Fig. 3). Sometimes the groups of different heights and periods can be separated even within one wake, as it is shown in Fig. 3a, where three groups of waves can be clearly identified. The highest waves (with a height of up to 1 m) usually belong to the first group and occur after the passage of several long, high-amplitude waves.

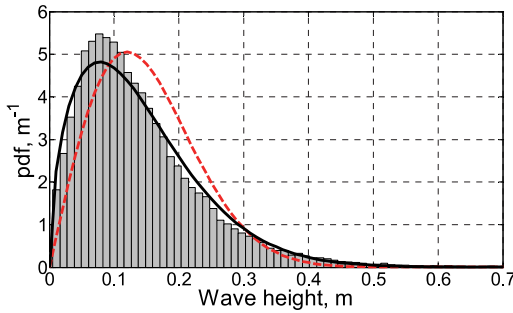


Fig. 4. Averaged distribution of wave heights within the wave wake; red dashed line corresponds to the Rayleigh distribution ($\sigma = 0.12$ m), black solid line corresponds to the Weibull distribution ($\sigma = 0.16$ m, $q = 1.53$) fitted using the maximum likelihood estimate.

The averaged distributions of wave heights within the vessel wake, computed by the up-crossing method, are demonstrated in Figs. 4 and 5. The averaging was performed over all 66 recorded events (Fig. 4) and for each specific ship that crossed the bay several times during the time of the observations (Fig. 5). The average distribution gathering the data from all ships might be reasonable, since all studied vessels are characterized by similar lengths, widths, draughts and operational speeds and induce similar wave wakes, and, therefore, can be considered as an averaged wake wave height distribution. It can be seen that most of wave heights are distributed within the interval < 30 cm and the number of particularly high waves in the wake is rather low. For example, the waves whose heights are larger than 40 cm constitute just 2% of the wave heights within one wake. For wakes from different vessels it varies from 1% for *Viking XPRS*, 2% for *Star* and 3% for *SuperStar*.

The obtained distributions of wave heights H within a wave wake are approximated by the mostly used probability density functions (pdf) in wave statistics: the one-parametric Rayleigh pdf

$$f_R(H, \sigma) = \frac{H}{\sigma^2} \exp\left[-\frac{H^2}{2\sigma^2}\right], \quad (1)$$

described by the only one scale parameter σ , measured in m, and two-parametric Weibull pdf

$$f_W(H, \sigma, q) = \frac{q}{\sigma} \left(\frac{H}{\sigma}\right)^{q-1} \exp\left[-\left(\frac{H}{\sigma}\right)^q\right], \quad (2)$$

described by a scale parameter σ and a shape parameter q , using a nonlinear least squares method. Rayleigh distribution describes amplitudes of narrow-band Gaussian processes. However, sea wave measurements often deviate from Rayleigh. This is why, in oceanology, e.g. for wind

wave fields, a generalization of Rayleigh distribution – two-parametric Weibull distribution is used. Since Rayleigh distribution fails to describe ship-generated waves, we follow the same scheme as for wind waves and apply two-parametric Weibull distribution for a better fit. Both approximated distributions are plotted in Figs. 4 and 5. It can be seen that Rayleigh pdf does not work well for description of the waves in the vessel wake. The best observed fit is for the *Viking XPRS*. However, Weibull pdf seems to be a fairly good model describing distribution of wave heights within a single vessel wake. Even though it underestimates the height of the distribution for waves of small (~ 10 cm) amplitude, it describes well the distribution of all larger wave heights > 15 cm. The mentioned discrepancy for small amplitude waves can be related to the existence of wind wave background, whose amplitudes were < 15 cm during most of the time of the experiment except a few days.

Approximated scale parameter σ remains the same for overall wave distribution (Fig. 4) and for distributions found for particular vessel types (Fig. 5) and is of the same order for both Rayleigh and Weibull pdfs. It changes from 0.1 m till 0.13 m for Rayleigh distribution and from 0.15 m to 0.16 m for Weibull distribution.

The shape parameter q in Weibull distribution varies more significantly. It is equal to 1.53 for overall distribution and reaches the value of 1.45 for *Star*, 1.52 for *SuperStar* and 1.71 for *Viking XPRS* vessels. This variety can be explained if we consider a physical meaning of the parameter q comparing Weibull distribution with Glukhovskiy distribution obtained for description of sea wave statistics at intermediate water depth (Glukhovskiy, 1966). Glukhovskiy distribution has been obtained semi-empirically for wind waves in the coastal zone of the Caspian Sea by including an additional parameter, the water depth. Since both Weibull and Glukhovskiy distributions represent a generalization of the Rayleigh distribution, we use this analogy and apply it to ship-generated waves in shallow water. For this purpose it is more convenient to consider cumulative distribution functions (cdf). For Weibull distributions it has the following form

$$F_W(H, \sigma, q) = 1 - \exp\left[-\left(\frac{H}{\sigma}\right)^q\right]. \quad (3)$$

The Glukhovskiy cdf is described by the following expression (Glukhovskiy, 1966)

$$F_G(H, \bar{H}, h) = 1 - \exp\left[-\frac{\pi}{4\left(1 + \frac{\bar{H}}{\sqrt{2\pi}h}\right)} \left(\frac{H}{\bar{H}}\right)^{\frac{2}{1-\bar{H}/h}}\right], \quad (4)$$

where \bar{H} is the mean wave height and h is the water depth. Comparing Eqs. (3) and (4) we find a connection between parameter σ and q in Eq. (3) and characteristics of wave field:

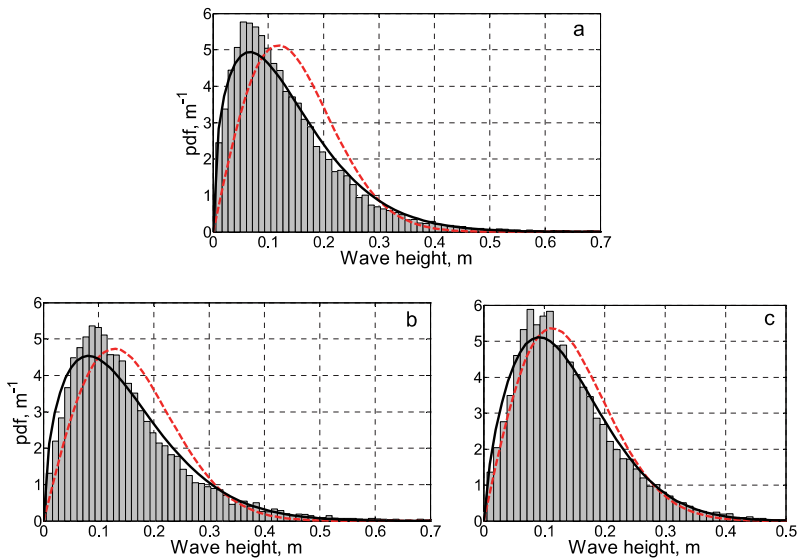


Fig. 5. Averaged distribution of wave heights within the wave wake of (a) *Star*, (b) *SuperStar* and (c) *Viking XPRS*; red dashed line corresponds to the fitted Rayleigh distribution with corresponding parameter σ (a) 0.12 m, (b) 0.13 m, (c) 0.11 m; black solid line corresponds to the fitted Weibull distribution with corresponding parameters (σ, q) (a) (0.15 m, 1.45), (b) (0.16 m, 1.52), (c) (0.15 m, 1.71) fitted using the maximum likelihood estimate.

$$q = \frac{2}{1 - \bar{H}/h}, \quad \sigma = \bar{H} \left(\frac{4}{\pi} + \left(\frac{2}{\pi} \right)^{3/2} \frac{\bar{H}}{h} \right)^{\frac{1-\bar{H}/h}{2}}. \quad (5)$$

Taking into account the water depth at the location of conducted measurements ($h = 2.7$ m) and applying the mean wave height ($\bar{H} = 0.14$ m), parameters of the Weibull distribution can be estimated as $\sigma \approx 0.16$ m and $q \approx 2.1$, which are close to the values calculated from the original data.

The averaged distributions of corresponding run-up heights on a beach, caused by a single wave wake are shown in Figs. 6 and 7 for overall run-up distribution and with respect to vessels of different types. Similar to wave heights, these distributions can also be approximated by Rayleigh and Weibull pdfs, which are marked by the corresponding lines in Figs. 6 and 7, and it can be seen that the Weibull distribution works quite well even for description of run-up heights. However, the shape parameters are more diversified for run-up heights. For the Rayleigh distribution, $\sigma = 0.38$ m for overall distribution and for *Star*, 0.40 m for *SuperStar* and 0.33 m for *Viking XPRS* vessels. Similar to wave heights, scale parameter in Weibull distribution for run-ups is slightly larger than the one for the Rayleigh pdf: $\sigma = 0.56$ m for overall distribution and for *Star*, 0.59 m for *SuperStar* and 0.49 m for *Viking XPRS* vessels. The shape parameter $q = 2.77$ for over-

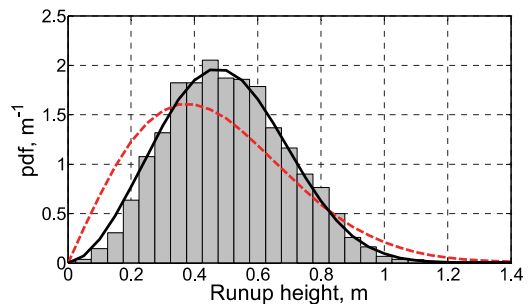


Fig. 6. Averaged distribution of run-up heights within the wave wake; red dashed line corresponds to the Rayleigh distribution ($\sigma = 0.38$ m), black solid line corresponds to the Weibull distribution ($\sigma = 0.56$ m, $q = 2.77$) fitted using the maximum likelihood estimate.

all distribution, 2.75 for *Star*, 2.93 for *SuperStar* and 2.70 for *Viking XPRS* vessels.

Knowing parameters of distributions, we can calculate the corresponding mean wave and run-up heights straight from the distribution:

$$\bar{H} = \int_0^{\infty} H f(H) dH, \quad (6)$$

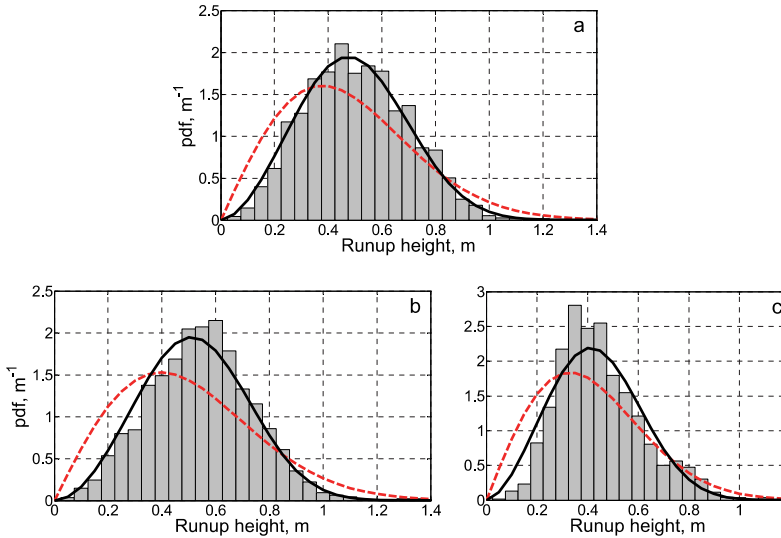


Fig. 7. Averaged distribution of run-up heights within the wave wake of (a) *Star*, (b) *SuperStar* and (c) *Viking XPRS*; red dashed line corresponds to the Rayleigh distribution with corresponding parameters σ (a) 0.38 m, (b) 0.40 m, (c) 0.33 m; black solid line corresponds to the Weibull distribution with corresponding parameters (σ, q) (a) (0.56 m, 2.75), (b) (0.59 m, 2.93), (c) (0.49 m, 2.70) fitted using the maximum likelihood estimate.

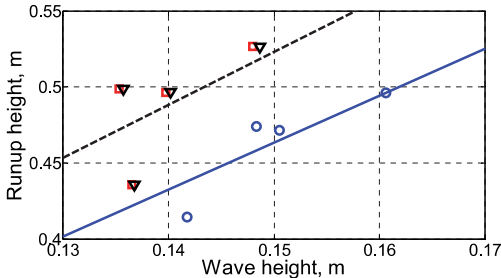


Fig. 8. Mean run-up and wave height in the wake, calculated from the original data (red squares) and reconstructed from Rayleigh (blue circles) and Weibull (black triangles) distributions; blue solid and black dashed lines correspond to the regression curve fitted heights calculated from the Rayleigh and Weibull distributions, respectively.

and consider an average wave amplification on a beach. The calculated values of mean wave and run-up heights, calculated from the original data and reconstructed from the obtained Rayleigh and Weibull distributions for overall statistics and for each vessel separately are presented in Fig. 8.

It is remarkable that original values of mean wave and run-up heights and those reconstructed from the Weibull distri-

bution are so close to each other that they practically coincide, which strongly indicates that Weibull distribution is an appropriate model for description of waves within a vessel wake. The heights reconstructed from Rayleigh distributions underestimate run-up observations by 10–20%. Based on the calculated data, the corresponding regression curves of wave amplification at the coast can be plotted (Fig. 8). Though regression lines, based on four points only, are not satisfactory, they can still indicate some trend. In the case of the Rayleigh and Weibull distributions they can be described by the following expressions

$$\bar{R} = 3.1\bar{H}, \tag{7}$$

$$\bar{R} = 3.5\bar{H}. \tag{8}$$

As it has been noticed before, the Rayleigh approximation gives smaller amplification at the coast and underestimates run-up heights.

For comparison, we estimate the amplification of non-breaking sinusoidal waves with a period $T = 10$ s, which corresponds to the period of the largest vessel waves, by the shallow water formula for long wave run-up on a plane beach (Didenkulova et al., 2007)

$$\frac{R}{H} = \pi \sqrt{\frac{2L}{\sqrt{gh}T}} \approx 6. \tag{9}$$

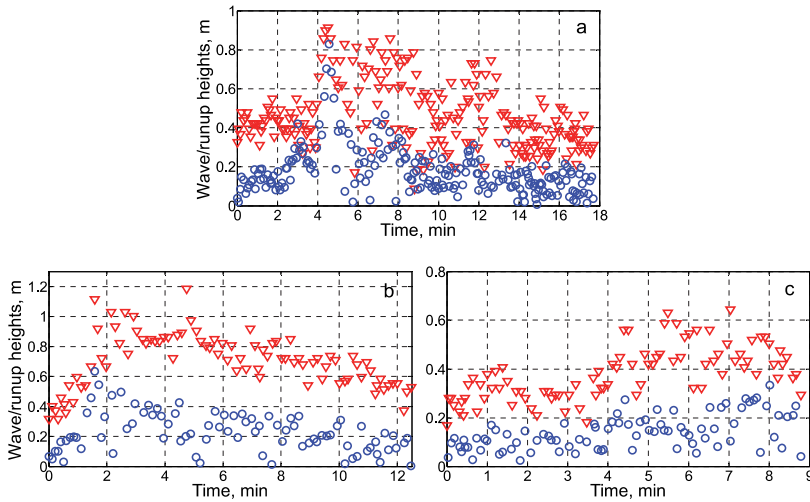


Fig. 9. Wave heights (blue circles) and corresponding run-up heights (red triangles) within the wake from (a) *SuperStar* (19 June 2009), (b) *Star* (20 June 2009) and (c) *Viking XPRS* (21 June 2009).

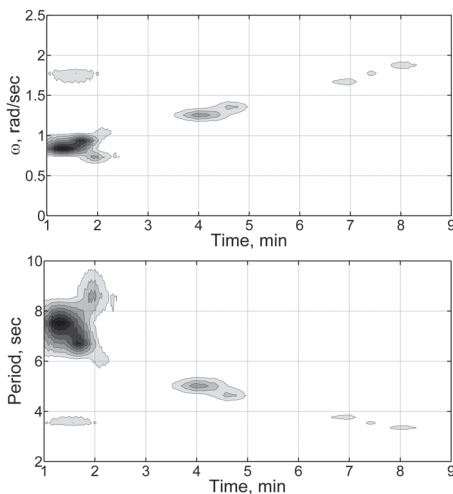


Fig. 10. Time-frequency spectrum for *SuperStar* (19 June 2009).

Here L is the distance to the shore (in our case $L = 100$ m), g is the gravity acceleration and h is the water depth ($h = 2.7$ m).

Thus, averaged amplification of vessel waves is almost twice as smaller than the one predicted by Eq. (9). This can be explained by strong dissipation during wave breaking, as very often vessel wakes break before reaching the coast (see Fig. 2).

4 Run-up of individual waves in the vessel wake

In order to better understand the details of individual wave run-up within the wake, we consider the run-up of three packets corresponding to three different types of vessels. As it has been mentioned before, the time at the echo sounder and at video recording was synchronized, making possible to identify the run-up of most of waves in the wake, except waves of very small amplitude (< 10 cm at the echo sounder record).

For this analysis we select a wave wake from *SuperStar*, which occurred on 19 June 2009 at 19:15; from *Star*, occurred on 20 June 2009 at 12:10; and from *Viking XPRS*, occurred on 21 June 2009 at 13:50. Corresponding wave and run-up heights for all of them are shown in Fig. 9.

It can be concluded from Fig. 9 that there is a fairly good correlation between wave and run-up data. Increase in the wave height generally corresponds to the increase in the run-up height. However, the maximum run-up in the wake does not always correspond to the maximum wave height. This is clearly seen in Fig. 9b and c, where the absolute maximum wave heights are not so pronounced as in Fig. 9a and are just slightly larger than for other waves.

At the same time Fig. 9a, with an outstanding peak for the highest wave, demonstrates numerous waves of much smaller height, which result in almost the same (just slightly smaller) run-up. This can be partially explained by different periods of wake waves, which is reflected in the time-frequency spectrum in Fig. 10.

The approach of three different groups with different periods is clearly seen in Fig. 10. The first group of waves, with peak period at 8 s, appears at the time moment of 1 min.

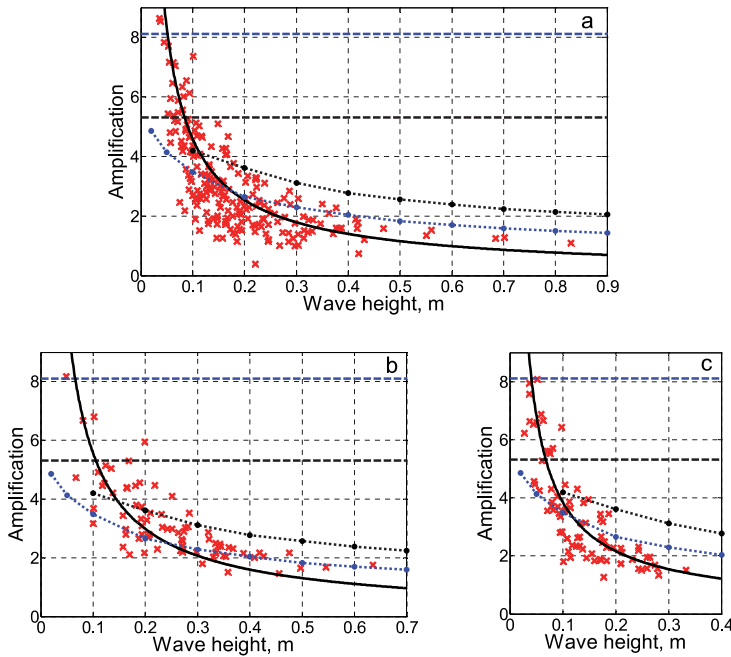


Fig. 11. Wave amplification on the beach plotted against wave height for wake waves from (a) *SuperStar* (19 June 2009), (b) *Star* (20 June 2009) and (c) *Viking XPRS* (21 June 2009). Dashed lines correspond to Eq. (9) and dotted lines correspond to calculation of breaking run-up with the characteristic period of 6 (blue) and 14 s (black). Black solid line corresponds to the power approximation described by Eq. (10).

Then, 3 min after, the second group with peak period at 5 s approaches. And finally, after 3 more minutes, the third group of waves with 4 s periods comes.

So, the structure of the wave packet is such that waves of longer period come first. At the same time the run-up height increases with decrease in the wave period (see Eq. 9) and this may explain why waves of the second group, which have smaller periods than the largest waves of the first group, produce the same run-up (see, time interval 4–8 min in Fig. 9a).

This effect may also be a key to the understanding of rapid beach erosion caused by fast-vessel wakes. The group structure of the wake works so that waves with the largest run-up heights come one after another resulting in the anomalous impact on the coast.

Another factor, which influences run-up height, is wave breaking, which affects waves of large amplitudes reducing their run-up. Observations show that very often the largest vessel induced waves break before they reach the coast (see, Fig. 2). Waves of larger amplitude break farther from the coast and dissipate stronger than smaller amplitude waves. This can be seen in Fig. 11 for wave amplification at the coast (R/H), where waves of smaller amplitude amplify stronger than the larger ones. For comparison, blue and black dashed horizontal lines correspond to the non-breaking run-

up on a plane beach (Eq. 9), calculated for waves with periods of 6 and 14 s. It can be seen that some smaller (probably, non-breaking) waves with wave heights < 20 cm may have the same amplification, but the majority of wake waves lie below this threshold.

The dotted lines in Fig. 11 represent the result of numerical simulation of wave amplification along a Pikakari beach profile. The numerical simulation is performed using the CLAWPACK (Conservation Laws Package) package (LeVeque, 2004), which models shallow water equations in the form of laws of conservation and allows formation and propagation of breaking waves parameterized by the shock waves. The propagation of such waves along a flat bottom is described in Pelinovsky and Rodin (2011); and Didenkulova et al. (2011). The calculated amplification curve decreases with an increase in the wave height, which is in a good agreement with the behavior of the experimental data. Waves of larger amplitude, which are more subject of wave breaking, are closer to the “breaking” curve, while smaller-amplitude waves are closer to the “non-breaking” line, what corresponds to our expectations.

The data from all three vessels in Fig. 11 can be very well described using the power regression curve (see, solid line in

Figs. 11)

$$\frac{R}{H} = aH^{-b}, \quad (10)$$

where the power coefficient varies within $0.75 \leq b \leq 0.95$ depending on the type of the vessel and dimensional coefficient changes within the range $0.4 \leq a \leq 1.0$. Obtained experimentally, Eq. (10) can be used for estimates of run-up heights from vessel generated waves.

5 Conclusions

The anomalous impact of waves from high-speed vessels on coasts is considered with respect to their specific group structure. The intensive vessel-induced waves and their run-ups are studied experimentally at the Pikakari beach in Tallinn Bay, the Baltic Sea, in summer 2009. In total, 66 wave wakes were recorded and 86 run-ups were measured from three different high-speed vessels: *Star*, *SuperStar* and *Viking XPRS*. It is shown that Weibull distribution can be a good model describing the distribution of wave heights in a single wake and corresponding run-up heights. This works for the overall distribution, as for wakes from different vessels. Both parameters of the Weibull distribution for wave heights can also be estimated from the Glukhovsky distribution for wind waves in shallow or intermediate water (Glukhovsky, 1966) and these estimates are in a good agreement with measured data. The mean wave and run-up heights, reconstructed from the Weibull distributions, demonstrate a great coincidence with the measurements. There is also a correspondence between mean wave and run-up heights showing that increase in one results in the increases in the other. It is found that, on average, vessel wave heights are amplified 3.5 times during 100 m of propagation to the coast.

The run-up of three particular wake waves, which correspond to three different vessels, is studied in detail. It is demonstrated that group structure of the wake, where the largest and the longest waves come first and waves of smaller amplitude and period come after, works so that waves with largest run-up heights come one after another resulting in the anomalous impact on the coast. This effect may be a key to understanding of the rapid beach erosion caused by fast vessel wakes.

Wave amplification varies significantly within a wake. Waves of large amplitude have very little amplification, which is explained by the influence of the wave breaking. At the same time small amplitude (< 20 cm) waves amplify significantly at the coast and can be described by the run-up of long non-breaking waves on a plane beach in the shallow water framework. Waves of moderate amplitude represent an intermediate case where wave breaking effects are still important, but they are influenced by wave dispersion and dissipation in the near bottom layer. For the description of these waves an empirical formula based on experimental data is provided.

Acknowledgements. This research was partially supported by the Federal Targeted Program "Research and educational personnel of innovation Russia" for 2009-2013, targeted financing by the Estonian Ministry of Education and Research (grant SF0140007s11), Estonian Science Foundation (Grant 8870), grants MK-1440.2012.5 and RFBR-12-05-33087. ID acknowledges the support provided by the Alexander von Humboldt Foundation and AR thanks DoRA 4 program. Authors thank Kevin Parnell and the team of Institute of Cybernetics (Tallinn, Estonia) for their help in organizing the experiment.

Edited by: E. Pelinovsky

Reviewed by: two anonymous referees

References

- Brown, E. D., Buchsbaum, S. B., Hall, R. E., Penhune, J. P., Schmitt, K. F., Watson, K. M., and Wyatt, D. C.: Observations of a nonlinear solitary wave packet in the Kelvin wake of a ship, *J. Fluid Mech.*, 204, 263–293, 1989.
- Didenkulova, I., Parnell, K. E., Soomere, T., Pelinovsky, E., and Kurennoy, D.: Shoaling and runup of long waves induced by high-speed ferries in Tallinn Bay, *J. Coast. Res., Special Issue*, 56, 491–495, 2009a.
- Didenkulova, I., Pelinovsky, E., and Soomere, T.: Long surface wave dynamics along a convex bottom, *J. Geophys. Res. Oceans*, 114, C07006, doi:10.1029/2008JC005027, 2009b.
- Didenkulova, I., Pelinovsky, E., Soomere, T., and Zahibo, N.: Runup of nonlinear asymmetric waves on a plane beach, in: *Tsunami & Nonlinear Waves*, edited by: Kundu, A., Springer, 175–190, 2007.
- Didenkulova, I., Pelinovsky, E., and Rodin, A.: Nonlinear interaction of large-amplitude unidirectional waves in shallow water, *Eston. J. Eng.*, 17, 289–300, 2011.
- Didenkulova, I. and Soomere, T.: Formation of two-section cross-shore profile under joint influence of random short waves and groups of long waves, *Mar. Geol.*, 289, 29–33, 2011.
- Garel, E., Fernández, L. L., and Collins, M.: Sediment resuspension events induced by the wake wash of deep-draft vessels, *Geo-Mar. Lett.*, 28, 205–211, 2008.
- Glukhovsky, B. H.: *Issledovanie morskogo vetrovogo volnenia (Study of sea wind waves)*, Leningrad, Gidrometeoizdat, 1966 (in Russian).
- Houser, C.: Sediment Resuspension by Vessel-Generated Waves along the Savannah River, Georgia, *J. Waterway, Port, Coastal Ocean Eng.*, 137, 246–257, 2011.
- Kurennoy, D., Soomere, T., and Parnell, K. E.: Variability in the properties of wakes generated by high-speed ferries, *J. Coast. Res. Special Issue* 56, 519–523, 2009.
- Kurennoy, D., Parnell, K. E., and Soomere, T.: Fast-ferry generated waves in south-west Tallinn Bay, *J. Coast. Res., Special Issue* 64, 165–169, 2011.
- LeVeque, R. J.: *Finite-volume methods for hyperbolic problems*, Cambridge Univ. Press, 2004.
- Neuman, D. G., Tapio, E., Haggard, D., Laws, K. E., and Bland, R. W.: Observation of long waves generated by ferries, *Canadian J. Remote Sens.*, 27, 361–370, 2001.
- Parnell, K. E. and Kofoed-Hansen, H.: Wakes from large high-speed ferries in confined coastal waters: Management approaches with

- examples from New Zealand and Denmark, *Coast. Manag.*, 29, 217–237, 2001.
- Parnell, K. E., McDonald, S. C., and Burke, A. E.: Shoreline effects of vessel wakes, Marlborough Sounds, New Zealand. *J. Coast. Res.*, Special Issue 50, 502–506, 2007.
- Parnell, K. E., Delpeche, N., Didenkulova, I., Dolphin, T., Erm, A., Kask, A., Kelpšaitė, L., Kurennoy, D., Quak, E., Räämet, A., Soomere, T., Terentjeva, A., Torsvik, T., and Zaitseva-Pärnaste, I.: Far-field vessel wakes in Tallinn Bay, *Estonian J. Eng.*, 14, 273–302, 2008.
- Pelinovsky, E. N. and Rodin, A. A.: Nonlinear deformation of a large-amplitude wave on shallow water, *Doklady Phys.*, 56, 305–308, 2011.
- Rapaglia, J., Zaggia, L., Ricklefs, K., Gelinis, M., and Bokuniewicz, H.: Characteristics of ships' depression waves and associated sediment resuspension in Venice Lagoon, Italy, *J. Mar. Syst.*, 85, 45–56, 2011.
- Soomere, T.: Fast ferry traffic as a qualitatively new forcing factor of environmental processes in non-tidal sea areas: a case study in Tallinn Bay, Baltic Sea, *Environ. Fluid Mech.*, 5, 293–323, 2005a.
- Soomere, T.: Wind wave statistics in Tallinn Bay, *Boreal Environ. Res.*, 10, 103–118, 2005b.
- Soomere, T.: Nonlinear components of ship wake waves, *Appl. Mech. Rev.*, 60, 120–138, 2007.
- Soomere, T., Parnell, K. E., and Didenkulova, I.: Implications of fast ferry wakes for semi-sheltered beaches: a case study at Aegna Island, Baltic Sea. *J. Coast. Res.*, Special Issue 56, 128–132, 2009.
- Soomere, T., Parnell, K. E., and Didenkulova, I.: Water transport in wake waves from high-speed vessels, *J. Mar. Syst.*, 88, 74–81, 2011.
- Torsvik, T., Didenkulova, I., Soomere, T., and Parnell, K. E.: Variability in spatial patterns of long nonlinear waves from fast ferries in Tallinn Bay, *Nonlin. Processes Geophys.*, 16, 351–363, doi:10.5194/npg-16-351-2009, 2009.

Paper II

Parnell K.E., Soomere T., Zaggia L., **Rodin A.**, Lorenzetti G., Rapaglia J., Scarpa G.M. 2015. Ship-induced solitary Riemann waves of depression in Venice Lagoon. *Physics Letters A*, 379, 555–559.



Ship-induced solitary Riemann waves of depression in Venice Lagoon



Kevin E. Parnell^{a,b}, Tarmo Soomere^{b,c,*}, Luca Zaggia^d, Artem Rodin^b,
Giuliano Lorenzetti^d, John Rapaglia^e, Gian Marco Scarpa^f

^a College of Marine and Environmental Sciences and Centre for Tropical Environmental and Sustainability Sciences, James Cook University, Queensland 4811, Australia

^b Institute of Cybernetics at Tallinn University of Technology, Akadeemia tee 21, 12618 Tallinn, Estonia

^c Estonian Academy of Sciences, Kohtu 6, 10130 Tallinn, Estonia

^d Institute of Marine Sciences, National Research Council, Castello 2737/F, 30122 Venice, Italy

^e Sacred Heart University Department of Biology, 5151 Park Avenue, Fairfield, CT 06825, USA

^f Università Ca' Foscari, Dorsoduro 3246, 30123 Venice, Italy

ARTICLE INFO

Article history:

Received 17 September 2014

Received in revised form 30 October 2014

Accepted 3 December 2014

Available online 8 December 2014

Communicated by F. Porcelli

Keywords:

Ship wakes

Bernoulli wake

Nonlinear waves

Shallow-water waves

Riemann wave

Bore formation

ABSTRACT

We demonstrate that ships of moderate size, sailing at low depth Froude numbers (0.37–0.5) in a navigation channel surrounded by shallow banks, produce depressions with depths up to 2.5 m. These depressions (Bernoulli wakes) propagate as long-living strongly nonlinear solitary Riemann waves of depression substantial distances into Venice Lagoon. They gradually become strongly asymmetric with the rear of the depression becoming extremely steep, similar to a bore. As they are dynamically similar, air pressure fluctuations moving over variable-depth coastal areas could generate meteorological tsunamis with a leading depression wave followed by a devastating bore-like feature.

© 2014 Elsevier B.V. All rights reserved.

1. Introduction

The wakes of ships range from the classical Kelvin wave groups [1,2] at low Froude numbers, to intricate nonlinear mechanisms at transcritical speeds [3], and to Mach-type systems at supercritical speeds [4,5]. It is commonly believed that the largest environmental impacts come from long and long-crested almost non-dispersive wave groups of significant amplitude [6,7]. Another recognized hazard is caused by solitonic waves that may result in high water velocities [8], elevate water levels at the shore [9] or build rogue waves [10]. The motion of a ship at finite depths also produces a depression region frequently called Bernoulli wake [11,12]. It is at times present at fairly low Froude numbers (down to 0.13 [13]) but is much more pronounced at moderate and high depth Froude numbers. It becomes often evident as a region of depression of nearly uniform depth [14–16], causes the draw-down effect (squat [17–22]) usually restricted to the navigation channel and may form structures similar to undular bore [23–25].

If the channel has adjacent harbor areas or wide banks, the depressions may cause extensive dropdown in the harbor water level [26], spread far away from the channel [27], or play the largest role in sediment resuspension [27–29]. They may penetrate to a distance of many hundreds of meters from the navigation channel [27,30]. The resulting events have a characteristic dominant, leading trough, followed by small crests [28].

The core new feature of our analysis is the description of striking features of ship wakes in a fairly realistic situation where a navigation channel is surrounded by wide but very shallow banks. The existing studies [15] suggest that in such situations the usual definition of the (depth-based) Froude number may lead to inconsistent results and unexpectedly high waves of elevation may occur at relatively modest Froude numbers.

The purpose of this paper is to provide evidence about unprecedentedly deep depression waves in this geometry and get some insight into how the resulting depression wave can be replicated, how far it can propagate and which are (fairly unexpected) implications from the described phenomenon for adjacent fields of wave science. The resulting long-living waves of depression obviously cannot be treated as linear or weakly nonlinear. We make an attempt to describe such events using fully nonlinear theory of shallow-water waves in terms of simple or Riemann waves [31,32].

* Corresponding author.

E-mail address: soomere@cs.ioc.ee (T. Soomere).

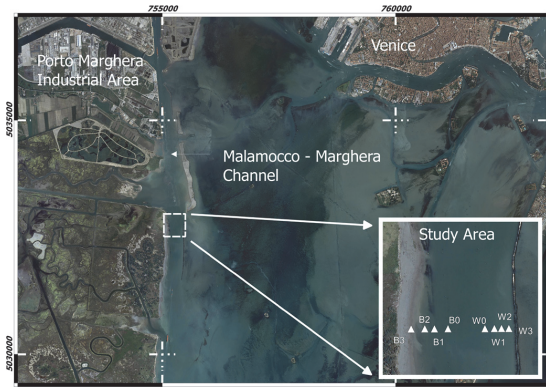


Fig. 1. The study area in the Malamocco–Marghera industrial channel. White triangles in the inset indicate the locations of pressure sensors in Fig. 2.

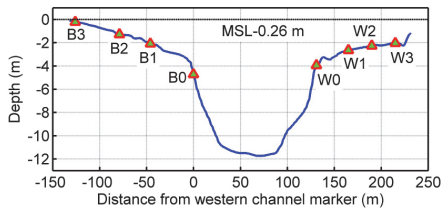


Fig. 2. Cross-section of the channel at the measurement site showing the location of pressure sensors (B0–B3, W0–W3). Distance is referenced to the western channel marker, and the depth is referenced to the local tidal datum (0.26 m below mean sea level (MSL)).

2. Ship-driven depressions

Venice Lagoon, the largest Italian lagoon (>500 km²), is extremely shallow (with an average depth of 0.8 m, the tidal range between 0.3 and 1.1 m) and crossed by numerous tidal channels and artificial waterways, as deep as 10 m or more. It underwent severe erosion after the construction of the Malamocco–Marghera industrial channel [33]. The channel (Fig. 1) is orientated almost north–south, 11–12 m deep and 60 m wide bottom with relatively steep slopes (~10%) that rise from this depth to about 4 m deep water (Fig. 2). On the western side of the channel, the water shoals at a constant slope (~3%) to a shoreline. The eastern side of the channel has a smaller slope of ~2% and is bordered by a permeable rock wall, the base of which is 90 m from the edge of the channel, at water depth ~2 m.

The measurements were performed using self-recording pressure sensors incorporated in various instruments (four InterOcean S4 current meters, one RBR Virtuoso wave gauge, one Ocean Seven CTD, two Esterline pressure sensors) at eight locations (Fig. 2). The InterOcean S4 instruments were fully time-synchronized while there may be some small error (± 10 s) for other instruments. Sensors at the edges of the channel were suspended from the channel markers, and all other sensors were mounted on the seabed. Data were collected at either 2 Hz or 5 Hz over four sampling periods of 2 to 6 days in March–April 2014. The data for three ships (Table 1) are selected out of about 90 recorded examples to illustrate the range of appearances of the wakes for ships with similar parameters.

Water level records (Fig. 3) are presented as actual water depths at the time of ship passage. The ships did not produce any substantial transient sign-variable wave groups or solitary waves of elevation evidently because of relatively low speeds (7.7–10.4 knots,

$Fr_d \sim 0.37$ –0.5). The dominant feature of the ship passage was a deep depression. The typical duration of an event from still water level preceding to still water level following was ~400 s, with the characteristic solitary trough (V-shaped wave of depression) lasting typically ~80 s. The characteristics of the depression produced by different vessels varied significantly. The maximum water level drop recorded (2.52 m from still water level at the shoreline side of the channel) was for *Abu Dhabi Star*, an unremarkable ship in terms of both its size and speed (Table 1).

A characteristic feature of the deepest depressions was the disparity of their maximum depths at the opposite margins of the channel. The maximum depth of the above depression by *Abu Dhabi Star* was only about 1.6 m on the lagoon side. *Domenico Loveli* produced a depression of 1.6 m on the lagoon side of the channel, but only 0.6 m on the shoreline side. The significant differences observed between the sides of the channel may reflect the position of the ship in the channel. Another reason may be the impact of the shape of the hulls. These depressions are, however, much larger than those previously reported [27,29,34].

The depressions were almost perfectly symmetric in time with respect to their deepest point at the margins of the navigational channel (locations B0 and W0 in Fig. 3). None of the recorded depressions had an elongated almost horizontal trough that is suggested by weakly nonlinear simulations [15,16]. This suggests that the depressions had strongly nonlinear nature.

The timing of the disturbance at subsequent sites (Fig. 3) indicates that the wave front moved obliquely with respect to the channel margin. Therefore, the subsequent recordings reflect the different parts of the wave crest. As around the measurement site the channel is essentially straight, its banks are almost homogeneous and the ship was moving at practically constant speed and direction, it is acceptable to assume that the properties of each depression only depend on the distance from the border of the channel.

The depression becomes gradually asymmetric with the distance from the channel margin. Its amplitude was usually smaller on the shoals compared to the channel edges but did not change significantly from one device to another (except at site B3, located in very shallow water where an increase in height was observed). The predominant process was an increase in the front/rear asymmetry of the wave profile. Its front slope became gradually less steep while the rear slope rapidly became steeper with the water surface exceeding the undisturbed level for a short period at the end of the some of the depression events. The asymmetry (defined as the ratio of typical values of the rear and front slopes) is usually well below 1.5 at sites W0 and B0 and increases to the level of 2–3 at sites B1 and B2, and to ~10 at sites W3 and B3. The overall appearance of the depression at sites B1–B3 and W1–W3 is a strongly skewed V-like shape. In most occasions an extremely steep section of the rear slope develops at the eastern (lagoon) side of the channel. Interestingly, virtually all records on the shoals demonstrate the development of a step, or a sequence of smaller steps on the rear slope of the depression wave.

3. Riemann waves

Based on the above arguments, we employ fully nonlinear 1D shallow-water equations for the description of the depression waves [31]:

$$\frac{\partial u}{\partial t} + u \frac{\partial u}{\partial x} + g \frac{\partial \eta}{\partial x} = 0, \quad \frac{\partial \eta}{\partial t} + \frac{\partial}{\partial x}[(h + \eta)u] = 0. \quad (1)$$

Here h is the unperturbed water depth, η is the water surface displacement, $u(x, t)$ is the depth-averaged horizontal velocity, g is

Table 1

Parameters of ships. The symbol C^* stands for the blocking coefficient (width \times draught/profile cross section area) and Fr_d is the depth-based Froude number.

Date	Time	Ship	Length, m	Width, m	Draught, m	Speed, knots	Direction of travel	C^*	Fr_d
28.03	8:30	<i>Pessada</i>	225	32	7	8.6	South	0.11	0.4
01.04	15:38	<i>Abu Dhabi Star</i>	183	32	7.8	7.7	North	0.14	0.37
22.04	6:50	<i>Domenico levoli</i>	146	20	6.6	10.4	South	0.07	0.5

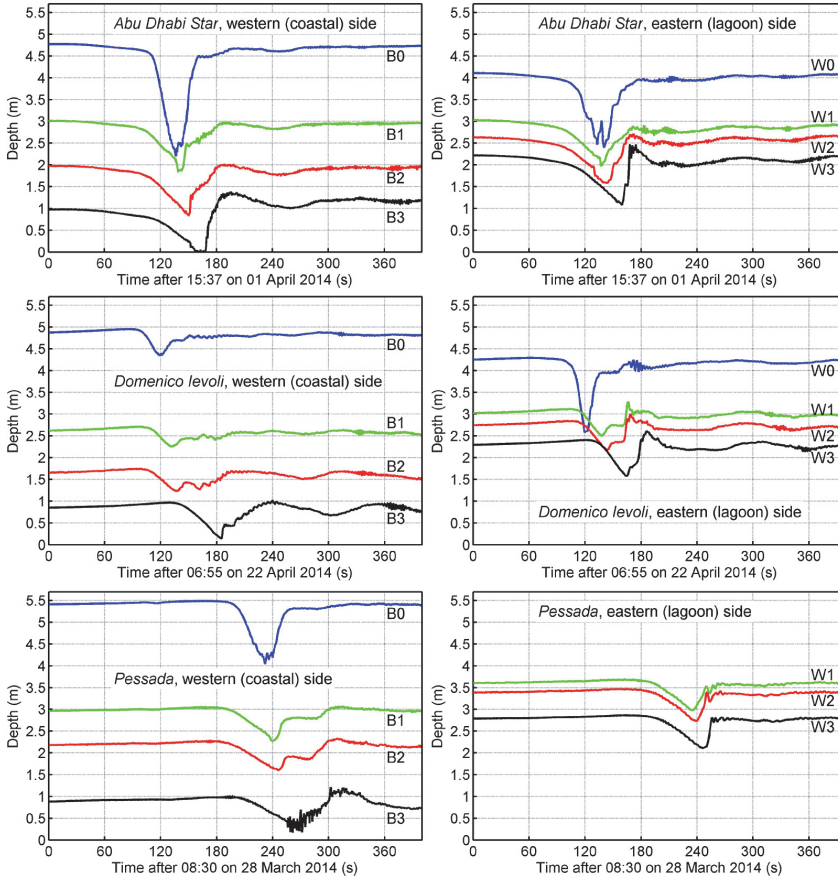


Fig. 3. Waves of depression driven by *Abu Dhabi Star*, *Domenico levoli* and *Pessada*. Data for W0 for the passage of *Pessada* is missing due to equipment failure. The largest depressions caused drying of the coastal slope at location B3.

acceleration due to gravity, x is the horizontal coordinate and t is time. Eqs. (1), formally, are exact equations for the waves of arbitrary amplitude if dispersion and dissipation can be neglected. They can be written in the flux form as follows:

$$\frac{\partial H}{\partial t} + \frac{\partial}{\partial x}(Hu) = 0, \quad \frac{\partial(Hu)}{\partial t} + \frac{\partial}{\partial x}\left(Hu^2 + \frac{gH^2}{2}\right) = 0, \quad (2)$$

where $H = h + \eta$ is the instantaneous total water depth. A classical solution to Eqs. (1), (2) is a so-called simple or Riemann wave that is well known in nonlinear acoustics [35,36]. It can be described via the shape of the water surface $H(x, t)$ and the associated flow speed:

$$H(x, t) = H_0[x - Vt], \quad u(x, t) = 2\left[\sqrt{gH(x, t)} - \sqrt{gh}\right], \quad (3)$$

where $H_0(x)$ describes the initial water surface profile. The local speed of nonlinear wave propagation is $V(x, t) = 3\sqrt{gH(x, t)} - 2\sqrt{gh}$. The Riemann waves of depression always propagate slower than the linear shallow-water wave speed \sqrt{gh} and tend to form a skewed shape with characteristic steep rear slope [31,32,37]. A Riemann wave of depression can only propagate over reasonable distances if its trough is not too deep: for $|\eta_{\max}| > (5/9)h$, the wave would almost instantly break [32,37]. This condition was only met at measurement site B3 located in less than 1 m deep water. Differently from several families of weakly nonlinear equations, solution (3) may be a long-living wave of depression. This solution has been often used to analyze the properties of waves produced, for example, by a wavemaker [32,37,38]. Here, ships play the role of a wavemaker.

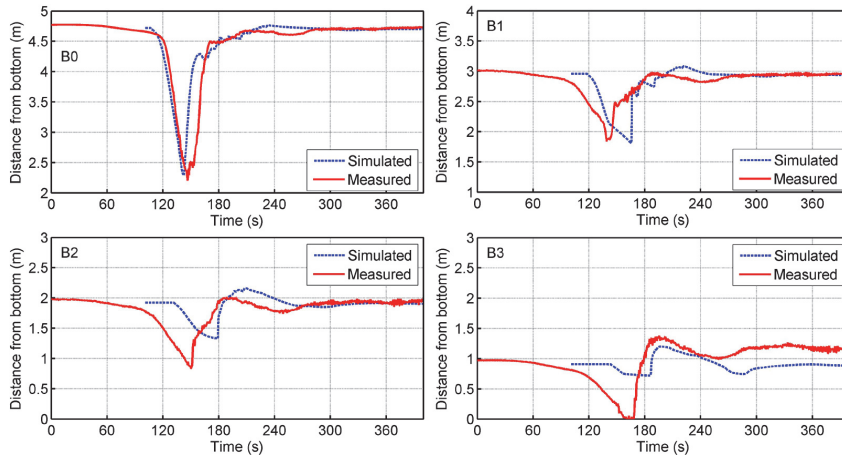


Fig. 4. Propagation of a numerically simulated Riemann wave matching the depression created by *Abu Dhabi Star* over the western side bank of the channel at measurement sites B0–B3.

4. Propagation of simulated Riemann waves

The propagation of depressions was simulated using the CLAW-PACK package, which solves Eqs. (2) with the finite volume method [39]. The numerical solution follows the mass conservation law with an accuracy of about $10^{-6}\%$ [38]. The boundary conditions were formulated as the Sommerfeld radiation condition. To smooth out small-scale ripples and other immaterial features of the measured profiles, at each side of the channel (near W0 or B0 in Fig. 4) the initial wave was assumed to have a Gaussian pulse of negative polarity. The amplitude, location and width of this pulse were chosen to match the maximum depth of the depression, its timing and the slope of the wave front at site W0 or B0. Another series of simulations (not shown) used an inverted shape of a Korteweg–de Vries soliton, defined in a similar manner, and led to almost coinciding results. This suggests that the basic properties of the propagation of the depression are largely defined by the slope and width of the disturbance. The flow velocity for this smoothed depression was defined using Eq. (3). The spatial grid step was 20 cm. Its refinement by 2–3 times leads to the difference in wave amplitudes of no more than 0.5%. The time step (0.5 s) has been chosen to satisfy the Courant–Friedrichs–Levy condition.

In spite of this rough approximation of the initial wave profile, the simulations replicate the major features of nonlinear propagation of depressions such as gradual smoothing of the wave front and development of steeper rear slope (Fig. 4). A certain time shift between the measured and simulated waves evidently reflects oblique propagation of the depressions with respect to the cluster of devices while the simulated wave front was assumed to propagate perpendicularly to the channel margin. The amplitude of the wave and the development of rear-front asymmetry (as defined above) are appreciably replicated at sites W1 and W2. The asymmetry of the simulated depression at W1–W3 and B1–B3 at times (when a step is developed in the rear slope) exceeds the asymmetry of the measured profile by an order of magnitude. The emergence of such steps in both recorded and simulated data is characteristic to the formation of the steep rear slope of large-amplitude Riemann waves of depression from Gaussian initial disturbances [38]. These steps are apparently fingerprints of reflected waves that propagate in the opposite direction to the depression wave if $|\eta_{\max}|$ approaches $(5/9)h$. Their replication is not perfect but clear qualitative match is evident at all sites. A mismatch between the measured and simulated amplitudes at site B3

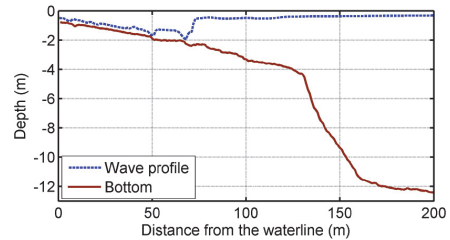


Fig. 5. The simulated wave profile produced by the depression wave of *Pessada* (Fig. 3) on the western side of the channel 80 s after reaching the channel margin. To the left of the trough there is sheet flow down the profile. Some fluctuations ahead of the shock are evidently caused by bottom profile irregularities.

is evidently related to the problems of replication of the drying effect.

Similarly to the measured data in Fig. 3, the propagation of the largest simulated depressions along the western (coastal) side of the channel led to almost drying out of the seabed (Fig. 5). For the largest waves along this shoreline the condition $|\eta_{\max}| > (5/9)h$ is usually met starting from a certain location along the profile. A shock-like rear slope of the trough appears almost instantaneously at this location and the wave propagates into the shallow area as a bore. In general these troughs can be well described by the numerical solution which in extreme cases can have different nonlinear effects [40].

5. Concluding remarks

Unexpectedly high (up to 2.5 m) solitary depression waves are generated by moderately-sized ships sailing at very moderate depth Froude numbers (<0.5) and blocking coefficients (<0.14) in channels surrounded by shallow banks. These depressions can propagate to a considerable distance (up to 500 m [27]) away from the navigation channel.

These disturbances are symmetric in time within the channel. The problem is specific to the case when the depression penetrates to a wide and shallow shoal (estuary, river bank, shallow lagoon, etc.). When moving as extremely long (typical periods of 40–50 s and lengths of 250–300 m) waves in very shallow water (2–3 m), they can be described in terms of strongly nonlinear sim-

ple or Riemann waves. Nonlinearity acts here in an expected way, by building up a steep rear slope or even bore-like features to the disturbance. This happens within less than ten seconds and over a distance of a few tens of meters.

A secondary impact of nonlinearity becomes evident as a temporary step-like profile of the rear slope. It is debatable which mechanism causes the small features seen in the observations at this site. For example, incipient undular bore formation probably modifies this part of the wake of *Pessada* at W1–W3 (Fig. 3) whereas a sort of reflection from the bottom may play a role in the evolution of *Domenico leovoli* wake at sites B3 and W1–W3 (Fig. 3). More importantly, the resulting water velocities, sediment resuspension and the overall environmental impact will be much (at least several times) larger than those evaluated based on the linear or weakly nonlinear approaches.

The presented material has important implications for re-evaluation of the chances of generation of a large tsunami wave of depression, or a similar wave preceded by a depression. The common understanding is that a meteorological tsunami is generated as a wave of elevation when an atmospheric disturbance moves at a near-critical speed. This wave may later develop, e.g., an *N*-wave preceded by a depression [41]. The dynamical similarity of ship wakes and meteorological tsunamis (a well-known feature explained in more detail in [42]) suggests that a substantial meteorological tsunami of depression can be directly generated by an atmospheric disturbance moving with a speed much less than the critical one along an abrupt scarp in the seabed, and that this process is possible for an often occurring geometry of seabed. Such tsunamis with a leading depression wave are eventually followed by a devastating bore-like feature.

Acknowledgements

The field studies were undertaken while K. Parnell was hosted by CNR-ISMAR, Venice, Italy, and were funded by the project Ritmare (SP3-WP3-A1). The underlying research into Riemann waves was funded by the Estonian Science Foundation (grant No. 9125), targeted financing by the Estonian Ministry of Education and Research (grant SF0140007s11), and through support of the European Regional Development Fund to the Centre of Excellence in Non-linear Studies CENS and project TERIKVANT (grant 3.2.0802.11-0043). A. Rodin is grateful for the support of the DoRa program to his PhD studies.

Appendix A. Supplementary material

Supplementary material related to this article can be found online at <http://dx.doi.org/10.1016/j.physleta.2014.12.004>.

References

- [1] J. Lighthill, *Waves in Fluids*, Cambridge University Press, 1978.
- [2] J.N. Newman, *Marine Hydrodynamics*, MIT Press, 1977.
- [3] T. Soomere, Nonlinear components of ship wake waves, *Appl. Mech. Rev.* 60 (2007) 120–138.
- [4] M. Rabaud, F. Moisy, Ship wakes: Kelvin or Mach angle?, *Phys. Rev. Lett.* 110 (2013) 214503.
- [5] A. Darmon, M. Benzaquen, E. Raphael, Kelvin wake pattern at large Froude numbers, *J. Fluid Mech.* 738 (2014) R3.
- [6] K.E. Parnell, H. Kofeod-Hansen, Wakes from large high-speed ferries in confined coastal waters: management approaches with examples from New Zealand and Denmark, *Coast. Manage.* 29 (2001) 217–237.
- [7] T. Soomere, Fast ferry traffic as a qualitatively new forcing factor of environmental processes in non-tidal sea areas: a case study in Tallinn Bay, Baltic Sea, *Environ. Fluid Mech.* 5 (2005) 293–323.
- [8] D. Neuman, E. Tapio, D. Haggard, K. Laws, R. Bland, Observation of long waves generated by ferries, *Can. J. Remote Sens.* 27 (2001) 361–370.
- [9] T. Soomere, K.E. Parnell, I. Didenkulova, Water transport in wake waves from high-speed vessels, *J. Mar. Syst.* 88 (2011) 74–81.
- [10] P. Peterson, T. Soomere, J. Engelbrecht, E. van Groesen, Soliton interaction as a possible model for extreme waves in shallow water, *Nonlinear Process. Geophys.* 10 (2003) 503–510.
- [11] W. Graff, Untersuchungen über die Ausbildung des Wellenwiderstandes im Bereich der Stauwellengeschwindigkeit in flachem, seitlich beschränktem Fahrwasser, *Schiffstechnik* 9 (1962) 110–122 (in German).
- [12] T. Jiang, *Ship Waves in Shallow Water*, Fortschritt-Berichte VDI, Reihe 12, Nr. 466, VDI Verlag, Düsseldorf, Germany, 2001.
- [13] C.E. Janson, Bernoulli waves in deep and shallow water at low speed, *Ship Technol. Res.* 49 (2002) 142–147.
- [14] P.G. Baines, *Topographic Effects in Stratified Flows*, Cambridge University Press, 1997.
- [15] T. Torsvik, G. Pedersen, K. Dysthe, *J. Waterw. Port Coast. Ocean Eng.* 135 (2007) 120.
- [16] T. Torsvik, I. Didenkulova, T. Soomere, K.E. Parnell, Variability in spatial patterns of long nonlinear waves from fast ferries in Tallinn Bay, *Nonlinear Process. Geophys.* 16 (2009) 351–363.
- [17] T. Constantine, On the movement of ships in restricted waterways, *J. Fluid Mech.* 9 (1961) 247–256.
- [18] P.M. Naghdi, M.B. Rubin, On the squat of a ship, *J. Ship Res.* 28 (1984) 107–117.
- [19] A. Millward, A review of the prediction of squat in shallow water, *J. Navig.* 49 (1996) 77–88.
- [20] T.P. Gourlay, Ship squat in water of varying depth, *Int. J. Marit. Eng.* 145 (2003) 1–8.
- [21] T.P. Gourlay, E.O. Tuck, The maximum sinkage of a ship, *J. Ship Res.* 45 (2001) 50–58.
- [22] T.P. Gourlay, A simple method for predicting the maximum squat of a high-speed displacement ship, *Mar. Technol.* 43 (2006) 146–151.
- [23] T. Akylas, On the excitation of long nonlinear water waves by a moving pressure distribution, *J. Fluid Mech.* 141 (1984) 455–466.
- [24] R.H.J. Grimshaw, N. Smyth, Resonant flow of a stratified flow over topography, *J. Fluid Mech.* 169 (1986) 429–464.
- [25] S.J. Lee, G.T. Yates, T.Y. Wu, Experiments and analyses of upstream-advancing solitary waves generated by moving disturbances, *J. Fluid Mech.* 199 (1989) 569–593.
- [26] B. Forsman, From bow to beach, in: *SSPA Highlights*, vol. 3, 2001, pp. 4–5.
- [27] J. Rapaglia, L. Zaggia, K. Ricklefs, M. Gelinias, H. Bokuniewicz, Characteristics of ships' depression waves and associated sediment resuspension in Venice Lagoon, Italy, *J. Mar. Syst.* 85 (2011) 45–56.
- [28] M. Gelinias, H. Bokuniewicz, J. Rapaglia, K.M.M. Lwiza, Sediment resuspension by ship wakes in the Venice Lagoon, *J. Coast. Res.* 29 (2013) 8–17.
- [29] G. Göransson, M. Larson, J. Althage, Ship-generated waves and induced turbidity in the Göta älv River in Sweden, *J. Waterw. Port Coast. Ocean Eng.* 140 (2014) 04014004, [http://dx.doi.org/10.1061/\(ASCE\)WW.1943-5460.0000224](http://dx.doi.org/10.1061/(ASCE)WW.1943-5460.0000224).
- [30] T.M. Ravens, R.C. Thomas, Ship wave-induced sedimentation of a tidal creek in Galveston bay, *J. Waterw. Port Coast. Ocean Eng.* 134 (2008) 21–29.
- [31] G.B. Whitham, *Linear and Nonlinear Waves*, Wiley, New York, 1974.
- [32] I.I. Didenkulova, N. Zahibo, A.A. Kurkin, E.N. Pelinovsky, Steepness and spectrum of a nonlinearly deformed wave on shallow waters, *Izvestiya Atmos. Ocean. Phys.* 42 (2006) 773–776.
- [33] A. Sarretta, S. Pillon, E. Molinaroli, S. Guerzoni, G. Fontolan, Sediment budget in the Lagoon of Venice, Italy, *Cont. Shelf Res.* 30 (2010) 934–949.
- [34] H. Balzerek, J. Kozłowski, Ship-induced riverbank and harbour damage. Evidence for claims processing, *Hydro International* (September 2007) 2–7.
- [35] O. Rudenko, S. Soluyan, *Theoretical Background of Nonlinear Acoustics*, Plenum, New York, 1977.
- [36] J.K. Engelbrecht, V.E. Fridman, E.N. Pelinovsky, *Nonlinear Evolution Equations*, Pitman Research Notes in Mathematics Series, vol. 180, Longman, London, 1988.
- [37] N. Zahibo, I. Didenkulova, A. Kurkin, E. Pelinovsky, Steepness and spectrum of nonlinear deformed shallow water wave, *Ocean Eng.* 35 (2008) 47–52.
- [38] I. Didenkulova, E. Pelinovsky, A. Rodin, Nonlinear interaction of large-amplitude unidirectional waves in shallow water, *Estonian J. Eng.* 17 (2011) 289–300.
- [39] R.J. LeVeque, *Finite-Volume Methods for Hyperbolic Problems*, Cambridge University Press, 2004.
- [40] E.N. Pelinovsky, A.A. Rodin, Transformation of a strongly nonlinear wave in a shallow-water basin, *Izvestiya Atmos. Ocean. Phys.* 48 (2012) 343–349.
- [41] S. Tadeipalli, C.E. Synolakis, Model for the leading waves of tsunamis, *Phys. Rev. Lett.* 77 (1996) 2141–2144.
- [42] I. Didenkulova, E. Pelinovsky, T. Soomere, Can the waves generated by fast ferries be a physical model of tsunami?, *Pure Appl. Geophys.* 168 (2011) 2071–2082.

Paper III

Rodin A., Soomere T., Parnell K.E., Zaggia L. 2015. Numerical simulation of the propagation of ship-induced Riemann waves of depression into the Venice Lagoon. *Proceedings of the Estonian Academy of Sciences*, 64, 22–35.



Numerical simulation of the propagation of ship-induced Riemann waves of depression into the Venice Lagoon

Artem Rodin^a, Tarmo Soomere^{a,b*}, Kevin E. Parnell^{a,c}, and Luca Zaggia^d

^a Institute of Cybernetics at Tallinn University of Technology, Akadeemia tee 21, 12618 Tallinn, Estonia

^b Estonian Academy of Sciences, Kohtu 6, 10130 Tallinn, Estonia

^c College of Marine and Environmental Sciences and Centre for Tropical Environmental and Sustainability Sciences, James Cook University, Queensland 4811, Australia

^d Institute of Marine Sciences, National Research Council, Castello 2737/F, 30122 Venice, Italy

Received 24 January 2015, revised 16 February 2015, accepted 17 February 2015, available online 4 March 2015

Abstract. Large in situ measured ship-induced depression waves (Bernoulli wakes) in the Malamocco–Marghera industrial channel of the Venice Lagoon are interpreted as long-living strongly nonlinear Riemann (simple) waves of depression. The properties of these depressions are numerically replicated using nonlinear shallow water theory and the CLAWPACK software. The further behaviour of measured depressions is analysed by means of replicating the vessel-induced disturbances with the propagation of initially smooth free waves. It is demonstrated that vessel-driven depressions of substantial height (>0.3 m) often propagate for more than 1 km from the navigation channel into areas of the lagoon of approximately 2 m water depth. As a depression wave propagates into the lagoon, its front slope becomes gradually less steep, but the rear slope preserves an extremely steep bore-like appearance and the amplitude becomes almost independent of the initial properties of the disturbance. Analysis suggests that even modest ships in terms of their size, sailing speed, and blocking coefficient may generate deep depressions that travel as compact and steep entities resembling asymmetric solitary waves over substantial distances into shallow water adjacent to navigation channels. Their impact may substantially increase the environmental impact of ship wakes in this and similar water bodies.

Key words: vessel wakes, nonlinear waves, shallow-water waves, Riemann wave, bore formation, Venice Lagoon.

1. INTRODUCTION

The classical theory of linear (Kelvin) ship waves (e.g., Wehausen, 1973; Newman, 1977; Lighthill, 1978; Kuznetsov et al., 2002) adequately describes the geometry of wave crests and several features of the distribution of wave heights for ships that sail steadily over a sea area of constant depth under low (depth- and length-based) Froude numbers. An increase in either of the Froude numbers leads to a wide range of nontrivial and often nonlinear phenomena. Sailing at moderate and near-critical depth Froude numbers ($0.6 \leq F_d < 1$) leads to the widening of the Kelvin wedge (the area filled with

waves that are stationary with respect to the ship) (Sorensen, 1973). This process is associated with the generation of long and long-crested leading waves. The resulting almost non-dispersive transient wave groups usually consist of a few crests that may result in substantial environmental impacts not only in the immediate vicinity of the sailing line (Parnell and Kofoed-Hansen, 2001) but also at a distance of many kilometres (Soomere, 2005; Parnell et al., 2007). These waves are often preceded by precursor solitons (Ertekin et al., 1984) that may be generated at depth Froude numbers as low as about 0.2 (Ertekin et al., 1986). Such structures often result in high water velocities (Neuman et al., 2001), elevate shoreline water levels (Soomere et al., 2011), and are capable of building long-living

* Corresponding author, soomere@cs.ioc.ee

rogue waves in shallow water (Peterson et al., 2003). An increase in the length-based Froude number at supercritical speeds may lead to Mach-type wave systems (Rabaud and Moisy, 2013; Darmon et al., 2014) in which the highest waves are located inside the Kelvin wedge (Noblesse et al., 2014).

Several components of vessel wakes may threaten ecosystems (Ali et al., 1999) and the users of the near-shore (Hamer, 1999) and the coast (Krylov, 2003) in regions where the levels of natural wave energy are normally small. Under specific conditions and in areas that are sheltered from ocean waves but exposed to significant ship traffic, vessel wakes may become a major factor in the dynamics of the coastal zone (Parnell and Kofoed-Hansen, 2001; Soomere, 2007). This feature has led to numerous attempts towards regulation of ship traffic in terms of the limitation of the wave height (Stumbo et al., 1999; Parnell and Kofoed-Hansen, 2001; Varyani, 2006). Most of these regulations set limits on just a single property of the wave field or on a characteristic single wave component of the entire system of disturbances generated by a vessel, usually the highest waves (Macfarlane et al., 2014). This policy is generally inadequate as a craft that operates in relatively shallow water usually excites an extremely complex wave pattern that may substantially vary both in physical and spectral space (Torsvik and Soomere, 2008; Sheremet et al., 2013; Torsvik et al., 2015). For example, a supercritical bore causes an abrupt elevation of water level that may result in a surge wave at the coast (Gourlay, 2001; Gourlay and Cook, 2004).

Moreover, this policy is often limited to the properties of either oscillatory motions of the water or to the waves of elevation. It is commonly accepted that for ship-generated disturbances the most significant environmental impacts come from almost non-dispersive wave groups of significant amplitude (Soomere, 2005). These groups, similar to tsunamis (Didenkulova et al., 2011b), may propagate over considerable distances, and may cause environmental damage and a hazard for people and property because their height and steepness (and consequently water velocities) are often amplified by shoaling. This understanding, however, implicitly reflects the properties of solutions of common equations for weakly nonlinear water waves (such as Korteweg–de Vries (KdV) or Kadomtsev–Pethviashvili equations). These equations may only have waves of elevation as their valid solitary-wave solutions.

A common effect of sailing at moderate and high depth Froude numbers (equivalently, in relatively shallow water) is the formation of a depression region (often called Bernoulli wake) in the ship's vicinity (Akylas, 1984; Grimshaw and Smyth, 1986; Lee et al., 1989). Its presence reflects a common feature of another class of weakly nonlinear disturbances – solutions of the KdV equation called undular bore, a phenomenon

known theoretically for more than 60 years (Benjamin and Lighthill, 1954; Peregrine, 1966). This effect is common in numerical experiments of one-dimensional ship motion where it becomes evident as a gradually lengthening region of depression of nearly uniform depth (Baines, 1997; Torsvik et al., 2009a, 2009b). It is a well-known feature in navigational channels where it causes the draw-down effect usually called squat (Constantine, 1961; Graff, 1962; Naghdi and Rubin, 1984). As it is a major source of danger in shallow water navigation (Millward, 1996; Gourlay, 2003), squat has been well documented (e.g. Gourlay and Tuck, 2001; Gourlay, 2006) and its forecast is made routinely (El-Kader et al., 2003).

Similar depression regions are always formed when a ship is sailing at moderate depth Froude numbers. They are often detected as dangerous water level draw-downs at the banks of navigable rivers (Balzerek and Kozłowski, 2007) or in harbours adjacent to shallow waterways (Forsman, 2001). While the depression area is usually thought to be concentrated in the vicinity of the hull, in some situations the depression may start travelling as a free wave. The situation is particularly complicated if the wave amplitude is large enough for nonlinearity to affect the wave propagation. As the wave propagates over shallow areas and finally impacts the shoreline, the effect of nonlinearity will lead to different behaviours of waves depending on the wave polarity. These differences have been extensively studied in tsunami research (e.g., Carrier et al., 2003; Fernando et al., 2008). However, most of the relevant studies have only addressed the classical solitary wave solutions to (weakly) nonlinear shallow-water equations, which are waves of elevation. The classical KdV model indicates that a sequence of elevation waves is rapidly formed from an initial depression (Arcas and Segur, 2012), with the leading elevation wave at the rear end of the depression being up to twice the height of the depression (Grimshaw et al., 2014).

The generation of a depression wave is particularly problematic if the navigation channel is surrounded by wide shallow-water areas. The classic case is the Venice Lagoon (Rapaglia et al., 2011). The depression waves may spread far away from the sailing line and substantial waves of depression have been reported at a distance of many hundreds of metres from the channel (Rapaglia et al., 2011). The rear of the depression often induces a bore-like feature at a certain distance from the generation area (Ravens and Thomas, 2008). The resulting events have a characteristic deep leading trough, followed by a set of crests (Gelinis et al., 2013). This scenario is common in the analysis based on non-dispersive shallow-water propagation in wave systems led by a wave of depression. Such systems are particularly prone to the formation of steep slopes and high velocities (Didenkulova et al., 2014). This is a

probable reason why ship-induced depression waves often play an unexpectedly large role in sediment resuspension (Rapaglia et al., 2011; Gelinas et al., 2013; Göransson et al., 2014).

Although weakly nonlinear theories provide an accurate qualitative picture of the various effects in areas to which depression waves propagate (Grimshaw et al., 2014), quantitative analysis of the fate of the largest examples of depression waves requires the application of fully nonlinear approaches. A recent study (Parnell et al., 2015) demonstrated that ships of fairly moderate size (blocking coefficient 0.07–0.14) and sailing at low to moderate depth Froude numbers (0.37–0.5) produce depressions with a depth up to 2.5 m at the border of the navigation channel. These waves decrease in height away from the channel but they obviously cannot be treated as linear or weakly nonlinear in the surrounding lagoon with the average depth of only 0.8 m. A feasible way to address these structures is the framework of fully nonlinear Riemann (or simple) waves (Whitham, 1974).

In this study we focus on the possibilities of numerical reconstruction of the propagation of such waves of depression in the Venice Lagoon. As discussed above, weakly nonlinear approaches are only conditionally valid for the depressions that may almost dry the seabed in shallow areas adjacent to the channel (Parnell et al., 2015). In the framework of fully nonlinear shallow-water theory, Riemann waves of depression may exist as free waves and propagate to substantial distances (Whitham, 1974; Didenkulova et al., 2006). The distinguishing feature of such waves, as is the case for ship-induced depression waves, is the development of a V -like shape with an extremely steep, often bore-like rear slope. It is likely that large-amplitude Riemann waves of depression become strongly asymmetric when they propagate into and through shallow water surrounding the navigation channel (Pelinovsky and Rodin, 2012).

The central question addressed in this paper is how far these waves may propagate from the region of generation. The previous research (Parnell et al., 2015) demonstrated that the technique of Riemann waves makes it possible to replicate the qualitative features of evolution of the wave shape over about 100 m along both almost horizontal and sloping shallow side banks of the channel. To shed light on the further evolution of these vessel wakes, it is necessary to reach a quantitative match of the simulated and measured wake properties. We first provide a systematic way to initialize the relevant numerical simulations so that the basic quantitative properties of ship wakes are satisfactorily reproduced for the entire sequence of wave measurement locations. Comparison of several dozens of reconstructions of the wave properties over side banks of the navigation channel provides an

indication of the reliability and uncertainty of these reconstructions. Finally, the evolution of several examples of numerical replications of the observed depressions is tracked over many hundred metres into the lagoon. The core result is an estimate of the distance at which such depressions still have a substantial amplitude and are capable of providing high near-bottom velocities.

2. DATA AND METHODS

2.1. Field observations of ship-induced waves of depression in the Venice Lagoon

The analysis of the propagation of depression waves in shallow water is based on measurements performed in spring 2014 in the Venice Lagoon, Italy. With a surface area of about 550 km² it is the biggest lagoon in the Mediterranean region (Brambati et al., 2003; Madricardo and Donnici, 2014). As this lagoon is an extremely shallow water body (average depth 0.8 m), its water circulation is mainly controlled by tidal excursion, which ranges between 0.3 and 1.1 m. Water exchange with the open sea occurs through three inlets, whose depths range from about 10 m to more than 17 m for the Malamocco inlet.

The lagoon was intensely modified through centuries with two main goals: preventing sediment deposition in the areas around the city of Venice (for defence purposes) and stabilization of the inlets and barrier islands. The first goal was achieved by a series of modifications, which ended with the diversions of larger rivers (Brenta and Piave) into the sea, completed in the 16th century. This intervention has played a role in aggravating more recent problems of subsidence, natural and human-caused, and sea-level rise. The second goal was also achieved with a series of adjustments that ultimately led to the protection of barrier islands with seawalls in the 18th century and the construction of jetties at the three inlets between the late 19th and the early 20th century (Brambati et al., 2003).

The development of the Porto Marghera Industrial Area between 1920 and 1970 directly to the west of Venice on the mainland coast (Fig. 1) was accompanied by dredging a new navigation channel (the Malamocco–Marghera channel, locally known as Canale dei Petrolì) connecting the industrial zone to the Malamocco inlet. With a total length of 20 km, a width of about 200 m in the east–west section and 100 m in the north–south section, and a depth of 12 m, this channel is able to accommodate medium-sized container ships, bulk carriers, and tankers. The channel leads to the south of Porto Marghera along the mainland coast for 14 km and then turns sharply towards the Malamocco inlet (Rapaglia et al., 2011).

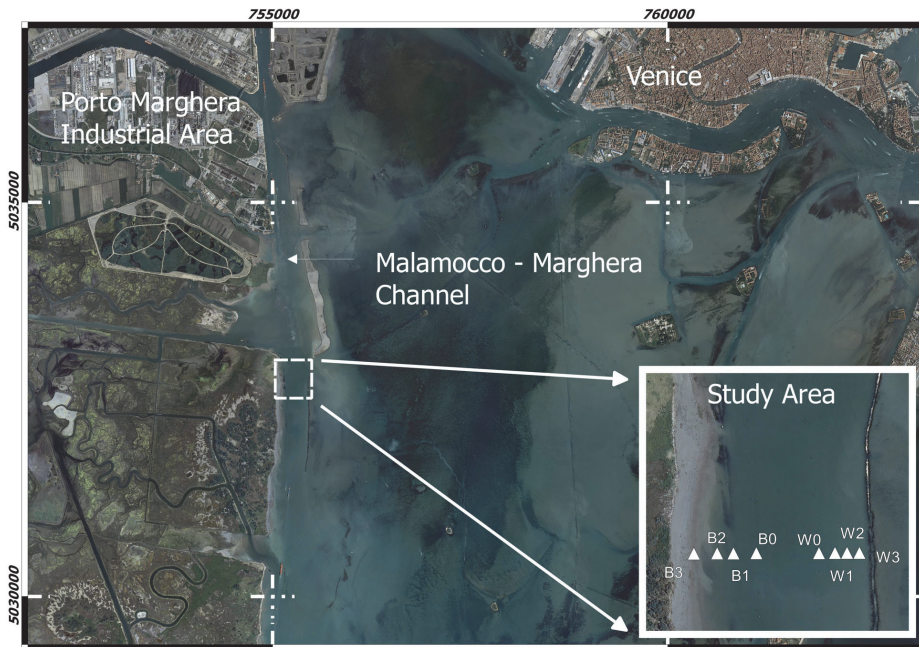


Fig. 1. Study area in the Malamocco–Marghera industrial channel in Venice. White triangles in the inset indicate the locations of pressure sensors in Fig. 2 (Parnell et al., 2015). Reprinted by permission from Elsevier.

As shown by the analysis of bathymetric surveys (Sarretta et al., 2010), severe erosion of the central lagoon basin occurred from 1970 to 2000, in the period following the opening of this waterway. Sediment transport studies by Defendi et al. (2010) showed that more recently the sediment loss from the Malamocco inlet was considerably lower than expected from the trend of bathymetric changes.

The potential environmental impact of ship traffic in this channel, in particular the impact of depression waves of substantial height generated in the channel and further penetrating into the lagoon, has been of considerable concern in the recent past (Rapaglia et al., 2011; Gelinat et al., 2013; Parnell et al., 2015). The trough of the depression waves is preceded by a much smaller crest and followed by a slightly larger crest. When propagating from the channel to the shoals of the lagoon, the depth of the trough decreases to some extent but the rear slope of the trough steepens and becomes bore-like. The greatest water velocities (measured near the seabed up to 2.1 m/s) and most of sediment resuspension are associated with the rear slope. Such disturbances travel many hundreds of metres into the lagoon. The frequent events of high hydrodynamic activity associated with ship traffic in the channel maintain the concentration of suspended sediment at

high levels for a considerable time. The suspended material may be transported by tidal currents and the currents associated with depression waves in the vicinity of the channel. Eventually sediment may be deposited in the navigation channel, where frequent dredging is required to maintain the navigation depth. The volume of dredged materials is comparable to the sedimentary budget of the lagoon as calculated from bathymetric changes (Autorità Portuale di Venezia, Venezia Porto Verde – Iniziativa ambientali per il Porto di Venezia, Venice, Jan 2010, http://newweb.riminifiera.it/upload_ist/AllegatiProgrammaEventi/Casarin%2009_368584.11.pdf).

2.2. Wake measurements

The wave measurements used in this study to initialize the calculations of nonlinear wave propagation over shallow areas were performed on the banks of the Malamocco–Marghera industrial channel (Fig. 1). At the study site, the channel is 11–12 m deep and its bottom is 60 m wide. This waterway is bordered by relatively steep slopes (~10%), which rise over 30–40 m so that the water depth decreases from 12 m to about 4 m (Fig. 2). The western (mainland) side of the channel bank has a constant slope (~3%). It is bordered by an

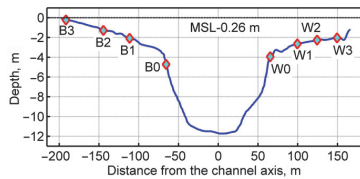


Fig. 2. Cross-section of the channel at the measurement site showing the location of pressure sensors (B0–B3, W0–W3). Distance is referenced to the channel axis, and the depth is referenced to the local tidal datum (0.26 m below mean sea level).

about 1 m high erosion scarp approximately 150 m from the channel edge. The eastern (lagoon) side bank of the channel has a depth of about 2 m and is separated from the rest of the lagoon by a semi-permeable rock wall. The wall was built about 90 m from the edge of the channel to prevent the penetration of ship wakes into shallow water areas of this part of the Venice Lagoon. The bottom of this bank has a relatively constant slope of ~2% towards the channel. Water moves freely through gaps in the wall between the channel and the lagoon; however, the wall absorbs most of the energy and momentum of vessel wakes.

The measurements were performed at eight locations (four on both sides of the channel) (Fig. 2). Wave-induced pressure fluctuations were recorded at either 2 Hz or 5 Hz using pressure sensors mounted on the seabed (B1–B3 and W1–W3 in Fig. 3) or suspended from the channel markers (B0 and W0). The sensors were incorporated in various time-synchronized self-recording instruments (four InterOcean S4 current meters, one RBR Virtuoso wave gauge, one Ocean Seven CTD, two Esterline pressure sensors). The maximum synchronization error is ± 10 s (Parnell et al., 2015), which is immaterial from the viewpoint of this study where only the magnitude and shape of the dis-

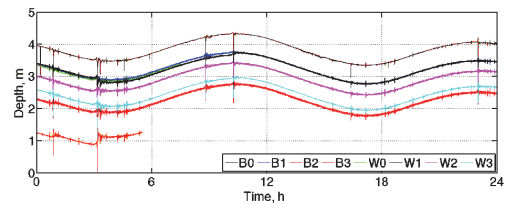


Fig. 3. A 24 h long record of vessel wakes on the western (coastal, B0–B4) and eastern (lagoon, W0–W4) sides of the channel. The locations of the instruments are shown in Fig. 2. The record begins at 12:00 on 01 April 2014. Data for locations W2 and W3 (used to characterize the wake of the *Abu Dhabi Star* in (Parnell et al., 2015) are partly missing due to an equipment failure. Note that gauges at W0 and B0 were not deployed on the seabed but were fixed to channel markers and that gauge B3 was moved by a strong wake about 3 h after the record begins.

turbances are employed. The reader is referred to Parnell et al. (2015) for further information.

Vessel wakes were recorded over four sampling periods of 2 to 6 days in March and April 2014. Figure 3 provides an example of water surface level records from different gauges as actual water depths at the measurement sites for the 24 hours' time interval from 12:00 on 01 April to 12:00 on 02 April 2014. It is generally expected that ships sailing at depth Froude numbers about 0.5 should excite transient sign-variable wave groups or solitary waves of elevation both in channels and in shallow areas of the open sea (Ertekin et al., 1986; Neuman et al., 2001; Soomere, 2007). Somewhat counter-intuitively but characteristic of this location (Rapaglia et al., 2011; Gelinas et al., 2013), the ships did not produce any substantial waves of elevation. This property can be to some extent explained by relatively low speeds (7–11.4 knots) and associated depth Froude numbers (0.34–0.53; Table 1).

Table 1. Parameters of ships and their sailing regimes. The symbol C^* stands for the blocking coefficient (width \times draught of the vessel/cross-sectional area of the channel) and $F_d = v/\sqrt{gH}$ (v is the ship's speed) is the depth-based Froude number

Ship	Velocity, knots	Length, m	Width, m	Draught, m	Type	C^*	F_d
<i>Vigor SW</i>	9.3	177	28	7.0	General cargo	0.10	0.43
<i>Pessada</i>	8.6	225	32	7.0	Bulk carrier	0.11	0.40
<i>Abu Dhabi Star</i>	7.7	183	32	7.8	Oil/Chemical tanker	0.14	0.36
<i>Aenne Rickmers</i>	8.0	195	30	9.0	Container ship	0.13	0.37
<i>Pirin</i>	10.3	169	24	6.0	Bulk carrier	0.07	0.48
<i>MSC Mia Summer</i>	7.3	216	27	9.9	Container ship	0.13	0.34
<i>Forza</i>	10.5	199	34	6.0	Ro-Ro	0.10	0.49
<i>Frauke</i>	10.6	160	24	8.5	Cargo	0.10	0.49
<i>Syn Tabit</i>	11.4	96	16	6.7	LPG tanker	0.05	0.53
<i>Constance</i>	11.0	86	12	3.8	General cargo	0.02	0.51
<i>Serenissima</i>	10.6	87	13	4.9	Passenger ship	0.03	0.49
<i>MRW Revenge</i>	7.0	82	11	4.6	General cargo	0.02	0.33

The dominant feature of many ship passages is a deep depression with a total duration of ~ 400 s with a solitary V -shaped trough typically lasting ~ 80 s (Parnell et al., 2015). It was shown previously that there is huge variability in the properties of wake waves of analogous ships in shallow open sea areas (Kurennoy et al., 2009). Similarly, the characteristics of the depression waves produced by different vessels vary significantly. Interestingly, the wake properties are often different on opposite sides of the channel for the same vessel (Parnell et al., 2015). This feature may reflect the position of the ship in the channel or the different morphology of the channel margins (or both).

The maximum water level drop recorded during the entire measurement campaign occurred with the passage of the *Abu Dhabi Star*, a relatively large but not exceptional ship sailing at a moderate speed (Parnell et al., 2015). The trough depth excited by this vessel at the western edge of the channel (location B0) was 2.52 m from still water level. As a small but quite long wave of elevation preceded the depression, the total water level dropdown was 2.58 m (Parnell et al., 2015). The depths of depression waves exceeded 1.5 m on several other occasions, which is much larger than previously reported (Balzerek and Kozłowski, 2007; Rapaglia et al., 2011; Göransson et al., 2014).

As none of the recorded depressions had an elongated almost horizontal trough (which is suggested by weakly nonlinear simulations; Torsvik et al., 2009a, 2009b), they apparently had a strongly nonlinear nature. The depressions were almost symmetric in time with respect to their deepest point at the margins of the navigational channel but became gradually asymmetric with propagation away from the channel (Fig. 4).

The amplitude of the wave clearly decreased when reaching the side bank but did not change significantly from one device to another over the bank. Instead, a front/rear asymmetry of the wave profile was developed. The front slope of the depression became gradually less steep while the rear slope rapidly became steeper and the overall appearance of the wave resembled a strongly skewed V -like shape. As suggested by weakly nonlinear analysis of such disturbances (Grimshaw et al., 2014), a

sequence of waves of elevation was developed at the end of the rear slope so that the water surface usually exceeded the undisturbed level at the end of some of the depression events. Almost all records revealed the development of a step or a sequence of smaller steps on the rear slope of the depression wave (Parnell et al., 2015). This is consistent with the results of numerical simulations of strongly nonlinear evolution of deep depression waves (Didenkulova et al., 2011a).

2.3. Interpretation of ship-driven depressions as Riemann waves

The presented material and a recent study (Parnell et al., 2015) show that weakly nonlinear approaches fail to replicate the properties and propagation of ship-induced depressions in shallow areas of the Venice Lagoon. Even if only a few ships are able to produce extremely large depression waves at the border of the navigation channel and the heights of these waves decrease away from the channel, on many occasions a depression of about 0.5 m penetrated to the surrounding shallow water areas. As the average depth of the lagoon in these areas is from 1 to 2 m (which is somewhat deeper than the average lagoon because of the strong erosion that followed the opening of the navigation channel), these waves are generally strongly nonlinear.

A feasible way to address the evolution and propagation of such depressions is the framework of simple or Riemann waves. The relevant technique, a valuable tool in nonlinear acoustics (Rudenko and Soluyan, 1977; Engelbrecht et al., 1988), has been applied to track long waves of any polarity in shallow water (Didenkulova et al., 2006; Zahibo et al., 2008). If the waves can be assumed to be (at least locally) long-crested, the motion of extremely long wave troughs produced by ships and propagating over very shallow water in ideal conditions can be approximately described by the following system of equations (Whitham, 1974):

$$\frac{\partial u}{\partial t} + u \frac{\partial u}{\partial x} + g \frac{\partial \eta}{\partial x} = 0, \quad \frac{\partial \eta}{\partial t} + \frac{\partial}{\partial x} [(h + \eta)u] = 0. \quad (1)$$

Here h is the unperturbed water depth, η is the water surface displacement, u is the depth-averaged horizontal velocity, $g = 9.81 \text{ m/s}^2$ is acceleration due to gravity, x is the horizontal coordinate along the wave propagation direction, and t is time. These equations are, formally, exact up to the wave breaking. They can be applied for the motion of long waves of any amplitude, even extremely high, on condition that dispersion does not play a perceptible role. As the ship-induced depressions with a duration of ~ 80 s are extremely long when propagating in 1–2 m deep water, this condition is effectively satisfied.

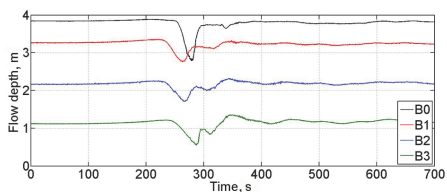


Fig. 4. Water surface time series in a wake produced by the *Vigor SW* on the western (coastal) side of the channel around 13:20 on 01 April 2014.

It is convenient to rewrite Eqs (1) in a flux form

$$\frac{\partial H}{\partial t} + \frac{\partial}{\partial x}(Hu) = 0, \quad \frac{\partial(Hu)}{\partial t} + \frac{\partial}{\partial x}\left(Hu^2 + \frac{gH^2}{2}\right) = 0, \quad (2)$$

where $H = h(x) + \eta(x)$ is the total water depth. A Riemann (or simple) wave is the classical solution to Eqs (2). For one-dimensional waves this solution can be presented as (Rudenko and Soluyan, 1977; Engelbrecht et al., 1988; Pelinovsky and Rodin, 2012):

$$H(x, t) = H_0[x - Vt], \quad u(x, t) = 2\left[\sqrt{gH(x, t)} - \sqrt{gh}\right], \quad (3)$$

where $H(x, t)$ is the shape of the water surface, $H_0(x)$ is the initial water surface profile, $u(x, t)$ is the associated flow speed, and \sqrt{gH} and $u(x, t) = \sqrt{gh}$ are long wave speeds (the maximum phase and group speed for surface waves at a given depth) for water depths of H and h , respectively. The properties of Riemann waves on water surface are extensively described e.g. by Whitham (1974), Didenkulova et al. (2006), Zahibo et al. (2008), and Pelinovsky and Rodin (2012). As is common for long water waves, it follows from Eqs (3) that the local speed of nonlinear wave propagation

$$V(x, t) = 3\sqrt{gH(x, t)} - 2\sqrt{gh} \quad (4)$$

depends on the local value of the total water depth H . As ship-induced disturbances addressed in this paper are waves of depression, from Eq. (4) it becomes clear that they propagate slower than the linear long wave speed \sqrt{gh} .

Differently from several families of weakly nonlinear equations (Grimshaw et al., 2014), solution (3) may be a long-living wave of depression. For this reason solution (3) has been often used to analyse the evolution, properties, and interactions of non-natural waves produced, for example, by a wavemaker (Didenkulova et al., 2006, 2011a; Zahibo et al., 2008). Such waves tend to form a skewed shape with a steep rear slope. There exists a sort of limiting amplitude for Riemann waves of depression. Such a wave can only survive for a reasonable time if its trough is not too deep. If the initial disturbance η (or the relative depth of the depression for waves propagating over an uneven seabed) exceeds the threshold $|\eta| = (5/9)h$, or equivalently, if the thickness of the water sheet at the deepest point of the trough is (Pelinovsky and Rodin, 2012)

$$H < H_{cr} = \frac{4}{9}h, \quad (5)$$

the trough velocity (4) becomes negative and different parts of the wave profile start to propagate in different

directions (in the coordinate system associated with the overall propagation of the disturbance). Consequently, the steep rear front is formed almost immediately and the wave would almost instantly break (Didenkulova et al., 2006; Zahibo et al., 2008). Some nonlinear effects such as a reflected wave from the shock front can occur (Pelinovsky and Rodin, 2012). However, at this instant, Eqs (1) fail to describe the further behaviour of the depression. It is likely that a bore-like feature is rapidly formed and that intense turbulence damps the energy of the motion.

2.4. Numerical simulation of ship-induced Riemann waves of depression

Simulations of ship-induced wave trough propagation and transformation over shallow banks are performed using the CLAWPACK software package of FORTRAN and Python subroutines. The major tool is the GEOCLAW package, a specialized version of CLAWPACK routines modified to address certain geophysical flow problems. This software solves the time-dependent hyperbolic system of partial differential Eqs (2) using the method of finite volumes (LeVeque, 2004). The quality of the simulations was monitored by means of tracking the exactness of the conservation of mass. This conservation law is satisfied with an accuracy of $10^{-6}\%$, a value used in earlier simulations of the propagation and interactions of Riemann waves (Didenkulova et al., 2011a). As we are interested in long-range propagation of waves of depression, Sommerfeld-type artificial radiation conditions (Sommerfeld, 1949) were applied at each side of the computational domain.

In this paper we work with depression-wave data recorded during one of the observation campaigns (three continuous records, about 30–36 h each; see Parnell et al., 2015 for information about the entire pool of records). These records contain 20 identifiable wakes. The larger examples of wakes were clearly identified and corresponded to particular ships (12 ships in total, Table 1). Five smaller wakes remained unidentified. To make the results comparable with the ones presented in (Parnell et al., 2015), simulations matching the wake of the *Domenico Ievoli* (22 April 2014) were added into the pool. As separate runs were made for waves propagating from the channel margin to the coast and the lagoon side, the pool of simulations contains 40 runs. The results of these simulations were compared with a total of 269 gauge signals (at some locations and times certain gauges were not working). Ship speeds were retrieved from data transmitted by the Automatic Identification System (AIS). Water level in each simulation was chosen as it was at the time of the ship passage.

2.5. Calibration of the initial conditions

The initial shapes of the depressions for simulations were constructed based on measured wake properties at the channel margins (B0 and W0). It is not obvious whether the measured depressions were forced disturbances or were already propagating as free waves. As we are specifically interested in the far field of the propagation of vessel wakes in the lagoon, to a first approximation we assumed that the depression was already travelling as a free wave at the margin of the channel. For ships moving in a strongly nonlinear regime the leading wave is a deep depression of a generally symmetric shape that resembles a Gaussian distribution with negative polarity (Torsvik and Soomere, 2008; Torsvik et al., 2009b). This assertion is consistent with a specific skewed V -like shape of the depression at the margins. This shape is a natural consequence of the evolution of initially smooth and symmetric deep depressions (Pelinovsky and Rodin, 2012). Based on these arguments, we assumed that the depression wave was initially (at the location of generation) symmetric with respect to time (or the ship motion).

It is also reasonable to presume that after some time (or at a certain distance from the sailing line) the details (shape, asymmetry, etc.) of vessel wakes are no longer directly connected with the properties of the hull and are defined by generic rules that govern the propagation of depressions of a certain amplitude. To test this assertion, we ran simulations with smooth soliton-like pulses and depressions of the shape of an inverted Gaussian bell. The exact shape of the initial pulse only insignificantly affected the results of simulations along the side banks. Therefore, to initialize ship-driven water disturbances we used a Gaussian bell shape of negative polarity

$$H_0(x) = A_0 \exp\left(-\frac{x^2}{l^2}\right). \quad (6)$$

Here A_0 is the initial amplitude of the trough and l is the characteristic half-size of the initial impulse.

To simulate the propagation of vessel wakes, the initial shape (6) was allowed to evolve over some distance in deeper water (the depth matching the average depth of the navigation area in the channel, Fig. 2), after which it propagated along the steep slope of the waterway (Fig. 5). The best visual match of the wave profile at the numerical gauge at the channel margin with those measured for vessels in Table 1 was found for the propagation time of 150 s (Fig. 5). This time was then used to initialize all the simulations.

The initial parameters of the depression were found iteratively from the match of two parameters of the simulated wake with the measured water level signal at the relevant channel margin (W0 or B0). Firstly, the amplitude A_0 was chosen so that the maximum

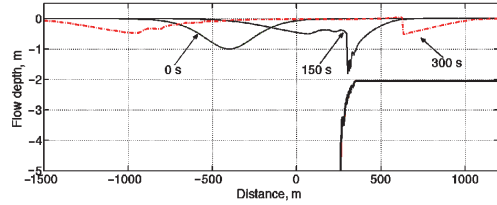


Fig. 5. Propagation of a depression pulse with the initial amplitude of 1 m in the navigation channel and over its lagoon-side slope at time instants 0, 150, and 300 s. Note the counter-propagating reflected wave at 150 and 300 s. The lowest line represents the model seabed (not shown for the model water depths >5 m).

simulated depression equalled the height of the measured depression. Secondly, the width $2l$ was chosen so that the width of the depression at 1/3 of the maximum depth equalled the similar width of the measured depression. As demonstrated in Fig. 5, the amplitudes of the initial smooth Gaussian-shaped depressions are much less than the heights of the depression waves at the channel margins.

The associated velocity field was derived from Eq. (3) and the sign of the velocities was assigned so as to ensure wave propagation away from the channel. The shape of the bottom profile within the limits of Fig. 2 was taken from the measurements that had a resolution of approximately 1 m. The measured data were linearly approximated to a grid with a step of 20 cm. A refinement of the grid step by 2–3 times led to maximum differences in wave amplitudes of less than 0.5%. The water depth was assumed to be constant in more remote locations. The length of the time step (0.5 s) was restricted by the Courant–Friedrichs–Levy condition.

To a first approximation, we ignored the mismatch of the propagation direction of simulated waves and the line of measurement devices in Fig. 2. In reality, the wave front moved obliquely (at an angle of about 45° ; Rapaglia et al., 2011) with respect to this line. Therefore, the subsequent recordings of devices at B1–B3 and W1–W3 reflect the properties of different parts of the wave crest. As the channel is essentially straight, it is natural to assume – similarly to the analysis in (Parnell et al., 2015) – that the channel banks are almost homogeneous. As the ships were moving at practically constant speed and direction, it is also acceptable to assume that the properties of each wave of depression mostly depend on the distance of the device from the relevant channel margin and that the properties of the bottom morphology along this distance affect different parts of the wave front in a similar manner. With these assumptions, the mismatch of the wave front propagation direction with the orientation of the line of

measurement devices will only lead to a certain shift in the timing of the measured and the simulated signal.

3. RESULTS

3.1. Simulated and measured wakes

Figures 6 and 7 present typical examples of the comparison of numerically replicated depressions with the measured data for each gauge over the beach-side and the lagoon-side bank of the channel, respectively. Although the initial wave shape is smooth and symmetric (and thus very different from the measured signal), the shape of the simulated wave (including the initial small and long wave of elevation) largely matches the measured wave profiles. This suggests that the numerical model reasonably describes the major

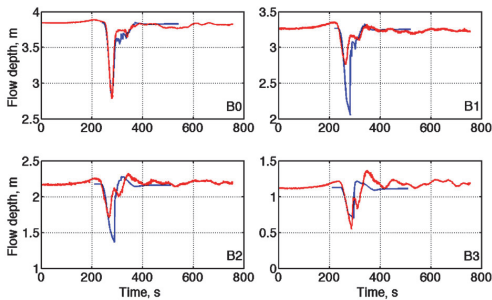


Fig. 6. Propagation of a numerically simulated Riemann wave matching the depression created by the *Vigor SW* over the beach-side bank of the channel at measurement sites B0–B3 on 01 April 2014 at 13:20. Red: measured profiles; blue: simulated profiles.

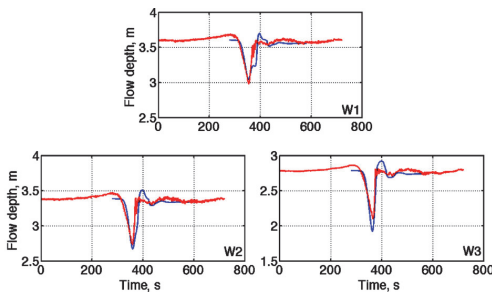


Fig. 7. Propagation of a numerically simulated Riemann wave matching the depression created by the *Pessada* over the lagoon-side bank of the channel at measurement sites W1–W3 (data from W0 are absent due to equipment failure) on 28 March 2014 at 8:30. Red: measured profiles; blue: simulated profiles.

features of wave propagation and transformation (such as the smoothing of the front slope of the wave and the steepening of the rear slope (see Figs 6 and 7)) in the framework of nonlinear shallow water theory. Although in the navigation channel weakly nonlinear approaches are apparently also adequate, the nonlinear framework should be applied at the side banks and in the lagoon. The height of the depression, although on some occasions replicated adequately at all measurement locations (Fig. 7), is often underestimated at intermediate locations W1, W2, B1, and B2. Interestingly, the match is particularly good at locations W3 and B3.

The condition $|\eta| > (5/9)h$ (Didenkulova et al., 2006; Zahibo et al., 2008) is usually satisfied starting from a certain location for largest waves on the coastal side of a channel. This means that in the strongly nonlinear environment a shock-like rear slope of the wave trough appears almost instantaneously and that the wave propagates into the shallow area as a bore (Parnell et al., 2015). Some fluctuations ahead of the shock are evidently caused by irregularities of the bottom profile. In general, even these wave troughs can be well described by the numerical solution, which in extreme cases can have different nonlinear effects (Pelinovskiy and Rodin, 2012).

Comparison of the maximum measured depression depths at different locations with the numerically replicated values (Fig. 8) demonstrates that the numerical approach tends to overestimate the wave height. The parameters of the linear regression line (in which the locations used for the calibration are excluded)

$$H_{\max(\text{measured})} = 0.27H_{\max(\text{simulated})} + 0.32 \quad (7)$$

show that simulations overestimate the wave amplitude on average by more than 40%. It is natural that the match is almost perfect for the locations at the channel

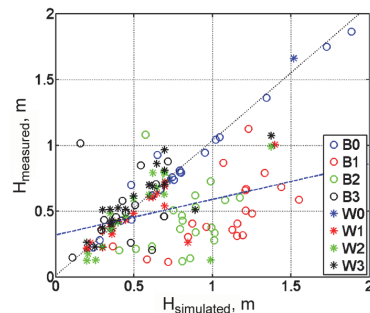


Fig. 8. Simulated and measured trough amplitudes for all 12 vessel passages with the regression lines for all measurement sites except calibration locations W0 and B0 (blue dashed line) and the most distant sites B3 and W3 only (black dotted line).

margins, where the initial parameters of virtual disturbances (6) were calibrated. The match is relatively poor for locations B1, B2, W1, and W2, where the maximum water level dropdown is often overestimated by a factor of two or even more. However, as Fig. 8 demonstrates, the match of measured and simulated depths of the depression is almost perfect at the remotest measurement locations B3 and W3. This feature suggests that the numerical model, even though it fails to reproduce some features of the near-field propagation of depression waves, eventually adequately replicates the future propagation of these waves into the lagoon. In general, it demonstrates a good agreement between calculated and real data considering the crudeness of the approximation in the mathematical model.

The spreading of calculated and measured data can be evaluated using the classical root mean square difference

$$\delta = \sqrt{\frac{1}{N} \sum_{n=1}^N (R_n^{\text{simulated}} / R_n^{\text{measured}} - 1)^2}. \quad (8)$$

Here, $R^{\text{simulated}}$ and R^{measured} are numerically calculated and measured maximum depths of the depression at different measurement locations, respectively, and N is the total number of comparable pairs of their values. The value of δ reaches 0.36 m when all measurements at W1–W3 and B1–B3 are involved. The spreading is considerably less, 0.26 m, for the lagoon-side most remote site W3.

3.2. Long-term propagation of simulated wakes into the lagoon

To estimate the practical significance of the permeable rock wall at the Malamocco–Marghera industrial channel and the risk of dangerous high-amplitude depressions followed by bore-like phenomena occurring in the Venice Lagoon (e.g., in case of the absence of such a wall along other sections of the channel), we simulated the further behaviour of the disturbances over a plane seabed. In other words, we ignored the wall and looked at the fate of such waves (with initial profiles chosen as described above) in water of constant depth.

As the simulations were in good agreement with the measured data, particularly at the most distant sites B3 and W3 from the channel, it is likely that the simulations adequately replicate the far-field situation in the lagoon. It is reasonable to use a constant depth in the lagoon instead of real bathymetry because the impact of the actual bottom on the wave propagation cannot be replicated by the model. Two processes have the largest effect on the wave motion. On the one hand, the depth in the lagoon is (at least over low tide) generally much less than 2 m and thus nonlinear effects tend to steepen the rear front of the depression much more strongly than

in the simulations. On the other hand, the wave loses its energy and compactness while interacting with and reflecting from the inhomogeneities of the bottom profile. Thus, the depth of the lagoon is assumed constant and equal to the water depth immediately at the channel side of the wall (2 m). As we are specifically interested in the far-field behaviour of the vessel wakes, in numerical experiments we ignored the presence of the coast for wakes propagating along the western bank and investigated also the possible fate of these depressions in water of constant depth.

It is debatable how large the ‘safe’ height of the depression far from the navigation channel is. A usual requirement is that the vessel-induced wave height H_{max} (in metres) should not exceed the limiting value (Parnell and Kofoed-Hansen, 2001)

$$H_{\text{max}} \leq 0.5 \sqrt{\frac{4.5}{T}} \quad (9)$$

at a still water depth of 3 m. Here T is the period of the waves in seconds. The usual period of high and dangerous vessel waves of elevation is 9–12 s (Parnell and Kofoed-Hansen, 2001; Soomere, 2007). For waves with a period 12.5 s the limiting value is $H_{\text{max}} = 0.3$ m. Although the effective period of depression waves is much longer, expression (9) becomes irrelevant for even longer waves. Also, waves below 0.3 m are usually harmless for coasts and their ecosystem. Moreover, disturbances below this height are already weakly nonlinear and evidently rapidly lose their bore-like properties. Based on these arguments, it can be assumed that a ‘safe’ trough amplitude for people and small boats in the lagoon, and possibly for the environment, is 0.3 m.

A typical example of a relatively large depression that propagates into the lagoon has the amplitude of the initial Gaussian-shaped depression $A_0 = 1$ m and the characteristic half-size $l = 200$ m. An initial depression (6) with these values matches well the shape and amplitude of the wake of the *Vigor SW* at the channel margin (Fig. 6) and is representative of the wakes that occur most frequently in the Malamocco–Marghera channel. Snapshots of the profile of this wave at selected time moments (Fig. 5) demonstrate that the depression develops a characteristic skewed V -like shape after some time. A time–space diagram (Fig. 9) shows that despite energy loss and reflection in the process of interaction with the slope of the channel, in the absence of the wall the wave height remains well over 0.3 m after a long incursion into the lagoon. The height of this depression falls to 0.3 m only after the pulse has travelled about 1500 m (equivalent to about 400 s) from the location of the wall. Even if we assume that the simulation overestimates the height of the depression (cf. Eq. (7)), the depression wave will cover at least 700–900 m before it becomes less than 0.3 m

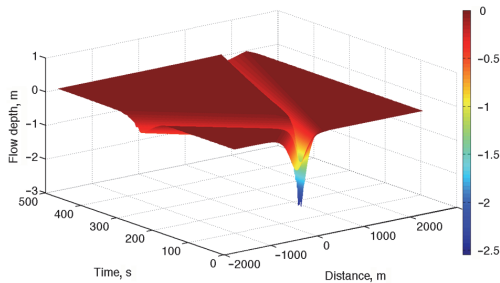


Fig. 9. Space–time (x – t) diagram of the simulated wave profile produced by the depression wave with the initial amplitude $A_0 = 1$ m propagating to the eastern (lagoon) side of the channel.

high. This conjecture is consistent with the observation by Rapaglia et al. (2011) that a 0.8 m high wave remained >0.3 m high at a distance of about 300 m from the channel margin.

Numerically replicated properties of a selection of wakes in the lagoon under the above-described initial and simulation conditions evolve in a very similar manner (Fig. 10). The initial propagation corresponds to the wave motion in idealized conditions (constant water depth equal to the depth of the bottom of the navigation channel) during which hardly any changes occur in the properties of the depressions. The wave amplitude increases rapidly when it reaches the beginning of the side slope of the channel. The maximum amplitude (comparable to the recorded values) is reached near the channel margin. Further propagation is accompanied by a gradual decrease in the amplitude whereas the amplitudes of different initial impulses rapidly level off and become almost equal after ~ 50 s (~ 200 m) propagation into the lagoon. Further changes in the waves are almost independent of the initial properties.

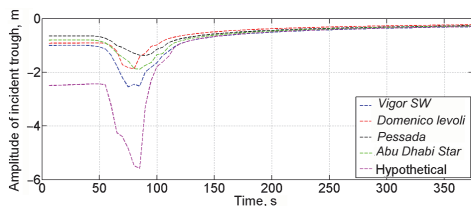


Fig. 10. Temporal evolution of numerically simulated trough amplitudes. The initial properties of the Gaussian-shaped depressions are as follows: *Vigor SW* (01 April 2014 at 13:20) – initial amplitude $A_0 = 1$ m and characteristic half-size $l = 200$ m; *Domenico levoli* (22 April 2014 at 06:50) – $A_0 = 0.92$ m, $l = 100$ m; *Pessada* (28 March 2014 at 8:30) – $A_0 = 0.65$ m, $l = 182.5$ m; *Abu Dhabi Star* (01 April 2014 at 15:38) – $A_0 = 0.8$ m, $l = 195$ m.

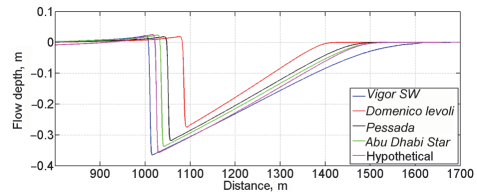


Fig. 11. Numerically simulated trough profiles in the Venice Lagoon after 300 s propagation time. The different locations of the wave trough are caused by different propagation speeds (4).

To understand how even larger-amplitude depressions may behave in the lagoon, we also consider a hypothetical case with characteristic half-size $l = 182.5$ m and extremely high initial amplitude of 2.5 m (matching the largest of the measured depression waves at the channel margin). This hypothetical disturbance creates an unrealistically deep depression (almost 6 m) at the channel slope. Its height is rapidly reduced to the level of real wakes at the channel margin and soon becomes almost equal to the height of the numerical replication of the largest measured wakes.

Importantly, the heights of all simulated wakes, including the very deep hypothetical one, level off after some propagation time (Fig. 10). This feature suggests that several real wakes may produce depressions of the maximum theoretically possible amplitude in the Venice Lagoon. Moreover, it is likely that the further propagation of such entities is almost independent of their initial amplitude. Consequently, even depressions of relatively modest amplitude may keep their height at a dangerous level over long distances.

The shapes of various measured and simulated depressions are largely different at the channel margin (Figs 6 and 7; see also Parnell et al., 2015). Similarly to the wave heights, the shapes of depressions also become similar after longer propagation distances (Fig. 11). Their characteristic features are a gently sloping front and a very steep rear, even at a distance of >1 km from the navigation channel. Although building up and keeping this shape may reflect specific features of the evolution of idealized Riemann waves and dispersion effects eventually triggering the formation of waves of elevation after some time, it is likely that the bore-like appearance of the rear of the depression waves may be preserved over substantial distances.

4. DISCUSSION AND CONCLUDING REMARKS

The environmental impacts of vessel-generated waves have received considerable attention in the international scientific and engineering literature. The increase in

water level associated with the leading edges of the waves is commonly regarded to be of largest environmental significance. With the exception of studies on sediment resuspension and turbidity (e.g., Rapaglia et al., 2011; Göransson et al., 2014) there have been few studies on the impacts of depression waves produced by various ships (Forsman, 2001). Previous research (Parnell et al., 2015) has demonstrated that unexpectedly high (up to 2.5 m) and extremely long depression waves are generated by moderately-sized ships sailing at very moderate depth Froude numbers (<0.5) and low blocking coefficients (<0.14) in channels surrounded by extensive shallow banks. These disturbances drive possibly significant but likely not exceptional water velocities (cf. Rapaglia et al., 2011) in the channel itself.

Our research addressed the possibility for these depression waves to propagate virtually freely away from the navigation channel and to penetrate onto wide and shallow shoals (estuary, river bank, shallow lagoon, etc.). These extremely long (typical periods of >40 s and associated lengths >250 m) waves experience transformations characteristic of strongly nonlinear Riemann waves on the water surface when they reach the channel margin (Parnell et al., 2015). Their front keeps a modest slope but their rear develops an extremely steep, near-breaking slope, or even a bore-like feature at a distance of much less than 100 m from the channel margin. The resulting water velocities and the overall possible environmental impact (Rapaglia et al., 2011; Gelinas et al., 2013) are likely much larger than those derived from common expressions for linear or weakly nonlinear waves (Parnell et al., 2015).

The simulations first of all demonstrate that a disturbance of considerable amplitude continues to move as a strongly nonlinear wave to a substantial distance. The amplitudes of very deep depressions rapidly (within 20–30 s) level off to a value that is apparently limited by the water depth. The multi-step structure of the rear slope (that exists at the margin of the navigation channel, equivalently, at the seaward slope of the shallow area, possibly owing to the presence of reflected wave components) disappears after a period of time. Importantly, the nonlinearity continuously acts towards building up a very steep rear slope of the depression and (in cases when dispersion can be neglected) the disturbance obtains a shape characteristic of Riemann waves of depression: a relatively gentle slope followed by a steep rear.

The amplitude of such depressions for the disturbances that are representative of the frequently occurring wakes in the Malamocco–Marghera channel in the Venice Lagoon remains at dangerous levels (>0.3 m) for distances of more than 1 km in our simulations. The actual depth of the lagoon is usually clearly smaller than the water depth at the channel side of the wall. The cause of this difference is that erosion on the channel

side has removed some sediment from the bottom as the wall was originally built on a flat bottom more or less simultaneously with the dredging of the channel. Therefore, it is reasonable to assume a shallower depth for the lagoon side of the wall than used in the model (2 m). This means that nonlinear effects are eventually greater than in the performed simulations and the steep bore-like feature may persist for an even longer time.

As the heights of all such depressions may become almost independent of their initial properties, even modest ships in terms of their size, sailing speed, and blocking coefficient may generate wakes that travel as compact entities over extensive areas of the lagoon adjacent to the navigation channels. Their impact may potentially lead to extensive resuspension and transport of bottom sediments and substantially increased levels of environmental consequences of ship wakes in this and similar water bodies. An adequate evaluation of these phenomena requires application of fully nonlinear approaches to describe the propagation of the depressions.

ACKNOWLEDGEMENTS

The research into Riemann waves was funded by the Estonian Science Foundation (grant No. 9125), targeted financing by the Estonian Ministry of Education and Research (grants SF0140007s11 and IUT33-3), and through support of the European Regional Development Fund to the Centre of Excellence in Non-linear Studies CENS. The field studies were undertaken while Kevin Parnell was hosted by CNR-ISMAR, Venice, Italy, and were funded by the project Ritmare (SP3-WP3-A1). The contributions of Giuliano Lorenzetti and Gian Marco Scarpa to fieldwork and data management are gratefully acknowledged.

REFERENCES

- Akylas, T. 1984. On the excitation of long nonlinear water waves by a moving pressure distribution. *J. Fluid Mech.*, **141**, 455–466.
- Ali, M. M., Murphy, K. J., and Langendorff, J. 1999. Interrelations of river ship traffic with aquatic plants in the River Nile, Upper Egypt. *Hydrobiologia*, **415**, 93–100.
- Arcas, D. and Segur, H. 2012. Seismically generated tsunamis. *Phil. Trans. R. Soc.*, **370**, 1505–1542.
- Baines, P. G. 1997. *Topographic Effects in Stratified Flows*. Cambridge Monographs on Mechanics. Cambridge University Press, Cambridge, UK.
- Balzerek, H. and Kozłowski, J. 2007. Ship-induced riverbank and harbour damage. Evidence for claims processing. *Hydro International*, **11**(8), 18–21.
- Benjamin, T. B. and Lighthill, M. J. 1954. On cnoidal waves and bores. *Proc. R. Soc. London A*, **224**, 448–460.

- Brambati, A., Carbognin, L., Quaia, T., Teatini, P., and Tosi, L. 2003. The Lagoon of Venice: geological setting, evolution and land subsidence. *Episodes*, **26**(3), 264–265.
- Carrier, G. F., Wu, T. T., and Yeh, H. 2003. Tsunami run-up and drawdown on a plane beach. *J. Fluid Mech.*, **475**, 79–99.
- Constantine, T. 1961. On the movement of ships in restricted waterways. *J. Fluid Mech.*, **9**, 247–256.
- Darmon, A., Benzaquen, M., and Raphael, E. 2014. Kelvin wake pattern at large Froude numbers. *J. Fluid Mech.*, **738**, Art. No. R3.
- Defendi, V., Kovačević, V., Zaggia, L., and Arena, F. 2010. Estimating sediment transport from acoustic measurements in the Venice Lagoon inlets. *Cont. Shelf Res.*, **30**, 883–893.
- Didenkulova, I. I., Zahibo, N., Kurkin, A. A., and Pelinovsky, E. N. 2006. Steepness and spectrum of a nonlinearly deformed wave on shallow waters. *Izv. Atmos. Ocean. Phys.*, **42**, 773–776.
- Didenkulova, I., Pelinovsky, E., and Rodin, A. 2011a. Nonlinear interaction of large-amplitude unidirectional waves in shallow water. *Estonian J. Eng.*, **17**, 289–300.
- Didenkulova, I., Pelinovsky, E., and Soomere, T. 2011b. Can the waves generated by fast ferries be a physical model of tsunami? *Pure Appl. Geophys.*, **168**, 2071–2082.
- Didenkulova, I. I., Pelinovsky, E. N., and Didenkulov, O. I. 2014. Run-up of long solitary waves of different polarities on a plane beach. *Izv. Atmos. Ocean. Phys.*, **50**, 532–538.
- El-Kader, F. A., El-Soud, M. S. A., El-Serafy, K., and Hassan, E. A. 2003. An integrated navigation system for Suez Canal (SCINS). *J. Navigation*, **56**, 241–255.
- Engelbrecht, J. K., Fridman, V. E., and Pelinowski, E. N. 1988. *Nonlinear Evolution Equations*. Pitman Research Notes in Mathematics Series, No. 180. Longman, London, 1988.
- Ertekin, R. C., Webster, W. C., and Wehausen, J. V. 1984. Ship-generated solitons. In *Proceedings of 15th Symposium on Naval Hydrodynamics, Hamburg, Federal Republic of Germany, September 2–7*. National Academy Press, Washington, D.C., pp. 347–364.
- Ertekin, R. C., Webster, W. C., and Wehausen, J. V. 1986. Waves caused by a moving disturbance in a shallow channel of finite width. *J. Fluid Mech.*, **169**, 275–292.
- Fernando, H. J. S., Braun, A., Galappatti, R., Ruwanpura, J., and Wirisinghe, S. C. 2008. Tsunamis: manifestation and aftermath. In *Large Scale Disasters*. Cambridge University Press, Cambridge, pp. 258–292.
- Forsman, B. 2001. From bow to beach. *SSPA Highlights*, No. 3/2001, 4–5.
- Gelinas, M., Bokuniewicz, H., Rapaglia, J., and Lwiza, K. M. M. 2013. Sediment resuspension by ship wakes in the Venice Lagoon. *J. Coast. Res.*, **29**, 8–17.
- Göransson, G., Larson, M., and Althage, J. 2014. Ship-generated waves and induced turbidity in the Göta Älv River in Sweden. *J. Waterw. Port Coast. Ocean Eng.*, **140**(3), 04014004.
- Gourlay, T. P. 2001. The supercritical bore produced by a high-speed ship in a channel. *J. Fluid Mech.*, **434**, 399–409.
- Gourlay, T. P. 2003. Ship squat in water of varying depth. *Int. J. Marit. Eng.*, **145**, 1–8.
- Gourlay, T. P. 2006. A simple method for predicting the maximum squat of a high-speed displacement ship. *Mar. Technol. Soc. J.*, **43**, 146–151.
- Gourlay, T. P. and Cook, S. M. 2004. Flow past a ship radiating a bore in a channel. *Proc. Inst. Mech. Eng. M. J. Eng. Marit. Environ.*, **218**, 31–40.
- Gourlay, T. P. and Tuck, E. O. 2001. The maximum sinkage of a ship. *J. Ship Res.*, **45**, 50–58.
- Graff, W. 1962. Untersuchungen über die Ausbildung des Wellenwiderstandes im Bereich der Stauwellengeschwindigkeit in flachem, seitlich beschränktem Fahrwasser. *Schiffstechnik*, **9**, 110–122.
- Grimshaw, R. H. J. and Smyth, N. 1986. Resonant flow of a stratified flow over topography. *J. Fluid Mech.*, **169**, 429–464.
- Grimshaw, R. H. J., Hunt, J. C. R., and Chow, K. W. 2014. Changing forms and sudden smooth transitions of tsunami waves. *J. Ocean Eng. Mar. Energy*, doi: 10.1007/s40722-014-0011-1
- Hamer, M. 1999. Solitary killers. *New Sci.*, **163**(2201), 18–19.
- Krylov, A. N. 2003. On the wave resistance and large ship waves. In *My Memoirs*. Politekhnika, Sankt-Peterburg, pp. 364–368 (in Russian).
- Kurennoy, D., Soomere, T., and Parnell, K. E. 2009. Variability in the properties of wakes generated by high-speed ferries. *J. Coast. Res.*, **SI 56**, 519–523.
- Kuznetsov, N., Maz'ya, V., and Vainberg, B. 2002. *Linear Water Waves: A Mathematical Approach*. Cambridge University Press.
- Lee, S. J., Yates, G. T., and Wu, T. Y. 1989. Experiments and analyses of upstream-advancing solitary waves generated by moving disturbances. *J. Fluid Mech.*, **199**, 569–593.
- LeVeque, R. J. 2004. *Finite-Volume Methods for Hyperbolic Problems*. Cambridge University Press.
- Lighthill, J. 1978. *Waves in Fluids*. Cambridge University Press.
- Macfarlane, G. J., Duffy, J. T., and Bose, N. 2014. Rapid assessment of boat-generated waves within sheltered waterways. *Aust. J. Civil Eng.*, **12**(1), 31–40.
- Madricardo, F. and Donnici, S. 2014. Mapping past and recent landscape modifications in the Lagoon of Venice through geophysical surveys and historical maps. *Anthropocene*, **6**, 86–96.
- Millward, A. 1996. A review of the prediction of squat in shallow water. *J. Navigation*, **49**, 77–88.
- Naghdi, P. M. and Rubin, M. B. 1984. On the squat of a ship. *J. Ship Res.*, **28**, 107–117.
- Neuman, D., Tapio, E., Haggard, D., Laws, K., and Bland, R. 2001. Observation of long waves generated by ferries. *Can. J. Remote Sens.*, **27**, 361–370.
- Newman, J. N. 1977. *Marine Hydrodynamics*. The MIT Press.
- Noblesse, F., He, J., Zhu, Y., Hong, L., Zhang, C., Zhu, R., and Yang, C. 2014. Why can ship wakes appear narrower than Kelvin's angle? *Eur. J. Mech. B/Fluids*, **46**, 164–171.
- Parnell, K. E. and Kofoed-Hansen, H. 2001. Wakes from large high-speed ferries in confined coastal waters: management approaches with examples from New Zealand and Denmark. *Coast. Manage.*, **29**, 217–237.

- Parnell, K. E., McDonald, S. C., and Burke, A. E. 2007. Shoreline effects of vessel wakes, Marlborough Sounds, New Zealand. *J. Coast. Res.*, SI **50**, 502–506.
- Parnell, K. E., Soomere, T., Zaggia, L., Rodin, A., Lorenzetti, G., Rapaglia, J., and Scarpa, G. M. 2015. Ship-induced solitary Riemann waves of depression in Venice Lagoon. *Phys. Lett. A*, **379**(6), 555–559.
- Pelinovsky, E. N. and Rodin, A. A. 2012. Transformation of a strongly nonlinear wave in a shallow-water basin. *Izv. Atmos. Ocean. Phys.*, **48**, 343–349.
- Peregrine, D. H. 1966. Calculations of the development of an undular bore. *J. Fluid Mech.*, **25**, 321–330.
- Peterson, P., Soomere, T., Engelbrecht, J., and van Groesen, E. 2003. Soliton interaction as a possible model for extreme waves in shallow water. *Nonlinear Proc. Geoph.*, **10**, 503–510.
- Rabaud, M. and Moisy, F. 2013. Ship wakes: Kelvin or Mach angle? *Phys. Rev. Lett.*, **110**, Art. No. 214503.
- Rapaglia, J., Zaggia, L., Ricklefs, K., Gelinis, M., and Bokuniewicz, H. 2011. Characteristics of ships' depression waves and associated sediment resuspension in Venice Lagoon, Italy. *J. Mar. Syst.*, **85**, 45–56.
- Ravens, T. M. and Thomas, R. C. 2008. Ship wave-induced sedimentation of a tidal creek in Galveston Bay. *J. Waterw. Port Coast. Ocean Eng.*, **134**, 21–29.
- Rudenko, O. and Soluyan, S. 1977. *Theoretical Background of Nonlinear Acoustics*. Plenum, New York, 1977.
- Sarretta, A., Pillon, S., Molinaroli, E., Guerzoni, S., and Fontolan, G. 2010. Sediment budget in the Lagoon of Venice, Italy. *Cont. Shelf Res.*, **30**, 934–949.
- Sheremet, A., Gravois, U., and Tian, M. 2013. Boat-wake statistics at Jensen Beach, Florida. *J. Waterw. Port Coast. Ocean Eng.*, **139**, 286–294.
- Sommerfeld, A. 1949. *Partial Differential Equations in Physics*. Elsevier.
- Soomere, T. 2005. Fast ferry traffic as a qualitatively new forcing factor of environmental processes in non-tidal sea areas: a case study in Tallinn Bay, Baltic Sea. *Environ. Fluid Mech.*, **5**, 293–323.
- Soomere, T. 2007. Nonlinear components of ship wake waves. *Appl. Mech. Rev.*, **60**, 120–138.
- Soomere, T., Parnell, K. E., and Didenkulova, I. 2011. Water transport in wake waves from high-speed vessels. *J. Mar. Syst.*, **88**, 74–81.
- Sorensen, R. M. 1973. Ship-generated waves. *Adv. Hydrosci.*, **9**, 49–83.
- Stumbo, S., Fox, K., Dvorak, F., and Elliot, L. 1999. The prediction, measurement, and analysis of wake wash from marine vessels. *Mar. Technol.*, **36**, 248–260.
- Torsvik, T. and Soomere, T. 2008. Simulation of patterns of wakes from high-speed ferries in Tallinn Bay. *Estonian J. Eng.*, **14**, 232–254.
- Torsvik, T., Didenkulova, I., Soomere, T., and Parnell, K. E. 2009a. Variability in spatial patterns of long nonlinear waves from fast ferries in Tallinn Bay. *Nonlinear Proc. Geoph.*, **16**, 351–363.
- Torsvik, T., Pedersen, G., and Dysthe, K. 2009b. Waves generated by a pressure disturbance moving in a channel with a variable cross-sectional topography. *J. Waterw. Port Coast. Ocean Eng.*, **135**, 120–123.
- Torsvik, T., Soomere, T., Didenkulova, I., and Sheremet, A. 2015. Identification of ship wake structures by a time-frequency method. *J. Fluid Mech.*, **765**, 229–251.
- Varyani, K. 2006. Full scale study of the wash of high speed craft. *Ocean Eng.*, **33**, 705–722.
- Wehausen, J. V. 1973. The wave resistance of ships. *Adv. Appl. Mech.*, **13**, 93–245.
- Whitham, G. B. 1974. *Linear and Nonlinear Waves*. Wiley, New York.
- Zahibo, N., Didenkulova, I., Kurkin, A., and Pelinovsky, E. 2008. Steepness and spectrum of nonlinear deformed shallow water wave. *Ocean Eng.*, **35**, 47–52.

Laevade tekitatud sügavate Riemanni üksiklainete levimine Venetsia laguunis

Artem Rodin, Tarmo Soomere, Kevin E. Parnell ja Luca Zaggia

Venetsia laguuni läbivas Malamocco-Marghera kanalil liikuvate laevade tekitatud ja kanali lähistel mõõdetud sügavaid ning pikka aega terviklike struktuuridena püsivaid üksiklaineid interpreteeritakse tugevalt mittelineaarsete madala vee võrrandite erilahendite, nn Riemanni (ehk lihtsate) lainetena. Nende liikuvate lohku peamised omadused kanali lähistel paiknevates mõõtepunktidetes on rekonstrueeritud tarkvaraga CLAWPACK. Lainelohkude edasist kulgemist ja transformeerumist laguuni kaugemates osades analüüsitakse mõõdetud lohku omadustega sobivate idealiseeritud alghäirituste numbrilise prognoosi teel. On näidatud, et ligikaudu 2 m sügavuses vees võivad laevade poolt kanalil tekitatud arvestatava sügavusega (>0,3 m) häiritused levida vähemalt 1 km kaugusele. Laguuni madalas vees levimisel muutub lainelohkude esinõlv järjest laugemaks, kuid taganõlv kujuneb kiiresti väga järsuks boori-taoliseks veevalliks. Algselt erineva sügavusega lainelohkude amplituud ühtlustub aegamisi ja kanalist eemal sõltub boori kõrgus peamiselt läbitud vahemaast. Analüüsi tulemustest järeldub, et isegi suhteliselt tagasihoidliku kiirusega sõitvate ja mitte eriti suurte laevade tekitatud lainelohud võivad levida negatiivseid üksiklaineid meenutavate järsu taganõlvaga kompaktsete häiritustena praktiliselt üle kogu laguuni. Selline võimalus suurendab märgatavalt laevalainete keskkonnamõju ruumilist ulatust kohtades, kus laevaliiklus toimub madalaveelistesse veekogudesse süvendatud kitsastes kanalites.

Paper IV

Didenkulova I., **Rodin A.** 2012. Statistics of shallow water rogue waves in Baltic Sea conditions: the case of Tallinn Bay. In: *IEEE/OES Baltic 2012 International Symposium*, 8–11 May 2012, Klaipėda, Lithuania; Proceedings. IEEE, doi: 10.1109/BALTIC.2012.6249221

Statistics of shallow water rogue waves in Baltic Sea conditions: the case of Tallinn Bay

I. Didenkulova^{1,2}, A. Rodin^{1,2}

¹Institute of Cybernetics, Tallinn University of Technology
Akadeemia tee 21, 12618 Tallinn, Estonia

²Nizhny Novgorod State Technical University
Minin str. 24, 603950 Nizhny Novgorod, Russia

Abstract- The properties of rogue waves in shallow water are analyzed based on records of sea surface elevation in Tallinn Bay, the Baltic Sea, measured at the water depth 2.7 m from 17 June to 1 July 2009 at a recording frequency of 5 Hz. The data set contains rogue waves, which occur in relatively calm weather conditions. Rogue waves are identified as those, whose wave height is at least twice larger than the significant wave height. The results obtained by both methods up-crossing and down-crossing are analyzed and compared. The statistics of rogue wave heights is studied together with the statistics of rogue wave crests and rogue wave troughs.

I. INTRODUCTION

Rogue waves in the coastal zone represent a serious danger for smaller ships, coastal structures and for people at the coast. It has been shown in [1-3] that most of accidents which result in human loss and ship damage occur in the nearshore. During the last 10 years 69 such accidents have been reported, which caused the death of 125 people and injury of 169 people. Even ship damages occurred mostly in the shallow region. Seven ship losses and 14 ship damages were reported in shallow waters [1]. The exceptionally large reported loss of lives and different kinds of injuries and damages suggests that the registration of rogue waves should be understood as an important goal worldwide and extreme events should be specifically documented everywhere where waves are measured for a long enough time interval. Doing so is one of a few feasible ways to reach more reliable statistics of the occurrence of smaller rogue wave events that do not result in any damage.

At the moment, the number of studies of rogue events in the coastal zone is rather limited and is reflected in the following publications [4-8]. The given paper also represents one of these studies and adds a new knowledge to the statistics of shallow-water rogue waves. It is a continuation of the work by [7, 8], which was focused on statistics of rogue waves in the coastal zone of Baltic Sea and based on measurements conducted near the coast of Aegna Island in the northern part of Tallinn Bay. Then existence of two different types of rogue waves with respect to their amplification factor has been demonstrated. In the given paper we present wave statistics, collected in June-July 2009 near Pikakari beach, in the southern part of Tallinn Bay. This statistics confirms some results presented in [7, 8] and also demonstrates some different effects, which is rather typical for rogue waves in shallow water, which are very much bathymetry-dependent [9, 10].

The paper is organized as follows. The wave measurements, the data set and its processing are described in Sec. II. The selected rogue waves and their statistics are analyzed in Sec. III. Main results are summarized in Conclusion.

II. WAVE MEASUREMENTS AND DATA PROCESSING

The measurements have been collected in the southern part of Tallinn Bay, Baltic Sea, near the coast of Pikakari beach (Fig. 1). The water surface profile has been recorded by ultrasonic echosounder, mounted on the top of a heavy tripod, located 100 m from the coast at the water depth of 2.7 m. The experimental equipment is described in [11].

Initial dataset represents a two-week record of water surface elevation (from 17 June to 1 July 2009) at a recording frequency of 5 Hz in relatively calm weather conditions. Since the location of the experiment was close to the port area with intense ship traffic, first of all, we needed to select only pure wind wave data. In order to do this we used only night data (from 0:00 to 7:00 am), when ship traffic was low, and also manually removed from the analysis the parts of records with accidentally late (after 0:00 a.m.) and early (before 7:00 a.m.) ship passages. Since ship waves have different period a specific wake structure, it was easy to identify them in the record.

The processed records have been subdivided by 20-minute intervals (totally, 274 20-minute intervals have been identified), where the significant wave height (H_s) was calculated using both up-crossing and down-crossing methods. Although, in general, these methods give similar results, their interpretation is different. Wave heights, extracted by the up-crossing method correspond

to the face slope of the wave, while wave heights, found by the down-crossing method correspond to the back slope of the wave. Both slopes of the wave are important from the rogue wave point of view and can lead to rogue wave accidents, though with different scenario. That is why below we keep datasets obtained using both methods.

The corresponding significant wave height distributions, obtained using up-crossing and down-crossing methods is demonstrated in Fig. 2. It can be seen that the significant wave height did not exceed 40 cm during the time of the experiment and most of the time stayed below 10 cm. It can also be seen in Fig. 2 that both up-crossing and down-crossing methods lead to the same distribution of H_s that means that statistically heights of face and back wave slopes are equivalent.

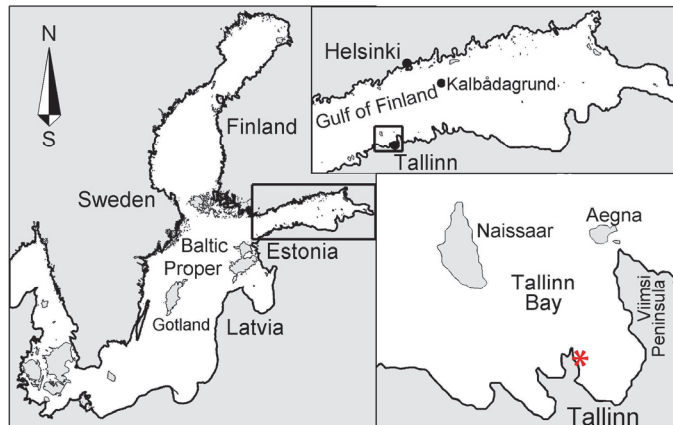


Fig. 1 The map of the study site, the location of the experiment is marked by the star.

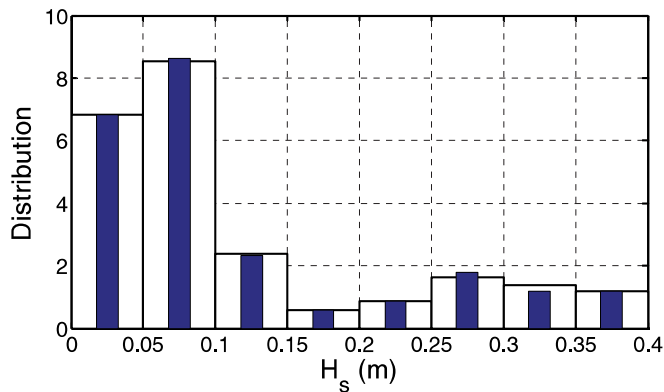


Fig. 2 Significant wave height distribution, obtained using down-crossing (white columns) and up-crossing (blue columns) methods.

With the reference to calculated significant wave heights, rogue wave events have been identified as those, whose wave height H_f is at least twice larger than the significant wave height within given 20-minute interval $H_f/H_s \geq 2$ [12]. In this way 51 rogue waves have been selected out of almost 180000 waves using the up-crossing method and 55 rogue waves – using down-crossing method. A Rayleigh distribution of wave heights, appropriate under a narrow-band Gaussian model for the sea surface elevation, would suggest that a rogue wave would occur about once in every 3000 wave events [12]; that is, about 60 times for our number of waves. Thus, the Rayleigh distribution slightly overestimates the number of rogue waves in the record of the nearshore region. Similar results have been obtained previously by [7] for the northern part of Tallinn Bay, near the coast of Aegna Island (Fig. 1).

The characteristic wave periods during the time of the experiment varied from 2 to 4 s and sometimes even less. In these cases the echo sounder resolution (5 Hz) was not sufficient enough to describe steep fronts of the corresponding rogue waves (Fig. 3). In the analysis below we mark these records as “low resolution records” and analyze both high-resolution dataset (excluding “low

resolution records”) and the full dataset (including “low resolution records”). Totally, 10 such “low resolution records” have been identified in the dataset obtained using up-crossing method and 12 records – in the dataset obtained using down-crossing method.

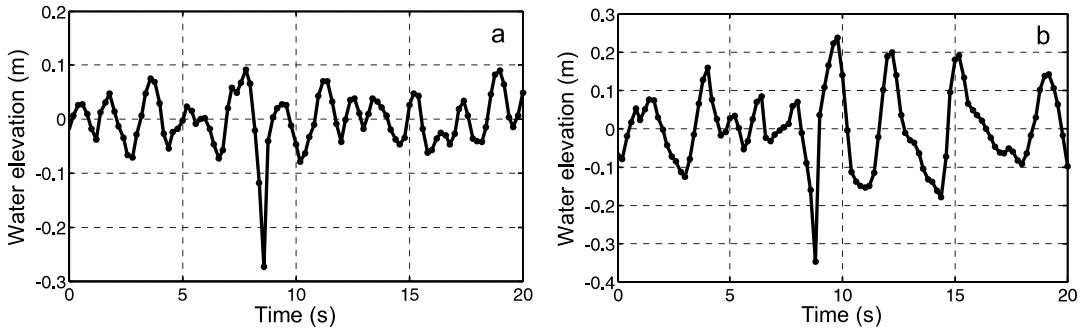


Fig. 3 Low resolution examples of rogue waves measured on 30 June (a) and 17 June 2009 (b).

It should also be mentioned that during the time of the experiment three rogue wave groups have been recorded. All three wave groups were measured on the same day – 25 June 2009, when the wind wave activity was very low (no more than 15 cm), and were identified by the down-crossing method (Fig. 4). One of these waves represents a typical shape for the deep-water wave group, where two high waves come one after another (Fig. 4a). It is also characteristic that this wave group was measured just before the weather changed and the wave amplitude started to grow. In other two cases two rogue waves belong to the same wave group, but located in different parts of the group as it is shown in Fig. 4b. Periods of rogue waves shown in Fig. 4 are very short and change from 1.5 s to 1.8 s, which corresponds to values of kh changing from 3.3 to 4.8 that are larger than $kh > 1.36$ and, therefore, observed rogue wave groups are generated by “deep-water” mechanisms.

For comparison, during 2008 experiment in the northern part of the Tallinn Bay, near the coast of Aegna Island, there were no such wave groups identified [7, 8].

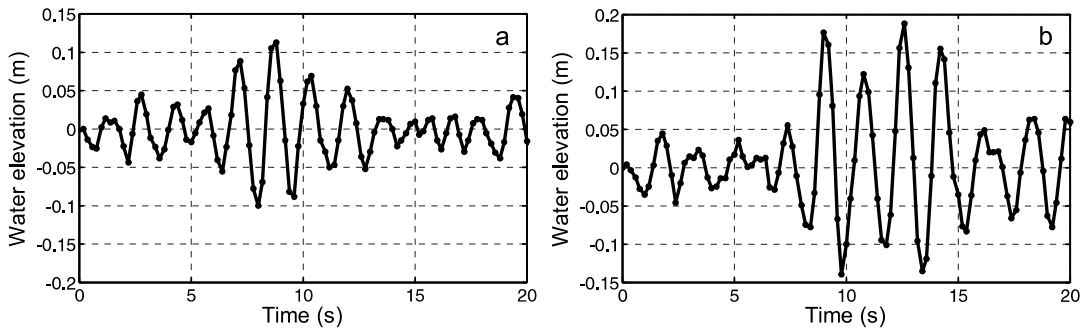


Fig. 4 Groups of rogue waves measured on 25 June 2009.

III. ROGUE WAVE STATISTICS

As it has been pointed out above, totally 51 rogue waves have been identified using the up-crossing method and 55 rogue waves – using down-crossing method. The scatter diagram of rogue wave height H_r and significant wave height H_s for different wave shapes is presented in Fig. 5. Observations are mostly close to the $H_r = 2H_s$ line with a few weak deviations mainly for waves of low resolution, which is logical, since the entire wave record is rather short and the probability of occurrence of rogue waves of a very large height is low. These deviations are even more evident in Fig. 6, where the amplification factor (the ratio of the rogue wave height to significant wave height) is shown. It can also be seen that some low resolution (high-frequency) records demonstrate an extreme wave amplification, which was also observed during 2008 experiment in the northern part of the Tallinn Bay, near the coast of Aegna Island [7]. Here, because of the lack of such measurements, it is hard to clearly identify this group of waves and the dependence on H_s is also not visible in comparison with [7]. However, the general tendency seems to be similar.

The distribution of rogue wave heights for up-crossing and down-crossing wave selection is shown in Fig. 7. It can be seen that face (Fig. 7a) and back (Fig. 7b) slopes of the rogue waves demonstrate similar, but slightly different behavior. In this way, for smaller wave heights (below 20 cm) it is more probable to meet the steep face slope, rather than the back slope of the wave. It can also be seen that in both up-crossing and down-crossing wave collections most of low-resolution waves were observed for intermediate values of H_f (30–70 cm).

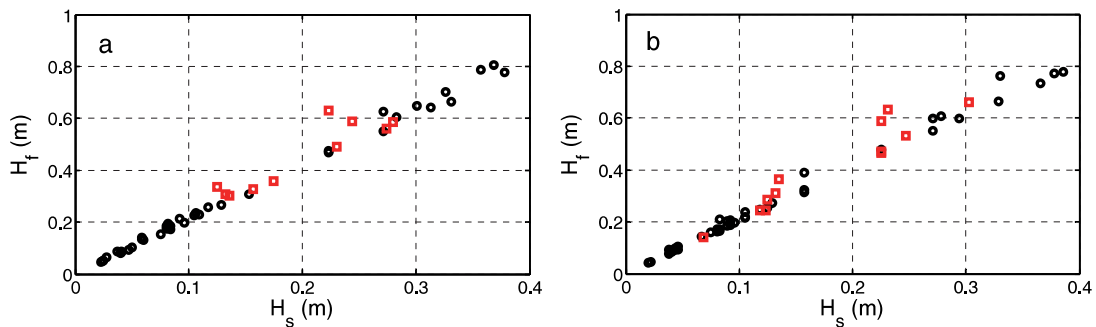


Fig. 5 Scatter diagram for rogue wave height H_f and significant wave height H_s for up-crossing (a) and down-crossing (b) wave selection. Red squares correspond to low-resolution rogue waves.

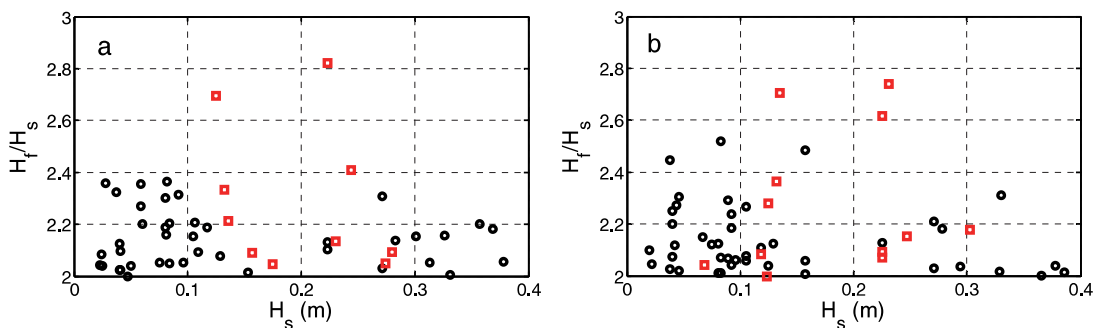


Fig. 6 Amplification factor of rogue waves for up-crossing (a) and down-crossing (b) wave selection. Red squares correspond to low-resolution rogue waves.

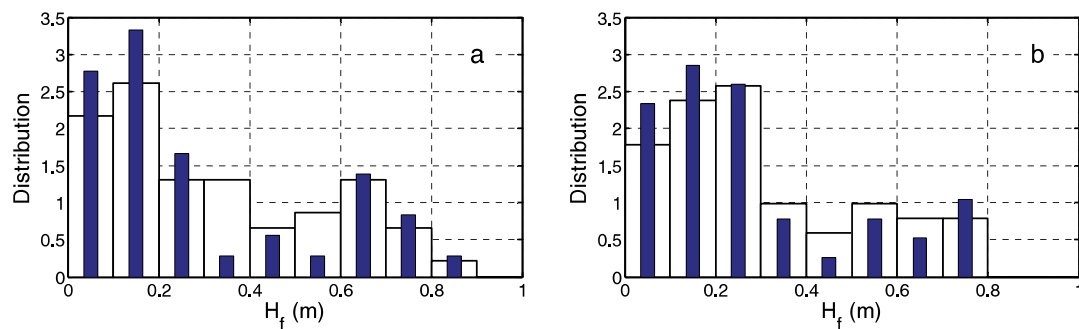


Fig. 7 Rogue wave height distribution for up-crossing (a) and down-crossing (b) wave selection; while columns correspond to the full rogue wave dataset and blue columns – to high-resolution events only.

Another interesting feature of rogue waves in the coastal zone can be concluded by looking at Fig. 8, where the distribution of rogue wave crests and troughs is plotted. It can be seen that at a very low wave activity (wave amplitudes below 10 cm) it is more probable to meet a deep wave trough rather than a high wave crest, while for wave amplitudes over 40 cm it is more probable to meet a high wave crest rather than a deep wave trough.

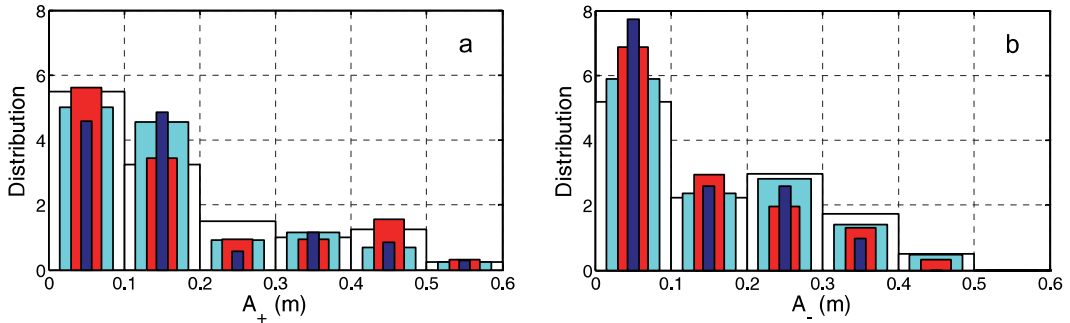


Fig. 8 Distribution of rogue wave crests (a) and rogue wave troughs (b). White and red columns correspond to all rogue wave amplitudes found by up-crossing method and to only high-resolution events respectively; light and dark blue columns correspond to all rogue wave amplitudes found by down-crossing method and to only high-resolution events respectively.

IV. CONCLUSION

The statistics of rogue waves in the coastal zone has been studied based on the two-week wave record of sea level oscillations in the coastal zone of the Baltic Sea. The experiment has been conducted 100 m far from the coast at 2.7 m depth in the southern part of Tallinn Bay, near the coast of Pikakari beach. Rogue waves were identified with respect to significant wave height ($H_j/H_s \geq 2$) by both up-crossing and down-crossing methods. Totally, 51 rogue waves (including 10 events with low resolution) have been found using the up-crossing method and 55 rogue waves (including 12 events with low resolution) – using down-crossing method. It has been shown, that Rayleigh distribution slightly overestimates the number of rogue waves in the record of the nearshore region.

Almost all identified rogue waves are single waves. However, among 55 rogue waves found by down-crossing method there are three rogue wave groups. One of these rogue wave groups represents a characteristic deep-water group structure with two large waves following one after another, while in other two groups two rogue waves are separated by other smaller waves.

It is shown that at a very low wave activity (wave amplitudes below 10 cm) it is more probable to meet a deep wave trough rather than a high wave crest, while for wave amplitudes over 40 cm it is more probable to meet a high wave crest rather than a deep wave trough. Also for smaller waves (wave heights below 20 cm) it is more probable to observe steep face slope, rather than the back slope of the wave.

ACKNOWLEDGMENT

Partial support from the targeted financing by the Estonian Ministry of Education and Research (grant SF0140007s11), Estonian Science Foundation (grant 8870), the EC Programme FP7-SST-2008-RTD-1 under grant agreement No 234175, Russian Foundation for Basic Research (Grants 11-05-00216, 11-05-92002 and 11-02-00483), Russian President Program (MK-1440.2012.5) and DoRa 4 program is acknowledged. This research was also supported by the European Union through support to the Estonian Centre of Excellence for Non-linear Studies CENS from the European Regional Development Fund.

REFERENCES

- [1] I. Nikolkina and I. Didenkulova. "Rogue waves in 2006 – 2010," *Nat. Hazards Earth Syst. Sci.*, vol. 11, pp. 2913-2924, 2011.
- [2] I. Nikolkina and I. Didenkulova. "Catalogue of rogue waves reported in media in 2006–2010," *Nat. Hazards*, vol. 61(3), pp. 989-1006, 2012.
- [3] P.C. Liu. "A chronology of freak wave encounters," *Geofizika*, vol. 24, pp. 57-70, 2007.
- [4] H. Chien, C-C. Kao and L.Z.H. Chuang. "On the characteristics of observed coastal freak waves," *Coastal Eng. J.*, vol. 44(4), pp. 301-319, 2002.
- [5] Z. Cherneva, P. Petrova, N. Andreeva and C. Guades Soares. "Probability distributions of peaks, troughs and heights of wind waves measured in the black sea coastal zone," *Coastal Eng.*, vol. 52, pp. 599-615, 2005.

- [6] B. Baschek and J. Imai. "Rogue Wave Observations Off the US West Coast," *Oceanography*, vol. 24(2), pp. 158-165.
- [7] I. Didenkulova and C. Anderson. "Freak waves of different types in the coastal zone of the Baltic Sea," *Nat. Hazards Earth Syst. Sci.*, vol. 10(9), pp. 2021-2029, 2010.
- [8] I. Didenkulova. "Shapes of freak waves in the coastal zone of the Baltic Sea (Tallinn Bay)," *Boreal Env. Res.*, vol. 16(Suppl A), pp. 138-148, 2011.
- [9] I. Didenkulova and E. Pelinovsky. "Rogue waves in nonlinear hyperbolic systems (shallow-water framework)," *Nonlinearity*, vol. 24, R1-R18, 2011.
- [10] A. Slunyaev, I. Didenkulova and E. Pelinovsky. "Rogue Waters," *Contemporary Physics*, vol. 52(6), pp. 571-590, 2011.
- [11] K. Parnell, N. Delpeche, I. Didenkulova, T. Dolphin, A. Erm, A. Kask, L. Kelpsaite, D. Kurennoy, E. Quak, A. Räämet, T. Soomere, A. Terentjeva, T. Torsvik and I. Zaitseva-Pärnaste. "Far-field vessel wakes in Tallinn Bay," *Est. J. Eng.*, vol. 14(4), pp. 273-302, 2008.
- [12] Ch. Kharif, E. Pelinovsky and A. Slunyaev. *Rogue waves in the ocean*, Springer, 2009.

Paper V

Rodin A., Didenkulova I., Nikolkina I. 2014. Run-up of large storm waves on Estonian coasts of the Baltic Sea. In: *IEEE/OES Baltic 2014 International Symposium*, 26–29 May 2014, Tallinn, Estonia; Proceedings. IEEE, doi: 10.1109/BALTIC.2014.6887886

Run-up of large storm waves on Estonian coasts of the Baltic Sea

A. Rodin, I. Didenkulova, I. Nikolkina
Institute of Cybernetics at Tallinn University of Technology
Akadeemia tee, 21
EE-12618 Tallinn
Estonia

Abstract- Analysis of maximal inundation of Estonian coasts of the Baltic Sea is conducted on 35-year wind wave simulations with WAM model forced by COSMO winds in the presence of ice. For each of selected along the Estonian Baltic Sea coast 18 beach profiles, the maximal significant wave heights and corresponding periods are found. The locations with available wave data are located at the water depth of about 10 to 20 m and at a distance up to 8 km from the shore. Run-up of these waves on Estonian beaches is calculated within the shallow water theory using the CLAWPACK software package (www.clawpack.org). The topography of the beach is taken from Geological field surveys and combined with GEBCO maps, where needed. We consider the case, when monochromatic waves of corresponding wave height and period are approaching the coast. For this we use boundary conditions of wave-maker located offshore and generating regular waves. Time and space step during all calculations of wave run-up remains constant (1 m and 1 s respectively). The estimates of maximal run-up are compared with the estimations made using different run-up formulas, available in the literature.

From the point of view of coastal structure design, it is very important to have an estimate of maximal expected inundation and run-up. This analysis is usually performed using different empirical engineering formulas obtained by means of field observations or by special flume experiments, see [1-7]. However, since in the coastal zone the waves are generally long, and Estonian sea coast is relatively shallow it can be possible to do this estimation by using nonlinear shallow water theory, what is proposed in the given paper. The results of calculations are compared with the estimations performed by different engineering formulas and the possibility of using the shallow water theory is revised. A good overview of empiric formulas available in the literature is given in [7].

Firstly we considered the Hunt [1] empirical formula for estimation of the run-up height as a function of beach slope α , and incident wave height H which was proposed based on the results of numerous flume tests

$$R = H\xi, \quad \xi = \alpha \sqrt{\frac{\lambda}{H_0}}, \quad (1)$$

where H_0 is the mean wave height and λ is the wave length of waves in deep water, ξ is so called Iribarren parameter (or surf-similarity parameter). Notation of this formula was changed by [2]. Instead of mean wave height it includes significant wave height H_s . In our case this formula leads to the same result.

On a dissipative sandy beach maximal run-up was described as linearly related to H_s , by [3]:

$$R = 0.035 + 0.71H_s. \quad (2)$$

Formula for the highest run-up on a gravel beach (based on experiments on a random wave run-up in a flume) was mentioned in [4]:

$$R = H_s \left(2.86 - 62.69 \left(\frac{H_s}{\lambda} \right) + 443.29 \left(\frac{H_s}{\lambda} \right)^2 \right). \quad (3)$$

For run-up on different sandy beaches (from reflective to dissipative) based on multiple measurements in [5,6] there was proposed the formula for beaches with slopes < 0.1 (due to the fact that Estonian coasts are very shallow, almost all the profiles we are using have slopes flatter than this value):

$$R = 0.05 \sqrt{H_{rms} \lambda}, \quad (4)$$

where H_{rms} is a deep-water root mean square wave height

$$H_{rms} = \frac{H_s}{\sqrt{2}}. \quad (5)$$

For beaches with slopes > 0.1 (or equal 0.1) the formula for run-up height will be:

$$R = 0.6\xi. \quad (6)$$

Analysis of maximal inundation of Estonian coasts of the Baltic Sea has been conducted based on 35-year wind wave simulations with WAM model forced by COSMO winds in the presence of ice. For this analysis we used beach profiles along the Estonian Baltic Sea coast, where good topographic data were available thanks to Geological field surveys (see Fig. 1).

Avoiding particularities, the most typical bottom profile for every beach have been taken from a bunch of profiles which were measured in 2006-2011 in the framework of state monitoring program of beaches [8-12] in 18 different locations of Estonian coast. So, 18 beach profiles were selected. In cases when the length of given profile was not enough for numerical calculations (either it was just too short, or given maximal height of profile was overflowed by the numerically modeled waves) it was extended using GEBCO maps.

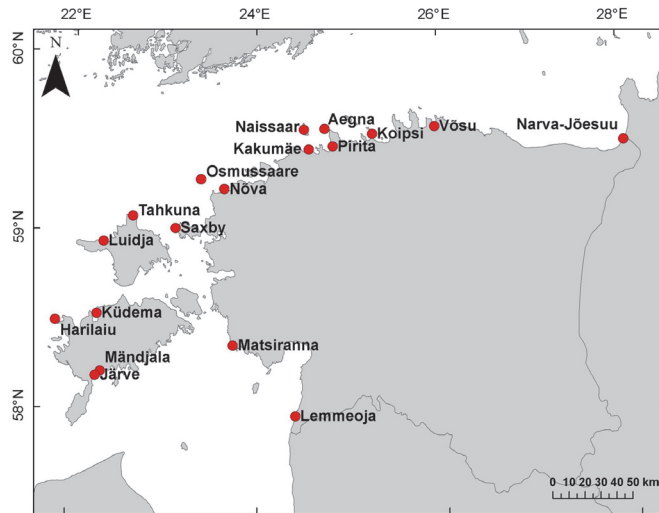


Fig.1. Locations of 18 beach profiles along Estonian coasts [13].

For all these profiles the maximal significant wave heights and corresponding periods were found in the nearest to the shoreline point, which corresponded to water depths from 9 to 28 m and distances from 1 to 8 km from the shore (see Table 1). The periods were changing from 8 sec to 11 sec. Significant wave heights varied between 3.3 m and 7.5 m. GPS coordinates for measured profiles were known, as well as the locations of the nearest computed wave gauges, which had registered waves taken as initial conditions.

Run-up of waves on Estonian beaches of real topography was calculated in the shallow water theory framework using the CLAWPACK software package (www.clawpack.org). We considered the case, when monochromatic waves of corresponding wave height and period were approaching the coast. Wave parameters and numerically calculated run-up heights and inundation distances are given in a Table 1. For this we used boundary conditions of wave-maker located offshore and generating regular waves. Time and space step during all calculations of wave run-up remained constant (1 m and 1 s respectively).

The calculated run-up heights for all these beaches are compared with described above formulas (1)-(6) and results of this comparison are given in Table 2. The maximal run-up heights of about 3 m are expected at Aegna, Naissaare and Osmussaare coasts. On Aegna Island it may lead to flooding of several houses located by the sea. Another place, where wave run-up of about 2 m is expected, is Kakumäe. This area is densely populated and, therefore, represents the most vulnerable to extreme wave hazard place.

The comparison of numerically calculated run-up heights with estimates performed by formulas (1)-(6) is graphically shown on Fig. 2. Formulas (2) and (3) generally overestimate numerical results and it can be explained by the specific type of studied beaches for which these formulas were suggested.

For instance, formula (3) was elaborated for gravel beaches in UK. Experimental set-up in [4] contained the random wave flume with a length of 42 m with the operating water depth ranging from 0.7 to 0.9 m. The beach slope was build or combined from particles with different diameter for a better fit to typical UK beaches. This also explains why formula (3) gives reasonable estimate for Estonian gravel beaches, such as Aegna and Osmussaare.

Formula (2) represents linear dependence of run-up height from the wave height and obviously cannot consider all of the factors and wave effects that might occur. It was elaborated for dissipative sandy beaches using field experiments at the Pacific coast of US (California, Torrey Pines Beach) included only certain wave regimes characteristic for this area. The local beach slope, in the region where the swash was measured, varied between 0.02 and 0.05, and incident wave heights were changing from 0.5 m to 1.5 m. So, it is not surprising that these estimates are not applicable for Estonian Baltic Sea coasts.

Formula (1) was based on flume experiments, where run-up heights were measured on a porous, rough continuous slope changing from 0.1 to 0.33 [1] and covered a wide range of wave regimes.

Formulas (4-6) were obtained using field experiments on natural beaches of Atlantic coast of US (North Carolina). Incident wave heights during experiments [5] varied from 0.4 m to 4 m. Their periods were in the range of 6 s to 16 s, and beach slopes - from 0.07 to 0.20. These parameters overlap with some wave parameters discussed in this work (see Table 1).

So, this explains why formulas (1) and (4-6) show comparably good overlapping with the computational results.

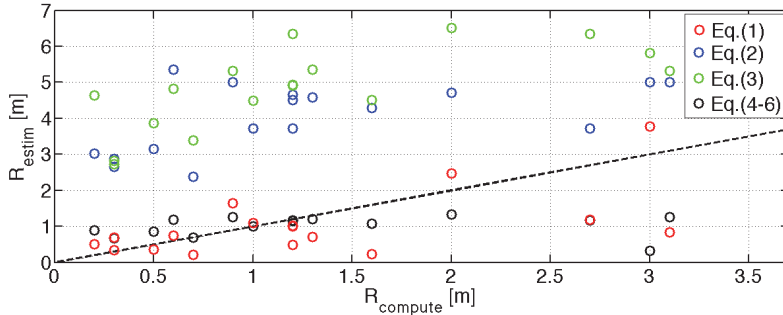


Fig.2. Comparison of calculated and estimated run-up heights.

TABLE I
EXTREME WAVE PARAMETERS COMPUTED AT DIFFERENT BEACHES ALONG ESTONIAN COASTS

Beach profile	Max H_s (m)	Water depth (m)	Max wave period (s)	Distance to the shore (km)	Beach slope α	Numerically calculated run-up height (m)	Numerically calculated inundation distance (m)
Aegna	7.0	17	11	0.75	0.028	3.1	35
Harilaid	6.0	15	10	1.65	0.009	1.6	26
Järve	3.7	9	8	8.40	0.044	0.3	3
Kakumäe	6.6	28	11	1.33	0.077	2.0	14
Koipsi	5.2	26	11	2.20	0.037	1.2	13
Küdeema	6.3	14	11	2.44	0.037	1.2	9
Lemmeoja	4.0	8	8	5.10	0.021	0.3	3
Luidja	7.5	11	11	6.82	0.026	0.6	7
Mändjala	3.7	9	8	6.45	0.043	0.3	8
Matsiranna	4.4	10	10	5.68	0.018	0.5	11
Naissaare	7.0	21	11	0.90	0.121	3.0	10
Narva-Jõesuu	3.3	14	8	1.90	0.013	0.7	14
Nõva	6.5	14	11	2.84	0.018	1.2	23
Osmussaare	5.2	26	11	1.25	0.043	2.7	27
Pirita	6.4	17	11	2.40	0.025	1.3	19
Saxby	5.2	11	11	3.17	0.047	1.0	8
Tahkuna	7.0	17	11	4.43	0.055	0.9	10
Võsu	4.2	15	10	7.83	0.023	0.2	6

Figure 3 shows the dependence of maximal run-up height on significant wave height. It can be seen that in general for all formulas and simulation run-up height grows with increase in the significant wave height. The smallest growth is observed for formulas (1) and (4)-(6). The same is observed in Fig. 4, where wave amplification (the ratio of run-up height and significant wave height) is plotted against significant wave height. On both Figs. 3 and 4 it can be seen that formulas (1) and (4)-(6) are in a relatively good agreement with numerical simulations performed using nonlinear shallow water theory, which demonstrates that nonlinear shallow water theory can be applied for calculation of wind wave run-up on the coast.

TABLE II
ESTIMATES OF MAXIMAL RUN-UP HEIGHTS AT DIFFERENT BEACHES ALONG ESTONIAN COASTS

Beach profile	Numerical simulation within shallow water theory (m)	Hunt 1959, Battjes 1974 (m)	Guza & Thornton 1982 (m)	Powell 1990 (m)	Holman 1986, Nielsen & Hanslow 1991 (m)
Aegna	3.1	0.8	5.0	5.3	1.3
Harilaid	1.6	0.2	4.3	4.5	1.1

Järve	0.3	0.7	2.7	2.8	0.7
Kakumäe	2.0	2.5	4.7	6.5	1.3
Koipsi	1.2	1.0	3.7	6.4	1.2
Küdemä	1.2	1.0	4.5	4.9	1.2
Lemmeoja	0.3	0.3	2.9	2.7	0.7
Luidja	0.6	0.7	5.4	4.8	1.2
Mändjala	0.3	0.7	2.7	2.8	0.7
Matsiranna	0.5	0.4	3.2	3.9	0.8
Naissaare	3.0	3.8	5.0	5.8	0.3
Narva-Jõesuu	0.7	0.2	2.4	3.4	0.7
Nõva	1.2	0.5	4.7	4.9	1.2
Osmussaare	2.7	1.2	3.7	6.4	1.2
Pirita	1.3	0.7	4.6	5.4	1.2
Saxby	1.0	1.1	3.7	4.5	1.0
Tahkuna	0.9	1.6	5.0	5.3	1.3
Võsu	0.2	0.5	3.0	4.6	0.9

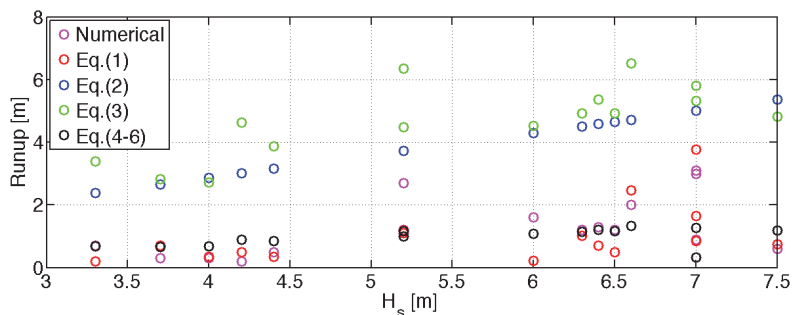


Fig.3. Calculated and estimated run-up heights versus significant wave height.

Thus, in this paper we compared run-up heights of extreme wind waves estimated by widely used engineering formulas with numerical calculations performed in the framework of nonlinear shallow water theory. It was shown that shallow water theory gives comparable estimate with some empiric formulas, which demonstrates the applicability of shallow water theory for calculation of run-up height of extreme wind waves on a beach.

For the worst case scenario - maximal significant wave height and period based on 35-year wind wave simulations with WAM model forced by COSMO winds, we assessed the wind wave hazard for Estonian coasts. According to our analysis, the most vulnerable to the waves hazard is Aegna and Kakumäe areas, where some buildings in a case of extreme waves can be flooded. Some buildings on Luidja, Mändjala, Matsiranna (Matsi), Narva-Jõesuu, Pirita, Tahkuna (Lehtma), Võsu beaches and Naissaare island are also situated close to the shore, though according to our calculations based on 35 year wave data, they should not be flooded. It should be mentioned, that in this work we restricted ourselves to wave hazard only and did not consider possible storm surge. Of course, together with storm surge the impact of extreme waves on the coast will be even more hazardous.

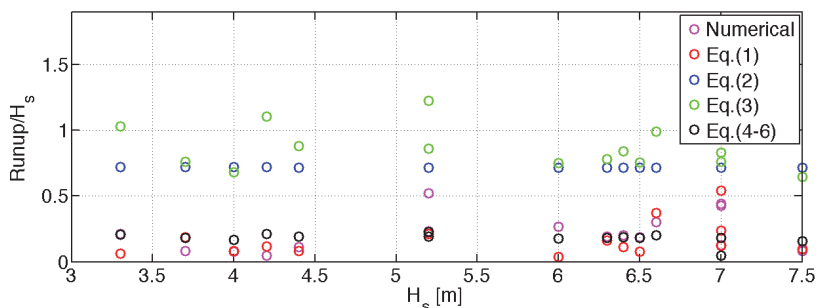


Fig.4. Wave amplification on the beach (ratio of run-up height to significant wave height) versus significant wave height.

ACKNOWLEDGMENT

This research was supported by targeted financing by the Estonian Ministry of Education and Research (grant SF0140007s11) and through support of the ERDF to the Centre of Excellence in Non-linear Studies CENS. AR is grateful to the support program for international doctoral studies in Estonia DoRa. ID acknowledges grant ETF8870.

REFERENCES

- [1] J. A. Hunt, „Design of seawalls and breakwaters,” *J. Waterw. Port C. Div.*, 85, 1959, pp. 123–152.
- [2] J.A. Battjes, “Runup distributions of waves breaking on slopes,” *Journal of the Waterways, Harbors, and Coastal Engineering*, 97 (WW1), 1974, pp. 91–114.
- [3] R.T. Guza, E.B. Thornton, “Swash oscillations on a natural beach,” *Journal of Geophysical Research*, 87 (C1), 1982, pp. 483–491.
- [4] K.A. Powell, “Predicting short term profile response for shingle beaches,” *HRWallingford SR Rept*, 1990, p. 219.
- [5] R.A. Holman, “Extreme value statistics for wave runup on a natural beach,” *Coastal Engineering*, 9, 1986, pp. 527–544.
- [6] P. Nielsen, D.J. Hanslow, “Wave runup distributions on natural beaches,” *Journal of Coastal Research*, 7(4), 1991, pp. 1139–1152.
- [7] A. Matias, J.J. Williams, G. Masselink, Ó. Ferreira, “Overwash threshold for gravel barriers,” *Coastal Engineering*, 63, 2012, pp. 48–61.
- [8] S. Suuroja, M. Karimov, A. Talpas and K. Suuroja, Mererannikute seire. Aruanne riikliku keskkonnaseire alamprogrammi “Mererannikute seire” täitmise 2006. aastal, Tallinn, 2007.
- [9] S. Suuroja, A. Talpas, K. Suuroja, “Eesti Riikliku Keskkonnaseire mererannikute seire allprogrammi 2007,” a aastaaruanne, Tallinn, 2008.
- [10] S. Suuroja, A. Talpas, K. Suuroja, “Eesti Riikliku Keskkonnaseire mererannikute seire allprogrammi 2008,” a aastaaruanne, Tallinn, 2009.
- [11] S. Suuroja, A. Talpas, K. Suuroja, “Eesti Riikliku Keskkonnaseire mererannikute seire allprogrammi 2009,” a aastaaruanne, Tallinn, 2010.
- [12] S. Suuroja, A. Talpas, K. Suuroja, “Eesti Riikliku Keskkonnaseire mererannikute seire allprogrammi 2010,” a aastaaruanne, Tallinn, 2011.
- [13] I. Didenkulova, T. Soomere, K. Pindsoo, S. Suuroja, “On the occurrence of non-reflecting cross-shore profiles along Estonian coasts of the Baltic Sea,” *Estonian Journal of Engineering*, 19 (2), 2013, pp.110–123.

**DISSERTATIONS DEFENDED AT
TALLINN UNIVERSITY OF TECHNOLOGY ON
CIVIL ENGINEERING**

1. **Heino Mölder.** Cycle of Investigations to Improve the Efficiency and Reliability of Activated Sludge Process in Sewage Treatment Plants. 1992.
2. **Stellian Grabko.** Structure and Properties of Oil-Shale Portland Cement Concrete. 1993.
3. **Kent Arvidsson.** Analysis of Interacting Systems of Shear Walls, Coupled Shear Walls and Frames in Multi-Storey Buildings. 1996.
4. **Andrus Aavik.** Methodical Basis for the Evaluation of Pavement Structural Strength in Estonian Pavement Management System (EPMS). 2003.
5. **Priit Vilba.** Unstiffened Welded Thin-Walled Metal Girder under Uniform Loading. 2003.
6. **Irene Lill.** Evaluation of Labour Management Strategies in Construction. 2004.
7. **Juhan Idnurm.** Discrete Analysis of Cable-Supported Bridges. 2004.
8. **Arvo Iital.** Monitoring of Surface Water Quality in Small Agricultural Watersheds. Methodology and Optimization of Monitoring Network. 2005.
9. **Liis Sipelgas.** Application of Satellite Data for Monitoring the Marine Environment. 2006.
10. **Ott Koppel.** Infrastruktuuri arvestus vertikaalselt integreeritud raudtee-ettevõtja korral: hinnakujunduse aspekt (Eesti peamise raudtee-ettevõtja näitel). 2006.
11. **Targo Kalamees.** Hygrothermal Criteria for Design and Simulation of Buildings. 2006.
12. **Raido Puust.** Probabilistic Leak Detection in Pipe Networks Using the SCEM-UA Algorithm. 2007.
13. **Sergei Zub.** Combined Treatment of Sulfate-Rich Molasses Wastewater from Yeast Industry. Technology Optimization. 2007.
14. **Alvina Reihan.** Analysis of Long-Term River Runoff Trends and Climate Change Impact on Water Resources in Estonia. 2008.
15. **Ain Valdmann.** On the Coastal Zone Management of the City of Tallinn under Natural and Anthropogenic Pressure. 2008.
16. **Ira Didenkulova.** Long Wave Dynamics in the Coastal Zone. 2008.
17. **Alvar Toode.** DHW Consumption, Consumption Profiles and Their Influence on Dimensioning of a District Heating Network. 2008.
18. **Annely Kuu.** Biological Diversity of Agricultural Soils in Estonia. 2008.

19. **Andres Tolli**. Hiina konteinerveod läbi Eesti Venemaale ja Hiinasse tagasisaadetavate tühjade konteinerite arvu vähendamise võimalused. 2008.
20. **Heiki Onton**. Investigation of the Causes of Deterioration of Old Reinforced Concrete Constructions and Possibilities of Their Restoration. 2008.
21. **Harri Moora**. Life Cycle Assessment as a Decision Support Tool for System optimisation – the Case of Waste Management in Estonia. 2009.
22. **Andres Kask**. Lithohydrodynamic Processes in the Tallinn Bay Area. 2009.
23. **Loreta Kelpšaitė**. Changing Properties of Wind Waves and Vessel Wakes on the Eastern Coast of the Baltic Sea. 2009.
24. **Dmitry Kurennoy**. Analysis of the Properties of Fast Ferry Wakes in the Context of Coastal Management. 2009.
25. **Egon Kivi**. Structural Behavior of Cable-Stayed Suspension Bridge Structure. 2009.
26. **Madis Ratassepp**. Wave Scattering at Discontinuities in Plates and Pipes. 2010.
27. **Tiia Pedusaar**. Management of Lake Ülemiste, a Drinking Water Reservoir. 2010.
28. **Karin Pachel**. Water Resources, Sustainable Use and Integrated Management in Estonia. 2010.
29. **Andrus Räämet**. Spatio-Temporal Variability of the Baltic Sea Wave Fields. 2010.
30. **Alar Just**. Structural Fire Design of Timber Frame Assemblies Insulated by Glass Wool and Covered by Gypsum Plasterboards. 2010.
31. **Toomas Liiv**. Experimental Analysis of Boundary Layer Dynamics in Plunging Breaking Wave. 2011.
32. **Martti Kiisa**. Discrete Analysis of Single-Pylon Suspension Bridges. 2011.
33. **Ivar Annus**. Development of Accelerating Pipe Flow Starting from Rest. 2011.
34. **Emlyn D.Q. Witt**. Risk Transfer and Construction Project Delivery Efficiency – Implications for Public Private Partnerships. 2012.
35. **Oxana Kurkina**. Nonlinear Dynamics of Internal Gravity Waves in Shallow Seas. 2012.
36. **Allan Hani**. Investigation of Energy Efficiency in Buildings and HVAC Systems. 2012.
37. **Tiina Hain**. Characteristics of Portland Cements for Sulfate and Weather Resistant Concrete. 2012.
38. **Dmitri Loginov**. Autonomous Design Systems (ADS) in HVAC Field. Synergetics-Based Approach. 2012.
39. **Kati Kõrbe Kaare**. Performance Measurement for the Road Network: Conceptual Approach and Technologies for Estonia. 2013.

40. **Viktorija Voronova**. Assessment of Environmental Impacts of Landfilling and Alternatives for Management of Municipal Solid Waste. 2013.
41. **Joonas Vaabel**. Hydraulic Power Capacity of Water Supply Systems. 2013.
42. **Inga Zaitseva-Pärnaste**. Wave Climate and its Decadal Changes in the Baltic Sea Derived from Visual Observations. 2013.
43. **Bert Viikmäe**. Optimising Fairways in the Gulf of Finland Using Patterns of Surface Currents. 2014.
44. **Raili Niine**. Population Equivalence Based Discharge Criteria of Wastewater Treatment Plants in Estonia. 2014.
45. **Marika Eik**. Orientation of Short Steel Fibres in Concrete: Measuring and Modelling. 2014.
46. **Maija Viška**. Sediment Transport Patterns Along the Eastern Coasts of the Baltic Sea. 2014.
47. **Jana Pöldnurk**. Integrated Economic and Environmental Impact Assessment and Optimisation of the Municipal Waste Management Model in Rural Area by Case of Harju County Municipalities in Estonia. 2014.
48. **Nicole Delpeche-Ellmann**. Circulation Patterns in the Gulf of Finland Applied to Environmental Management of Marine Protected Areas. 2014.
49. **Andrea Giudici**. Quantification of Spontaneous Current-induced Patch Formation in the Marine Surface Layer. 2015.
50. **Tiina Nuuter**. Comparison of Housing Market Sustainability in European Countries Based on Multiple Criteria Assessment. 2015.
51. **Erkki Seinre**. Quantification of Environmental and Economic Impacts in Building Sustainability Assessment. 2015.